

Computational Investigations of Some Molecular Properties,  
their Perturbation by External Electric Fields, and their use in  
Quantitative Structure-to-Activity Relationships

by

Shahin Sowlati Hashjin

A Thesis Submitted to Saint Mary's University, Halifax, Nova Scotia,  
in Partial Fulfillment of the Requirements for the  
Degree of Master of Science in Applied Science

June 12, 2013, Halifax, Nova Scotia

Copyright Shahin Sowlati Hashjin, 2013

Approved: Dr. Chérif F. Matta  
Supervisor  
Department of Chemistry  
Mount Saint Vincent University

Approved: Dr. Lou Massa  
External Examiner  
Faculty of Chemistry and Physics  
Hunter College  
City University New York

Approved: Dr. Cory Pye  
Supervisory Committee Member  
Department of Chemistry

Approved: Dr. Timothy Frasier  
Supervisory Committee Member  
Department of Biology

Approved: Dr. Madine VanderPlaat  
Graduate Studies Representative

Date: June 12, 2013

## Dedication

To my parents  
And brothers Shervin and Shayan

## Acknowledgements

I am grateful to several people, without the help of whom this thesis could not have been completed. First and foremost I would like to thank my supervisor Dr. Chérif F. Matta whose invaluable guidance, support and advice helped me the most through this program and whom I learned a lot from.

I would like to thank the committee members, Dr. Cory C. Pye and Dr. Timothy Frasier, for their useful comments, suggestions, corrections, and discussions during the committee meetings. I would also like to thank Dr. Lou Massa who has accepted to be the external examiner.

My thanks also go to my co-authors of the papers presented in this thesis: Dr. André D. Bandrauk, Dr. René V. Bensasson, Dr. Vicent Zoete, and Dr. Daniel Dauzonne.

I was fortunate to have the chance of attending the memorable lectures on density functional theory of Dr. Axel D. Becke last year which was a great learning opportunity.

I would like to thank Dr. Shant Shahbazian for his help and advice and also Jessica L. Churchill for proof reading and her helpful suggestions.

Finally I like to thank my family for their support over all these years.

Shahin Sowlati Hashjin

Computational Investigations of Some Molecular Properties, their Perturbations by  
External Electric Fields, and their use in Quantitative Structure-to-Activity Relationships

by  
Shahin Sowlati Hashjin

**Abstract**

This thesis consists of three quantum chemical investigations. The first investigates the changes in the chemical bond in strong electric fields, a necessary first step for understanding the behaviour of a substrates or drugs in enzyme active sites where such fields are ubiquitous. The second study traces the atomic origins of the sharp peaks in the dipole moment near the transition states of chemical laser reactions. The *Quantum Theory of Atoms in Molecules* is used to decompose the dipole moment surfaces into atomic contributions. Since these peaks can be exploited in the laser control, this knowledge adds another layer of control on tuneable reactions through the choice of reactants maximizing the laser-molecule interaction. The last study outlines a quantitative structure-to-activity study relating the observed anti-carcinogenic and anti-inflammatory activities of 150 molecules to calculated electronic properties, reducing the cost, time, and effort in the design of anticancer and anti-inflammatory drugs.

June 12, 2013

## Table of content

	<b>Introduction</b>	1
<b>1.</b>	<b>Chapter 1: The Chemical Bond In External Electric Field</b>	21
	<b>Summary</b>	21
<b>1.1.</b>	<b>Introduction</b>	22
<b>1.2.</b>	<b>Methods and Computation</b>	26
<b>1.2.1.</b>	The Molecular Set	26
<b>1.2.2.</b>	Electronic Structure Calculations	26
<b>1.2.3.</b>	Field Strengths and Directions	28
<b>1.2.</b>	<b>Results and Discussion</b>	33
<b>1.2.1.</b>	The Energy and the Dipole Moment of a Diatomic Molecule in an External Homogenous Electric Field	37
1.3.1.1.	<i>The Energy Expression</i>	
1.3.1.2.	<i>The Role of Permanent Dipole Moment and of Polarizability in Determining the Response to an External Field</i>	
<b>1.3.2.</b>	The Equilibrium Bond Length (Inter-Nuclear Separation) in an External Homogenous Electric Field	47
1.3.2.1.	<i>Trends in Equilibrium Bond Lengths in an External Field</i>	
1.3.2.2.	<i>Electric Field-Perturbed Morse Potential</i>	
<b>1.3.3.</b>	IR Vibrational Stark Effects and Bond Force Constants in External Fields	58
1.3.3.1.	<i>General Considerations</i>	
1.3.3.2.	<i>Inability of UQCISD to Reproduce the Vibrational Stark-shift in Nitric Oxide</i>	
1.3.3.3.	<i>A Simple Model to Account for the Vibrational Stark-shift in Diatomics</i>	
<b>1.4.</b>	<b>Conclusion</b>	70
	<b>References</b>	73
<b>2.</b>	<b>Chapter 2: Dipole Moment Surface of the <math>\text{CH}_4 + \cdot\text{X} \rightarrow \text{CH}_3\cdot + \text{HX}</math> (<math>\text{X} = \text{F}, \text{Cl}</math>) Reaction from Atomic Dipole Moment Surfaces, and the Origin of the Sharp Extrema in the Dipole Moment near the Transition State</b>	79
	<b>Summary</b>	79
<b>2.1.</b>	<b>Introduction</b>	80
<b>2.2.</b>	<b>Atomic Contributions to the Total Dipole for Electrically-Neutral System</b>	83
<b>2.3.</b>	<b>Computational Methods</b>	85
<b>2.4.</b>	<b>Conventions and Units</b>	86
<b>2.5.</b>	<b>Results and Discussion</b>	87
<b>2.5.1.</b>	General Features of the Potential Energy and Dipole Moment Surfaces	87
<b>2.5.2.</b>	Atomic and Group Charges Surfaces	91
<b>2.5.3.</b>	Atomic and Group Dipolar Polarization in the Reactants and Products	94
<b>2.5.4.</b>	The Dipole Moment surface of the $\text{CH}_4 + \cdot\text{F} \rightarrow \text{CH}_3\cdot + \text{HF}$ Reaction	98
<b>2.5.5.</b>	The Dipole Moment surface of the $\text{CH}_4 + \cdot\text{Cl} \rightarrow \text{CH}_3\cdot + \text{HCl}$ Reaction	110
<b>2.6.</b>	<b>Conclusion</b>	116
	<b>References</b>	118

<b>3.</b>	<b>Chapter 3: Physicochemical properties of exogenous molecules correlated with their biological efficacy as protectors against carcinogenesis and inflammation</b>	122
	<b>Summary</b>	122
<b>3.1.</b>	<b>Introduction</b>	123
<b>3.2.</b>	<b>Methods</b>	124
<b>3.2.1.</b>	Biological methods	124
<b>3.2.2.</b>	Computational methods	124
3.2.2.1.	<i>Semiempirical quantum mechanical calculations</i>	
3.2.2.2.	<i>Calculations of the vertical ionisation potential IP and of the electron affinity (EA) by density functional theory (DFT)</i>	
<b>3.2.3.</b>	Data treatment and analyses	127
3.2.3.1.	<i>Relation of IP, E(HOMO) and the oxidation potential at neutral pH</i>	
3.2.3.2.	<i>Biological quantitative structure-activity relationships (QSAR)</i>	
<b>3.3.</b>	<b>Results and Discussion</b>	128
<b>3.3.1.</b>	Cancer chemoprevention efficacy <i>in vivo</i>	128
3.3.1.1.	<i>Correlations between redox properties of phenolic derivatives (P) and their inhibitory effects on mice neoplasia</i>	
3.3.1.2.	<i>Correlations between electron-donating ability of 3-nitroflavones (NF) and their inhibitory activity of the onset and progression of aberrant crypt foci (ACF) in rat colon</i>	
3.3.1.3.	<i>Correlations between electron-donating ability of 3-nitroflavones (NF) and their efficacy to inhibit angiogenesis</i>	
<b>3.3.2.</b>	Induction of a cancer-protective enzyme, NAD(P)H-quinone reductase 1 (NQO1)	144
3.3.2.1.	<i>Induction of NQO1 by diphenols (DP)</i>	
3.3.2.2.	<i>Induction of NQO1 by phenylpropenoids (PP)</i>	
3.3.2.3.	<i>Induction of NQO1 by flavonoids (F)</i>	
3.3.2.4.	<i>Induction of NQO1 by by triterpenoids (TP)</i>	
<b>3.3.3.</b>	Inhibition of topoisomerases involved in DNA replication and transcription	167
<b>3.3.4.</b>	Inflammation suppressive capacity	172
<b>3.4.</b>	<b>Conclusion</b>	173
	<b>References</b>	178
<b>4.</b>	<b>Chapter 4: Closing Remarks</b>	184
<b>5.</b>	<b>Appendix</b>	187

## Introduction

Computational chemistry combines computer science and theoretical chemistry with the goal of helping chemists to deepen their understanding of the problem at hand, but also to solve their practical wet-lab problems at hand. This subfield of chemistry, which intersects with quantum mechanics on one hand and with chemical biology on another, has gained undeniably increasing role in fundamental and applied chemical research in the past decade or so [1-8].

A principal strength of computational chemistry is that its results can not only be in close agreement with experiment, but also can accurately *predict* and *describe* never-seen-before chemical phenomena and/or the properties of molecules yet to be synthesized. The deviations from exact results are due to assumption of several simplification and approximation in the process of solving the Schrödinger equation numerically (iteratively) and also sometime in the following simplification of the statistical mechanical treatment of the results of the electronic structure calculation to obtain bulk properties of matter. A clearly unsolved problem in computational chemistry is that of the solvent effects, precisely due to the enormously complex statistical mechanical problem that this entails. Further, both computational and experimental results have their own inherent limitations in both accuracy and precision.

Based on the computational framework, there is a long list of atomic and molecular properties which can be calculated by standard modern computational chemistry software (e.g. Gaussian, GAMESS, MolPro, HyperChem, Jaguar, etc.), such as atomic and molecular energies, molecular geometries (bond lengths, bond angles and

dihedrals), vibrational frequencies, charge distributions, absorption intensities, molecular orbital energies, ionization energies, reaction barriers, and the geometries and energies of transition state [1-8].

Depending on the system one wishes to study, there may be several computational schemes to choose from. For small systems, there are highly accurate methods available. However, for larger systems such as proteins, in order to obtain reasonably accurate results in practical time, simpler methods are often the only practical methods that are applicable. The development of linear scaling algorithms in parallel with the unprecedented developments in computer hardware and software and massive parallelization give reasons to expect far more accurate methods to reach proteins in their applicability and in the not too distant future [9-24].

An important goal of a standard quantum computational chemistry software is to solve the molecular Schrödinger equation approximately. There are innumerable texts outlining the Hartree-Fock approximation and the methods that build on it, as these are also often reviewed in theses. The author does not find this necessary to repeat this review in this thesis yet again, but we will just mention a few salient points to set the tone of this thesis.

A fundamental postulate of quantum mechanics is that a quantum system is fully described by a mathematical function of the many particles' coordinates and spins known as state- or wavefunction  $\psi$ , which contains all the information that can be known about the system. The wavefunction must be antisymmetric in the interchange of the coordinates and spins of any two particles in an ensemble of fermions, i.e., particles with half-integral spin such as a collection of electrons in an atom or a molecule. The



information can then be extracted from the wavefunction through the operation of linear Hermitian operators.

In one dimension and for a one-particle system, the wavefunction satisfies the time-dependent Schrödinger [25] equation:

$$-(\hbar/2\pi i) \partial\psi(x, t)/\partial t = -(\hbar^2/8m\pi^2) \partial^2\psi(x, t)/\partial x^2 + V(x, t)\psi(x, t) \quad (1)$$

Max Born [26, 27] was the first to advance the interpretation of the wavefunction as probability *amplitude*. The *probability* of finding a particle at the time  $t$  in a certain region along the  $x$ -axis is given then by:

$$|\psi(x, t)|^2 \quad (2)$$

Frequently, chemical problems can be approached satisfactorily without the explicit inclusion of time-dependence, which is a great simplification. Thus, instead of solving Eqn. (1), in this case one has to solve the simpler time-independent form of the Schrödinger equation (Eqn. 1-3), which describes the stationary states of the system, in one-dimension:

$$-(\hbar^2/8m\pi^2) \partial^2\psi(x)/\partial x^2 + V(x)\psi(x) = E\psi(x) \quad (3)$$

As mentioned above, finding (approximate) solutions to the time-independent Schrödinger equation is one of the core problems of computational quantum chemistry.

Described in terms of position vectors of electron and nuclei ( $\mathbf{r}$  and  $\mathbf{R}$  respectively), written in atomic units, the Hamiltonian operator for a multi-particle system is as follows:

$$\begin{aligned}
H = & -\sum_{i=1}^N \frac{1}{2} \nabla_i^2 - \sum_{A=1}^M \frac{\nabla_A^2}{2M_A} - \sum_{i=1}^N \sum_{A=1}^M \frac{Z_A}{r_{iA}} + \sum_{i=1}^N \sum_{j>i}^N \frac{1}{r_{ij}} + \\
& \sum_{A=1}^M \sum_{B>A}^M \frac{Z_A Z_B}{R_{AB}}
\end{aligned}
\tag{4}$$

wherein, the first and second terms are the kinetic energy of the electrons and the nuclei respectively, the third term is nuclear-electron attraction, and the fourth and fifth term describe the electron-electron and nuclear-nuclear repulsions, respectively.

Central to quantum chemistry is the Born-Oppenheimer (BO) approximation [28], which assumes that, due to the difference of their masses, the motion of electrons is much faster than that of the nuclei. As a consequence, it is possible to consider that electrons are moving in a fixed field generated by clamped nuclei. This approximation decouples the motion of the electrons from that of the nuclei, the nuclear positions become a parameter and the nuclei move in the potential created by the electrons as one varies the positions of the nuclei. It is only within the framework of the BO approximation that concepts such as the potential energy surface (PES) and even the dipole moment itself have a physical meaning [2].

The BO approximation allows one to add the second term in equation 4 (the nuclear-nuclear repulsion term) at the end of the calculation, after solving the electronic problem approximately. In other words, the last term can be regarded as a classical parameter that does not affect the form of eigenfunction, adding only a constant to the eigenvalues.

The remaining terms in equation 4 form the electronic Hamiltonian operator of a multi-particle system:

$$H\psi = E\psi \tag{5}$$

Therefore Hamiltonian of a system explicitly depends on the electronic coordinates while the dependence on the nuclear coordinates remains parametrical. The total energy of the system is obtained by adding the nuclear repulsion, as a constant, to the electronic energy.

The second approximation in what is nowadays standard quantum chemistry is the orbital approximation, that is, replacing the  $N$ -electron wavefunction with  $N$  one-electron wavefunctions (spin orbitals). This simplification avoids the correlation among electrons and introduces an error in the resulting energy as it keeps the electrons uncorrelated. This problem is tackled to some extent in post HF and DFT methods. Employing basis set as linear combination of basis functions to avoid complicated equations in the solutions of HF equations is another choice for simplification. Most current computational approaches ignore the finite dimensions of the nuclei which are treated as point charges, leading to (non-physical) cusps in the wavefunction and in the electron density at their positions. Relativistic effects are important only in the calculations including heavy atoms due to average electronic speeds that can become sizable fraction of  $c$  especially the core electrons, and since in this thesis we are only concerned with light atoms these effects are safely ignored. There are also other assumption/simplifications such as use of Gaussian basis functions which compared to Slater type ones are less accurate in reproducing the behaviour of the atomic orbitals near the nuclei, for precisely their inability to approach the cusp, and at long ranges as they decay more slowly, but are far more computationally efficient since the product of two Gaussian functions is a third Gaussian.

The main streams in computational quantum chemistry outlined above can be termed collectively "*wavefunction methods of calculation*" [31,32], but there are other important branches of theoretical computational chemistry, namely, the valence-bond method [29,30] and density functional theory (DFT) [33,34]. Valence bond methods are usually only practical for the smallest system and because of that are far less frequently utilized than the two other streams [35]. Wavefunction-based methods can further branch into *ab initio* (including variational methods such as Hartree-Fock and post Hartree-Fock methods such as configuration interaction (CI) and coupled cluster methods (CC), and perturbative methods such as Møller-Plesset  $n^{\text{th}}$  order perturbation theory (MP $n$ )), and semi-empirical schemes (such as AM1, PM3, INDO, MINDO, EHT, etc.) in which some experimental parameters are included to approximate the values of computationally demanding integrals.

Density functional theory methods are conceptually constructed on the basis of the first Hohenberg-Kohn (HK) theorem which states there is a one to one relation between the energy of a system and its electron density distribution [36]. In other words, the ground state density uniquely determines the external potential. In this regard energy of the system as a functional of the electron density is defined as  $E[\rho] = T[\rho] + E_{ne}[\rho] + E_{ee}[\rho]$  where right hand side terms are electronic kinetic energy, nuclei-electron attraction and electron-electron repulsion energy terms respectively. However the H-K theorem is an "existence" theorem that does not tell us how to find this unique *functional* relation between external potential and the electron density. The second H-K theorem suggests that the lowest energy of the system can be delivered through the functional  $F_{HK}[\rho] = T[\rho] + E_{ee}[\rho]$ , only and only if the employed electron density is

the true ground state density; a variational principle similar to that in wavefunction methods. It is through the second Kohn-Sham (KS) theorem [37] that modern DFT methods work, where the energy of the molecule is considered as a deviation from a fictitious non-interacting reference system. This leads to K-S equations which can be solved iteratively and yield K-S orbitals that are further used to construct the electron density. The sum of kinetic energy and electron-electron repulsion deviations from their classical counterparts are called exchange-correlation energy ( $E_{xc}$ ) which has to be approximated.

Besides these electronic structure methods, there are also molecular mechanics (MM) and molecular dynamical (MD) methods [38-40], which the latter is employed mainly for modeling biomolecules. There are also hybrid methods, such as QM/MM methods [41,42], in which some parts of a system are studied by more accurate quantum mechanical approaches (accuracy in focus) and less significant parts of the same system are modelled by molecular mechanics (speed of computation is in focus).

Computational chemists use different methods and different software to study their systems of interest which may be an atom, an ion, a diatomic molecule, a complex molecule such as a catalyst in a reaction, a solid, an enzyme, metabolism of a recently designed drug, a large protein, or a multi-step reaction. In 1959 Mulliken and Roothaan [43] made a brilliant pronouncement on the efficiency of quantum chemistry, which can be undoubtedly generalized to *computational chemistry*:

*Looking toward the future, it seems certain that colossal rewards lie ahead from large quantum-mechanical calculations of the structure of matter.*

Later in 1984 H. F. Schaefer [44] commented:

*We are confident that by the year 2000, essentially all fields of chemistry will acknowledge the accuracy of Mulliken and Roothaan's prophecy.*

Even later in 2000, Barden and Schaefer [45] made a new note on Mulliken and Roothaan in which they predicted that:

*by the year 2100, those 'colossal rewards' will have been largely realized, and their consequences will be so striking that essentially all fields of science will acknowledge the accuracy of Mulliken and Roothaan's prophecy.*

Computational chemistry indeed has opened new doors to all fields of chemistry and enabled chemists to ask new questions, and predict/answer them. Any single study reveals something new, adds something to our knowledge, sheds light on some aspect of the phenomenon being studied, and finds a puzzle piece and its correct place to complete the "big picture": understanding the universe.

All the studies presented in this thesis are briefly described in the following paragraphs after a short introduction to Quantum Theory of Atoms In Molecules (QTAIM) [46-51] which is employed in the second study (chapter 2) and will be used in the future to extend the investigations outlined in chapters 1 and 3.

Founded by Richard F. W. Bader, the roots of the QTAIM can be traced back to the sixties [52-55] and was further developed in seventies [56-58] and eighties [51,59-62] of the past century. This theory is today well-known and established, emphasizing the importance of the electron density in the description, explanation, and understanding the chemical phenomena, and providing a line that connects empirical chemistry to its quantum mechanical roots. There is a link between chemical concepts and quantum

mechanics “as we live in only one world” [48] and QTAIM is what we need to make this link. The theory provides a solid theoretical basis for core chemical concepts such as chemical structure, chemical reactivity, and chemical stability. Quantum mechanics is brought into application to atoms in molecules by definition of open “quantum subsystem” as a bounded region in a closed system [47].

Within the framework of the theory, every atom has its own contribution to molecular properties which add up to the corresponding molecular values [63]. In this regard, the theory is called the quantum mechanics of open subsystems, such open subsystems as atoms in molecules or crystals or even a solvated electron [64].

The theory has also made it possible to generalize the “global” statement of the virial theorem [65], which correlates potential and kinetic energies of a molecule to its “local” form which is then defined at each point in space [61]. The theorem is also defined for a subspace and leads to the natural definition of an atomic energy as is well documented in the QTAIM literature.

Since its birth, the quantum theory of atoms in molecules has grown conceptually as well as technically, and nowadays several standard software implement it as their principal focus. The field is still opened and fast developing [66].

The applicability of the QTAIM extends over a wide range of research areas such as drug discovery [67-69] and protein modeling [70-74], solid state [75-78], biochemistry [79], and ultrahigh resolution X-ray crystallography [80-82]. It is now common to take advantage of the QTAIM’s capability of analyzing various isolated or dynamic systems [83].

This thesis, in part, uses the QTAIM as a tool to answer some important questions, the answer of which is by necessity "regional", *i.e.*, ascribing a global phenomenon to a particular region in a molecule or reacting system. QTAIM analysis of the first and the last study presented in this thesis is currently under investigation.

The present thesis includes three separate studies. The first two are contributions to theoretical chemical physics-physical chemistry. In the first of these studies the effects of strong external electric fields on the properties of the chemical bond are elucidated, quantitated, and a theoretical foundation using diatomic molecules as a test case is provided. In the second study, we determine the relative role of every atom in a reacting system in the overall changes of the system's dipole moments especially near the transition state of the reaction. The importance of this study is to help understand what determines the height of these dipole peaks, peaks that can be exploited in the laser control of reaction as previously demonstrated [84]. The third study is a contribution to theoretical chemical biology. In this study, quantum chemistry is used in the modeling and in the prediction of the anti-carcinogenic and anti-inflammatory properties of a large variety of molecules.

The three studies that constitute this thesis use the modern tools of computational quantum chemistry to explain and predict patterns of chemical reactivity and, in the third, their reflection in the biology of the studied molecules. In this thesis, the *structures* and *properties* of molecules are studied in different environments with the goal of gaining insight to their chemistry, physics, reactivities, and biological activities.

The first study in the thesis elucidates the response of molecules to external electric fields of magnitudes that are commonly encountered in an enzyme active site or



in modern nanoscience tools such as a scanning tunnelling microscope (STM). In this study, key properties of the chemical bond such as bond length, force constant, vibrational frequency, and important molecular properties such as total energies and dipole moments of several diatomic molecules, homonuclear and heteronuclear, are studied in presence of a range of external electric fields. The authors plan to extend this study to include field effects on the common topological and QTAIM properties such as the electron density at the bond critical point, the delocalization index, and the atomic charges. The effects of external electric fields on different molecules, especially biological molecules of importance, are of considerable interest and many important studies have been conducted addressing this issue. However, to the best of the author's knowledge, a systematic QTAIM study of these effects, with a few exceptions in the literature, is lacking to a great extent. The first study presented here is a preliminary investigation upon which the author plans to build.

The second study outlines the changes in structures and electrical properties of reactants, following changes in their dipole moment surfaces as they reach the products passing through the transition state region. The question the study attempts to answer is about the atomic origins (the principal atomic contributor(s)) to the observed very sharp peaks in the dipole moment surfaces of two reacting systems  $\text{CH}_4 + \cdot\text{X} \rightarrow \text{CH}_3\cdot + \text{HX}$  ( $\text{X} = \text{F}, \text{Cl}$ ) near the region of their respective transition states. A dipole moment surface is the response surface of the dipole moment as a function of the reaction coordinate, similar in construction to a potential energy surface except that the energy axis is replaced by the electric dipole moment. The QTAIM provides a rigorous partitioning of the dipole moment of a system into two origin-independent contributions, namely atomic

polarization (AP) and charge transfer (CT). In this study this approach is applied for the well-known laser-induced chemical reactions  $\text{CH}_4 + \cdot\text{X} \rightarrow \text{CH}_3\cdot + \text{HX}$  (X= F, Cl) for which it has been shown that the dipole moment and the polarizability tensor components along the reactions coordinate undergo dramatic changes near transition state [84]. The systems' dipole moment surfaces are decomposed, by means of the QTAIM, into atomic and/or group contributions. The atomic origins of these sharp peaks in dipole moment surfaces for both reactions are discussed besides the comparison between the atomic polarization and charge transfer contributions.

The ultimate part of the thesis represents a change in emphasis, that is, focusing on developing empirical correlations between structure and activity or "quantitative structure activity relationship" (QSAR) study [85-88]. QSAR studies are based on the assumption that similar compounds give similar responses or have similar activities.

The last chapter, thus, summarizes a chemical descriptor based QSAR study of a large number of molecules with known potency as anti-carcinogenic and inflammatory agents. In this type of QSAR studies various molecular descriptor such as electronic, energetic, and geometric are used and the best descriptors selected empirically through the strength of their correlation with the known activity. The correlations between properties related to the electron donating ease indices (predictor variable) such as ionization potential and energy of highest occupied molecular orbital of different classes of molecules are found to be correlated to various extents to concrete biological properties such as inhibitory effects on mice neoplasia, on ACF in rat colon, angiogenesis etc.. Such studies are of importance at least from two aspects. First, they may shed light

on the *mechanism(s)* of drug action. Second, they can be used in the *design* of new and more effective and less toxic drugs.

In such a chemical descriptor based QSAR study where energetic and electronic properties are of importance and electron releasing ease is the descriptor, QTAIM analysis can be beneficial. QTAIM may enable one to predict the active “region” of the compound. In this way, the chemical descriptor based QSAR is reduced to fragment based or group contribution QSAR. The exploration of the active part of the molecule makes design/proposing new compounds possible [69].

## References

- (1) P. v. R. Schleyer; *Encyclopaedia of Computational Chemistry*; John Wiley and Sons: Chichester, UK, 1998.
- (2) L. Piela; *Ideas of Quantum Chemistry*; Elsevier: Amsterdam, 2007.
- (3) E. G. Lewars; *Computational Chemistry: Introduction to the Theory and Applications of Molecular and Quantum Mechanics (Second Edition)*; Springer: New York, 2011.
- (4) C. J. Cramer; *Essentials of Computational Chemistry: Theories and Models*; John Wiley & Sons, Ltd.: New York, 2002.
- (5) S. M. Bachrach; *Computational Organic Chemistry*; John Wiley and Sons, Inc.: Hoboken, New Jersey, 2007.
- (6) F. Jensen; *Introduction to Computational Chemistry*; John Wiley and Sons Ltd.: West Sussex (UK), 2007.
- (7) K. Krogh-Jespersen; *Introduction to Computational Chemistry*; Dept. of Chemistry and Chemical Biology, Rutgers, The State University of New Jersey: New Brunswick, NJ (USA), 2004.
- (8) D. C. Young; *Computational Chemistry: A Practical Guide for Applying Techniques to Real World Problems*; Wiley-Interscience: New York, 2001.
- (9) L. Huang, H. Bohorquez, C. F. Matta, L. Massa; The Kernel Energy Method: Application to Graphene and Extended Aromatics. *Int. J. Quantum Chem.* **2011**, 4150-4157.
- (10) L. Huang, L. Massa, J. Karle; Quantum kernels and quantum crystallography: Applications in biochemistry. *Quantum Biochemistry: Electronic Structure and Biological Activity*; Wiley-VCH: Weinheim, 2010, pp 3-60.
- (11) L. Huang, L. Massa, J. Karle; Kernel energy method applied to vesicular stomatitis virus nucleoprotein. *Proc. Natl. Acad. Sci. USA* **2009**, *106*, 1731-1736.
- (12) L. Huang, L. Massa, J. Karle; The Kernel Energy Method: Application to a tRNA. *Proc. Natl. Acad. Sci. USA* **2006**, *103*, 1233-1237.
- (13) L. Huang, L. Massa, J. Karle; Kernel energy method: Application to insulin. *Proc. Natl. Acad. Sci. USA* **2005**, *102*, 12690-12693.
- (14) L. Huang, L. Massa, J. Karle; Kernel energy method: Application to DNA. *Biochemistry* **2005**, *44*, 16747-16752.
- (15) L. Huang, L. Massa, J. Karle; Kernel energy method illustrated with peptides. *Int.*

- J. Quantum Chem.* **2005**, *103*, 808-817.
- (16) S. Hua, W. Hua, S. Li; An efficient implementation of the generalized energy-based fragmentation approach for general large molecules. *J. Phys. Chem. A* **2010**, *114*, 8126-8134.
  - (17) L. Hung, E. A. Carter; Accurate simulations of metals at the mesoscale: Explicit treatment of 1 million atoms with quantum mechanics. *Chem. Phys. Lett.* **2009**, *475*, 163-170.
  - (18) D. Fedorov, K. Kitaura; *The Fragment Molecular Orbital Method: Practical Applications to Large Molecular Systems*; CRC Press: Boca Raton, Florida, 2009.
  - (19) X. He, J. Z. H. Zhang; A new method for direct calculation of total energy of protein. *J. Chem. Phys.* **2005**, *122*, 031103-1-031103-4.
  - (20) Y. Mei, D. W. Zhang, J. Z. H. Zhang; New method for direct linear-scaling calculation of electron density of proteins. *J. Phys. Chem. A* **2005**, *109*, 2-5.
  - (21) S. Li, W. Li, T. Fang; An efficient fragment-based approach for predicting the ground-state energies and structures of large molecules. *J. Am. Chem. Soc.* **2005**, *127*, 7215-7226.
  - (22) G. E. Scuseria; Linear scaling density functional calculations with gaussian orbitals. *J. Phys. Chem. A* **1999**, *103*, 4782-4790.
  - (23) T.-S. Lee, J. P. Lewis, W. Yang; Linear-scaling quantum mechanical calculations of biological molecules: The divide-and-conquer approach. *Comput. Mater. Sci. Volume 12, 1998, Pages 259-277* **1998**, *12*, 259-277.
  - (24) M. C. Strain, G. E. Scuseria, M. J. Frisch; Achieving linear scaling for the electronic quantum coulomb problem. *Science* **1996**, *271*, 51-53.
  - (25) E. Schrödinger; *Collected Papers on Wave Mechanics together with Four Lectures on Wave Mechanics, Third (Augmented) English Edition*; American Mathematical Society - Chelsea Publishing: Providence, Rhode Island, 1982.
  - (26) M. Born; Quantenmechanik der stoßvorgänge. *Z. Physik* **1926**, *38*, 803-827.
  - (27) M. Born; Zur quantenmechanik der stoßvorgänge. *Z. Physik* **1926**, *37*, 863-867.
  - (28) M. Born, R. Oppenheimer; Zur Quantentheorie der Moleküle (On the Quantum Theory of Molecules). *Ann. Phys.* **1927**, *84*, 457-484.
  - (29) S. Shaik, P. C. Hiberty; *A Chemist's Guide to Valence Bond Theory*; John Wiley and Sons, Inc.: New Jersey, 2008.
  - (30) G. A. Gallup; *Valence Bond Methods*; Cambridge University Press: Cambridge,

2002.

- (31) A. Szabo, N. S. Ostlund; *Modern Quantum Chemistry: Introduction to Advanced Electronic Structure Theory*; Dover Publications, Inc.: New York, 1989.
- (32) I. N. Levine; *Quantum Chemistry, (Sixth Edition)*; Pearson Prentice Hall: Upper Saddle River, New Jersey, 2009.
- (33) R. G. Parr, W. Yang; *Density-Functional Theory of Atoms and Molecules*; Oxford University Press: Oxford, 1989.
- (34) W. Koch, M. C. Holthausen; *A Chemist's Guide to Density Functional Theory, (Second Edition)*; Wiley-VCH: New York, 2001.
- (35) R. Hoffmann, S. Shaik, P. C. Hiberty; A conversation on VB vs MO theory: A never-ending rivalry? *Acc. Chem. Res.* **2003**, *36*, 750-756.
- (36) P. Hohenberg, W. Kohn; Inhomogeneous electron gas. *Phys. Rev. B* **1964**, *136*, 864-871.
- (37) W. Kohn, L. J. Sham; Self consistent equations including exchange and correlation effects. *Phys. Rev. A* **1965**, *140 (4A)*, 1133-1138.
- (38) J. W. Ponder, D. A. Case; Force fields for protein simulations. *Adv. Protein Chem.* **2003**, *66*, 27-85.
- (39) T. Schlick; *Molecular Modeling and Simulation: An Interdisciplinary Guide*; Springer: New York, 2002.
- (40) A. Warshel; *Computer Modeling of Chemical Reactions in Enzymes and Solutions*; John Wiley and Sons, Inc.: New York, 1991.
- (41) H. M. Senn, W. Thiel; QM/MM methods for biomolecular systems. *Angew. Chem. Int. Ed.* **2009**, *48*, 1198-1229.
- (42) F. R. Clemente, T. Vreven, M. J. Frisch; Getting the most out of ONIOM: Guidelines and pitfalls. *Quantum Biochemistry: Electronic Structure and Biological Activity*; Wiley-VCH: Weinheim, 2010, pp 61-83.
- (43) R. S. Mulliken, C. C. J. Roothaan; Broken Bottlenecks and the Future of Molecular Quantum Mechanics. *Proc. U. S. Natl. Acad. Sci.* **1959**, *45*, 394-398
- (44) H. F. Schaefer; *Quantum Chemistry: The development of Ab Initio Methods in Molecular Electronic Structure Theory*. Clarendon Press, Oxford (1984)
- (45) C. J. Barden, H. F. Schaefer; Quantum Chemistry in the 21<sup>st</sup> Century. *Pure Appl. Chem.* **2000**, *72*, 1405-1423

- (46) R. F. W. Bader; *Atoms in Molecules: A Quantum Theory*; Oxford University Press: Oxford, U.K., 1990.
- (47) C. F. Matta, R. J. Boyd; *The Quantum Theory of Atoms in Molecules: From Solid State to DNA and Drug Design*; Wiley-VCH: Weinheim, 2007.
- (48) P. L. A. Popelier; *Atoms in Molecules: An Introduction*; Prentice Hall: London, 2000.
- (49) R. F. W. Bader; The quantum mechanical basis of conceptual chemistry. *Monatsh. Chem.* **2005**, *136*, 819-854.
- (50) R. F. W. Bader, T. T. Nguyen-Dang; Quantum theory of atoms in molecules - Dalton revisited. *Adv. Quantum Chem.* **1981**, *14*, 63-124.
- (51) R. F. W. Bader, T. T. Nguyen-Dang, Y. Tal; A topological theory of molecular structure. *Rep. Prog. Phys.* **1981**, *44*, 893-948.
- (52) R. F. W. Bader, I. Keaveny, P. E. Cade; Molecular charge distributions and chemical binding II. First-row diatomic hydrides. *J. Chem. Phys.* **1967**, *47*, 3381-3402.
- (53) R. F. W. Bader, W. H. Henneker, P. E. Cade; Molecular charge distributions and chemical binding. *J. Chem. Phys.* **1967**, *46*, 3341-3363.
- (54) R. F. W. Bader, A. K. Chandra; A view of bond formation in terms of molecular charge distributions. *Can. J. Chem.* **1968**, *46*, 953-966.
- (55) R. F. W. Bader, A. D. Bandrauk; Molecular charge distributions and chemical binding III. The isoelectronic series N<sub>2</sub>, CO, BF and C<sub>2</sub>, BeO, LiF. *J. Chem. Phys.* **1968**, *49*, 1653-1665.
- (56) R. F. W. Bader, P. M. Beddall; Virial field relationship for molecular charge distributions and the spatial partitioning of molecular properties. *J. Chem. Phys.* **1972**, *56*, 3320-3328.
- (57) S. Srebrenik, R. F. W. Bader; Towards the development of the quantum mechanics of a subspace. *J. Chem. Phys.* **1975**, *63*, 3945-3961.
- (58) S. Srebrenik, R. F. W. Bader, T. T. Nguyen-Dang; Subspace quantum mechanics and the variational principle. *J. Chem. Phys.* **1978**, *68*, 3667-3679.
- (59) J. Hernández-Trujillo, F. Cortés-Guzmán, D.-C. Fang, R. F. W. Bader; Forces in molecules. *Chemical Concepts from Quantum Mechanics, Faraday Discussions, Vol. 135*; Royal Society of Chemistry: Cambridge, pp 79-95.
- (60) R. F. W. Bader, Y. Tal, S. G. Anderson, T. T. Nguyen-Dang; Quantum topology: Theory of molecular structure and its change. *Israel J. Chem.* **1980**, *19*, 8-29.

- (61) R. F. W. Bader; Quantum topology of molecular charge distributions. III. The mechanics of an atom in a molecule. *J. Chem. Phys.* **1980**, *73*, 2871-2883.
- (62) R. F. W. Bader, H. Essen; The characterization of atomic interactions. *J. Chem. Phys.* **1984**, *80*, 1943-1960.
- (63) C. F. Matta, R. F. W. Bader; An experimentalist's reply to "What is an atom in a molecule?" *J. Phys. Chem. A* **2006**, *110*, 6365-6371
- (64) R. F. W. Bader; Principle of stationary action and the definition of a proper open system *Phys. Rev. B* **1994**, *49*, 13348-13356
- (65) J. C. Slater; The virial and molecular structure *J. Chem. Phys.* **1933**, *1*, 687-691
- (66) Sh. Shahbazian; Beyond the orthodox QTAIM: motivations, current status, prospects and challenges. *Found. Chem.* (2012) doi:10.1007/s10698-012-9170-0
- (67) C. F. Matta; *Quantum Biochemistry: Electronic Structure and Biological Activity*; Wiley-VCH: Weinheim, 2010.
- (68) C. F. Matta, A. A. Arabi; Electron-density descriptors as predictors in quantitative structureactivity/property relationships and drug design. *Future Med. Chem.* **2011**, *3*, 969-994.
- (69) C. F. Matta, A. A. Arabi, D. F. Weaver; The bioisosteric similarity of the tetrazole and carboxylate anions: Clues from the topologies of the electrostatic potential and of the electron density. *Eur. J. Med. Chem.* **2010**, *45*, 1868-1872.
- (70) M. Song, C. M. Breneman, J. Bi, N. Sukumar, K. P. Bennett, S. Cramer, N. Tugcu; Prediction of protein retention times in anion-exchange chromatography systems using support vector regression. *J. Chem. Inf. Comput. Sci.* **2002**, *42*, 1347-1357.
- (71) C. F. Matta, R. F. W. Bader; An atoms-in-molecules study of the genetically-encoded amino acids. I. Effects of conformation and of tautomerization on geometric, atomic, and bond properties. *Proteins: Struct. Funct. Genet.* **2000**, *40*, 310-329.
- (72) C. F. Matta, R. F. W. Bader; Atoms-in-molecules study of the genetically-encoded amino acids. II. Computational study of molecular geometries. *Proteins: Struct. Funct. Genet.* **2002**, *48*, 519-538.
- (73) C. F. Matta, R. F. W. Bader; Atoms-in-molecules study of the genetically-encoded amino acids. III. Bond and atomic properties and their correlations with experiment including mutation-induced changes in protein stability and genetic coding. *Proteins: Struct. Funct. Genet.* **2003**, *52*, 360-399.
- (74) R. F. W. Bader, C. F. Matta, F. J. Martín; Atoms in medicinal chemistry. *Medicinal Quantum Chemistry*; Wiley-VCH: Weinheim, 2003, pp 201-231.



- (75) C. Gatti; Chemical bonding in crystals: New directions. *Z. Kristallogr.* **2005**, *220*, 399-457.
- (76) C. Gatti, P. Macchi; *Modern Charge Density Analysis*; Springer: Germany, 2011.
- (77) P. Mori-Sanchez, A. M. Pendás, V. Luaña; A classification of covalent, ionic, and metallic solids based on the electron density. *J. Am. Chem. Soc.* **2002**, *124*, 14721-14723.
- (78) V. Luaña, A. Costales, P. Mori-Sánchez, M. A. Blanco, A. Martín Pendás; Topological properties of the electron density of solids and molecules. Recent developments in Oviedo. *Acta Cryst. A* **2004**, *60*, 434-437.
- (79) A. A. Arabi, C. F. Matta; Where is energy stored in adenosine triphosphate? *J. Phys. Chem. A* **2009**, *113*, 3360-3368.
- (80) V. G. Tsirelson, R. P. Ozerov; *Electron Density and Bonding in Crystals: Principles, Theory and X-ray Diffraction Experiments in Solid State Physics and Chemistry*; Institute of Physics Publishing: New York, 1996.
- (81) P. Coppens; *X-ray Charge Densities and Chemical Bonding*; Oxford University Press, Inc.: New York, 1997.
- (82) T. S. Koritsanszky, P. Coppens; Chemical applications of X-ray charge-density analysis. *Chem. Rev.* **2001**, *101*, 1583-1628.
- (83) C. F. Matta, S. Sowlati-Hashjin, A. D. Bandrauk; Dipole Moment Surface of the  $\text{CH}_4 + \text{X} \rightarrow \text{CH}_3^{\bullet} + \text{HX}$  (X=F,Cl) Reactions from Atomic Dipole Moment Surfaces, and the Origins of the Sharp Extrema of the Dipole Moments near the Transition States. *J. Phys. Chem. A* doi: 10.1021/jp401555h
- (84) A. D. Bandrauk, E. S. Sedik, and C. F. Matta; Effect of absolute laser phase on reaction paths in laser-induced chemical reactions. *J. Chem. Phys.* **2004**, *121*, 7764-7775
- (85) C. Hansch; A quantitative approach to biochemical structure-activity relationships. *Acc. Chem. Res.* **1969**, *2*, 232-239.
- (86) C. Hansch; Structure-activity relationships of chemical mutagens and carcinogens. *Sci. Total Environ.* **1991**, *109/110*, 17-29.
- (87) C. Hansch, A. Leo; *Exploring QSAR: Fundamentals and Applications in Chemistry and Biology*; American Chemical Society: Washington, DC, 1995. (5) A. Williams *Free Energy Relationships in Organic and Bio-Organic Chemistry*; Royal Society of Chemistry (RSC): Cambridge (UK), 2003.

- (88) M. S. Tute; Principles and practice of Hansch analysis: a guide to structure-activity correlation for the medicinal chemist. *Advances in Drug Research* (Vol. 6); Academic Press: London, 1971, pp 1-77.

## Chapter 1

# The Chemical Bond in External Electric Fields<sup>1</sup>

### Summary

It is shown that experimentally-observable field-free molecular properties can be used to predict a diatomic molecule's response to an external field. The response properties include the total energy, the equilibrium bond length under the perturbing field, and the vibrational Stark shift. The model proposed employs in its construction the field-free equilibrium bond length, the bond dissociation energy, the polarizability and dipole moment functions (related to the Raman- and IR-intensities, respectively), the vibrational frequency, and the curvature of the potential energy surface. The departing point for this paper is the important work of B. Delley [*J. Mol. Struct. (THEOCHEM)* **1998**, 434, 229] where a field-perturbed potential is proposed as a linear combination of a field-free Morse potential and a term representing the perturbation. The perturbation term in the original proposal is proportional to the internuclear separation leading to infinities at the dissociation limit. This term is replaced in this account by the expression of the energy change due to the molecule-field interaction which reaches a constant asymptotic limit proportional to the sum of the polarizabilities of the separated atoms. The model is shown to capture the essential physics of bond length change in the field and simultaneously the accompanying vibrational Stark shift by testing it on a set of nine diatomics [five homo-nuclear ( $H_2$ ,  $N_2$ ,  $O_2$ ,  $F_2$ , and  $Cl_2$ ) and four hetero-nuclear (HF, HCl, CO, and NO)] covering a wide range and combinations of dipole moments and polarizabilities. Electronic structure calculations were conducted at two levels of theory (QCISD, and DFT-B3LYP) utilizing the same basis set [6-311++G(3df,2pd)]. All results for all molecules agree closely at these two levels of theory, but QCISD is found to be incapable

---

<sup>1</sup> This Chapter is based on the paper: Sowlati-Hashjin, S.; Matta, C. F. (2013) "The chemical bond in external electric fields. energies, geometries, and vibrational Stark shifts in diatomic molecules"; *Journal of Chemical Physics* **139**, accepted - in press, scheduled for issue 11 of 21 Sept. 13.

of reproducing the Stark effect of the NO molecule (and for which further testing at the Hartree Fock, MP2, DFT-mPW1PW91, and CCSD has been performed).

## 1.1. Introduction

The interaction of molecules with external fields [1,2], such as those associated with laser radiation, can be used to control chemical reactions [3-13]. The electrical component of the radiation dominates its interaction with matter when the speed of the electronic motion is small compared to the speed of light as in the lighter elements of the periodic table. The interaction of the time-varying electric field of an intense IR laser radiation [14-18], or that of a strong static electric field [19], with a reacting system can significantly alter its potential energy surface (PES) and reaction kinetics.

The simplest PES is that describing the energy of a diatomic as a function of the internuclear separation. This paper reports a systematic computational study of the effects of external static uniform electric fields on diatomics with the goal of relating the field-induced changes in the PES with the accompanying field-induced changes in other molecular, atomic, and bond properties. Another simplification adopted in this paper to limit the study of the effects of *static uniform external electric fields*, which is what will be meant by "field", "E-fields", "EF", *etc.*

Two functional groups carrying opposite charges of  $\pm 0.5 e^-$ , typically present in an enzyme active site for example, generate fields between  $\sim 10^8$  and  $\sim 10^9 \text{ Vm}^{-1}$  at their center when separated by 10 to 30 Å, respectively. These local fields can induce observable effects such as vibrational Stark shifts in the IR frequencies of a host molecule trapped into an active site. Stark shifted vibrational frequencies of a substrate can be exploited to probe the strength and direction of the electric fields in its active site,

in effect acting as a "*local reporter of its electrostatic environment*" in the words of Boxer *et al* [20].

Examples of "*local reporter*" molecules include carbon monoxide (C=O) attached to the Fe of the porphyrin ring in myoglobin [21], and the nitrile- ( $-C\equiv N$ ) containing substrates in the active site of human aldose reductase enzyme (hALR2) [20]. From the changes in the vibrational Stark shifts of the nitrile group, Boxer *et al.* were able to estimate a *change* of  $10^8 \text{ Vm}^{-1}$  in the electric field accompanying a single point mutation at the active site [20]. Zhang *et al.* have recently demonstrated that an accurate modeling of the electric charges in the cavity of hALR2 is essential for the accurate prediction of the mutation-induced Stark shift in the vibrational frequencies of the nitrile group.<sup>22</sup>

Molecules can also be exposed to fields from sources external to the organism, whether applied in an experiment or in the crystal environment of the molecule, for example. In a theoretical study of a set of 20 common non-linear optical materials, Spackman, Munshi and Jayatilaka have shown that the crystal fields to which molecules are typically exposed to are in the range  $\sim 0.8$  to  $3.4 \times 10^9 \text{ Vm}^{-1}$  (16 compounds), in the range  $\sim 7$  to  $9 \times 10^9 \text{ Vm}^{-1}$  (3 compounds), and reaching a maximal value of  $\sim 1.6 \times 10^{10} \text{ Vm}^{-1}$  for the remaining compound in the set [23]. Fields of magnitudes in the range  $\sim 10^9 \text{ Vm}^{-1}$  have been shown to quadruple the rate constant of double proton transfer reactions [19]. Fields of such strength can be used as "tweezers" to guide a chemical reaction through a particular channel when more than one channel link a set of reactants to different sets of products, as Shaik *et al.* have shown in the case of bond activation by porphyrin-based catalysts [24]. Fields of  $10^8 \text{ Vm}^{-1}$  can also accelerate photosynthetic reactions by an order of magnitude [25-27] and significantly decrease the enzymatic

activity of cytochrome c oxidase [28].

Experimentally, one can apply strong external electric fields to a surface, an interface, or a crystal. External fields between the tip and the sample in a scanning tunneling microscope (STM) can reach magnitudes of  $\sim 3 \times 10^9 \text{ Vm}^{-1}$  for a tip-sample separation of  $\sim 2 \text{ \AA}$  and a bias voltage of  $\sim 0.6 \text{ V}$  [29]. Technical difficulties limit the maximal strength of macroscopic fields applied to a crystal during an X-ray crystallographic diffraction experiments to *ca.*  $10^7 \text{ Vm}^{-1}$  [30], two orders of magnitude weaker than the fields inside a molecule. The resulting (small) field-induced changes in diffraction patterns have been observed for sometime [31-36], and often require for their observation the use of intense synchrotron sources, low temperatures, and efficient data collection methodologies. Tsirelson, Gorfman, and Pietsch [30, 37] developed the theory of X-ray diffraction from field-perturbed crystals and demonstrated that the shift in atomic positions in the unit cell is  $\sim 100$  times more significant than the polarization of the atomic electronic clouds in determining the field-induced perturbation to the diffraction pattern [30].

Several authors report response properties of molecules in external fields. For example, the response of vibrational frequencies, IR intensities, HOMO-LUMO gaps, and geometries of some hydrocarbons to external fields have reported at the DFT-B3LYP/6-311++G(2d,2p) level of theory [38]. In that study, the fields parallel/antiparallel to the dipole moment of the molecule ("physicist convention") were found to elongate/shorten the bond lengths respectively, except the H-C bond in methane which was found to be elongated by fields in both directions [38]. Vibrational frequencies exhibit a red shift for fields applied parallel to the dipole moment of the

molecule and blue shift for antiparallel fields. IR intensities and HOMO-LUMO gaps, however, do not appear to exhibit simple trends in response to the applied fields [38]. Nakatsuji *et al.* have studied the molecular geometries of CO, NH<sub>3</sub>, C<sub>2</sub>H<sub>2</sub>, and CH<sub>4</sub>, under a field strength of 0.1 atomic units (a.u.) [39], and CO, CO<sub>2</sub>, NH<sub>3</sub>, C<sub>2</sub>H<sub>2</sub>, C<sub>2</sub>H<sub>4</sub>, H<sub>2</sub>CO, under a field strength of 0.005 a.u. ( $\sim 2.5 \times 10^9 \text{ Vm}^{-1}$ ) [40] and have shown that, in general, fields in both directions elongate the bond lengths of non-polar bonds (C-H). Kairys *et al.* have studied the geometry and vibrations of the OH<sup>-</sup> anion and have shown that applying electric fields of magnitudes up to 0.1 a.u. in both directions lengthen the bond of OH<sup>-</sup> [41]. Some time ago, Delley investigated the effects of strong external fields on vibrational frequencies and dissociation energies of small molecules: N<sub>2</sub>, NaCl, H<sub>2</sub>O, and SF<sub>6</sub> [42]. Mata, Molins, Alkorta, and Espinosa [43] studied the effect of external fields on the geometries, topological bond properties [44, 45] and bond dissociation energies of the strong hydrogen bond in the H-F...H-F dimer.

In this paper, we report a computational study of the effects of external fields on the properties of strong bonds in diatomics with the goal of finding a coherent description that accounts for the simultaneous responses of the different molecular and bond properties to external fields. Each molecule in a set of first to third row homo- and heteronuclear diatomics is subjected to fields of various strengths along its  $C_\infty$ -axis (in two opposite directions in the case of the heterodiatomics). The studied properties include: The total vibrationless molecular energy ( $E$ ), the (equilibrium) bond length ( $R$ ), the bond force constant ( $k$ ), and the vibrational frequency ( $\nu$ ). Field effects on other bond properties, including topological properties, will be discussed elsewhere.

## 1.2. Method and Computations

### 1.2.1. The Molecular Set

The series of diatomic molecules studied in this work is selected from the first and up to and including the third row of the periodic table. Relativistic effects are expected to be negligible for these light elements and are not accounted for in the present calculations. The set of diatomic molecules includes five homo-nuclear diatomic molecules ( $\text{H}_2$ ,  $\text{N}_2$ ,  $\text{O}_2$ ,  $\text{F}_2$ ,  $\text{Cl}_2$ ), and four hetero-diatomic molecules ( $^{+1.22}\text{C}-\text{O}^{-1.22}$ ,  $^{+0.75}\text{H}-\text{F}^{-0.75}$ ,  $^{+0.44}\text{N}-\text{O}^{-0.44}$ ,  $^{+0.26}\text{H}-\text{Cl}^{-0.26}$ ) that cover a range of bond polarity (these partial charges are obtained from the QTAIM theory at the gas-phase equilibrium geometries as described below). Calculations were performed on all compounds in their ground electronic states.

### 1.2.2. Electronic Structure Calculations

Only the ground electronic states of the diatomics were considered in this study, these are:  $^1\Sigma_g^+$  for closed-shell homonuclear dimers,  $^1\Sigma^+$  for closed-shell heteronuclear dimers,  $^2\Pi_r$  in the case of NO, and  $^3\Sigma_g^-$  in the case of  $\text{O}_2$ .

To increase the confidence in the results, calculations were conducted using two significantly different underlying electronic structure methods, namely, (i) quadratic configuration interaction with single and double excitations (QCISD) [46], and (ii) density functional theory (DFT) Becke's hybrid exchange functional [47] and Lee-Yang-Parr correlation functional [48] (B3LYP). To keep the discussion simple, a single (large) polarized split-valence basis set augmented with diffuse functions on all atoms [6-311++G(3df,2pd)] was employed in all calculations (the inclusion of diffuse functions is important for the description of electron densities under external fields). The unrestricted



formulations of QCISD and of B3LYP have been used for open-shell molecules, atoms, and ions.

Molecular geometries were optimized with and without external fields within convergence thresholds of  $2 \times 10^{-6}$  and  $1 \times 10^{-6}$  hartree/bohr (a.u.) for the residual maximum forces and root-mean square forces on the nuclei, respectively.

Electronic structure calculations, geometry optimizations, and frequency calculations were all conducted using the Gaussian 09 program [49]. All reported frequencies are those obtained directly from the calculation (unscaled) [50].

Both levels of theory QCISD and B3LYP generally yield results that agree both absolutely and in trends. Thus, unless mentioned otherwise, the discussion and quoted results are primarily those of the QCISD calculations. The full set of QCISD and DFT-B3LYP results are provided in the **Appendix** (page 186).

There is one exception to the close agreement of QCISD and B3LYP, and this is in the trends in field effects on the frequencies and force constants of NO for which QCISD and B3LYP give widely different trends and absolute values. To determine which of these two levels of theory is more credible in this case, similar calculations were conducted at four additional levels of theory: Coupled clusters [51-53] with single and double excitations (CCSD), Møller-Plesset second order perturbation theory [54] with full excitation including core electrons, Hartree-Fock (HF) self consistent field (SCF) level [55], and the DFT functional mPW1PW91 [56].

### 1.2.3. Field Strengths and Directions

Electric fields from  $5.14 \times 10^8$  to  $5.14 \times 10^{10} \text{ Vm}^{-1}$  ( $= 0.001$  to  $0.01$  a.u.) were applied along the molecular  $C_\infty$ -axis (the  $z$ -axis of the coordinate system, **Figure 1**), since fields aligned with the bonds maximally affect the vibrational frequencies [57]. Any field directed obliquely on the internuclear axis can always be decomposed into an (anti)parallel and a perpendicular component.

Disregarding orientation dependence of field effect on non-spherically symmetric electronic systems, the order of magnitude of the rate of electron tunneling ionization ( $\omega$ ) from a molecule in an external electric field can be estimated from the well-known formula [58, 59]:

$$\omega(t) = 4 \frac{\omega_0}{|\mathbf{E}|} (2\text{IP})^{5/2} \exp\left[-\frac{2}{3} \frac{(2\text{IP})^{3/2}}{|\mathbf{E}|}\right] \quad (1)$$

where  $|\mathbf{E}| = E$  is the electric field strength, IP is the vertical ionization potential, both quantities in a.u., and  $\omega_0$  is the atomic unit of frequency ( $4 \times 10^{16} \text{ s}^{-1}$ ). Tunneling ionization rates calculated from Eq. (1) using the experimental IPs of the nine diatomics are collected in **Table 1**.

Chemical reactions generally happen on a time scale of  $\sim 10$  to  $10^4$  fs [60]. One can take the reciprocal of the longest time of this range ( $10^{-4} \text{ fs}^{-1}$ ) as the maximal acceptable average tunneling ionization rate for a molecule in the field. An arbitrary threshold of  $\omega \cong 10^{11} \text{ s}^{-1}$  can thus be considered reasonable. From **Table 1**, a field strength of  $5.14 \times 10^9 \text{ Vm}^{-1}$  ( $0.01$  a.u.) can be taken as an upper ionization threshold for the maximum field strength (except for the alkali metal dimers  $\text{Li}_2$  and  $\text{Na}_2$  which are excluded from this study in view of their low ionization potential). That being said, the

results described below show that fields of up to  $9.1 \times 10^{12} \text{ Vm}^{-1}$  (0.02 a.u.) do not induce changes in trends and are, thus, also kept as an upper extreme limiting case.

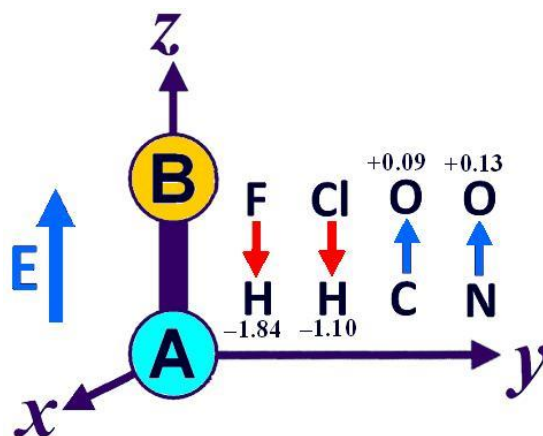


**Figure 1**

Orientation of heteronuclear molecules along axis in the coordinate system where A and B refer to the less and more electronegative atom, respectively. Atom A is placed at the origin and the internuclear axis aligned along the  $z$ -axis. The electronegativity ranking is taken according to Pauling to be:<sup>57</sup> H (2.1) < C (2.5) < N (3.0)  $\approx$  Cl (3.0) < O (3.5) < F (4.0). The electric field  $\mathbf{E}$  is positive when oriented as in this figure, pointing to the positive  $z$ -direction, and negative when pointing to the negative  $z$ -direction. The arrows on the symbols of the diatomics points at the direction of the permanent (field-free) molecular dipole moment with the value of the dipole moment calculated at the QCISD level to two decimal places in debyes (a  $\pm$  sign indicates a parallel/antiparallel orientation with respect to both the  $z$ -axis and the  $\mathbf{E}$ -field).

Heteronuclear molecules are subjected to fields in the two opposite (nonequivalent) directions: Parallel and antiparallel to the  $C_{\infty}$ -axis. The molecules are oriented in the coordinate system by placing the least electronegative atom (Pauling's scale) [61] at the origin and the second atom along the positive  $z$ -axis. The Cartesian coordinate system and orientation of the diatomics are displayed in **Figure 1**. Whenever a field is mentioned without its magnitude what is being referred to, is the field with the strongest magnitude. Hence,  $\mathbf{E}_+$  or  $\bar{\mathbf{E}}_+$  mean a field of magnitude  $1.03 \times 10^{10} \text{ Vm}^{-1} = 2.0 \times 10^{-2} \text{ a.u.}$  oriented to

point in the positive direction of the  $z$ -axis shown in **Figure 1** while  $\mathbf{E}_+$  or  $\bar{\mathbf{E}}_-$  is a field of the same strength but pointing in the opposite direction.

*In this paper, the dipole moment vector is directed according to the "physicists convention", [62, 63] i.e., it originates at the negative end and points to the positive end, and can be denoted by  $^{+--}$  where  $\boldsymbol{\mu}$  symbolizes the dipole moment (e.g.  $^{\delta+}\text{H} \leftarrow \text{Cl}^{\delta-}$ , where  $\delta$  indicates a partial atomic charge). On the other hand, all electric fields, external or within the dipoles, originate at positive charges (sources) and end at negative charges (sinks). (Note that the Gaussian 09 program orients electric fields in the reverse direction). Thus, all E-fields in this paper have the same direction and sign as the  $z$ -axis along which they are aligned (**Figure 1**) and are uniform (as in an infinite parallel-plate capacitor). These conventions ensure that a dipole is in its most stable direction (the direction that minimizes its energy in the field) when parallel to the external field since  $E_{\mathbf{E}} = -\boldsymbol{\mu} \cdot \mathbf{E}$  [62]. With these conventions, a *stabilizing* (energy lowering) orientation of the dipole is *parallel* to that of the external field and can be given the symbol  $^{+--} \left[ \begin{array}{c} \boldsymbol{\mu} \\ \leftarrow \end{array} \right]_-$ , where the arrow below the brackets is the direction of the field. On the other hand,  $^{+--} \left[ \begin{array}{c} \boldsymbol{\mu} \\ \rightarrow \end{array} \right]_-$  symbolizes an *antiparallel* and *destabilizing* (energy raising) orientation of the dipole with respect to the external field. When quoting other authors' work their conventions have been converted to the ones used in this paper if needed.*

All studied diatomic molecules are oriented in the coordinate system so that one of the two atoms is at the origin and the other lying in the positive side of the  $z$ -axis. In the case of heterodiatomics, the least electronegative atom is the one placed at the origin as shown in **Figure 1**. *This convention is independent of the direction of the permanent*

*molecular dipole*. Thus, in two instances the dipole points at the origin (H←F and H←Cl) and in the other two it points away from the origin (C→O and N→O) as depicted in the figure [the arrows between the atomic symbols indicate the direction of the permanent (field-free) molecular dipole which changes in magnitude in external fields and can also change direction, as described below in length].

**Table 1**

Calculated tunneling ionization rate ( $s^{-1}$ ), equation (1), of the diatomic molecules using experimental first ionization potentials (IPs). (IPs were obtained from Ref. 73).

E  (au)	<u>Homonuclear Diatomics (<math>D_{\infty h}</math>)</u>						<u>Heteronuclear Diatomics (<math>C_{\infty v}</math>)</u>				
	H <sub>2</sub>	Li <sub>2</sub>	Na <sub>2</sub>	N <sub>2</sub>	O <sub>2</sub>	F <sub>2</sub>	Cl <sub>2</sub>	HF	HCl	CO	NO
0.030	$6.39 \times 10^{14}$	$7.53 \times 10^{16}$	$7.59 \times 10^{16}$	$5.20 \times 10^{14}$	$5.90 \times 10^{15}$	$5.20 \times 10^{14}$	$8.14 \times 10^{15}$	$3.41 \times 10^{14}$	$3.54 \times 10^{15}$	$1.71 \times 10^{15}$	$2.48 \times 10^{16}$
0.020	$9.11 \times 10^{12}$	$4.50 \times 10^{16}$	$4.87 \times 10^{16}$	$6.53 \times 10^{12}$	$3.46 \times 10^{14}$	$6.53 \times 10^{12}$	$5.93 \times 10^{14}$	$3.32 \times 10^{12}$	$1.48 \times 10^{14}$	$4.48 \times 10^{13}$	$4.11 \times 10^{15}$
0.010	$1.56 \times 10^7$	$5.69 \times 10^{15}$	$7.65 \times 10^{15}$	$7.70 \times 10^6$	$4.12 \times 10^{10}$	$7.70 \times 10^6$	$1.36 \times 10^{11}$	$1.83 \times 10^6$	$6.42 \times 10^9$	$4.79 \times 10^8$	$1.11 \times 10^{13}$
0.007	$1.41 \times 10^2$	$7.63 \times 10^{14}$	$1.23 \times 10^{15}$	$5.03 \times 10^1$	$1.40 \times 10^7$	$5.03 \times 10^1$	$8.15 \times 10^7$	6.22	$9.21 \times 10^5$	$2.07 \times 10^4$	$5.49 \times 10^{10}$
0.005	$2.30 \times 10^{-5}$	$4.55 \times 10^{13}$	$9.41 \times 10^{13}$	$5.34 \times 10^{-6}$	$2.92 \times 10^2$	$5.34 \times 10^{-6}$	$3.58 \times 10^3$	$2.77 \times 10^{-7}$	6.02	$2.00 \times 10^{-2}$	$4.04 \times 10^7$
0.003	$2.54 \times 10^{-21}$	$4.82 \times 10^{10}$	$1.76 \times 10^{11}$	$2.17 \times 10^{-22}$	$2.63 \times 10^{-9}$	$2.17 \times 10^{-22}$	$1.85 \times 10^{-7}$	$3.00 \times 10^{-46}$	$3.65 \times 10^{-12}$	$1.58 \times 10^{-33}$	1.49
0.001	$9.89 \times 10^{-109}$	$1.40 \times 10^{-5}$	$9.60 \times 10^{-4}$	$5.62 \times 10^{-105}$	$3.65 \times 10^{-65}$	$5.62 \times 10^{-105}$	$1.61 \times 10^{-59}$	$1.48 \times 10^{-111}$	$7.01 \times 10^{-74}$	$5.95 \times 10^{-86}$	$2.42 \times 10^{-38}$

We remind the reader that while the permanent molecular dipole moment generally points in the direction expected on the basis their different electronegativities due to the inter-atomic transfer of charge as in  $^{+0.75}\text{H}-\text{F}^{-0.75}$  or  $^{+0.26}\text{H}\leftarrow\text{Cl}^{-0.26}$ , there are known exceptions where the positive end of the dipole points at the atom bearing a net negative charge such as  $^{+1.22}\text{C}\rightarrow\text{O}^{-1.22}$  and  $^{+0.44}\text{N}\rightarrow\text{O}^{-0.44}$ . The reasons for this unexpected direction of the dipole moment (unexpected on the basis of the net flow of electronic charge alone) has been discussed elsewhere [64] and is due to a large and opposite atomic polarization term [65-67], that is, a distortion of the charge cloud of an atom in a molecule that not only cancels the charge transfer dipole but can even result in a reversal of the molecular dipole opposite to the charge transfer dipole moment. The interplay of the charge transfer dipole and the atomic polarization dipole has been recently studied over the entire potential energy surface of the reactive collision of halogens with methane [68].

### 1.3. Results and Discussion

**Table 2** summarizes the properties of all nine studied molecules in the field free case and in the presence of the strongest considered field strength of  $0.02 \text{ a.u.} = 1.03 \times 10^{10} \text{ Vm}^{-1}$  (in both directions in the case of hetero diatomic molecules). The properties investigated for each of the nine molecules in this work include the total energy ( $E$ ), the change in the total energy due to the external field ( $\Delta E$ ), the molecular dipole moment ( $\mu$ ), the equilibrium bond length ( $R$ ) (or internuclear separation), the force constant ( $k$ ), and the harmonic vibrational frequency ( $\nu$ ). The table is organized so as to list, for every

molecular property, three values: The field-free value in the middle row flanked by the values under the strongest studied field strength ( $1.03 \times 10^{10} \text{ Vm}^{-1}$ ) in the two opposite directions. Since for homonuclear diatomics the two field directions are equivalent, they are taken as a positive field.

The field response of each of these molecular properties is discussed separately below. For the purpose of a clearer discussion, it helps to group the nine molecules in two separate categories (homonuclear and heteronuclear) since the behavior of the two groups differ significantly.



**Table 2**

Molecular, bond, and atomic properties of diatomics with and without an electric field ( $\mathbf{E}_{\pm}$ ) of  $\pm 1.03 \times 10^{10} \text{ Vm}^{-1} = \pm 2.0 \times 10^{-2} \text{ a.u.}^{(a)}$

Property	Field	H <sub>2</sub>	N <sub>2</sub>	O <sub>2</sub>	F <sub>2</sub>	Cl <sub>2</sub>	H←F <sup>(b)</sup>	H←Cl <sup>(b)</sup>	C→O <sup>(b)</sup>	N→O <sup>(b)</sup>
$E$ (a.u.)	$\overline{\mathbf{E}}_+$	-1.17365	-109.35884	-150.11470	-199.27451	-919.39999	-100.32095	-460.31704	-113.14531	-129.70479
	0	-1.17235	-109.35590	-150.11162	-199.27218	-919.39185	-100.33424	-460.32223	-113.14149	-129.70083
	$\overline{\mathbf{E}}_-$						-100.34986	-460.33429	-113.14401	-129.70285
$\Delta E$ (eV)	$\overline{\mathbf{E}}_+$	-0.0354	-0.0800	-0.0838	-0.0634	-0.2215	0.3616	0.1412	-0.1039	-0.1078
	$\overline{\mathbf{E}}_-$						-0.4250	-0.3282	-0.0686	-0.0550
$\mu$ (debye) <sup>(c)</sup>	$\overline{\mathbf{E}}_+$	-0.3317	-0.7477	-0.783	-0.5916	-2.0783	-1.5403	-0.2219	0.8965	0.8865
	0	0.0000	0.0000	0.0000	0.0000	0.0000	-1.8358	-1.0949	0.0846	0.1247
	$\overline{\mathbf{E}}_-$						-2.1284	-1.9721	-0.719	-0.6352
BL(Å)	$\overline{\mathbf{E}}_+$	0.7446	1.0983	1.2015	1.3962	2.0059	0.9100	1.2702	1.1234	1.1472
	0	0.7426	1.0975	1.1995	1.3938	1.9974	0.9146	1.2736	1.1285	1.1504
	$\overline{\mathbf{E}}_-$						0.9212	1.2828	1.1356	1.1556
$k$ (mDyneÅ <sup>-1</sup> )	$\overline{\mathbf{E}}_+$	11.35	47.42	25.62	10.78	6.16	11.38	5.65	39.53	37.01
	0	11.52	47.70	26.26	10.94	6.51	11.04	5.57	38.18	34.91
	$\overline{\mathbf{E}}_-$						10.78	5.27	36.26	33.29
$\nu$ (cm <sup>-1</sup> )	$\overline{\mathbf{E}}_+$	4372.5	2397.3	1648.9	981.5	546.8	4272.5	3041.8	2234.4	2055.4
	0	4405.3	2404.5	1669.2	988.6	562.2	4207.8	3021.0	2196.0	1996.4
	$\overline{\mathbf{E}}_-$						4104.4	2939.0	2140.0	1949.3

- (a) Data based on calculations at the (U)QCISD/6-311++G(3df,2pd) level of theory for all properties and molecules [except for the force constants and frequencies of NO which were obtained at the UQCISD/6-311++G(3df,2pd) level of theory].
- (b) The arrow between the atomic symbols depicts the direction of the field free (permanent) dipole moment. Note that this direction may flip sides under a strong external field in the opposite direction [see also footnote (c)].
- (c) A negative dipole moment points to the left ( $-\mu \equiv \bar{\mu}$ ) and one that is positive to the right with respect to the other vectors indicated by arrows in this table [see also footnote (b)].

### 1.3.1. The Energy and the Dipole Moment of a Diatomic Molecule in an External Homogenous Electric Field

#### 1.3.1.1 The Energy Expression

The expansion of the energy  $E$  of a diatomic molecule in an external homogenous electric field ( $\mathbf{E}$ ) as a power series takes the form [69]:

$$E(\mathbf{E}, r) = E_0(r) - \mu_0(r)E \cos \theta - \frac{1}{2} \alpha_{//0}(r)E^2 \cos^2 \theta - \alpha_{\perp 0}(r)E^2 \sin^2 \theta + O(E^{n \geq 3}), \quad (2)$$

where  $E_0$  and  $\mu_0$  are the field-free energy and (permanent) dipole moment, respectively, and both of which are functions of the internuclear separation ( $r$ ),  $E = |\mathbf{E}|$  is the magnitude of the external electric field that makes an angle  $\theta$  with the internuclear axis,  $\alpha_{//0}$  and  $\alpha_{\perp 0}$  are the field-free parallel and perpendicular polarizability tensor components, and the last term collects all higher order terms.

Similarly, the  $i^{\text{th}}$  cartesian component of the total molecular dipole moment vector under the field,  $\mu_i(\mathbf{E}, r)$ , may be expressed as the sum of the permanent (field free) component,  $\mu_{i0}(r)$ , plus the induced dipole represented by the remainder of terms in Eq. (3):

$$\mu_i(\mathbf{E}, r) = \mu_{i0}(r) + \alpha_{//0}(r)E \cos \theta + 2\alpha_{\perp 0}(r)E \sin \theta + O(E^{n \geq 2}). \quad (3)$$

Plots of the molecular dipole moments  $\boldsymbol{\mu}$  of the nine studied diatomic molecules as a function of the external fields are displayed in **Figure 2**. From the figure it is clear that within the range of the electric field strengths considered in this study the molecular dipole moment  $\boldsymbol{\mu}$  of all nine molecules, whether homo- or hetero dimeric, is directly proportional to the applied field strength over the entire range of field strengths and orientations. The Pearson linear regression coefficient relating each molecular dipole

moment to the external field is unity to three decimals, and this includes the doubled range of fields in the case of heterodiatomics due to the flipping of the sign of the electric field from parallel to antiparallel. Because of this proportionality of the dipole moment and the electric field strength, the higher terms in Eq. (2) can be ignored [70].

Further, in this work we only consider fields that are co-linear with the molecular axis (parallel  $\theta = 0$ , or antiparallel  $\theta = \pi$  radians) and hence Eq. (2) can be further simplified and rearranged to define the field-induced change in the energy (field stabilization or destabilization),  $\Delta E$ , as:

$$\Delta E \equiv E - E_0 = \mp \mu_0(r)E - \frac{1}{2} \alpha_{//0}(r)E^2, \quad (4)$$

where the dipole term assumes a negative sign for parallel (stabilizing, energy lowering) fields and a positive sign for antiparallel field. From now on, the subscript "0" will be dropped from the symbols for dipole moment and polarizability when it is clear from the context that the parameter of interest is the field-free parameter.

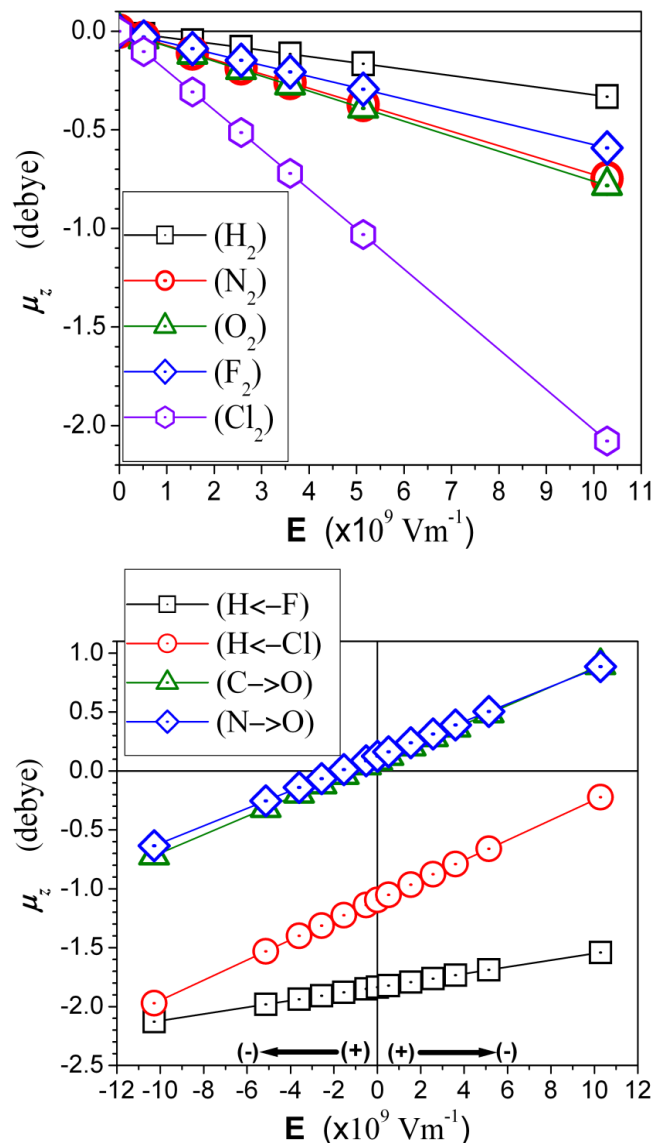


**Figure 2**

Plots of the molecular dipole moment (in debye) as a function of the electric field ( $\mathbf{E}$ ) strength for the homonuclear diatomics (*top*), and as a function of the field strength and direction for the heteronuclear diatomics (*bottom*). *The following statement in square brackets applies to this figure and to Figures 3-5 as well:*

[The electric field magnitude is given in  $10^9 \text{ Vm}^{-1}$ . The convention of assigning directions to the field is given by the arrows parallel to the abscissa of the plot (*right*) in which the field changes direction halfway through the abscissa. In the inset of the bottom plot, each molecule is drawn in the orientation it has with respect to the external fields with a small arrow between the atomic symbols depicting the orientation of the permanent molecular dipole moment with respect to the external field (also see **Figure 1**). Except when stated otherwise, all plotted results were obtained at the (U)QCISD/6-311++G(3df,2pd) level of theory.]

### 1.3.1.2. *The Role of the Permanent Dipole Moment and of the Polarizability in Determining the Response to an External Field*

**Table 3** lists the experimental and calculated polarizabilities and permanent dipole moments of the nine molecules considered in this work. The table has been sorted in the order of increasing polarizability within each of the two groups of molecules. The values listed in the table shows that the selected molecules in each group cover a wide range of each of the polarizability and of the dipole moment. The homo-nuclear diatomics molecular set includes H<sub>2</sub> which exhibits a polarizability as low as 0.8 Å<sup>3</sup> and up to the highly polarizable Cl<sub>2</sub> for which  $\alpha \approx 4.6 \text{ \AA}^3$ . On the other hand, the hetero-nuclear diatomics molecular set includes various combinations of polarizability and permanent dipole moment. Thus, HF has a significant dipole moment of 1.8 debye and a polarizability as low as that of H<sub>2</sub>; CO and NO have small permanent dipole moments (of  $\sim 0.1$  debye) and sizeable polarizabilities of  $\sim 1.8 \text{ \AA}^3$ ; and finally HCl has both a sizable dipole moment (1.1 debye) and a sizable polarizability of  $\sim 2.5 \text{ \AA}^3$ . (See **Table 3**). The listing in the table also shows the excellent agreement between the measured and calculated parameters.

The form of equation (4) and the relative combinations of permanent dipole moments and polarizability for each molecule lead one to anticipate their response to an external electric field as long as the response of the dipole moment remains essentially linear (which is true for all nine studied molecules over the entire range of field strengths and directions considered in this work).

The functional dependence of the energy lowering due to the field for each of the nine diatomics is displayed in **Figure 3** where plots for homonuclear molecules are

collected together at the top of the figure and those for the heteronuclear diatomics at the bottom.

For homonuclear diatomics, the dipolar term in Eq. (4) vanishes of course and hence (a) all fields are energy lowering to all molecules in this group due to the non-linear term which is always negative, and (b) the energy lowering is proportional to the square of the field strength.

A glance at the plots in **Figure 3 (top)** shows that the molecule that is least affected by the field is H<sub>2</sub>, the one with the smallest polarizability among the homonuclear diatomics. In contrast, the figure also shows that the molecule with the largest polarizability, Cl<sub>2</sub>, is the most stabilized by the field. The curves representing the response of the remaining homonuclear diatomics fall into their relative places in the plot according to their respective polarizabilities, and numerically, at the highest studied field of  $1.03 \times 10^{10} \text{ Vm}^{-1}$ , we can sort the homodimers X<sub>2</sub> in order of increasing polarizability noticing a corresponding rise in the magnitude of the stabilization energy ( $\alpha_{//}$  in  $\text{\AA}^3 / \Delta E$  in eV): H<sub>2</sub> (1.0176 / -0.0354) < F<sub>2</sub> (1.7655 / -0.0634) < O<sub>2</sub> (2.2099 / -0.0838)  $\approx$  N<sub>2</sub> (2.2167 / -0.0800) < Cl<sub>2</sub> (6.1443 / -0.2215). The mild discrepancy in the observed trend in the case of O<sub>2</sub> (slightly smaller polarizability than N<sub>2</sub> but slightly larger magnitude of field stabilization) might be related to the different nature of its ground electronic state (open shell, triplet) that of all remaining singlet closed shell homodimers.

A numerical fit through the origin of  $\Delta E = aE^2$ , where  $a$  is the constant of proportionality, yields, when  $\Delta E$  is expressed in eV and  $E$  in multiples of  $10^9 \text{ Vm}^{-1}$ ,  $a = -2.0948$  (in units of  $3.204 \times 10^{-31} \text{ } \epsilon_0^{-1} \text{ m}^3$ , where the permittivity of free space,  $\epsilon_0$ , is expressed in  $\text{C.m}^{-1}\text{V}^{-1}$ ) for the molecule exhibiting the most pronounced stabilization in

response to the field ( $\text{Cl}_2$ ). For the least pronounced case ( $\text{H}_2$ ), and in the same units,  $a = -0.3345$ . The corresponding values of  $a$  in for the remaining molecules are:  $\text{F}_2$  ( $-0.5997$ ),  $\text{N}_2$  ( $-0.7574$ ), and  $\text{O}_2$  ( $-0.7931$ ). Each one of the five linear regression correlations yield  $r^2 = 1.0000$  which indicates a perfectly linear energetic stabilization of the five homonuclear diatomics in response to the external field strength over the entire range of studied fields.

The lower plot of **Figure 3** displays the (de)stabilization energy of the heteronuclear diatomic molecules as a function of the direction and magnitude of the applied field. The plot can be conceptually divided into three behavioral modes. The first response type is that of HF, which is practically linear with the field strength over the entire range and which can be fit to a linear regression equation  $\Delta E = bE$ , where  $b$  is found to be  $0.0383$  (in multiples of  $1.602 \times 10^{-28} \text{ C.m} = 48.02 \text{ debye}$ , when  $\Delta E$  is expressed in eV and  $E$  in multiples of  $10^9 \text{ Vm}^{-1}$ ) is the constant of proportionality with a squared linear regression coefficient of  $0.9953$  indicating a close to perfectly linear correlation. This linear dependence of the energy of HF on the field strength is expected since HF has the highest dipole moment [ $\mu(\text{exptl./calc.}) = 1.8262/1.8358 \text{ debye}$ ] and in the same time the lowest polarizability [ $\alpha_{ij} = 0.8658 \text{ \AA}^3$ ] of all molecules under study (**Table 3**), and hence its field-response is dominated by the linear (dipolar) term in Eq. (4).



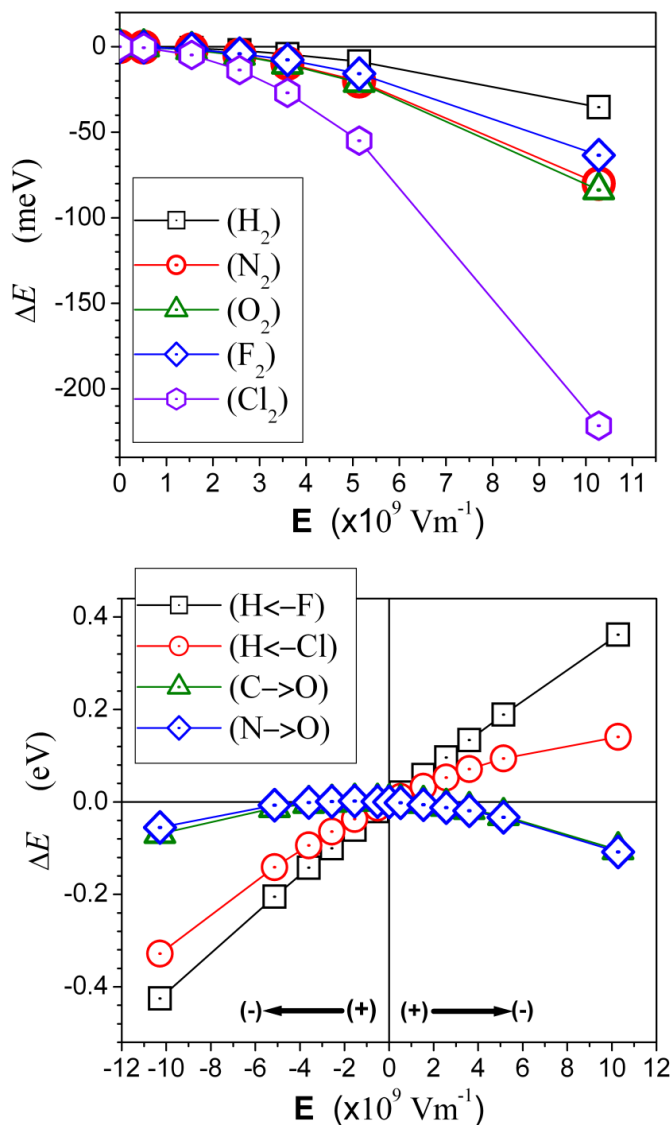


**Figure 3**

The change in the total energy ( $\Delta E$ ) without ZPE or vibrational corrections as a function of the electric field ( $\mathbf{E}$ ) strength for the homo-nuclear diatomics in milli-electron volts (meV) (*top*), and as a function of the field strength and direction for the hetero-nuclear diatomics in electron volts (eV) (*bottom*). The change in the total energy is defined:  $\Delta E = E(\mathbf{E}) - E_0$ , where  $E(\mathbf{E})$  is the total energy in a finite non-zero field  $\mathbf{E}$  and  $E_0$  the energy of the ground state in absence of external fields (energies of the field-free ground state molecules and their perturbed values under the strongest field considered in this study are listed in **Table 3**). (See end statement of the caption of **Figure 2** in square brackets).

The second behavioral mode of the heterodiatomics is that exhibited by CO and NO, two molecules with feeble permanent dipole moments [ $\mu_{\text{CO}}(\text{exptl./calc.}) = 0.1098/0.0846$  debye and  $\mu_{\text{NO}}(\text{exptl./calc.}) = 0.1587/0.1247$  debye] but significant polarizabilities [ $\alpha_{//,\text{NO}} = 2.2085 \text{ \AA}^3$  and  $\alpha_{//,\text{CO}} = 2.2911 \text{ \AA}^3$ ]. As a consequence, these two molecules exhibit trends not dissimilar to those of the homonuclear diatomics in that they are generally stabilized by both field directions. At the weaker studied field strengths however, CO and NO are first slightly destabilized in *antiparallel* fields due to their weak dipole moment until the field strength reaches approximately  $2.57 \times 10^9$  and  $3.60 \times 10^9 \text{ Vm}^{-1}$ , respectively, when the total energy is lowered again (**Figure 3**) as the external field becomes sufficiently strong to reverse the direction of the molecular dipole moment into alignment and induce a parallel dipole moment (**Figure 2**).

Because of the small (and possibly negligible) dipole moments of CO and NO, we attempt a linear regression of their field stabilization energies against the squared electric field, *i.e.*, a fit through the origin of  $\Delta E = aE^2$ . This fitting yields for CO an  $r^2$  of 0.9258 and  $a = -8.158 \times 10^{-4}$  (in units of  $3.204 \times 10^{-31} \epsilon_0^{-1} \text{ m}^3$  where  $\epsilon_0$  is in  $\text{C.m}^{-1}\text{V}^{-1}$ ,  $\Delta E$  in eV, and  $E$  in multiples of  $10^9 \text{ Vm}^{-1}$ ); while for NO  $r^2 = 0.8308$  and  $a = -7.703 \times 10^{-4}$  (in the same units). The strength of the linear correlation as judged from  $r^2$  is significantly stronger for CO [the molecule with the smaller permanent dipole moment of 0.0846 debye, and hence an almost vanishing first (dipolar) term in Eq. (3), approaching a homonuclear diatomic in this respect] than for NO which has a stronger permanent dipole moment of 0.1247 debye (**Table 3**).

**Table 3**

Experimental and calculated polarizabilities (in cubic angstroms,  $\text{\AA}^3$ ) and permanent dipole moments (in debye) of the ground states of the diatomic molecules considered in this study.

Diatomics	$\alpha(\text{exptl.})^{(a)}$	$\alpha_{\text{avg.}}^{(b)}$	$\alpha_{\parallel}^{(b)}$	$\alpha_{\perp}^{(b)}$	$ \mu (\text{exptl.})^{(a)}$	$\mu^{(b,c)}$
<i>Homonuclear (<math>D_{\infty h}</math>)</i>						
H <sub>2</sub> ( $v = 0, J = 0$ )	0.8023	0.6045	1.0176	0.3980		
F <sub>2</sub>	1.38	1.1341	1.7655	0.8184		
O <sub>2</sub>	1.5812	1.4793	2.2099	1.1141		
N <sub>2</sub>	1.7403	1.7307	2.2167	1.4876		
Cl <sub>2</sub>	4.61	4.4377	6.1443	3.5844		
<i>Heteronuclear (<math>C_{\infty v}</math>)<sup>(d)</sup></i>						
H←F	0.80	0.7123	0.8658	0.6356	1.8262	-1.8358
N→O	1.70	1.6441	2.2085	1.3619 <sup>(e)</sup>	0.1587	0.1247
C→O	1.95	1.9306	2.2911	1.7504	0.1098	0.0846
H←Cl	2.63, 2.77	2.4285	2.5958	2.3449	1.1086±0.0003	-1.0949

(a) Experimental data from Ref. [65].

(b) Calculated values are at the (U)QCISD/6-311++G(3df,2pd) level of theory.

(c) The signs of the permanent dipole moments indicate their relative orientation with respect to the coordinate system displayed in **Figure 1**.

(d) The arrows between the atomic symbols indicate the direction of the dipole moment according to the physicist convention [58, 59].

(e) The NO molecule is an odd open shell-molecule with two degenerate  $\pi^*$  orbitals, one of which is half filled. The Gaussian 09 program does not allow for partial occupation of molecular orbitals and hence the calculated perpendicular polarizability tensor components are unequal, being respectively  $\alpha_{xx} = 1.2945 \text{\AA}^3$  and  $\alpha_{yy} = 1.4292 \text{\AA}^3$ . The entry in the table is their average.

Finally, and between these two extremes one finds the curve representing the response of HCl to the field. This molecule is considerably polarizable ( $\alpha_{\parallel} = 2.5958 \text{\AA}^3$ ), second only to Cl<sub>2</sub> ( $\alpha_{\parallel} = 6.1443 \text{\AA}^3$ ) in the set of nine studied molecules and also has the second stronger permanent dipole moment ( $\mu = 1.0949$  debye) in the set (**Table 2**). Therefore, for HCl the two terms in Eq. (3) have important contributions in the lowering of its energy in the field and cannot be fitted with only one of the two terms separately.

From an examination of the curve representing the response of the stabilization energy of HCl to the external field in the bottom plot of **Figure 3**, we note that the

destabilization of the antiparallel field (the segment of the curve in the first quadrant) is softer in its rise with the magnitude of the external field than the stabilization of the parallel field. This inversion asymmetry through the origin of this plot can be rationalized by examining the rate of change of the stabilization energy with the field by taking the derivative of the expression of  $\Delta E$  [Eq. (4)] with respect to the field strength:

$$\text{slope} = \frac{\partial(\Delta E)}{\partial E} = \begin{cases} -\mu_0 - \alpha_{\parallel} E & \text{(parallel)} \\ +\mu_0 - \alpha_{\perp} E & \text{(antiparallel)} \end{cases} \quad (5)$$

In the third quadrant (parallel fields for HCl) both terms in Eq. (4) have the same (negative) sign and hence the slope is not constant and decreases monotonously with the field strength. At the origin (when  $\mathbf{E} = 0$ ), the tangent to the curve equals the field-free dipole  $\mu_0$ . Upon moving to the first quadrant (antiparallel fields) the dipole moment enters in the expression for the slope with a positive sign and thus at small magnitudes of the electric field the slope is positive (the curve is rising) and steadily decreasing with  $|\mathbf{E}|$  (tapering curve) until  $\alpha_{\perp} E = \mu_0$  when the slope become zero (the tangent to the curve at this point is a horizontal line). At field strengths beyond this point, the slope changes sign and the curve takes a downturn. Our data points did not reach fields of enough strength to bring the curve to its turning point, but the curve in **Figure 3** clearly exhibits the expected form.

### 1.3.2. The Equilibrium Bond Length (Inter-Nuclear Separation) in an External Homogenous Electric Field

#### 1.3.2.1. Trends in Equilibrium Bond Lengths in an External Field

**Figure 4** and **Table 2** show the trend of changes in the equilibrium bond lengths,  $\Delta R$ , of the nine molecules versus the electric field strength. The  $\Delta R$  is defined:

$$\Delta R = R_E - R_0 \quad (6)$$

where  $R_0$  and  $R_E$  are the field-free and with-field equilibrium bond lengths, respectively. The plot for homo-nuclear diatomics (*left*) shows that increasing the external electric field strength always lengthens the internuclear separation in these molecules. The response of heteronuclear diatomic (*right*), however, depends on the relative orientations of the field and the molecule.

The field-induced response of the bond length is clearly non-linear for the five studied homo-nuclear diatomics (**Figure 4**). On the bases of the correlation coefficients within the studied range of fields strengths (**Table 4**), these non-linear functional dependencies of the bond length on  $E$  are well described, phenomenologically, by:

$$R_E = R_0 \times \exp(\gamma E) \quad (7)$$

where  $\gamma$  is a constant of dimensions reciprocal of  $E$ . The table also collects regression equations according to exponential (**I**) and linear (**II**) models of the field-induced response of the given bond property of each of the nine molecules within the range and orientations of the studied fields. From the listed values of the correlation coefficients in the table,  $0.862 (\text{O}_2) \leq r^2 \leq 0.881 (\text{H}_2)$ , one can see that the exponential relation captures reasonably well the bond stretching under the field for homo-diatomics, with  $r^2$  values always higher than the linear model for these molecules. The same conclusion applies for

all four hetero-diatomic molecules, albeit with less difference between the exponential and the linear model as the values in **Table 4** indicate.

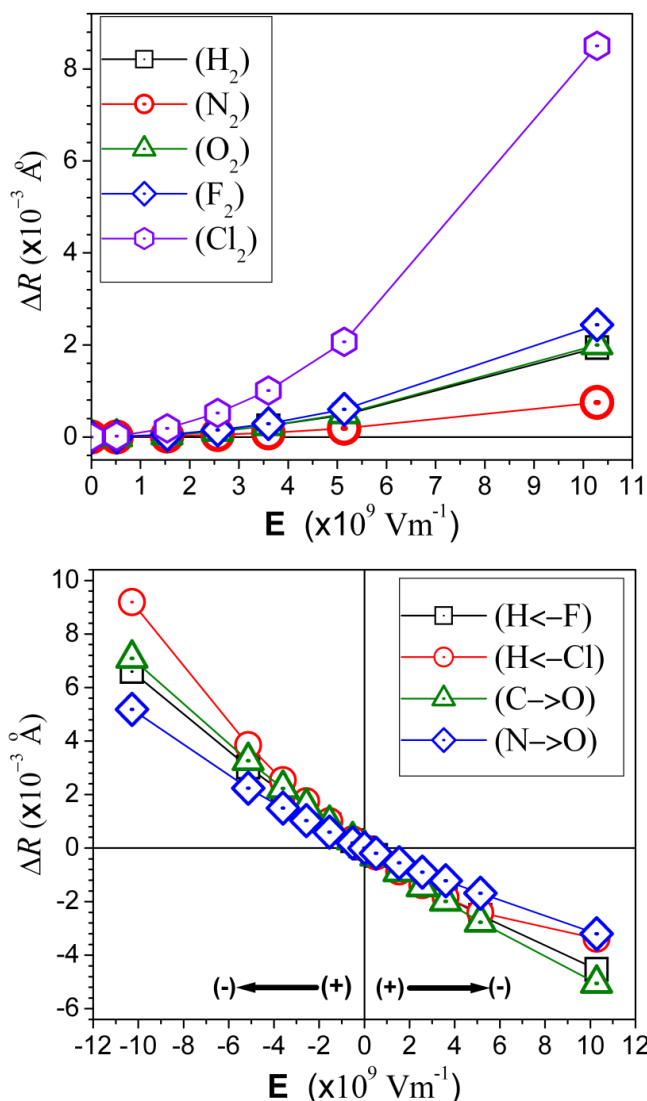


**Figure 4**

Plots of the change in the bond lengths ( $\Delta R$ ), at the optimized geometry, as a function of the electric field ( $\mathbf{E}$ ) strength for the homo-nuclear diatomics (*top*), and as a function of the field strength and direction for the hetero-nuclear diatomics (*bottom*); all in  $\text{m}\text{\AA}$ . The change in the BL is defined:  $\Delta R = R(\mathbf{E}) - R(0)$ , where  $R(\mathbf{E})$  is the bond length in the field and  $R(0)$  the bond length of the ground state in absence of external fields (bond lengths of the field-free ground state molecules are listed in **Table 2**). (See end statement of the caption of **Figure 2** in square brackets).

For HCl and HF, all *parallel* fields increasingly stretch the bond with increasing field strength, *antiparallel* fields compress the bond but to a lesser extent. From **Table 2**, parallel  $E_-$  stretches HF and HCl by 0.0066 and 0.0092 Å, respectively. On the other hand, the antiparallel  $E_+$  compresses HF and HCl by only 0.0045 and 0.0034 Å, respectively.

**Table 4**

Regression correlations between some bond properties and the applied field.

Bond Property ( $P$ )	Model	H <sub>2</sub>	N <sub>2</sub>	O <sub>2</sub>	F <sub>2</sub>	Cl <sub>2</sub>	H←F	H←Cl	C→O	N→O
BL (Å)	BL <sub>0</sub>	0.7426	1.0975	1.1995	1.3938	1.9974	0.9146	1.2736	1.1285	1.1504
	<b>I</b> $\gamma$	$5.298 \times 10^{-2}$	$1.406 \times 10^{-2}$	$3.353 \times 10^{-2}$	$3.482 \times 10^{-2}$	$8.422 \times 10^{-2}$	$-3.039 \times 10^{-1}$	$-2.467 \times 10^{-1}$	$-2.686 \times 10^{-1}$	$-1.783 \times 10^{-1}$
	$r^2$	0.881	0.877	0.862	0.868	0.873	0.976	0.859	0.980	0.957
	<b>II</b> $\eta$	$1.534 \times 10^{-4}$	$5.943 \times 10^{-5}$	$1.579 \times 10^{-4}$	$1.923 \times 10^{-4}$	$6.695 \times 10^{-4}$	$-5.402 \times 10^{-4}$	$-6.102 \times 10^{-4}$	$-5.894 \times 10^{-4}$	$-3.988 \times 10^{-4}$
	$r^2$	0.849	0.852	0.847	0.846	0.845	0.975	0.857	0.979	0.956
	$k$ (mdyne/Å)	$k_0$	11.52	47.70	26.26	10.94	6.51	11.04	5.57	38.18
<b>I</b> $\gamma$		$-3.012 \times 10^{-1}$	$-1.217 \times 10^{-1}$	$-4.965 \times 10^{-1}$	$-2.914 \times 10^{-1}$	-1.090	1.562	1.663	2.125	2.643
$r^2$		0.874	0.872	0.873	0.876	0.871	0.953	0.770	0.972	0.991
<b>II</b> $\eta$		$-1.351 \times 10^{-2}$	$-2.263 \times 10^{-2}$	$-5.025 \times 10^{-2}$	$-1.247 \times 10^{-2}$	$-2.775 \times 10^{-2}$	$3.349 \times 10^{-2}$	$1.829 \times 10^{-2}$	$1.589 \times 10^{-1}$	$1.788 \times 10^{-1}$
$r^2$		0.849	0.849	0.851	0.848	0.848	0.952	0.783	0.978	0.987
$\nu$ (cm <sup>-1</sup> )		$\nu_0$	4405.3	2404.5	1669.2	988.6	562.2	4207.8	3021.0	2196.0
	<b>I</b> $\gamma$	$-1.604 \times 10^{-1}$	$-6.131 \times 10^{-2}$	$-1.292 \times 10^{-1}$	$-1.822 \times 10^{-1}$	$-5.804 \times 10^{-1}$	$9.953 \times 10^{-1}$	$8.440 \times 10^{-1}$	1.069	1.317
	$r^2$	0.872	0.873	0.873	0.872	0.872	0.958	0.772	0.972	0.992
	<b>II</b> $\eta$	-2.591	$-5.713 \times 10^{-1}$	-1.606	$-5.651 \times 10^{-1}$	-1.212	8.177	4.998	4.583	5.100
	$r^2$	0.849	0.849	0.850	0.848	0.846	0.962	0.778	0.975	0.990

- (a) Regression model **I** is the exponential model,  $P_E = P_0 \exp(\gamma E)$ , where  $P_0$  and  $P_E$  denote the field-free and field-perturbed property, respectively, listed in the corresponding left-most column; and the regression model **II** is a linear model of the form  $P_E = P_0 + \eta E$  (both models were constructed with  $E$  expressed in units of  $10^9$  Vm<sup>-1</sup>). The table lists the regression constants  $\gamma$  and  $\eta$  in the first line for each model followed by the corresponding calculated squared correlation coefficient  $r^2$ . The number of data points (different field strengths, in addition to the field free data point, and for heteroatomics different field strengths in the opposite direction as well):  $n = 6$  for homonuclear diatomics and  $n = 13$  for heteronuclear diatomics. The units of the constant  $\gamma$  are reciprocal atomic units of electric field, and those of  $\eta$  are the same as  $P$  multiplied by reciprocal of the units of the electric field.
- (b) Total energy without ZPE of thermodynamic corrections.
- (c) The QTAIM integrated charge on the electropositive atom. In case of diatomics, the positive atom is as indicated by the partial charges.



The bond length of the two heterodiatomics with very small permanent dipole moment (CO and NO) behave in a peculiar manner that differ from the other heterodiatomics that possess large permanent dipole moments. Surprisingly, *parallel* (rather than antiparallel) fields compress these two molecules quite significantly, by 0.0051 and 0.0032 Å for CO and NO. Antiparallel fields stretch the bond to a *lesser* (rather than to a larger) extent than their compression by the parallel field, the stretching being, respectively, 0.0071 and 0.0052 Å. It may be predicted from these trends that *only fields that have a parallel component* of sufficient strength can break the H–X (X = F, Cl) bonds, but any fields of sufficient strength (other than fields perpendicular to the interatomic axis) can dissociate the NO and the CO molecules since there will always be a component that is either parallel or antiparallel. In this respect, CO and NO behave similarly to homonuclear diatomics.

### 1.3.2.2. *Electric Field-Perturbed Morse Potential*

Delley has developed a simple but important model to account for the observed field effects on the bond lengths and on the harmonic frequencies of molecules subjected to external electric fields [42]. This author proposed  $V(r) = D_e(1 - y)^2 + Fr$  as a generalized Morse potential [71] that includes a field-perturbation term ( $Fr$ ) where  $F = F(\mathbf{E})$  has the dimensions of force. The *form* of the equations that followed from this proposal<sup>42</sup> are correct and hence it yields equations that achieve excellent statistical fits to direct numerical results [42]. Unless we have missed a crucial point in Delley's paper, this proposed perturbed Morse potential does not appear to yield the correct asymptotic behavior. For if  $Fr > 0$ , the proposed potential will go to infinity at infinite interatomic

separation [ $V(\infty) = +\infty$ ]. On the other hand, if  $Fr < 0$ , then the asymptotic limit is  $V(\infty) = -\infty$ . In either case the limit is non-physical. We do not wish, however, to downplay the *importance* of Delley's proposal and subsequent derivations that we essentially retrace, with some modification and generalization, but from a different starting point.

Following steps similar to those first proposed by Delley's (with modification), we propose a perturbed Morse potential whereby instead of  $Fr$  we insert the explicit form of the effect of a homogenous field on the potential energy of a diatomic molecule as given by equation (4). Further, and in addition to the parallel orientation (the only orientation allowed in Delley's paper), we also account for the possibility of the antiparallel orientation as well. With these changes, the field-perturbed Morse potential takes the form:

$$V(r) = D_e (1 - \zeta)^2 \mp \mu_0(r)E - \frac{1}{2} \alpha_{ij}(r)E^2, \quad (8)$$

where,

$$\zeta = e^{-a(r-R_0)}, \quad (9)$$

and where  $r$  is the internuclear separation,  $a = \sqrt{k/2D_e}$  is a constant of dimensions of  $[\text{length}]^{-1}$  related to the curvature (or force constant  $k$ ) of the potential energy curve at the field-free equilibrium distance  $R_0$  and which can be taken as the reciprocal of the width of the potential well, and  $D_e$  the (bottom of well) dissociation energy (a positive quantity for a bound state), and where parallel fields are expressed with a negative number in front of the dipolar term and antiparallel fields with a positive sign. Our perturbed potential expressed in Eq. (9) has the following desirable features: (a) It incorporates the explicit expression for the energy change in the field; (b) it takes into account the two field orientations (via the  $\mp$  sign) and which can be generalized straightforwardly to any

oblique field orientation with respect to the internuclear axis by retaining the terms containing  $\cos\theta$  and  $\sin\theta$  in Eq. (3); and finally and importantly (c) it does have the correct asymptotic limits where  $\mu_0(r \rightarrow \infty) = 0$  and  $\alpha(r \rightarrow \infty) = \text{constant}$ , where this constant is the sum of the polarizabilities of the separate atoms.

A re-expression of Eq. (9) yields the expression for the equilibrium bond length under the external field:

$$R_{\mathbf{E}} = R_0 - \frac{1}{a} \ln \zeta, \quad (10)$$

where  $\zeta$  is obtained by applying the equilibrium condition,  $\partial V / \partial r = 0$ , to Eq. (8), yielding:

$$\zeta = \frac{1}{2} \left( 1 + \sqrt{1 \mp c_1 E - c_2 E^2} \right), \quad (11)$$

where

$$c_1 \equiv \frac{2}{aD_e} \frac{\partial \mu_0}{\partial r}, \quad \text{and} \quad c_2 \equiv \frac{1}{aD_e} \frac{\partial \alpha_{\parallel}}{\partial r}. \quad (12)$$

Only the positive root of the quadratic equation  $\zeta^2 - \zeta - \frac{1}{4}(\mp c_1 E - c_2 E^2) = 0$  is retained since otherwise  $\zeta$  would vanish in the field-free case, which is clearly unphysical. It is important to note that for homonuclear diatomics,  $c_1$  vanishes since  $\partial \mu_0 / \partial r = 0$ , the latter equality being the reason for which they are IR inactive. Thus for homonuclear diatomics Eq. (11) has the simpler form  $\zeta = \frac{1}{2} \left( 1 + \sqrt{1 - c_2 E^2} \right)$  and the response of the bond length to the field is exclusively dependent on the slope of the polarizability function, upon which the intensity of the Raman signal depends.

Since we did not obtain the derivatives necessary for the explicit calculation of  $c_1$  and  $c_2$  in this preliminary work, and in order to test the validity of the mathematical form

of equations (10) to (12), we resort to a numerical fitting the results of which are summarized in **Table 5**. For homo-nuclear diatomics, the fitting includes, in addition to the field-free value of the bond length, six values of the bond length under increasingly strong fields up to the maximal field intensity considered in this work of  $1.03 \times 10^{10} \text{ Vm}^{-1}$ , *i.e.* 7 data points, with a data-to-fitting parameters ratio of 7:1. In the case of the heteronuclear diatomics, both  $c_1$  and  $c_2$  are finite, the range of the external field varies from  $-1.03 \times 10^{10} \text{ Vm}^{-1}$  to  $+1.03 \times 10^{10} \text{ Vm}^{-1}$  (13 data points), and the ratio of data/parameters (13:2). Thus in both cases the data/parameters ratio is  $\geq 6.5$  which is generally believed to satisfy the minimum requirement for robust statistics.

**Table 5**

Regression parameters, correlation coefficients, and root mean square deviations of bond lengths obtained from a fitting to Eq. (9).<sup>(a)</sup>

	$1/a$ (Å)	$c_1$ ( $10^9 \text{ mV}^{-1}$ )	$c_2$ ( $10^{18} \text{ m}^2 \text{V}^{-2}$ )	$r^2$	RMSD (Å)
H <sub>2</sub>	0.36151		$2.02 \times 10^{-4}$	0.99997	$1.37 \times 10^{-6}$
N <sub>2</sub>	0.24742		$1.14 \times 10^{-4}$	0.99991	$8.60 \times 10^{-7}$
O <sub>2</sub>	0.24029		$3.11 \times 10^{-4}$	0.99997	$1.31 \times 10^{-6}$
F <sub>2</sub>	0.18832		$4.81 \times 10^{-4}$	0.99999	$1.16 \times 10^{-6}$
Cl <sub>2</sub>	0.32370		$9.56 \times 10^{-5}$	0.99996	$6.69 \times 10^{-6}$
H←F	0.41746	$-5.15 \times 10^{-3}$	$8.31 \times 10^{-5}$	1.00000	$1.32 \times 10^{-6}$
H←Cl	0.50913	$-4.73 \times 10^{-3}$	$2.05 \times 10^{-4}$	0.99999	$3.19 \times 10^{-6}$
C→O	0.30016	$-7.80 \times 10^{-3}$	$1.05 \times 10^{-4}$	1.00000	$1.60 \times 10^{-6}$
N→O	0.23524	$-6.72 \times 10^{-3}$	$1.43 \times 10^{-4}$	0.99920	$1.55 \times 10^{-5}$

(a)Data based on calculations at the (U)QCISD/6-311++G(3df,2pd) level of theory.

The values of the squared correlation coefficients and those of the root mean square deviations (RMSD) in **Table 5** demonstrate that the fitted and directly calculated values of the bond length as a function of  $\mathbf{E}$  are perfectly correlated for each one of the

nine studied molecules. **Table 6** lists the directly calculated equilibrium bond lengths under different field strengths and direction for the set of the nine studied molecules. The

**Table 6**

Directly calculated equilibrium internuclear separations (bond lengths) in Å under different fields and those obtained from the regression parameters listed in **Table 4** using Eq. (19).<sup>(a)</sup>

$E(\times 10^9 \text{ Vm}^{-1})^{(b,c)}$	H <sub>2</sub>	N <sub>2</sub>	O <sub>2</sub>	F <sub>2</sub>	Cl <sub>2</sub>	H←F	H←Cl	C→O	N→O
-10.28									
(←)						0.92115	1.28281	1.13556	1.15560
						0.92254	1.28152	1.13734	1.15781
						0.15	-0.10	0.16	0.19
-5.14									
(←)						0.91759	1.27746	1.13174	1.15266
						0.91792	1.27713	1.13216	1.15325
						0.04	-0.03	0.04	0.05
-3.60									
(←)						0.91663	1.27615	1.13070	1.15192
						0.91678	1.27599	1.13091	1.15223
						0.02	-0.01	0.02	0.03
-2.57									
(←)						0.91601	1.27536	1.13003	1.15145
						0.91609	1.27527	1.13014	1.15163
						0.01	-0.01	0.01	0.02
-1.54									
(←)						0.91542	1.27462	1.12939	1.15102
						0.91544	1.27459	1.12943	1.15110
						0.00	0.00	0.00	0.01
-0.51									
(←)						0.91484	1.27394	1.12877	1.15061
						0.91484	1.27393	1.12878	1.15063

$\mathbf{E}(\times 10^9 \text{ Vm}^{-1})^{(b,c)}$	H <sub>2</sub>	N <sub>2</sub>	O <sub>2</sub>	F <sub>2</sub>	Cl <sub>2</sub>	H←F	H←Cl	C→O	N→O
						0.00	0.00	0.00	0.00
0	0.74262	1.09752	1.19947	1.39376	1.99741	0.91456	1.27362	1.12847	1.15042
	0.74262	1.09752	1.19947	1.39376	1.99741	0.91456	1.27362	1.12847	1.15042
	0.00	0.00	0.00	0.00	0.00	0.00	0.00	0.00	0.00
0.51 (→)	0.74263	1.09752	1.19947	1.39376	1.99743	0.91429	1.27331	1.12817	1.15023
	0.74262	1.09752	1.19947	1.39377	1.99743	0.91429	1.27331	1.12818	1.15022
	0.00	0.00	0.00	0.00	0.00	0.00	0.00	0.00	0.00
1.54 (→)	0.74267	1.09754	1.19951	1.39381	1.99760	0.91376	1.27275	1.12758	1.14987
	0.74266	1.09754	1.19951	1.39381	1.99759	0.91378	1.27273	1.12763	1.14988
	0.00	0.00	0.00	0.00	0.00	0.00	0.00	0.00	0.00
2.57 (→)	0.74274	1.09757	1.19959	1.39391	1.99793	0.91324	1.27224	1.12702	1.14952
	0.74274	1.09757	1.19959	1.39391	1.99792	0.91332	1.27217	1.12713	1.14960
	0.00	0.00	0.00	0.00	0.00	0.01	-0.01	0.01	0.01
3.60 (→)	0.74286	1.09761	1.19971	1.39405	1.99842	0.91275	1.27178	1.12648	1.14920
	0.74286	1.09761	1.19971	1.39405	1.99842	0.91291	1.27165	1.12668	1.14937
	0.00	0.00	0.00	0.00	0.00	0.02	-0.01	0.02	0.01
5.14 (→)	0.74310	1.09771	1.19997	1.39436	1.99948	0.91205	1.27121	1.12570	1.14873
	0.74310	1.09771	1.19997	1.39436	1.99947	0.91237	1.27093	1.12611	1.14915
	0.00	0.00	0.00	0.00	0.00	0.04	-0.02	0.04	0.04
10.28									
(→)	0.74456	1.09827	1.20147	1.39620	2.00591	0.91003	1.27024	1.12342	1.14722
	0.74456	1.09827	1.20147	1.39620	2.00591	0.91130	1.26903	1.12498	1.14935
	0.00	0.00	0.00	0.00	0.00	0.14	-0.10	0.14	0.19

(a) All data are based on calculations at the (U)QCISD/6-311++G(3df;2pd) level of theory.

(b) The direction of the field with respect to the permanent molecular dipole moment is indicated by the arrow, while the permanent dipole moment is indicated by the arrow between the atomic symbols.

(c) For every field there are three rows: The top row is the value calculated directly from the Gaussian 09 program, the middle row is the value obtained from using the regression parameters  $c_1$  and  $c_2$  listed in **Table 4** and obtained from a fitting of bond lengths using Eq. (10).

table shows that in addition to a universal agreement of trends (shortening or lengthening of the bond under a given field compared to another value or direction of the field), there is a remarkable quantitative agreement between the directly calculated values and those obtained from the regression equations in both absolute and relative (%) terms. The agreement is such that we had to retain up to the fifth decimal in the values of the bond lengths (expressed in Å) for the difference between the two values to become discernable.

### **1.3.3. IR Vibrational Stark Effect and Bond Force Constants in External Fields**

#### *1.3.3.1. General Considerations*

We have seen in the previous section that external fields stretch homonuclear diatomics but may stretch or compress heteronuclear diatomics. Generally, stretching a chemical bond weakens it since stretching to infinity is by definition a bond breaking. A sensitive measure of bond strength [72] (its stiffness, so to speak) is the force constant,  $k$ , which is independent of the masses of the bonded atoms. Another, gauge of the strength of the bonding is the vibrational frequency,  $\nu$ , both  $\nu$  and  $k$  being related and both being experimentally measurable.

To be able to discuss the Stark-shift experienced by all nine molecules on an equal footing, we define the field-induced change in the force constant and that in the harmonic frequency of a given bond as:

$$\Delta k = k_E - k_0 \tag{13}$$

and



$$\Delta\nu = \nu_E - \nu_0 \quad (14)$$

**Figure 5** displays plots of  $\Delta k$  and  $\Delta\nu$  for all molecules studied as a function of the external field strength and direction. As the figure and **Table 2** demonstrate, external fields always reduce  $k$  for all of the five studied homonuclear diatomic molecules, an effect which is maximal in the case of  $\text{O}_2$  ( $k_0 = 26.26 \text{ mdyne}\times\text{\AA}^{-1}$ ,  $k_E = 25.62 \text{ mdyne}\times\text{\AA}^{-1}$ ). The reduction in the force constant of homonuclear diatomics is surprisingly *not* minimal for  $\text{N}_2$ , a molecule bound by one of the strongest chemical bonds known [ $k_0(\text{N}\equiv\text{N}) = 47.70 \text{ mdyne}\times\text{\AA}^{-1}$ ]. Instead, bonds that are only 1/4<sup>th</sup> as stiff (H–H and F–F) exhibit the smallest field-induced softening: In  $\text{mdyne}\times\text{\AA}^{-1}$ , the force constants of these two bonds drops from 11.52 to 11.35 for  $\text{H}_2$ , and from 10.94 to 10.78 for  $\text{F}_2$ . In other words, the magnitude of the field-induced softening of homonuclear chemical bonds appears to bear no simple relation to its stiffness in field-free conditions.

The ordering of the magnitude of the Stark-shift by molecule is different than that of the force constants due to its dependence on the reduced mass ( $M_{\text{red}}$ ). Thus,  $\text{N}_2$  and  $\text{F}_2$  show the smallest Stark-shift, while  $\text{H}_2$  - the molecule with the smallest reduced mass - the largest (**Figure 4** and **Table 2**). A glance to **Figure 4** shows that, generally, both  $\Delta k$  and  $\Delta\nu$  are not linear functions of the field strength, the non-linearity being more visually discernable from the plots of the homo-nuclear diatomics.

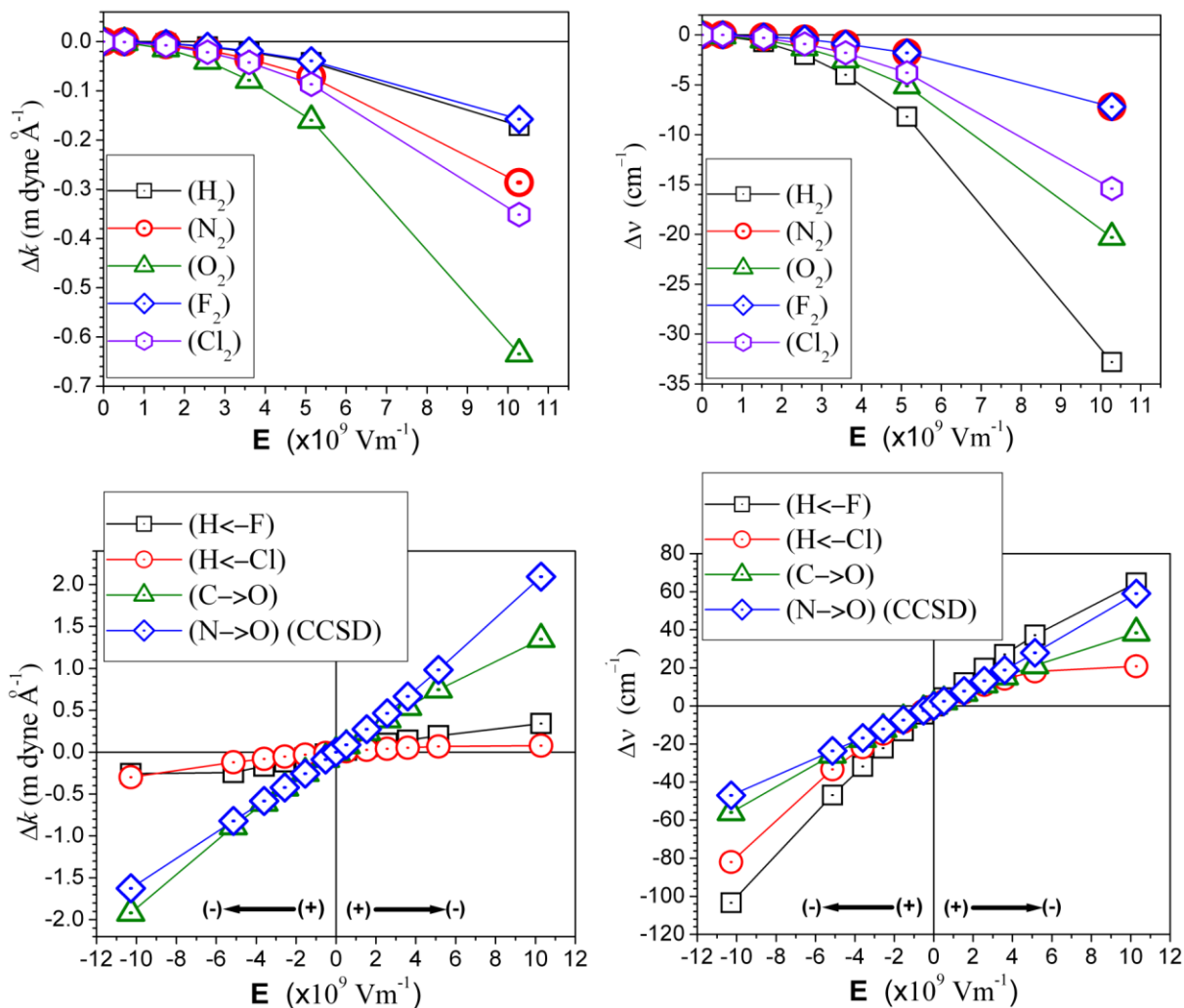


**Figure 5**

Plots of the change in the force constants in  $\text{m dynes} \times \text{\AA}^{-1}$  ( $\Delta k$ , left), and of the change in the harmonic frequencies in  $\text{cm}^{-1}$  ( $\Delta \nu$ , right plots) and as functions of the electric field ( $\mathbf{E}$ ) strength for the homonuclear diatomics (top), and as functions of the field strength and direction for the heteronuclear diatomics (bottom). The change is defined:  $\Delta P = P_{\mathbf{E}} - P_0$ , where  $P_{\mathbf{E}}$  and  $P_0$  are either  $\nu$  or  $k$  with and without  $\mathbf{E}$ , respectively (the value of  $\nu$  and  $k$  for the field free molecules can be found in **Table 2**). All data are obtained at the (U)QCISD/6-311++G(3df,2pd) level of theory except those for NO which were obtained at the UCCSD/6-311++G(3df,2pd) level for reasons described in **Section 3.3.2.** of the text. (See end statement of the caption of **Figure 2** in square brackets and also **Figure 6**).

For all hetero-nuclear diatomics, parallel fields on one hand decrease  $k$  (soften the bond) to various extents for the two halogen halides and on the other have the opposite effect (stiffen the bond) for CO and NO, as can be seen from the entries in **Table 2**. The same observation can be reached by noting the rising positive values of  $\Delta k$  in the first quadrant of the lower right plot of **Figure 4**. HCl exhibits the least pronounced change in response to the field, in  $\text{mdyne}\times\text{\AA}^{-1}$ :  $k = 5.57$ ,  $k_{\mathbf{E}+}$  (antiparallel, stiffer) = 5.65;  $k = 5.57$ ,  $k_{\mathbf{E}-}$  (parallel, softer) = 5.27. In contrast, NO (a bond with considerable stiffness) exhibits the largest change, in  $\text{mdyne}\times\text{\AA}^{-1}$  (CCSD level of theory):  $k = 34.91$ ,  $k_{\mathbf{E}+}$  (parallel, stiffer) = 37.01;  $k_{\mathbf{E}-}$  (antiparallel, softer) = 33.29.

### 1.3.3.2. *Inability of UQCISD to Reproduce the Vibrational Stark-Shift of Nitric Oxide*

Interestingly, the (U)QCISD/6-311++G(3df,2pd) level of theory, the principal level of theory utilized in this paper, fails to reproduce physically-meaningful trends of the  $\Delta k$  and  $\Delta\nu$  field-responses of the NO molecule (all remaining properties notwithstanding). (The full data set can be found in the **Appendix**).

The field-response of the force constant and of the harmonic frequency of this molecule calculated at the UQCISD/6-311++G(3df,2pd) level of theory, each, lie on a parabolic curve. This parabolic relationship is a far cry from the linear response of  $k$  to the field observed for the remaining eight molecules including CO (which is similar to NO in its dipole moment, polarizability, field-free force constant, and charge separation). The parabolic curve is also inconsistent with the linear response of  $k$  and  $\nu$  of NO obtained in response to the perturbing fields at the B3LYP/6-311++G(3df,2pd) level of theory.

In order to resolve the inconsistency in favor of one or the other levels of theory (QCISD or B3LYP), we have tested the field-effect on the force constant of this molecule at four additional commonly used computational levels of theory using the same basis (**Figure 6**). The details of these computations are outlined in **Section 2.2**.

A glance at **Figure 6** shows that the various levels of theory yield very different field-free force constants for NO, these values in  $\text{mdyne}\times\text{\AA}^{-1}$  are: H-F (43.33), MP2 (88.66), B3LYP (34.32), mPW1PW91 (36.17), CCSD (34.91), and QCISD (29.09). The consensus value appears to be centered around the value obtained from the CCSD calculation, *i.e.*, around  $35 \text{ mdyne}\times\text{\AA}^{-1}$ . MP2 appears to dramatically overestimate this value while QCISD under estimate it.

The experimental (*field-free*) frequency for this molecule is reported to be  $1904 \text{ cm}^{-1}$  [73], while the theoretical methods, in order of increasing absolute deviation from the experimental value, are [Method ( $v_{\text{calc.}}$ , deviation from experimental value; all in  $\text{cm}^{-1}$ ): B3LYP (1979, +75); QCISD (1822, -82); CCSD (1996, +92); mPW1PW91 (2032, +128); HF (2224, +320); MP2 (3181, +1277)]. The unscaled B3LYP frequency of NO is thus the closest in agreement with experiment, outperforming even CCSD in this case.

The Stark shift is consistent at all levels of theory and is reflected in the slopes of the curves of  $k$  as a function of  $\mathbf{E}$  and of the level of theory which are displayed in **Figure 6**. The slopes of these curves (in  $10^{-9} \text{ mdyne}\times\text{\AA}^{-1}\times\text{V}^{-1}\times\text{m}$ ) and the corresponding squared correlation coefficients ( $r^2$ ) of the regression lines, respectively, obtained at the various levels of theory are: H-F (0.178/0.999), MP2 (3.323/0.996), B3LYP (0.121/0.995), mPW1PW91 (0.126/0.995), CCSD (0.174/0.997). Thus, five different levels of theory, including the highly accurate CCSD, predict a linear response of the force constant (and

hence of the frequency) of NO to the external field strength, just as any of the other eight molecules. It is concluded that QCISD while reproducing well the *field-free frequency* is incapable of correctly reproducing the associated Stark-shift. Because of this failure of QCISD to properly describe the vibrational Stark shift of NO, the values of  $k$  and  $\nu$  listed for this molecule in all tables and figures in this paper are obtained from UCCSD/6-311++G(3df,2pd) calculations.

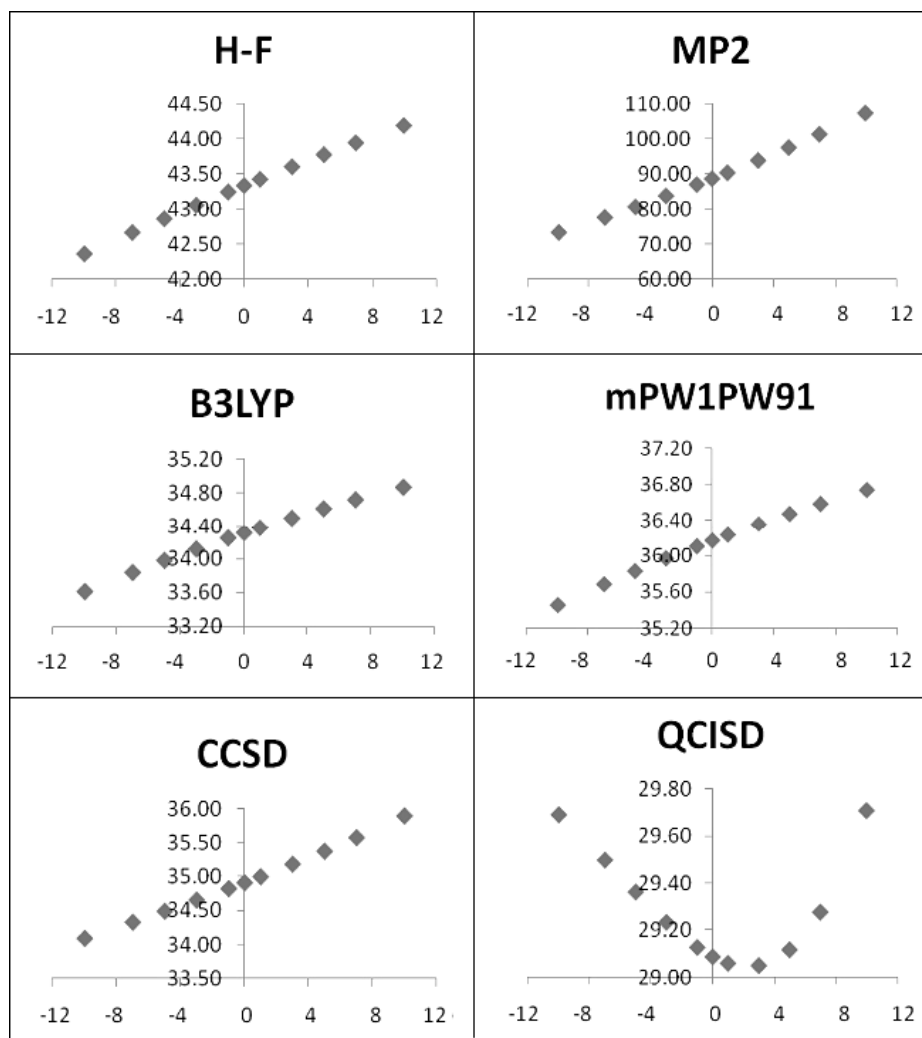


**Figure 6**

Plots of the force constant,  $k$ , of the bond in N–O (in  $\text{mdyn} \times \text{\AA}^{-1}$ ) as a function of the electric field ( $\mathbf{E}$ ) strength and direction (in  $10^9 \text{ Vm}^{-1}$ ) obtained from six different underlying electronic structure methods (levels of theory) all using the same basis set [6-311++G(3df,2pd)]: Hartree Fock (H-F), Møller-Plesset second order perturbation theory (MP2), density functional theory using the two functionals B3LYP and mPW1PW91, coupled clusters with single and double excitations (CCSD), and quadratic configuration interaction with single and double excitations (QCISD). Except for the vibrational frequency and force constant of the NO molecule, the QCISD is the level used to obtain all other results presented and discussed in this paper. The QCISD results have been compared with those obtained at the B3LYP, and both levels of theory were found to yield very similar absolute and relative results and trends (the full set of B3LYP results can be found in the **Appendix**). The convention of assigning directions to the field is the same as in all previous figures.

### 1.3.3.3. A Simple Model to Account for the Vibrational Stark-Shift in Diatomics

We now develop a simple model, closely related to that developed by Delley [42], to rationalize the observed trends in the field-response of  $k$  and of  $\nu$ .

All the bonds we are investigating in this study are of the strong covalent type (including some of the strongest bonds known in chemistry such as the  $\text{N}\equiv\text{N}$  bond), hence the behavior near the bottom of the well is accurately represented by the harmonic approximation. In that approximation, the  $k$  and  $\nu$  are related by the well-known expression:

$$\nu = \frac{a}{\pi} \sqrt{\frac{D_e}{2M_{\text{red.}}}} = \frac{1}{2\pi} \sqrt{\frac{k}{M_{\text{red.}}}} \quad , \quad (15)$$

where  $M_{\text{red.}}$  is the reduced mass.

To account for the field effect on the frequencies we first take the second derivative of the field-free Morse potential given by Eq. (8) after setting  $\mathbf{E} = 0$  to obtain:

$$\frac{\partial^2 V}{\partial r^2} = 2a^2 D_e (2\zeta^2 - \zeta) \quad , \quad (16)$$

which when evaluated at  $r = R_0$  yields:

$$\left. \frac{\partial^2 V}{\partial r^2} \right|_{r=R_0} = 2a^2 D_e = k \quad , \quad (17)$$

which is the field free force constant. But since the field alters the equilibrium bond

length, *i.e.*,  $R_0 \xrightarrow{\mathbf{E}} R$ , we keep  $\zeta$  and solve for  $k_{\mathbf{E}}$  to obtain:

$$k_{\mathbf{E}} = 2a^2 D_e \left\{ \frac{1 + 4(\mp c_1 \mathbf{E} - c_2 \mathbf{E}^2) + [1 + 4(\mp c_1 \mathbf{E} - c_2 \mathbf{E}^2)]^{1/2}}{2} \right\} \quad , \quad (18)$$

which upon setting  $\mathbf{E} = 0$  yields back the field-free force constant:

$$k_{\mathbf{E}=0} \equiv k_0 = 2a^2 D_e = k = 4\pi^2 \nu^2 M_{\text{red.}} \quad . \quad (19)$$

Using the last equality in Eq. (19) to convert the harmonic force constant into the corresponding frequencies yields:

$$\nu_{\mathbf{E}} = \kappa \nu_0, \quad (20)$$

where

$$\kappa \equiv \sqrt{\frac{1}{2} \left[ 1 + 4(\mp c_1 \mathbf{E} - c_2 \mathbf{E}^2) \right]^{1/2} \left\{ 1 + \left[ 1 + 4(\mp c_1 \mathbf{E} - c_2 \mathbf{E}^2) \right]^{1/2} \right\}}. \quad (21)$$

From Eqs. (20) and (21) it is clear that the field-perturbed frequency  $\nu_{\mathbf{E}}$  is given by the field-free value  $\nu_0$  multiplied by the dimensionless factor  $\kappa$  which depends on both the magnitude and direction of the external field. When  $\kappa(\mathbf{E}) > 1$  this corresponds to a hypsochromic shift, while a bathochromic shift corresponds to  $\kappa(\mathbf{E}) < 1$ . Obviously  $\kappa(\mathbf{E} = 0) \equiv \kappa_0 = 1$  yields the field-free frequency. This formula should therefore explain all the trends in **Figure 4**, whether the Stark shift is to higher or lower frequencies.

From the discussion above, the necessary ingredients to evaluate the frequency under any given field is the field-free frequency  $\nu_0$  weighted by  $\kappa$ . The latter,  $\kappa$ , can be evaluated, in principle, from a knowledge of the field-free IR and Raman intensities since it depends on  $c_1$  and  $c_2$  defined in Eq. (11). For homonuclear diatomics,  $c_1 = 0$ , and hence Eq. (20) reduces to:

$$\kappa \equiv \sqrt{\frac{1}{2} \left[ 1 - 4c_2 \mathbf{E}^2 \right]^{1/2} \left\{ 1 + \left[ 1 - 4c_2 \mathbf{E}^2 \right]^{1/2} \right\}}. \quad (22)$$

The derivatives of the dipole moment and polarizability with respect to bond length were not explicitly evaluated in this preliminary study, but instead regression estimates of  $c_1$  and  $c_2$  were obtained from the non-linear fitting of Eq. (9) (**Table 5**), as explained above.



Non-linear regression with more than one fitting parameter differs from linear regression in that there are usually several local minima of the function being optimized. There are no guarantees, therefore, that the numerical minimization of residuals will locate the "global minimum", only a "local minimum" of the function that depends on the initial guess is all that can be guaranteed.

**Table 7** lists the field-free and Stark-shifted frequencies calculated directly from the Gaussian 09 program against those estimated using the fitted values of the  $c_1$  and  $c_2$  parameters (listed in **Table 5**) by substitution into Eqs. (20-22) for each one of the nine molecules at every value of the external field. **Table 7** also lists the signed percent errors

**Table 7**

Directly calculated harmonic vibrational frequencies (in  $\text{cm}^{-1}$ ) under different fields and those obtained from the regression parameters listed in **Table 4** using Eq. (19).<sup>(a)</sup>

$\mathbf{E}$ ( $\times 10^9 \text{ Vm}^{-1}$ ) <sup>(b,c)</sup>	$\text{H}_2$	$\text{N}_2$	$\text{O}_2$	$\text{F}_2$	$\text{Cl}_2$	$\text{H}\leftarrow\text{F}$	$\text{H}\leftarrow\text{Cl}$	$\text{C}\rightarrow\text{O}$	$\text{N}\rightarrow\text{O}$ <sup>(d)</sup>
-10.28 ( $\leftarrow$ )						4104.4	2939.0	2140.0	1949.3
						3908.9	2754.9	1953.3	1783.0
-5.14 ( $\leftarrow$ )						-4.76	-6.26	-8.73	-8.53
						4161.0	2987.7	2170.3	1972.7
-3.60 ( $\leftarrow$ )						4082.5	2922.4	2096.5	1915.1
						-1.89	-2.19	-3.40	-2.92
-2.57 ( $\leftarrow$ )						4176.0	2999.3	2178.5	1979.6
						4125.8	2959.2	2131.2	1944.8
-1.54 ( $\leftarrow$ )						-1.20	-1.34	-2.17	-1.76
						4185.6	3006.3	2183.7	1984.3
-0.51 ( $\leftarrow$ )						4152.8	2980.8	2152.6	1962.4
						-0.79	-0.85	-1.43	-1.10
0						4194.8	3012.6	2188.7	1989.0
						4178.1	3000.0	2172.6	1978.5
0.51 ( $\rightarrow$ )						-0.40	-0.42	-0.74	-0.53
						4203.6	3018.4	2193.6	1993.9
0						4202.0	3017.0	2191.4	1992.9
						-0.04	-0.05	-0.10	-0.05
0						4207.8	3021.0	2196.0	1996.4
						4405.3	2404.5	1669.2	988.6
0						562.2	4213.4	3024.7	2200.3
						4405.3	2404.5	1669.2	988.6
0						0.00	0.00	0.00	0.00
						0.00	0.00	0.00	0.00
0.51 ( $\rightarrow$ )						0.13	0.12	0.20	0.16
						4405.2	2404.5	1669.1	988.6
0.51 ( $\rightarrow$ )						562.2	4212.0	3023.5	2198.3
						4405.0	2404.4	1669.0	988.4
0.51 ( $\rightarrow$ )						562.2	4224.5	3031.8	2209.0
						4224.5	3031.8	2209.0	2005.9

$\mathbf{E}$ ( $\times 10^9 \text{ Vm}^{-1}$ ) <sup>(b,c)</sup>	H <sub>2</sub>	N <sub>2</sub>	O <sub>2</sub>	F <sub>2</sub>	Cl <sub>2</sub>	H←F	H←Cl	C→O	N→O <sup>(d)</sup>
	-0.01	0.00	-0.01	-0.02	0.00	0.30	0.28	0.49	0.35
1.54 (→)	4404.6	2404.4	1668.7	988.5	561.9	4220.0	3028.0	2202.8	2004.2
	4402.1	2403.6	1667.3	986.9	562.1	4245.5	3044.5	2225.5	2017.4
	-0.06	-0.03	-0.08	-0.16	0.04	0.60	0.55	1.03	0.66
2.57 (→)	4403.3	2404.1	1667.9	988.2	561.3	4227.7	3031.9	2207.2	2009.6
	4396.5	2401.8	1664.0	983.9	561.9	4265.2	3055.2	2240.8	2027.6
	-0.15	-0.09	-0.23	-0.44	0.10	0.89	0.77	1.53	0.89
3.60 (→)	4401.3	2403.6	1666.7	987.8	560.4	4234.9	3035.3	2211.3	2015.3
	4388.1	2399.2	1659.0	979.3	561.5	4283.6	3063.8	2255.2	2036.3
	-0.30	-0.18	-0.46	-0.86	0.21	1.15	0.94	1.98	1.04
5.14 (→)	4397.2	2402.7	1664.1	986.9	558.5	4245.1	3039.1	2217.3	2024.3
	4370.0	2393.7	1648.3	969.4	560.8	4308.7	3072.9	2274.8	2046.9
	-0.62	-0.37	-0.95	-1.77	0.42	1.50	1.11	2.60	1.12
10.28 (→)	4372.5	2397.3	1648.9	981.5	546.8	4272.5	3041.8	2234.4	2055.3
	4261.6	2360.9	1583.4	908.2	556.6	4372.5	3071.6	2325.0	2061.6
	-2.54	-1.52	-3.97	-7.46	1.78	2.34	0.98	4.06	0.31

- (a) All data except for NO are based on calculations at the (U)QCISD/6-311++G(3df,2pd) level of theory.
- (b) The direction of the field with respect to the permanent molecular dipole moment is indicated by the arrow, while the permanent dipole moment is indicated by the arrow between the atomic symbols.
- (c) For every field there are three rows: The top row is the value calculated directly from the Gaussian 09 program, the middle row is the value obtained from using the regression parameters  $c_1$  and  $c_2$  listed in Table 4 [and obtained from a fitting of bond lengths, Eq. (10)] using Eq. (20).
- (d) The  $c_1$  and  $c_2$  parameters for NO were obtained as all others from a fitting of bond lengths at the UQCISD/6-311++G(3df,2pd), but the directly calculated vibrational frequencies were obtained from UCCSD/6-311++G(3df,2pd) as explained in the text.

in the estimated versus the directly calculated values of the frequencies. A glance at the table reveals, first, that the modeling described here recovers the correct trends of bathochromic or hypsochromic Stark shifts as a function of the field strength and direction. Second, it reveals that the absolute errors are insignificant especially at relatively low-to -intermediate field strengths, and that the large absolute and relative errors are usually at the strongest field values. Overall, the agreement between the directly calculated frequencies and those estimated from Eqs. (20-22) is no less than *remarkable* given the approximations of the model and the statistical "local minimum" nature of the fitted solution. The modeling outlined above appears to capture the essential physics of the Stark shift.

#### 1.4. Conclusions

A number of molecular and bond properties of a set of five homo-nuclear and four hetero-nuclear diatomic molecules are studied as functions of external homogenous static electric fields. The homo-nuclear diatomics include H<sub>2</sub>, N<sub>2</sub>, O<sub>2</sub>, F<sub>2</sub>, and Cl<sub>2</sub>, and the hetero-nuclear diatomics include HF, HCl, CO, and NO. The molecules were selected to cover a wide range of combinations of permanent dipole moments and polarizabilities: (1) The selected *homonuclear* diatomics, all of which have - naturally - no permanent dipole moment, range in polarizability from H<sub>2</sub> (0.8 Å<sup>3</sup>) to Cl<sub>2</sub> (4.6 Å<sup>3</sup>); (2) the selected *heteronuclear* diatomics include those with a large permanent dipole moment and a small polarizability such as HF ( $\mu = 1.8$  debye,  $\alpha = 0.8$  Å<sup>3</sup>), those with a negligible dipole moment but sizable polarizability such as CO ( $\mu = 0.1$  debye,  $\alpha = 2.0$  Å<sup>3</sup>), and those with

a large dipole moment and a large polarizability such as HCl ( $\mu = 1.1$  debye,  $\alpha = 2.6 \text{ \AA}^3$ ). The response of the total energy to the field  $\Delta E$  is shown to depend on the relative sizes of the dipolar and polarizability terms in the energy expression of each individual molecule, totally consistent with the observed calculated trends.

Delley was first to propose a field-perturbed Morse potential in the form of a linear combination of the field-free Morse potential and a term that introduce the totality of the field effect on the potential energy surface [42]. The field term in Delley's perturbed Morse potential leads to infinities in energy at infinite internuclear separations, which is non-physical. The work of Delley, however, is of great importance in that all his subsequent derivations are correct. Instead of an *ad hoc* term in the perturbed potential, we have introduced the explicit energy expression of a diatomic in a homogenous external field and allowed for both the parallel and antiparallel orientations. In doing so, and by following steps similar to those of Delley, we have refined a simple yet powerful and predictive model that account for the response of the energies, the bond lengths, the harmonic vibrational frequencies, and the force constants to external fields.

The model presented here is shown to capture in a unified manner the essential physics determining the change in bond length in an external field and the associated Stark shift. A statistical fitting of *one* parameter,  $c_2$ , proportional to the rate of change of the polarizability with internuclear separation (hence related to Raman intensities), is shown to capture the essential physics of the bond length elongation in an external field and the associated bathochromic Stark shift of the homo-nuclear diatomic molecules. In the case of the heteronuclear diatomics, which are both Raman- and IR-active, an additional parameter proportional to the rate of change of the dipole moment with the

bond length (hence related to IR intensities),  $c_1$ , is necessary to explain both the bond length changes in the fields and the concomitant bathochromic or hypsochromic Stark shifts (depending on the orientation of the molecule in the field).

Since we did not calculate  $c_1$  and  $c_2$  explicitly, a statistical fitting was employed to obtain reasonable estimates of  $c_1$  and  $c_2$  from the observed trends in field-induced bond length variations. The two parameters were then employed in the expressions for the field-induced bond length alterations and Stark shifts and which were shown to recover the directly calculated values with a remarkable accuracy.

The model presented here demonstrates the predictability of the field-responses from the *field-free* molecular properties with only a parametric dependence on the external electric field. It is also emphasized that the prediction of equilibrium bond lengths under perturbing fields and the accompanying Stark-shift require knowledge of quantities that are all *measurable* from field-free experiments, at least in principle. These (directly or indirectly) experimentally accessible quantities include the bond dissociation energy, the Raman- and IR-intensities, the equilibrium bond length, the vibrational frequency, and the curvature of the potential energy surface at the equilibrium bond length.

## References

- (1) M. Ed. Mohan *Atoms and Molecules in Laser and External Fields*; Alpha Science Ltd.: Oxford, UK, 2008.
- (2) P. Schmelcher, W. E. Schweizer *Atoms and Molecules in Strong External Fields*; Plenum Press: New York, 2010.
- (3) S. Chelkowski, A. D. Bandrauk, P. B. Corkum; Efficient molecular dissociation by a chirped ultrashort infrared laser pulse. *Phys. Rev. Lett.* **1990**, *65*, 2355.
- (4) R. S. Judson, H. Rabitz; Teaching lasers to control molecules. *Phys. Rev. Lett.* **1992**, *68*, 1500-1503.
- (5) W. S. Warren, H. Rabitz, M. Dahleh; Coherent control of quantum dynamics: The dream is alive. *Science* **1993**, *259*, 1581.
- (6) A. D. Bandrauk (Ed.) *Molecules in Laser Fields*; M. Dekker, Publisher, New York, 1994.
- (7) A. Assion, T. Baumert, M. Bergt, T. Brixner, B. Kiefer, V. Seyfried, M. Strehle, Gerber G.; Control of chemical reactions by feedback-optimized phase-shaped femtosecond laser pulses. *Science* **1998**, *282*, 919-922.
- (8) D. Meshulach, Y. Silberberg; Coherent quantum control of 2-photon transitions by a femtosecond laser-pulse. *Nature* **1998**, *396*, 239-242.
- (9) A. D. Bandrauk, Y. Fujimura, R. J. Gordon, (Eds.) *Laser Control and Manipulation of Molecules (ACS Symposium Series)*; Oxford University Press, American Chemical Society: Oxford, 2002.
- (10) A. D. Bandrauk, M. Delfour, LeBris C.,(Eds.) *Quantum Control - Mathematical and Numerical Challenges*; American Mathematical Society: New York, 2003.
- (11) M. Shapiro, P. Brumer *Principles of the Quantum Control of Molecular Processes*; Wiley - Inter: New York, 2003.
- (12) M. Dantus, V. V. Lozovoy; Experimental coherent laser control of physicochemical processes. *Chem. Rev.* **2004**, *104*, 1813-1859.
- (13) V. S. Letokhov *Laser Control of Atoms and Molecules*; Oxford University Press: Oxford UK, 2007.
- (14) M. Y. Ivanov, D. R. Matusek, J. S. Wright; Altered reaction dynamics: Lowered barriers and bound states induced by intense infrared laser fields. *Chem. Phys. Lett.* **1996**, *255*, 232-237.

- (15) D. R. Matusek, M. Y. Ivanov, J. S. Wright; IR laser enhancement of the H + H<sub>2</sub> reaction on an accurate dipole moment surface. *Chem. Phys. Lett.* **1996**, *258*, 255-259.
- (16) M. Y. Ivanov, D. R. Matusek, J. S. Wright; Exchange reactions in intense infrared laser fields. *Phys. Rev. A* **1996**, *54*, 5159-5170.
- (17) A. D. Bandrauk, E. S. Sedik, C. F. Matta; Laser control of reaction paths in ion-molecule reactions. *Mol. Phys.* **2006**, *104*, 95-102.
- (18) A. D. Bandrauk, E. S. Sedik, C. F. Matta; Effect of absolute laser phase on reaction paths in laser-induced chemical reactions. *J. Chem. Phys.* **2004**, *121*, 7764-7775.
- (19) A. A. Arabi, C. F. Matta; Effects of external electric fields on double proton transfer kinetics in the formic acid dimer. *Phys. Chem. Chem. Phys. (PCCP)* **2011**, *13*, 13738-13748.
- (20) I. T. Suydam, C. D. Snow, V. S. Pande, S. G. Boxer; Electric fields at the active site of an enzyme: Direct comparison of experiment with theory. *Science* **2006**, *313*, 200-204 (erratum 29 September 2006).
- (21) H. Lehle, J. M. Kriegl, K. Neienhaus, P. Deng, S. Fengler, G. U. Nienhaus; Probing electric fields in protein cavities by using the vibrational Stark effect of carbon monoxide. *Biophys. J.* **2005**, *88*, 1978-1990.
- (22) X. Wang, X. He, J. Z. H. Zhang; Predicting mutation-induced stark shifts in the active site of a protein with a polarized force field. *J. Phys. Chem. A* **2013**, ASAP, DOI: 10.1021/jp312063h.
- (23) M. A. Spackman, P. Munshi, D. Jayatilaka; The use of dipole lattice sums to estimate electric fields and dipole moment enhancement in molecular crystals. *Chem. Phys. Lett.* **2007**, *443*, 87-91.
- (24) S. Shaik, S. P. de Visser, D. Kumar; External electric field will control the selectivity of enzymatic-like bond activations. *J. Am. Chem. Soc.* **2004**, *126*, 11746-11749.
- (25) S. Franzen, R. F. Goldstein, S. G. Boxer; Electric-Field Modulation of Electron-Transfer Reaction-Rates in Isotropic Systems - Long-Distance Charge Recombination in Photosynthetic Reaction Centers. *J. Phys. Chem.* **1990**, *94*, 5135-5149.
- (26) A. Gopher, Y. Blatt, M. Schonfeld, M. Y. Okamura, G. Feher, M. Montal; The Effect of an Applied Electric-Field on the Charge Recombination Kinetics in Reaction Centers Reconstituted in Planar Lipid Bilayers. *Biophys. J.* **1985**, *48*, 311-



320.

- (27) Z. D. Popovic, G. J. Kovacs, P. S. Vincett, G. Alegria, P. L. Dutton; Electric-Field Dependence of Recombination Kinetics in Reaction Centers of Photosynthetic Bacteria. *J. Chem. Phys.* **1986**, *110*, 227-237.
- (28) P. M. Moroney, T. A. Scholes, P. C. Hinkle; Effect of Membrane-Potential and pH Gradient on Electron-Transfer in Cytochrome-Oxidase. *Biochem.* **1984**, *23*, 4991-4997.
- (29) Y. A. Hong, J. R. Hahn, H. Kanga; Electron transfer through interfacial water layer studied by scanning tunneling microscopy. *J. Chem. Phys.* **1998**, *108*, 4367-4370.
- (30) S. G. Gorfman, V. G. Tsirelson, U. Pietscha; X-ray diffraction by a crystal in a permanent external electric field: General considerations. *Acta Cryst. A* **2005**, *61*, 387-396.
- (31) H. Graafsma, J. Majewski, D. Cahen, P. Coppens; Ionic displacements and piezoelectric constants of AgGaS<sub>2</sub> from X-ray diffraction of a crystal in an external field. *J. Solid State Chem.* **1993**, *105*, 520-527.
- (32) H. Graafsma, G. W. J. C. Heunen, C. Schulze; A new synchrotron-based diffraction technique for perturbation crystallography. *J. Appl. Cryst.* **1998**, *31*, 414-422.
- (33) J. Stahn, A. Pucher, T. Geue, A. Daniel, U. Pietsch; Electric-field-induced electron density response of GaAs and ZnSe. *Europhys. Lett.* **1998**, *44*, 714-720.
- (34) J. Stahn, U. Pietsch, P. Blaha, K. Schwarz; Electric-field-induced charge-density variations in covalently bonded binary compounds. *Phys. Rev. B* **2001**, *63*, 165205-1\_10.
- (35) N. K. Hansen, P. Fertey, R. Régis Guillot; Studies of electric field induced structural and electron-density modifications by X-ray diffraction. *Acta Cryst. A* **2004**, *60*, 465-471.
- (36) R. Guillot, P. Fertey, N. K. Hansen, P. Alle, E. Elkaïm, C. Lecomte; Diffraction study of the piezoelectric properties of low quartz. *Eur. Phys. J. B* **2004**, *42*, 373-380.
- (37) V. G. Tsirelson, S. V. Gorfmana, U. Pietschb; X-ray scattering amplitude of an atom in a permanent external electric field. *Acta Cryst. A* **2003**, *59*, 221-227.
- (38) D. Rai, H. Joshi, A. D. Kulkarni, S. P. Gejji, R. K. Pathak; Electric field effects on aromatic and aliphatic hydrocarbons: A density-functional study. *J. Phys. Chem. A* **2007**, *111*, 9111-9121.

- (39) H. Nakatsuji, T. Hayakawa, T. Yonezawa; Molecules in an electric field. Model for molecular geometry. *J. Am. Chem. Soc.* **1981**, *103*, 7426-7432.
- (40) Y. Honda, H. Nakatsuji; Force concept for predicting the geometries of molecules in an external electric field. *Chem. Phys. Lett.* **1998**, *293*, 230-238.
- (41) V. Kairys, J. D. Head; Electric field effects on the geometry and vibrations of charged molecules: the hydroxide ion case. *Chem. Phys. Lett.* **1998**, *288*, 423-428.
- (42) B. Delley; Vibrations and dissociation of molecules in strong electric fields: N<sub>2</sub>, NaCl, H<sub>2</sub>O and SF<sub>6</sub>. *J. Mol. Struct. (THEOCHEM)* **1998**, *434*, 229-237.
- (43) I. Mata, E. Molins, I. Alkorta, E. Espinosa; Effect of an external electric field on the dissociation energy and the electron density properties: The case of the hydrogen bonded dimer HF...HF. *J. Chem. Phys.* **2009**, *130*, 044104\_1-16.
- (44) R. F. W. Bader; *Atoms in Molecules: A Quantum Theory*; Oxford University Press: Oxford, U.K., 1990.
- (45) C. F. Matta, R. J. Boyd (Eds.) *The Quantum Theory of Atoms in Molecules: From Solid State to DNA and Drug Design*; Wiley-VCH: Weinheim, 2007.
- (46) J. A. Pople, M. Head-Gordon, K. Raghavachari; Quadratic configuration interaction - a general technique for determining electron correlation energies. *J. Chem. Phys.* **1987**, *87*, 5968-5975.
- (47) A. D. Becke; Density-functional thermochemistry.3. The role of exact exchange. *J. Chem. Phys.* **1993**, *98*, 5648-5652.
- (48) C. Lee, W. Yang, R. Parr; Development of the Colle-Salvetti correlation-energy formula into a functional of the electron-density. *Phys. Rev. B* **1988**, *37*, 785-789.
- (49) Frisch, M. J., Trucks, G. W., Schlegel, H. B., Scuseria, G. E., Robb, M. A., Cheeseman, J. R., Scalmani, G., Barone, V., Mennucci, B., Petersson, G. A., Nakatsuji, H., Caricato, M., Li, X., Hratchian, H. P., Izmaylov, A. F., Bloino, J., Zheng, G., Sonnenberg, J. L., Hada, M., Ehara, M., Toyota, K., Fukuda, R., Hasegawa, J., Ishida, M., Nakajima, T., Honda, Y., Kitao, O., Nakai, H., Vreven, T., Montgomery Jr, J. A., Peralta, J. E., Ogliaro, F., Bearpark, M., Heyd, J. J., Brothers, E., Kudin, K. N., Staroverov, V. N., Keith, T., Kobayashi, R., Normand, J., Raghavachari, K., Rendell, A., Burant, J. C., Iyengar, S. S., Tomasi, J., Cossi, M., Rega, N., Millam, J. M., Klene, M., Knox, J. E., Cross, J. B., Bakken, V., Adamo, C., Jaramillo, J., Gomperts, R., Stratmann, R. E., Yazyev, O., Austin, A. J., Cammi, R., Pomelli, C., Ochterski, J. W., Martin, R. L., Morokuma, K., Zakrzewski, V. G., Voth, G. A., Salvador, P., Dannenberg, J. J., Dapprich, S., Daniels, A. D., Farkas, O., Foresman, J. B., Ortiz, J. V., Cioslowski, J., and Fox, D. J.; Gaussian Inc.: Wallingford CT, 2010.

- (50) J. B. Foresman, A. Frisch; *Exploring Chemistry with Electronic Structure Methods, (Second Edition)*; Gaussian, Inc.: Pittsburgh, 1996.
- (51) I. Shavitt, R. J. Bartlett; *Many-Body Methods in Chemistry and Physics: MBPT and Coupled-Cluster Theory*; Cambridge University Press: Cambridge, 2009.
- (52) G. E. Scuseria, C. L. Janssen, H. F. Schaefer III; An efficient reformulation of the closed-shell coupled cluster single and double excitation (CCSD) equations. *J. Chem. Phys.* **1988**, *89*, 7382-7387.
- (53) G. D. Purvis III, R. J. Bartlett; A full coupled-cluster singles and doubles model - the inclusion of disconnected triples. *J. Chem. Phys.* **1982**, *76*, 1910-1918.
- (54) C. Müller, M. S. Plesset; Note on an approximation treatment for many-electron systems. *Phys. Rev.* **1934**, *46*, 618-22.
- (55) A. Szabo, N. S. Ostlund; *Modern Quantum Chemistry: Introduction to Advanced Electronic Structure Theory*; Dover Publications, Inc.: New York, 1989.
- (56) C. Adamo, V. Barone; Exchange functionals with improved long-range behavior and adiabatic connection methods without adjustable parameters: The mPW and mPW1PW models. *J. Chem. Phys.* **1998**, *108*, 664-675.
- (57) K. Hermansson; O-H bonds in electric fields: electron densities and vibrational frequency shifts. *Chem. Phys. Lett.* **1995**, *233*, 376-382.
- (58) P. B. Corkum, N. H. Burnett, F. Brunel; *Phys.Rev.Lett.* **1989**, *62*, 1259.
- (59) L. D. Landau, E. M. Lifshitz *Quantum Mechanics*; Pergamon Press: New York, 1965.
- (60) M. Gruebele, A. H. Zewail; Ultrafast reaction dynamics. *Phys. Today* **1990**, *Vol. 43 (Issue 5, May)*, 24-33.
- (61) L. Pauling; *The Nature of the Chemical Bond, (Third Ed.)*; Cornell University Press: Ithaca, N.Y., 1960.
- (62) J. W. Hovick, J. C. Poler; Misconceptions in sign conventions: Flipping the electric dipole moment. *J. Chem. Edu.* **2005**, *82*, 889.
- (63) C. A. Coulson *Electricity*; Oliver and Boyd: London, 1961.
- (64) C. F. Matta, R. J. Gillespie; Understanding and interpreting electron density distributions. *J. Chem. Educ.* **2002**, *79*, 1141-1152.

- (65) R. F. W. Bader *Atoms in Molecules: A Quantum Theory*; Oxford University Press: Oxford, U.K., 1990.
- (66) T. A. Keith Atomic Response Properties. *The Quantum Theory of Atoms in Molecules: From Solid State to DNA and Drug Design*; Wiley-VCH: Weinheim, 2007.
- (67) R. F. W. Bader, C. F. Matta; Properties of atoms in crystals: Dielectric polarization. *Int. J. Quantum Chem.* **2001**, *85*, 592-607.
- (68) C. F. Matta, S. Sowlati-Hashjin, A. D. Bandrauk; Dipole moment surfaces of the  $\text{CH}_4 + \cdot\text{X} \rightarrow \text{CH}_3\cdot + \text{HX}$  ( $\text{X} = \text{F}, \text{Cl}$ ) reactions from atomic dipole moment surfaces, and the origins of the sharp extrema of the dipole moments near the transition states. *J. Phys. Chem. A* **2013**, *117*, In press, published online (DOI: 10.1021/jp401555h).
- (69) D. M. Bishop, B. Lam, S. T. Epstein; The Stark effect and polarizabilities for a diatomic molecule. *J. Chem. Phys.* **1988**, *88*, 337-341.
- (70) A. D. Buckingham, B. J. Orr; Molecular hyperpolarizabilities. *Quart. Rev. Chem. Soc.* **1967**, *21*, 195-212.
- (71) P. Morse; Diatomic molecules according to the wave mechanics. II. Vibrational levels. *Phys. Rev.* **1929**, *34*, 57-64.
- (72) T. L. Cottrell; *The Strength of Chemical Bonds (Second Ed.)*; Butterworths: London, 1958.
- (73) NIST <http://webbook.nist.gov/chemistry/>; The National Institute of Standards and Technology: Washington DC, 2013.
- (74) D. R. Lide *CRC Handbook of Chemistry and Physics 87th Edition*; CRC Press: 2006.

## Chapter 2

# Dipole Moment Surface of the $\text{CH}_4 + \cdot\text{X} \rightarrow \text{CH}_3\cdot + \text{HX}$ ( $\text{X} = \text{F}, \text{Cl}$ ) Reaction from Atomic Dipole Moment Surfaces, and the Origin of the Sharp Extrema in the Dipole Moment near the Transition State<sup>2</sup>

## Summary

The partitioning of the dipole moment of an isolated molecule or that of a reacting system is reviewed and applied to a dynamic reacting system whereby the system's dipole moment surface is constructed in parallel to its potential energy surface. The dipole moment surface is then decomposed into two origin-independent surfaces: (1) An atomic polarization (AP) surface and a charge transfer (CT) surface. The dipole moment surface as well as its two composing AP and CT surfaces are all further broken down into atomic and/or group contributions with the aid of the quantum theory of atoms in molecules (QTAIM). This approach is applied to the title's laser-induced chemical reactions [ $\text{CH}_4 + \text{X}\cdot \rightarrow \text{CH}_3\cdot + \text{HX}$  ( $\text{X} = \text{F}, \text{Cl}$ )] previously studied by Bandrauk *et al.* [*J. Chem. Phys.*, **121**, 7764-7775 (2004)], and which were found to exhibit marked peaks in the dipole moment and in the polarizability tensor component at (or near) the transition state. These peaks afford a means to control the kinetics of these reactions with the proper adjustment of an external laser field intensity and phase. The entrance channel potentials of these reactions have recently been probed by photodetachment spectroscopy by Bowman and collaborators [*J. Chem. Phys.* **134**, 191102, 1-4 (2011)]. The understanding of the origin of the peaks in the dipole moment can provide, eventually, an additional layer of control

---

<sup>2</sup> This Chapter is based on the paper: C. F. Matta, S. Sowlati-Hashjin and A. D. Bandrauk "Dipole Moment Surface of the  $\text{CH}_4 + \cdot\text{X} \rightarrow \text{CH}_3\cdot + \text{HX}$  ( $\text{X} = \text{F}, \text{Cl}$ ) Reaction from Atomic Dipole Moment Surfaces, and the Origin of the Sharp Extrema in the Dipole Moment near the Transition State" *J. Phys. Chem.* Published online, In Press, DOI: 10.1021/jp401555h (2013).

in the design of reactions tunable by external fields through the proper selection of the reactants to maximize the field-molecule interaction.

## 2.1. Introduction

The manipulation of the amplitude and the relative phase of laser pulses are nowadays achievable in the laboratory and can be exploited in the coherent control of molecular radiative processes [1-5]. Ultrashort pulses have been generated with phase stabilized carrier-envelopes [6, 7] allowing for the study of the effects of the absolute phase (*e.g.*, asymmetric ionization) and leading to measurement of the absolute phase [8-10].

Intense infra red (IR) lasers can lower the activation energy barriers, and hence accelerate chemical reactions [11-13], effects that are quite general as confirmed by quantum mechanical calculations [14]. The experimental IR intensities for the dissociative ionization of diatomics such as HCl [15] were correctly predicted in the vicinity of  $10^{14} \text{ Wcm}^{-2}$  using a quasistatic model of barrier suppression [16].

For a linear system aligned along the  $z$ -axis, the effective potential of the field molecule system as a function of the reaction coordinate ( $s$ ) can be written approximately as [17]:

$$V_{\text{eff.}}(s) \approx V(s) - \mu_z(s)E_0 \cos(\phi) - \frac{1}{2} \alpha_{zz}(s)E_0^2 \cos^2(\phi), \quad (1)$$

where  $V(s)$  is the field-free potential,  $\mu_z$  and  $\alpha_{zz}$  are the components of the dipole moment and of the polarizability parallel to the  $C_3$  axis,  $E_0$  the amplitude and  $\phi$  the phase of the external electromagnetic field. Eq. (1) emphasizes the importance of both the system's dipole  $\mu$  and polarizability  $\alpha$  in describing laser-molecule interactions.

Using quantum mechanical calculations, we have shown that for the  $\text{CH}_4 + \cdot\text{X} \rightarrow \text{CH}_3\cdot + \text{HX}$  ( $\text{X} = \text{F}, \text{Cl}$ ) reaction, the dipole moment (along the  $C_3$  axis) and the diagonal

polarizability tensor elements all exhibit sharp peaks near the coordinate of the transition state (TS) [17, 18]. Similar peaks to the one observed for the two reactions studied in this paper [17] were previously found in the case of the H + H<sub>2</sub> reaction in both the total system's dipole moment and polarizability surfaces [19]. We note that the polarizability, by being proportional to  $\langle r^3 \rangle$ , has been recently shown to provide a basis for the definition of atomic volumes for free atoms and for atoms in molecules, volumes that were shown to be highly insensitive to the level of theoretical calculation [20].

The title reactions are of interest as sources of chemical lasers due to the large inversion of vibrational population in the H–X product [21]. The parallel ( $z$ ) components of the dipole ( $\mu_z$ ) and of the polarizability ( $\alpha_{zz}$ ) of the system is found to exhibit remarkably sharp extrema near the transition state (TS) region. When X = F, these peaks are on the side of the products, but are on the side of the reactants in the case of X = Cl.

Therefore, and through Eq. (1), one can anticipate a maximal effect of the external field on the reacting system near the TS region where the field-molecule interaction, approximated by the two last terms, is extremized. Because of these two terms, the phase  $\phi$  and the amplitude  $E_0$  of the external field can be tuned to eliminate, or even invert, the potential energy barrier. The inversion of a barrier means that a transition state can be converted into a temporary bound state through interaction with the external field, as has already been demonstrated in the case of the Cl + CH<sub>4</sub> reaction [17, 18]. In the case of the F + CH<sub>4</sub> reaction, the coupling with the field eliminates the barrier and can result into a barrierless reaction leading from reactants to products with zero-activation energy barrier.

These results suggest the possibility of a coherent control of such reaction paths as a function of the absolute phase of the external field. Recent work has re-examined these reactions by photodetachment of the halogen anion in collision with CH<sub>4</sub> by Bowman and coworkers [22].

An understanding of the physical process that gives rise to these extrema in the dipole moment and polarizability surfaces can lead to the design of reacting systems with sharper peaks, providing another layer of control of the reaction-radiation system. This paper has two purposes: (1) To briefly review and summarize the partitioning of the dipole moment of a polyatomic system into atomic and interatomic charge transfer contributions, using the quantum theory of atoms in molecules (QTAIM) [23-25], and then (2) to use this partitioning to decompose the dipole moment surface of the reacting system, *i.e.*,  $\mu_z = \mu_z(s)$ , into atomic and inter-atomic components.

This decomposition of the dipole moment into additive contributions has the purpose of elucidating the atomic origins of the very large peaks near the TS in the dipole moment surface. The dipole moment of the system (supermolecule) is calculated at several points along the reaction path and is then decomposed into atomic terms each consisting of two contributions: A charge transfer term ( $\mu_{CT}$ ) arising from the transfer of electronic charge to or from an atom to its bonded neighbors, and an atomic polarization term ( $\mu_{AP}$ ) due to the distortion of the electron density within the atomic basin itself away from spherical symmetry [23, 26-28].



## 2.2. Atomic Contributions to the Total Dipole for an Electrically-Neutral System

The dipole moment ( $\boldsymbol{\mu}$ ) of a system of interacting atoms, e.g. atoms forming a molecule or two approaching reactant molecules, *etc.*, can be always be decomposed into atomic contributions [23, 26-28]:

$$\boldsymbol{\mu} = \sum_{\Omega} \left[ -\int_{\Omega} \mathbf{r}_{\Omega} \rho(\mathbf{r}) d\mathbf{r} + \left( Z_{\Omega} - \int_{\Omega} \rho(\mathbf{r}) d\mathbf{r} \right) \mathbf{R}_{\Omega} \right] \quad (2a)$$

$$\boldsymbol{\mu} = \sum_{\Omega} \left[ \underbrace{\boldsymbol{\mu}_{\text{ap}}(\Omega)}_{\text{atomic dipolar polarization term}} + \underbrace{q(\Omega)\mathbf{R}_{\Omega}}_{\text{origin-dependent atomic charge transfer term}} \right] = \sum_{\Omega} \boldsymbol{\mu}(\Omega) \quad (2b)$$

where

$$\mathbf{r} = \mathbf{r}_{\Omega} + \mathbf{R}_{\Omega}, \quad (2c)$$

and where  $q(\Omega)$  is the net charge of atom  $\Omega$  bounded by a zero-flux surface and a given outer isodensity envelope, often taken to be the density envelope of  $\rho = 0.001$  au,  $\mathbf{r}_{\Omega}$  the position vector with the origin placed at the nucleus of atom  $\Omega$ , and  $\mathbf{R}_{\Omega}$  the position of the nucleus of  $\Omega$  in the arbitrary molecular coordinate system. The arbitrariness of the molecular coordinate system is the reason for origin dependence of the second term in the sum of eq 2 (the sum itself, of course, is origin independent). The dipole moment of an atom in a polyatomic system is, thus, the result of the vector sum of two terms: (1) An *atomic dipolar polarization term* [ $\boldsymbol{\mu}_{\text{AP}}(\Omega)$ ] which is, in general, origin dependent since an atom in a molecule is usually electrically charged; and (2) a *charge transfer (or bond dipole) term* [ $q(\Omega)\mathbf{R}_{\Omega}$ ] which results from the flow of electronic charge between  $\Omega$  and its bonded atoms. The atomic polarization term,  $\boldsymbol{\mu}_{\text{AP}}$ , is static not dynamic and is nonzero

only for nonspherically symmetric electron densities whereby the center of the electronic charge does not coincide with the position of the nucleus.

The decomposition afforded by Eq. (2) of the system's dipole moment as written is exact but not unique. Its non-uniqueness arises because every charge transfer term  $[q(\Omega)\mathbf{R}_\Omega]$  is origin-dependent since it depends on the chosen coordinate system via the set of nuclear coordinates  $\{\mathbf{R}_\Omega\}$ . As a consequence, the atomic dipole moments  $[\boldsymbol{\mu}(\Omega)]$  are themselves origin dependent. [It should be clear that the vectorial sum of any of the infinite number of sets  $\{\boldsymbol{\mu}(\Omega)\}$  always yields the system's dipole ( $\boldsymbol{\mu}$ )].

To eliminate this origin-dependence, Bader *et al.* define terms that account for the charge transfer from an atom to each of its bonded neighbours, explicitly [26, 29]. In this manner, the molecular dipole moment  $\boldsymbol{\mu}$  is decomposed into origin-independent additive atomic contributions [for which we reserve the symbol  $\boldsymbol{\mu}(\Omega)$  henceforth in this paper]:

$$\boldsymbol{\mu} = \sum_{\Omega} \boldsymbol{\mu}(\Omega) = \sum_{\Omega} \left\{ \boldsymbol{\mu}_{\text{AP}}(\Omega) + \underbrace{\sum_{\Omega' \neq \Omega} q(\Omega') [\mathbf{R}_{\text{bcp}}(\Omega | \Omega') - \mathbf{R}_\Omega]}_{\text{origin-independent charge transfer term}} \right\} \quad (3)$$

where  $\mathbf{R}_{\text{bcp}}(\Omega/\Omega')$  is the position vector of the bond critical point (bcp) along the bond path linking the nuclei of  $\Omega$  and  $\Omega'$  and which is located on the interatomic surface  $S(\Omega|\Omega')$  separating their basins. The sum in Eq. (3) runs over all atoms (or groups)  $\Omega'$  linked to and sharing a surface with atom  $\Omega$ . This is the desired *origin-independent* decomposition of the molecular dipole moment into individual atomic contributions:

$$\boldsymbol{\mu}(\Omega) = \boldsymbol{\mu}_{\text{AP}}(\Omega) + \boldsymbol{\mu}_{\text{CT}}(\Omega), \quad (4a)$$

where

$$\boldsymbol{\mu}_{\text{CT}}(\Omega) = \sum_{\Omega' \neq \Omega} q(\Omega') [\mathbf{R}_{\text{bcp}}(\Omega | \Omega') - \mathbf{R}_{\Omega}] \quad (4b)$$

The atomic polarization dipole,  $\boldsymbol{\mu}_{\text{AP}}$ , defined already in Eq. (2), measures the departure of a given atomic electron density from a spherically-symmetric distribution. The results in Eqs. (3) and (4) can be readily shown to reduce to Eq. (2). A book chapter by Keith entitled "Atomic Response Properties" [30], thoroughly derives and generalizes the partitioning of the so-called "null properties" such as the dipole moment and its derivatives into atomic contributions.

### 2.3. Computational Methods

Unrestricted second-order Møller-Plesset perturbation theory [31] calculations that include inner shell excitations [UMP2(full)] were conducted using a 6-311++G(2d,2p) Pople-type basis set [17]. Geometry optimizations, the tracing of reaction paths (according to the algorithm due to Gonzalez and Schlegel) [32], and the calculation of the final electron density distributions were all performed at the same computational level using Gaussian 98 [33]. The average expectation value of  $\langle S^2 \rangle \pm$  the standard deviation is  $0.760 \pm 0.009$  for the F+CH<sub>4</sub> and  $0.763 \pm 0.006$  for the Cl+CH<sub>4</sub> system, deviating, in the worst case by less than  $\sim 3\%$  from the ideal value of  $s(s + 1) = 0.75$  ( $s$  here being the net spin), and hence well within the recommended maximal tolerance of 10% deviation [34]. Calculations at the MP2 level of theory, especially of molecular and of atomic (atoms-in-molecules) electrostatic properties have been shown to be highly reliable [35].

The electron densities obtained at twelve different points on each one of the two reaction path, the progress on which is described by the intrinsic reaction coordinate (IRC) [36, 37], were analyzed according to the quantum theory of atoms in molecules (QTAIM) [23-25] using the program AIMAll/AIMStudio [38].

## 2.4. Conventions and Units

In this paper, the studied systems are electrically neutral; hence, their dipole moment is origin-independent. The "physicists convention" is adopted in this work for the labelling of the dipole moment vector [39, 40]. In this convention, the dipole moment vector originates at the negative pole and points to the positive pole, *i.e.*, opposite to the electric field inside the dipole (symbolically:  $\overset{+}{\mu} \overset{-}{\leftarrow}$  where  $\mu$  symbolizes the dipole moment (*e.g.*,  $\overset{\delta+}{\text{H}} \overset{\delta-}{\text{---}} \text{F}$ ). With this convention, the dipole is in its most stable direction when *parallel* to an external electric field since the field-molecule energy is expressed by:  $U_E = -\mu \cdot E$  [39]. To provide a sense for the sign of the dipole moment, **Figure 1** exhibits the Cartesian coordinate system in which the reacting systems are placed. For example, if  $\mu_z$  has a positive sign, then it points toward the positive direction of the  $z$ -axis, and *vice versa*. The dipole moments in this paper are given in atomic units (au), defined as the dipole moment of two opposite and equal charges of one atomic unit ( $e$ ) separated by the Bohr radius ( $a_0$ ), [1 au of dipole moment = 2.5418 debyes (D) [41], the latter unit being the one used in the Gaussian program].

Regarding reaction direction, the  $\text{CH}_4 + \cdot\text{X} \rightarrow \text{CH}_3\cdot + \text{HX}$  is taken as the forward reaction. In this work, we only consider the attack whereby the halogen atom, the transferred hydrogen atom, and the carbon are colinear. Focusing on the collinear attack

is not a limitation since the electric field of the laser will align these species in this manner within a small angularly-smearred thermal distribution. Whenever we refer to "the hydrogen atom" we mean the hydrogen atom that is directly involved in the reaction, and not the other three methyl atoms unless stated otherwise.

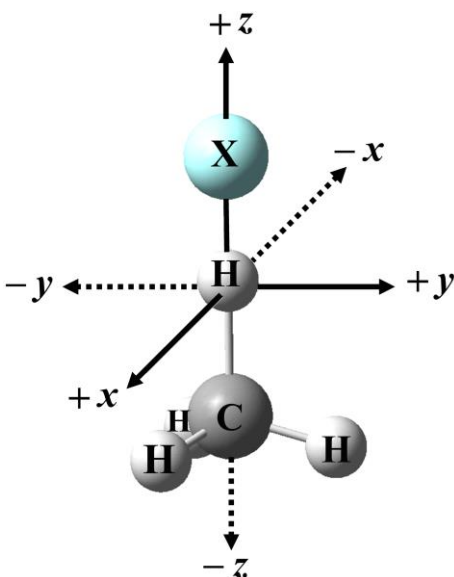


**Figure 1**  
Orientation of reacting system in the coordinate system used for all calculations.

## 2.5. Results and Discussion

### 2.5.1. General Features of the Potential Energy and Dipole Moment Surfaces

The calculated and experimental energy barriers and energies of reaction compare well with experiment [17]. The energy barriers, in kcal/mol, are as follows (X = F / X = Cl):

(a) The barriers to the forward reactions are 4.6/9.3, values that decrease to 2.3/5.0 with the inclusion of ZPE corrections, compare well with the experimental values [42] of 1.2/3.8; (b) the barriers to the back reactions are calculated to be 36.3/2.6, that become 37.6/3.7 with ZPE corrections, comparing well with the experimental value for the X = Cl reaction (2.3) [43] (we were unable to locate an experimental value for the X = F reaction in the literature). Finally, the calculated reaction energies, in kcal/mol are –

31.7/+6.6, which becomes  $\Delta H(298\text{ K})$  of  $-34.6/+2.0$  after applying thermodynamic corrections, compares relatively well with the experimental values [44] of  $-31/1$ . The entropy of the system is not expected to change significantly in such strongly interacting systems over a narrow range of reaction coordinates. To sum-up, the reaction  $X = \text{F}$  is spontaneous as written, but not the  $X = \text{Cl}$  reaction, and the latter has an energy barrier that is  $\sim 3$  kcal/mol higher than the former. Further, the chosen level of theory yields physically-meaningful and realistic energies.

**Figure 2** exhibits ball-and-stick models of the optimized geometries of the reactants, transition states, and products of both reactions. The two potential energy curves tracing the minimum energy path from reactants to products for both reactions are reproduced in the top panel of **Figure 3**. We have shown that the  $X = \text{F}$  reaction can be made barrierless and that the potential energy surface of the  $X = \text{Cl}$  can even be inverted forming a bound state at the reaction coordinate of the transition state through the proper choice of the laser phase and intensity [17].

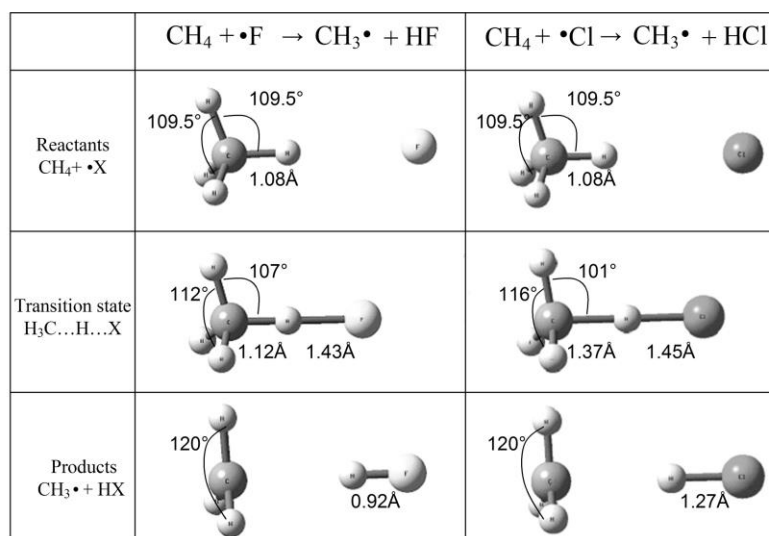


**Figure 2**

Ball-and-stick representation of the optimized geometries of the reactants, transition state structures, and products the  $\text{CH}_4 + \cdot\text{X} \rightarrow \text{CH}_3\cdot + \text{XH}$  ( $X = \text{F}, \text{Cl}$ ) reaction with the

umbrella angle (in degrees) and key inter-atomic distances (in Å) indicated. (Reproduced with permission of the *American Institute of Physics* from Ref. <sup>15</sup>).

The second panel of **Figure 3** shows that there is a drastic change near the TS region in the umbrella angle, defined as the  $\angle \text{H}'\text{-C-H}\dots\text{X}$  angle (see caption of **Figure 3**) which goes from the ideal tetrahedral value of approximately  $109.5^\circ$  to  $90^\circ$  in the products separated at infinity. For  $\text{X} = \text{F}$ , the change in the umbrella angle is steeper than for  $\text{X} = \text{Cl}$  and occurs late, well into the products region (*ca.*  $0.0 \leq s \leq +2.0$  au) and centered on  $s = +1.0$  au. The change in the umbrella angle is smoother in the case of  $\text{X} = \text{Cl}$ , is centered at the TS ( $s = 0.0$  au), and happens over a wider range (*ca.*  $-1.0 \leq s \leq +2.0$  au).

The overall system's dipole moment follows the rate of change in this (and other) geometrical parameters as already noted before [17] and as can be visually seen by comparing the middle and bottom panels of **Figure 3**. Thus, there exists a sharp peak in the dipole moment of the  $\text{X} = \text{F}$  reaction shortly after the transition state, reaching  $\mu = -1.705$  au at a reaction coordinate  $s = 0.40$  au (to two decimals). In the case of the  $\text{X} = \text{Cl}$ , there exists also a sharp peak, of  $\mu = -1.141$  au, less pronounced than for  $\text{X} = \text{F}$ , and significantly, occurs at the transition state ( $s = 0.00$  au). The negative sign of the "dipole moment well" indicates that the dipole points at a direction opposite to the  $z$ -axis of the chosen coordinate system.

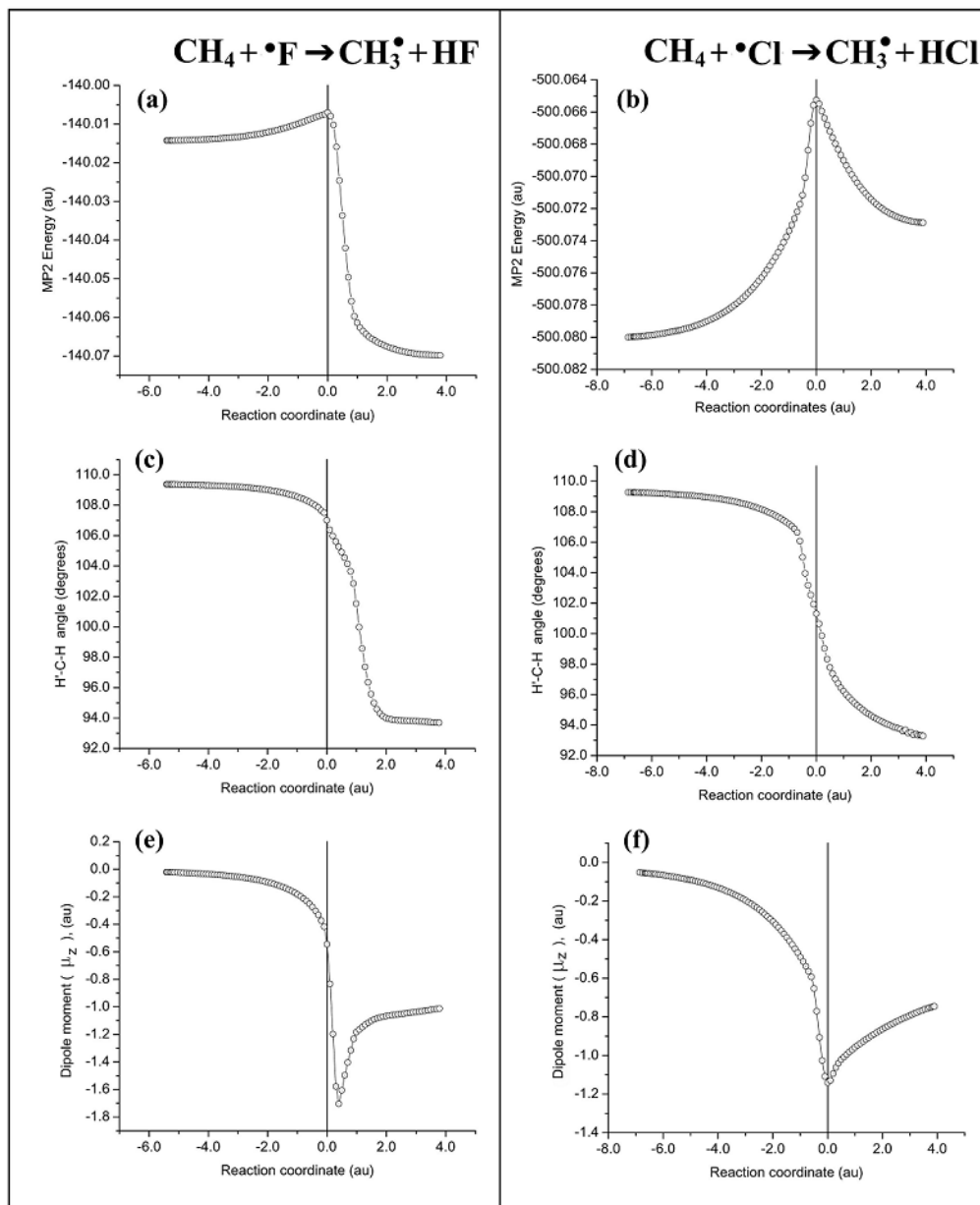


**Figure 3**

Properties as a function of the reaction coordinate  $s$ , in other words, response surfaces of the reaction  $\text{CH}_4 + \cdot\text{X} \rightarrow \text{CH}_3\cdot + \text{XH}$  [ $\text{X} = \text{F}$  (left column),  $\text{Cl}$  (right column)]. In every plot, reactants have  $s < 0$  and products  $s > 0$ , while the transition state occurs at  $s = 0$ . (a, b) Total energies in atomic units; (c, d) the umbrella angle  $\angle \text{H}'\text{-C-H}$  in degrees,  $\text{H}'$  being one of the three equivalent umbrella hydrogen atoms and  $\text{H}$  being the atom transferred in the reaction; and (e, f) the dipole moment in atomic units along the  $z$ -axis. (Reproduced with permission of the *American Institute of Physics* from Ref.[17]).



### 2.5.2. Atomic and Group Charges Surfaces

We first examine the evolution of atomic and group charges as the reaction progresses from reactants to products passing by the transition state. The reaction starts with the approach of the neutral halogen atom X from infinity toward the methane molecule with the concomitant formation of the X–H bond and, simultaneously, the severing of the bond linking the transferring hydrogen atom (referred to simply as "H") to its parent methane molecule. A considerable reorganization of electronic charge can be expected as the reaction progresses. This is so since the halogen starts at infinity as a neutral isolated atom and ends-up becoming an "atom-in-a-molecule" in the products (H–X) where it gains a significant negative charge at the expense of the hydrogen atom which forms the positive end of the dipole.

**Figure 4** displays the atomic and group charges as function of the reaction progress coordinate  $s$  for both reactions. Each of the two plots is partitioned into four quadrants, the upper half being the side of positively charged species, the bottom that of the negatively charged species, the left side being that of the reactants and the right that of the products. Naturally, X, is exactly neutral at infinity and H– and –CH<sub>3</sub> are close to neutrality with opposite small partial charges of magnitude  $|q| = 0.002$  au (being negative for H). In the products, CH<sub>3</sub><sup>•</sup> is obviously an open-shell neutral free radical species, and H–X is a highly polar molecule with a significant degree of charge separation (<sup>+0.738</sup>H–F<sup>–0.738</sup>, and <sup>+0.215</sup>H–Cl<sup>–0.215</sup>) and, consequently, a large dipole moment pointing to the hydrogen atom of magnitudes  $\mu(\text{HF}) = 0.737$  au and  $\mu(\text{HCl}) = 0.464$  au.

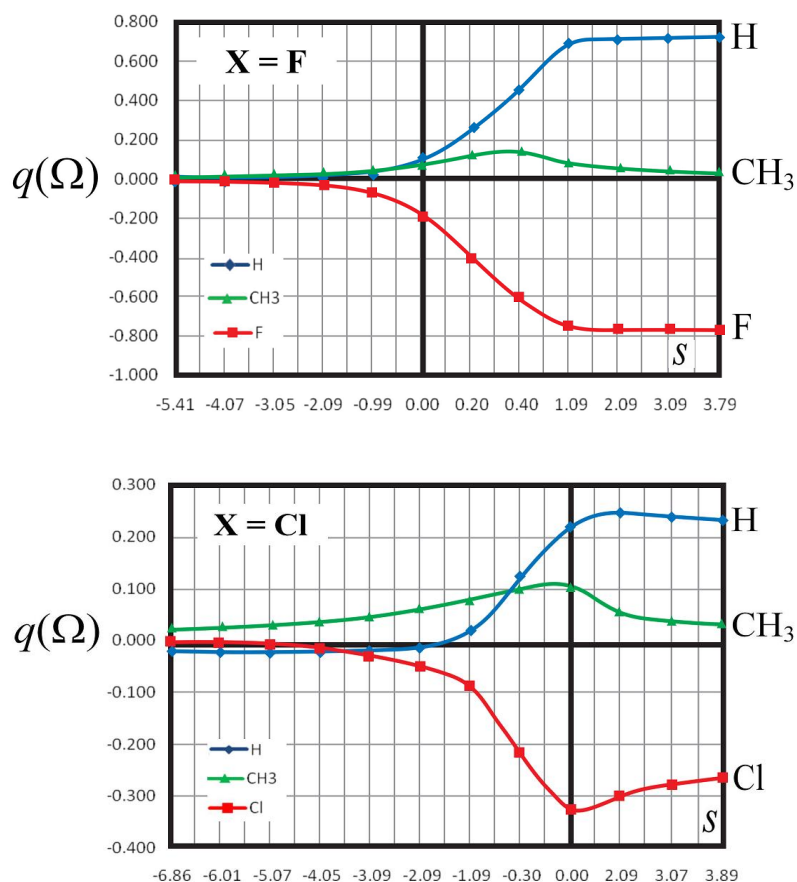


**Figure 4**

Atomic (H, F, and Cl) and group (CH<sub>3</sub>) net electric charges as functions of the reaction coordinate ( $s$ ) for the two studied  $\text{CH}_4 + \text{X} \rightarrow \text{CH}_3 + \text{HX}$  ( $\text{X} = \text{F}, \text{Cl}$ ) reactions. All plotted data are in atomic units.

An examination of **Figure 4** and of **Table 1** reveals that the most significant changes for the  $\text{X} = \text{F}$  reaction happen after the TS. The charge on F at the TS is  $-0.18$  au, only 25% of its maximal magnitude in an isolated HF molecule. The negative charge on F reaches  $-0.76$  au before it slightly decrease in magnitude, after having lost the electron reservoir that  $\text{CH}_3$  provides, to reach its asymptotic value of  $-0.74$  au in the HF molecule.

**Table 1**

Atomic (H, F, and Cl) and group (CH<sub>3</sub>) net electric charges as functions of the reaction coordinate ( $s$ ) for the two studied CH<sub>4</sub> + <sup>\*</sup>X → CH<sub>3</sub><sup>\*</sup> + HX (X = F, Cl) reactions. (All data in atomic units, those for the respective transition states are in bold typeface, and those corresponding to the dipole moment peak in italics).

CH <sub>4</sub> + <sup>*</sup> F → CH <sub>3</sub> <sup>*</sup> + HF				CH <sub>4</sub> + <sup>*</sup> Cl → CH <sub>3</sub> <sup>*</sup> + HCl			
$s(X=F)$	H	F	CH <sub>3</sub>	$s(X=Cl)$	H	Cl	CH <sub>3</sub>
-5.41	-0.007	-0.007	0.014	-6.86	-0.020	-0.003	0.023
-4.07	-0.005	-0.013	0.018	-6.01	-0.022	-0.004	0.026
-3.04	-0.003	-0.020	0.023	-5.07	-0.022	-0.008	0.031
-2.09	0.003	-0.033	0.031	-4.05	-0.022	-0.016	0.038
-0.99	0.022	-0.065	0.043	-3.09	-0.018	-0.028	0.046
<b>0.00</b>	<b>0.111</b>	<b>-0.183</b>	<b>0.072</b>	-2.09	-0.006	-0.052	0.058
0.20	0.271	-0.393	0.122	-1.09	0.021	-0.095	0.074
<i>0.40</i>	<i>0.478</i>	<i>-0.619</i>	<i>0.141</i>	-0.30	0.125	-0.226	0.101
1.09	0.688	-0.756	0.069	<b>0.00</b>	<b>0.224</b>	<b>-0.326</b>	<b>0.103</b>
2.09	0.709	-0.764	0.055	2.09	0.245	-0.296	0.051
3.09	0.719	-0.762	0.044	3.07	0.238	-0.278	0.040
3.79	0.721	-0.759	0.037	3.89	0.233	-0.266	0.033

It is noteworthy to remark that the charge on F reaches its maximally negative value at  $s \approx 1.09$  au slightly after the position of the peak in the dipole moment which occurs at  $s = 0.40$  au. This observation hints at the possible retardation effect of the internal atomic or group dipolar polarization in a direction opposite to the charge transfer contribution. Finally, and importantly, the behavior of the charge surface of H is close to being a mirror image of that of F, reflected into the  $q(\Omega) = 0.00$  axis.

A glance at the corresponding plot for the X = Cl reaction in **Figure 4** shows several differences from the X = F reaction. First, the reader is asked to realize that the range span of the ordinate axis of the charge  $q(\Omega)$  for the X = F reaction is more than 2.5 times wider than that of the X = Cl reaction. This reflects the much smaller magnitudes of the atomic charges in the HCl molecule (0.215 au), only ~29% of those in HF (0.738 au). The second observation is that the charge transfer occurs more gradually and reaches

its peak exactly at the TS, *i.e.*, at  $s = 0.00$  au, in contrast to the delayed charge transfer that characterizes the  $X = F$  reaction. In both reaction, there is a transient bump in the positive charge of the  $\text{CH}_3$  group of  $q(\text{CH}_3, X = F, s = 0.40 \text{ au}) = 0.141 \text{ au}$  and  $q(\text{CH}_3, X = \text{Cl}, s = 0.00 \text{ au}) = 0.103 \text{ au}$  coinciding in both cases with the reaction coordinate of maximum dipole moment magnitude. This peak is, however, short-lived and quickly tends to the asymptotic electrical neutrality of the  $\text{CH}_3^\bullet$  radical.

These observations indicate that the reaction is not driven by a harpoon mechanism, since the charge transfer occurs very late (at the TS or later).

### 2.5.3. Atomic and Group Dipolar Polarization in the Reactants and the Products

Before exploring the evolution of the dipole moment and its composing terms over the path of the reaction, it is instructive to dissect the dipole moment of the species that have an internal dipole moment components along the  $z$ -axis (the axis of the reaction), even if these components cancel when added vectorially. **Figure 5** displays plots of the electron density contours of an isolated  $\text{CH}_4$  molecule in a plane that contains the carbon atom and two of the hydrogen atoms, and of the HF and HCl molecules in a plane containing the two nuclei, respectively. The charges, the total atomic or group dipole moments as well as its composing atomic polarization (AP) and charge transfer (CT) terms are displayed numerically and graphically in the figure. All drawings in this figure are to scale (approximately) including the scales of the three density contour plots with respect to one another - so the reader can compare the size of the electron clouds of the three molecules visually.

The top panel of **Figure 5** reveals that each hydrogen atom in methane is slightly negatively charged [ $q(\text{H}, \text{CH}_4) = -0.002$  au]. This very small charge transfer is insufficient for any significant charge transfer dipole contribution,  $\mu_{\text{CT}}$  being only a mere 0.002 au pointing at the carbon atom. The bulk-part of the dipole moment of the hydrogen atom is due to its distortion from spherical symmetry, and its ( $\mu_{\text{AP}} = -0.151$  au) accounts for  $\sim 99\%$  of the total atomic dipole ( $\mu = -0.153$  au), all dipoles pointing at the carbon atom. The carbon atom itself has zero contribution in both the AP and the CT terms as required by symmetry. The zero dipole moment of  $\text{CH}_4$  implies that the vector addition of the other tetrahedrally-oriented dipoles of the remaining three hydrogen atoms cancel exactly that of any given hydrogen atom.

The density and dipole moment components of HF (in au:  $\mu = -0.737$ ,  $\mu_{\text{AP}} = +0.544$ , and  $\mu_{\text{CT}} = -1.281$ ) are displayed in the middle panel of **Figure 5**. The total permanent dipole moment of HF ( $\mu = -0.737$  au) is clearly dominated by the dipole of the halogen, which itself is the result of a primary contributor ( $\mu_{\text{CT}} = -1.083$  au) counteracted by a lesser, but still important, internal polarization term ( $\mu_{\text{AP}} = +0.423$  au). Visually, one can see the distortion of the F from spherical symmetry in the "onion bulb" looking form of the displayed electron density contours. The considerable charge transfer in this molecule is such that the density within the basin of the fluorine atom polarizes to counteract the change due to the transfer of charge. To quote Bader and Cortés-Guzman's<sup>45</sup> words: "*There appears to be a Le Chatellier principle at work – one that states that two open systems brought into contact respond in such a way as to minimize the overall changes in form and energy, resulting in many cases in a conservation of energy.*"

Finally, the bottom panel of **Figure 5** depicts the density map and dipole moment components of HCl (in au:  $\mu = -0.464$ ,  $\mu_{\text{AP}} = +0.052$ , and  $\mu_{\text{CT}} = -0.516$ ). The dipole of the chlorine atom is quite different from its smaller and more compact halogen, fluorine. (Compare the much larger and more diffuse electron cloud of Cl to that of F in **Figure 5**). Charge transfer is more dominant than atomic polarization in the case of Cl compared to that of F. The single most dominant term is  $\mu_{\text{CT}}(\text{Cl}) = -0.357$  au which is *ca.* 77% of the magnitude of the molecular dipole moment. In both cases, H contributes a little net dipole that reinforces that of the halogen [in au:  $\mu(\text{HF}) = -0.077$ ,  $\mu(\text{HCl}) = -0.045$ ]. The dipole of H is the results of the near cancellation of a CT term, parallel to the molecular and halogen net dipole, and an antiparallel AP term (**Figure 5**).

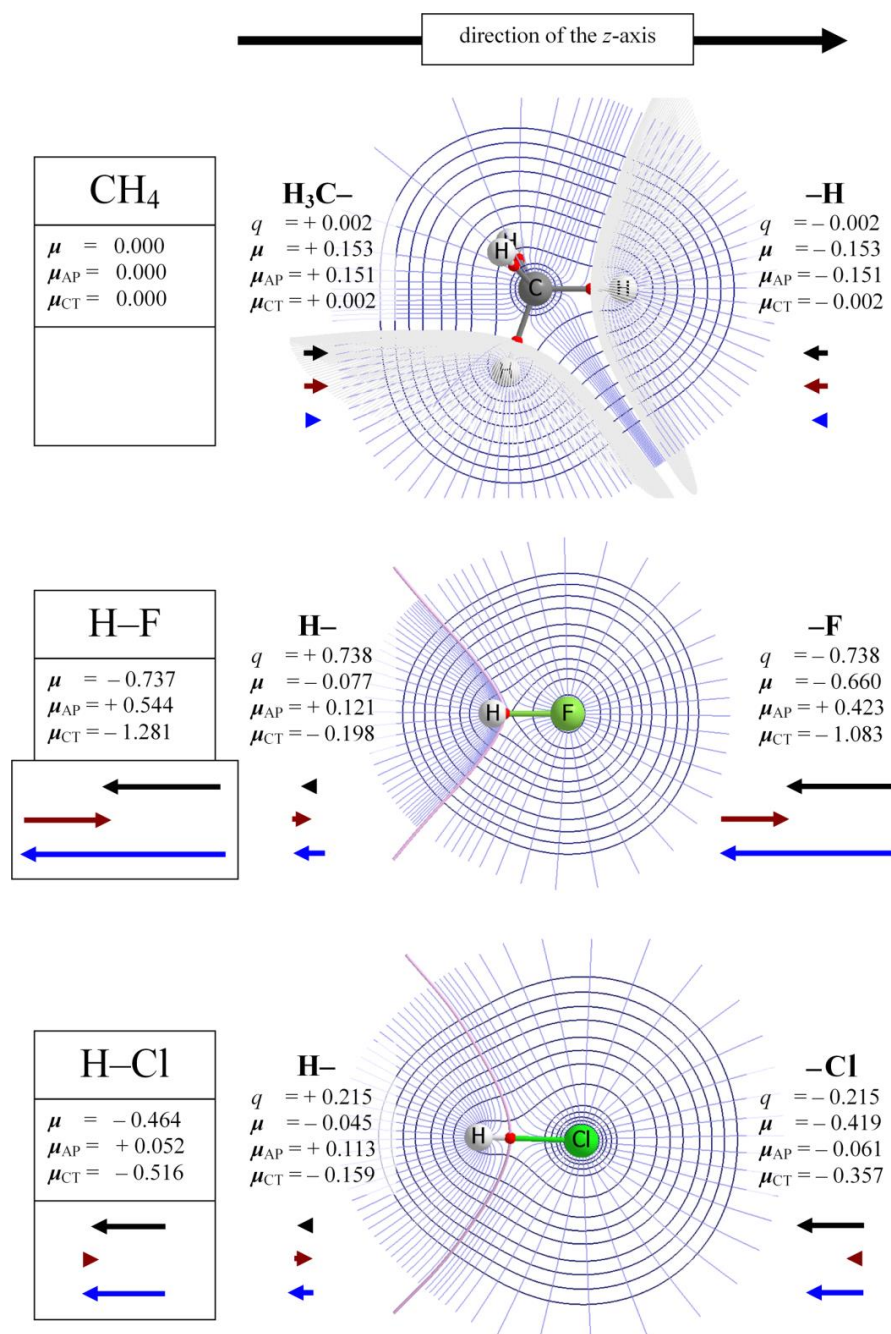


**Figure 5**

Electron density contour maps with their associated gradient vector fields in the H-C-H plane of CH<sub>4</sub> and a plane containing the C<sub>∞</sub>-axis in HF and HCl plane along with the interatomic surfaces intersecting the respective planes (the values of the contours from the outside isodensity contour inward are: 0.001, 0.002, 0.004, 0.008, 0.02, 0.04, 0.08, 0.2, 0.4, 0.8, 2.0, 4.0, 8.0 au). The numerical labels indicate the contribution of the given

atom or group (in the case of CH<sub>3</sub>) to the given term in the dipole moment expression: The total dipole ( $\mu$ ), the atomic polarization term ( $\mu_{AP}$ ), and the charge transfer term ( $\mu_{CT}$ ). The net charge of the atom or group is labelled  $q$ . The respective total system dipole moment and its two components are listed in the middle box at the far left. Below each atom or group is a display of the direction and relative magnitude of the dipole moment along the  $z$ -axis ( $\mu$  = top/black,  $\mu_{AP}$  = middle/brown-red, and  $\mu_{CT}$  = bottom/blue). (All numerical entries in this figure are in atomic units, and all density plots and vector representation of dipole contribution are to scale among and across the three systems). (Key interatomic distance in Å:  $d(\text{H}_3\text{C}-\text{H}) = 1.0830$ ,  $d(\text{H}-\text{F}) = 0.9179$ , and  $d(\text{H}-\text{Cl}) = 1.2703$ , all optimized at the level of theory used in this work).

#### 2.5.4. The Dipole Moment Surface of the CH<sub>4</sub> + <sup>•</sup>F → CH<sub>3</sub><sup>•</sup> + HF Reaction

**Figure 6** exhibits the functional dependence of the total dipole moment as well as the separate sums of the atomic AP and of the atomic CT terms composing it for the X = F system. The plot suggests that from the reactants separated by infinity and up to  $s = 0.40$  au, the point on the reaction path of peak in the system's dipole moment, the dipole moment of the system closely follows the charge transfer term. After the  $s = 0.40$  au, there is a sudden jump in the contribution of the AP term cancelling, partially, the effect of the charge transfer term (which also loose in magnitude). The net result is a diminution of the dipole moment magnitude beyond  $s = 0.40$  au until it plateaus at its asymptotic value of  $-0.737$  au, that of a free HF molecule.

For a better understanding of the origin of these overall behaviors, each one of these curves is partitioned into atomic and group contributions. The results are summarized in **Table 2** and graphically displayed in **Figure 7**. **Table 2** (and **Table 3**, discussed below) lists the individual components of the dipole moment of every atom in the system as a function of the reaction coordinates.



**Table 2**

Atomic contributions to the total system dipole moment for several points along the reaction coordinate ( $s$ ) for the  $\text{CH}_4 + \text{F} \rightarrow \text{CH}_3 + \text{HF}$  system. (All entries are in atomic units).

$\Omega$	$s \rightarrow$	<b>-5.414</b>	<b>-4.074</b>	<b>-3.045</b>	<b>-2.086</b>	<b>-0.991</b>	<b>0.000</b>	<b>0.200</b>	<b>0.400</b>	<b>1.092</b>	<b>2.091</b>	<b>3.091</b>	<b>3.790</b>
F	$\mu_{\text{AP}}(z)$	0.011	0.011	0.011	0.009	0.008	0.019	0.071	0.163	0.355	0.389	0.406	0.413
	$\mu_{\text{CT}}(z)$	-0.019	-0.030	-0.045	-0.068	-0.125	-0.321	-0.676	-1.052	-1.122	-1.133	-1.129	-1.124
	$\mu(z)$	-0.008	-0.019	-0.034	-0.059	-0.117	-0.303	-0.606	-0.890	-0.767	-0.744	-0.723	-0.710
H	$\mu_{\text{AP}}(z)$	-0.130	-0.118	-0.106	-0.090	-0.065	-0.022	0.017	0.048	0.113	0.118	0.121	0.124
	$\mu_{\text{CT}}(z)$	-0.026	-0.037	-0.051	-0.071	-0.113	-0.230	-0.401	-0.480	-0.279	-0.271	-0.261	-0.256
	$\mu(z)$	-0.156	-0.156	-0.157	-0.162	-0.179	-0.251	-0.384	-0.432	-0.166	-0.154	-0.140	-0.132
C	$\mu_{\text{AP}}(z)$	0.011	0.016	0.022	0.028	0.035	0.009	-0.062	-0.147	-0.139	-0.073	-0.089	-0.098
	$\mu_{\text{CT}}(z)$	-0.018	-0.025	-0.033	-0.044	-0.067	-0.131	-0.248	-0.319	-0.179	-0.141	-0.122	-0.111
	$\mu(z)$	-0.007	-0.009	-0.011	-0.016	-0.032	-0.122	-0.310	-0.466	-0.317	-0.215	-0.211	-0.209
H(a)	$\mu_{\text{AP}}(x)$	0.000	0.000	0.000	0.000	0.000	0.000	0.000	0.000	0.000	0.000	0.000	0.000
	$\mu_{\text{AP}}(y)$	-0.142	-0.142	-0.141	-0.141	-0.140	-0.137	-0.132	-0.129	-0.134	-0.137	-0.139	-0.140
	$\mu_{\text{AP}}(z)$	0.050	0.050	0.050	0.050	0.050	0.050	0.046	0.044	0.037	0.019	0.016	0.014
	$\mu_{\text{CT}}(x)$	0.000	0.000	0.000	0.000	0.000	0.000	0.000	0.000	0.000	0.000	0.000	0.000
	$\mu_{\text{CT}}(y)$	0.000	0.000	0.001	0.003	0.006	0.020	0.041	0.054	0.041	0.042	0.039	0.037
	$\mu_{\text{CT}}(z)$	0.000	0.000	0.000	-0.001	-0.002	-0.006	-0.012	-0.016	-0.008	-0.003	-0.003	-0.002
	$\mu(x)$	0.000	0.000	0.000	0.000	0.000	0.000	0.000	0.000	0.000	0.000	0.000	0.000
H(b)	$\mu(y)$	-0.142	-0.141	-0.140	-0.138	-0.134	-0.116	-0.091	-0.075	-0.094	-0.095	-0.100	-0.103
	$\mu(z)$	0.050	0.050	0.049	0.049	0.048	0.044	0.034	0.028	0.029	0.016	0.013	0.012
	$\mu_{\text{AP}}(x)$	-0.123	-0.123	-0.122	-0.122	-0.121	-0.118	-0.114	-0.111	-0.116	-0.119	-0.120	-0.121
	$\mu_{\text{AP}}(y)$	0.071	0.071	0.071	0.070	0.070	0.068	0.066	0.064	0.067	0.069	0.069	0.070
	$\mu_{\text{AP}}(z)$	0.050	0.050	0.050	0.050	0.050	0.050	0.046	0.044	0.037	0.019	0.016	0.014

$\Omega$	$s \rightarrow$	<b>-5.414</b>	<b>-4.074</b>	<b>-3.045</b>	<b>-2.086</b>	<b>-0.991</b>	<b>0.000</b>	<b>0.200</b>	<b>0.400</b>	<b>1.092</b>	<b>2.091</b>	<b>3.091</b>	<b>3.790</b>	
H(c)	$\mu_{CT}(x)$	0.000	0.000	0.001	0.002	0.005	0.018	0.036	0.047	0.035	0.036	0.033	0.032	
	$\mu_{CT}(y)$	0.000	0.000	-0.001	-0.001	-0.003	-0.010	-0.021	-0.027	-0.020	-0.021	-0.019	-0.018	
	$\mu_{CT}(z)$	0.000	0.000	0.000	-0.001	-0.002	-0.006	-0.012	-0.016	-0.008	-0.003	-0.003	-0.002	
	$\mu(x)$	-0.123	-0.122	-0.121	-0.120	-0.116	-0.101	-0.079	-0.065	-0.081	-0.083	-0.087	-0.089	
	$\mu(y)$	0.071	0.071	0.070	0.069	0.067	0.058	0.045	0.037	0.047	0.048	0.050	0.052	
	$\mu(z)$	0.050	0.050	0.049	0.049	0.048	0.044	0.034	0.028	0.029	0.016	0.013	0.012	
	$\mu_{AP}(x)$	0.123	0.123	0.122	0.122	0.121	0.118	0.114	0.111	0.116	0.119	0.120	0.121	
	$\mu_{AP}(y)$	0.071	0.071	0.071	0.070	0.070	0.068	0.066	0.064	0.067	0.069	0.069	0.070	
	$\mu_{AP}(z)$	0.050	0.050	0.050	0.050	0.050	0.050	0.046	0.044	0.037	0.019	0.016	0.014	
	$\mu_{CT}(x)$	0.000	0.000	-0.001	-0.002	-0.005	-0.018	-0.036	-0.047	-0.035	-0.036	-0.033	-0.032	
CH <sub>3</sub>	$\mu_{CT}(y)$	0.000	0.000	-0.001	-0.001	-0.003	-0.010	-0.021	-0.027	-0.020	-0.021	-0.019	-0.018	
	$\mu_{CT}(z)$	0.000	0.000	0.000	-0.001	-0.002	-0.006	-0.012	-0.016	-0.008	-0.003	-0.003	-0.002	
	$\mu(x)$	0.123	0.122	0.121	0.120	0.116	0.101	0.079	0.065	0.081	0.083	0.087	0.089	
	$\mu(y)$	0.071	0.071	0.070	0.069	0.067	0.058	0.045	0.037	0.047	0.048	0.050	0.052	
	$\mu(z)$	0.050	0.050	0.049	0.049	0.048	0.044	0.034	0.028	0.029	0.016	0.013	0.012	
	$\mu_{AP}(z)$	0.161	0.165	0.171	0.178	0.185	0.159	0.077	-0.017	-0.029	-0.016	-0.041	-0.055	
	$\mu_{CT}(z)$	-0.018	-0.025	-0.034	-0.047	-0.073	-0.150	-0.285	-0.366	-0.202	-0.151	-0.130	-0.119	
	$\mu(z)$	0.143	0.140	0.137	0.131	0.112	0.009	-0.208	-0.383	-0.231	-0.167	-0.171	-0.173	
	System (sum)	$\mu(z)$	-0.038	-0.057	-0.063	-0.090	-0.183	-0.545	-1.197	-1.705	-1.165	-1.064	-1.035	-1.013
	System (ab initio)	$\mu(z)$	-0.021	-0.034	-0.054	-0.090	-0.183	-0.545	-1.197	-1.704	-1.164	-1.064	-1.034	-1.015
$\Delta$		0.017	0.023	0.009	0.000	0.000	0.000	0.000	0.001	0.001	0.000	0.001	-0.002	

The first entries list the  $z$ -components for X, the transferred H, and C, since these are the only components that are non-zero by symmetry. These are followed by all the components of the overall, AP, and CT dipoles of the three remaining hydrogen atoms, and the  $z$ -component of the methyl (CH<sub>3</sub>) as a group. The system's overall vector sum (the system dipole reconstructed from the atomic dipoles) followed by the system's dipole moment obtained directly from the *ab initio* calculation are listed at the bottom of the table. The small difference listed at the bottom of the table is due to the cumulative numerical integration errors in the calculation of the atomic dipoles from the electron density. The smallness of this difference (error) is a measure of the quality and precision of the atomic integrations.

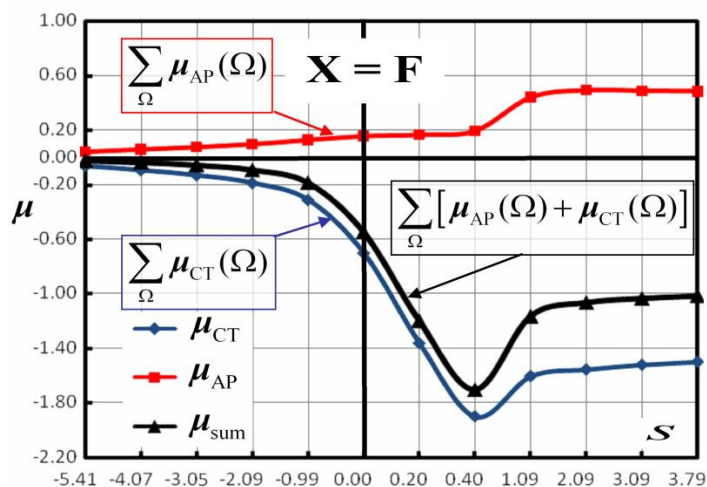


**Figure 6**

Decomposition of the system's total dipole moment of the CH<sub>4</sub> + F → CH<sub>3</sub> + HF system as a function of the reaction coordinate,  $\mu = \mu(s)$ , as the vector sum of an atomic polarization terms [itself the vector sum of atomic dipolar polarizations,  $\sum_{\Omega} \mu_{AP}(\Omega)$ ], and a charge transfer terms which is composed of the vector sum of individual atomic charge transfer terms [ $\sum_{\Omega} \mu_{CT}(\Omega)$ ]. (All quantities are in atomic units).

The top panel of **Figure 7** follows the net dipole  $\mu$  of each atom/group and that of the total system. It is seen that the fluorine atom, in general, makes the most dominant contribution, this is especially visible at reaction coordinates higher than  $\sim 0.2$  au. At the peak itself, one can see that H and CH<sub>3</sub> also contribute to the depression of the overall dipole surface, albeit to a smaller extent than F. All group contributions point in the same direction as that of the total system dipole over the full dipole surface with the exception of that of H, which flips sign at the TS to get aligned with the rest of the atoms on the products side of the surface.

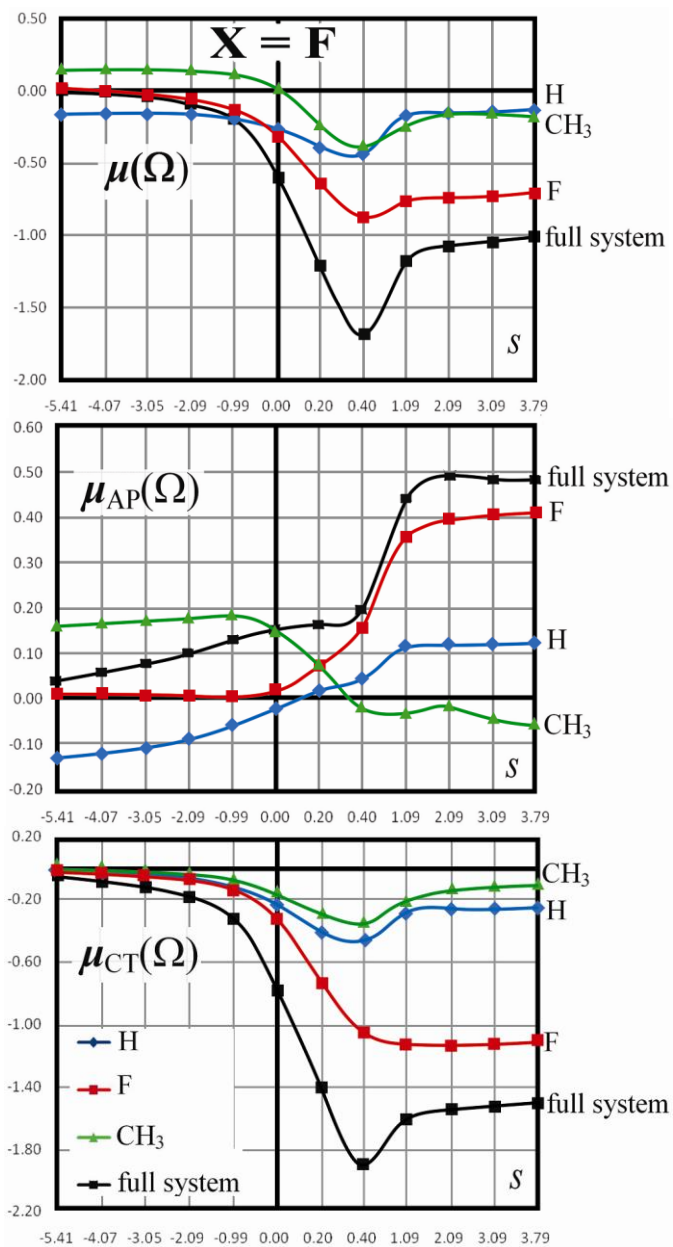


**Figure 7**

Atomic and methyl group total dipolar polarizations,  $\mu(\Omega)$ , and their respective component internal atomic (or group) polarization terms  $\mu_{\text{AP}}(\Omega)$  and charge transfer terms  $\mu_{\text{CT}}(\Omega)$ , as functions of the coordinate ( $s$ ) of the  $\text{CH}_4 + \text{F} \rightarrow \text{CH}_3 + \text{HF}$  reaction. (All quantities are in atomic units).

The scales of the first and last panels of **Figure 7** are comparable, but that of the middle panel is an order of magnitude smaller (magnifying the subtle changes in

the AP component). The middle panel shows that generally  $\mu_{AP}$  changes in a direction opposite to the change of  $\mu_{CT}$  as a function of  $s$ , an observation true for the full system, F, and H, but not as clear-cut for the CH<sub>3</sub> group, the dipole and its components of which have rather small magnitudes. In the case of F, the reverse behavior of  $\mu_{AP}$  compared to  $\mu_{CT}$  can be visually appreciated by comparing the shape of the component dipole moment surfaces for that atom in the middle and bottom plots. These observations give some credence to the notion that a Le Chatelier-type principle may be in operation. It appears, however, that the Le Chatelier principle may only be operational in cases of significant  $\mu_{CT}$  magnitudes.

**Table 3**

Atomic contributions to the total system dipole moment for several points along the reaction coordinate ( $s$ ) for the  $\text{CH}_4 + \cdot\text{Cl} \rightarrow \text{CH}_3\cdot + \text{HCl}$  system. (All entries are in atomic units).

$\Omega$	$s \rightarrow$	<b>-6.857</b>	<b>-6.008</b>	<b>-5.072</b>	<b>-4.054</b>	<b>-3.086</b>	<b>-2.091</b>	<b>-1.092</b>	<b>-0.300</b>	<b>0.0000</b>	<b>2.095</b>	<b>3.070</b>	<b>3.894</b>
Cl	$\mu_{\text{AP}}(z)$	-0.016	-0.021	-0.027	-0.035	-0.045	-0.059	-0.076	-0.049	0.001	-0.025	-0.031	-0.035
	$\mu_{\text{CT}}(z)$	-0.008	-0.013	-0.024	-0.042	-0.072	-0.123	-0.211	-0.464	-0.627	-0.508	-0.472	-0.451
	$\mu(z)$	-0.024	-0.034	-0.051	-0.077	-0.117	-0.182	-0.287	-0.513	-0.626	-0.532	-0.504	-0.486
H	$\mu_{\text{AP}}(z)$	-0.138	-0.133	-0.126	-0.115	-0.102	-0.085	-0.063	-0.012	0.032	0.087	0.096	0.102
	$\mu_{\text{CT}}(z)$	-0.022	-0.028	-0.038	-0.054	-0.077	-0.113	-0.168	-0.298	-0.358	-0.278	-0.257	-0.244
	$\mu(z)$	-0.160	-0.162	-0.164	-0.169	-0.179	-0.197	-0.231	-0.310	-0.326	-0.191	-0.161	-0.141
C	$\mu_{\text{AP}}(z)$	0.018	0.022	0.025	0.031	0.037	0.040	0.040	-0.012	-0.076	-0.060	-0.060	-0.061
	$\mu_{\text{CT}}(z)$	-0.032	-0.038	-0.046	-0.057	-0.072	-0.094	-0.127	-0.196	-0.224	-0.132	-0.110	-0.097
	$\mu(z)$	-0.014	-0.016	-0.020	-0.026	-0.036	-0.054	-0.086	-0.208	-0.300	-0.192	-0.171	-0.158
H(a)	$\mu_{\text{AP}}(x)$	0.000	0.000	0.000	0.000	0.000	0.000	0.000	0.000	0.000	0.000	0.000	0.000
	$\mu_{\text{AP}}(y)$	-0.141	-0.141	-0.141	-0.140	-0.140	-0.139	-0.137	-0.134	-0.133	-0.139	-0.140	-0.141
	$\mu_{\text{AP}}(z)$	0.050	0.050	0.050	0.050	0.050	0.050	0.051	0.050	0.046	0.023	0.018	0.015
	$\mu_{\text{CT}}(x)$	0.000	0.000	0.000	0.000	0.000	0.000	0.000	0.000	0.000	0.000	0.000	0.000
	$\mu_{\text{CT}}(y)$	0.002	0.002	0.003	0.005	0.007	0.011	0.017	0.037	0.045	0.039	0.036	0.034
	$\mu_{\text{CT}}(z)$	-0.001	-0.001	-0.001	-0.002	-0.002	-0.004	-0.005	-0.009	-0.009	-0.003	-0.002	-0.002
	$\mu(x)$	0.000	0.000	0.000	0.000	0.000	0.000	0.000	0.000	0.000	0.000	0.000	0.000
	$\mu(y)$	-0.140	-0.139	-0.138	-0.136	-0.133	-0.128	-0.120	-0.097	-0.088	-0.100	-0.104	-0.107
	$\mu(z)$	0.049	0.049	0.048	0.048	0.047	0.047	0.045	0.042	0.037	0.019	0.015	0.013
	$\mu_{\text{AP}}(x)$	-0.122	-0.122	-0.122	-0.122	-0.121	-0.120	-0.119	-0.116	-0.115	-0.120	-0.121	-0.122
H(b)	$\mu_{\text{AP}}(y)$	0.071	0.071	0.070	0.070	0.070	0.069	0.069	0.067	0.066	0.069	0.070	0.070
	$\mu_{\text{AP}}(z)$	0.050	0.050	0.050	0.050	0.050	0.050	0.051	0.050	0.046	0.023	0.018	0.015
	$\mu_{\text{CT}}(x)$	0.001	0.002	0.003	0.004	0.006	0.009	0.015	0.032	0.039	0.034	0.031	0.030

$\Omega$	$s \rightarrow$	<b>-6.857</b>	<b>-6.008</b>	<b>-5.072</b>	<b>-4.054</b>	<b>-3.086</b>	<b>-2.091</b>	<b>-1.092</b>	<b>-0.300</b>	<b>0.0000</b>	<b>2.095</b>	<b>3.070</b>	<b>3.894</b>
H(c)	$\mu_{CT}(y)$	-0.001	-0.001	-0.002	-0.002	-0.004	-0.005	-0.009	-0.018	-0.022	-0.019	-0.018	-0.017
	$\mu_{CT}(z)$	-0.001	-0.001	-0.001	-0.002	-0.002	-0.004	-0.005	-0.009	-0.009	-0.003	-0.002	-0.002
	$\mu(x)$	-0.121	-0.120	-0.119	-0.118	-0.115	-0.111	-0.104	-0.084	-0.076	-0.087	-0.090	-0.092
	$\mu(y)$	0.070	0.069	0.069	0.068	0.066	0.064	0.060	0.049	0.044	0.050	0.052	0.053
	$\mu(z)$	0.049	0.049	0.048	0.048	0.047	0.047	0.045	0.042	0.037	0.019	0.015	0.013
	$\mu_{AP}(x)$	0.122	0.122	0.122	0.122	0.121	0.120	0.119	0.116	0.115	0.120	0.121	0.122
	$\mu_{AP}(y)$	0.071	0.071	0.070	0.070	0.070	0.069	0.069	0.067	0.066	0.069	0.070	0.070
	$\mu_{AP}(z)$	0.050	0.050	0.050	0.050	0.050	0.050	0.051	0.050	0.046	0.023	0.018	0.015
	$\mu_{CT}(x)$	-0.001	-0.002	-0.003	-0.004	-0.006	-0.009	-0.015	-0.032	-0.039	-0.034	-0.031	-0.030
	$\mu_{CT}(y)$	-0.001	-0.001	-0.002	-0.002	-0.004	-0.005	-0.009	-0.018	-0.022	-0.019	-0.018	-0.017
CH <sub>3</sub>	$\mu_{CT}(z)$	-0.001	-0.001	-0.001	-0.002	-0.002	-0.004	-0.005	-0.009	-0.009	-0.003	-0.002	-0.002
	$\mu(x)$	0.121	0.120	0.119	0.118	0.115	0.111	0.104	0.084	0.076	0.087	0.090	0.092
	$\mu(y)$	0.070	0.069	0.069	0.068	0.066	0.064	0.060	0.049	0.044	0.050	0.052	0.053
	$\mu(z)$	0.049	0.049	0.048	0.048	0.047	0.047	0.045	0.042	0.037	0.019	0.015	0.013
	$\mu_{AP}(z)$	0.167	0.170	0.174	0.180	0.186	0.191	0.193	0.139	0.063	0.008	-0.007	-0.016
	$\mu_{CT}(z)$	-0.034	-0.040	-0.049	-0.062	-0.079	-0.105	-0.143	-0.222	-0.252	-0.142	-0.118	-0.052
	$\mu(z)$	0.133	0.130	0.125	0.118	0.107	0.086	0.050	-0.083	-0.189	-0.134	-0.124	-0.119
System (sum)	$\mu(z)$	-0.031	-0.040	-0.055	-0.077	-0.107	-0.294	-0.468	-0.906	-1.141	-0.856	-0.789	-0.746
System (ab initio)		-0.052	-0.065	-0.089	-0.128	-0.189	-0.294	-0.468	-0.906	-1.141	-0.857	-0.789	-0.747
$\Delta$		-0.021	-0.025	-0.034	-0.051	-0.082	0.000	0.000	0.000	0.000	-0.001	0.000	-0.001



**Figure 8** contains a set of three electron density plots similar to the one for the free molecules already discussed above (**Figure 5**), but now obtained for the total reacting  $X = F$  system at three key reaction coordinates: The top panel representing the far reactant side ( $s = -5.41$  au), the middle is at the reactant coordinate of peak dipole moment ( $s = 0.40$  au), and finally the last is on the far product side ( $s = +3.79$  au). As anticipated from **Figure 6**, the reactants exhibit very little charge transfer at  $s = -5.41$  au where the distance separating H from F is  $2.433 \text{ \AA}$ , only slightly smaller than the sum of their van der Waals radii [46] ( $1.2+1.35 = 2.6 \text{ \AA}$ ). At this reaction coordinate, there exists a weak interaction linking the F and H atoms as evidenced by the presence of bond path characterized by  $\rho_{\text{bcp}}(\text{H|F}) = 0.006$  au (a low density at the bond critical point, typical of weak van der Waals complexes). At the same time, at this coordinate the C–H bond path is identical to the ones linking C with the three remaining hydrogen atoms,  $\rho_{\text{bcp}}(\text{C|H}) = 0.283$  au.

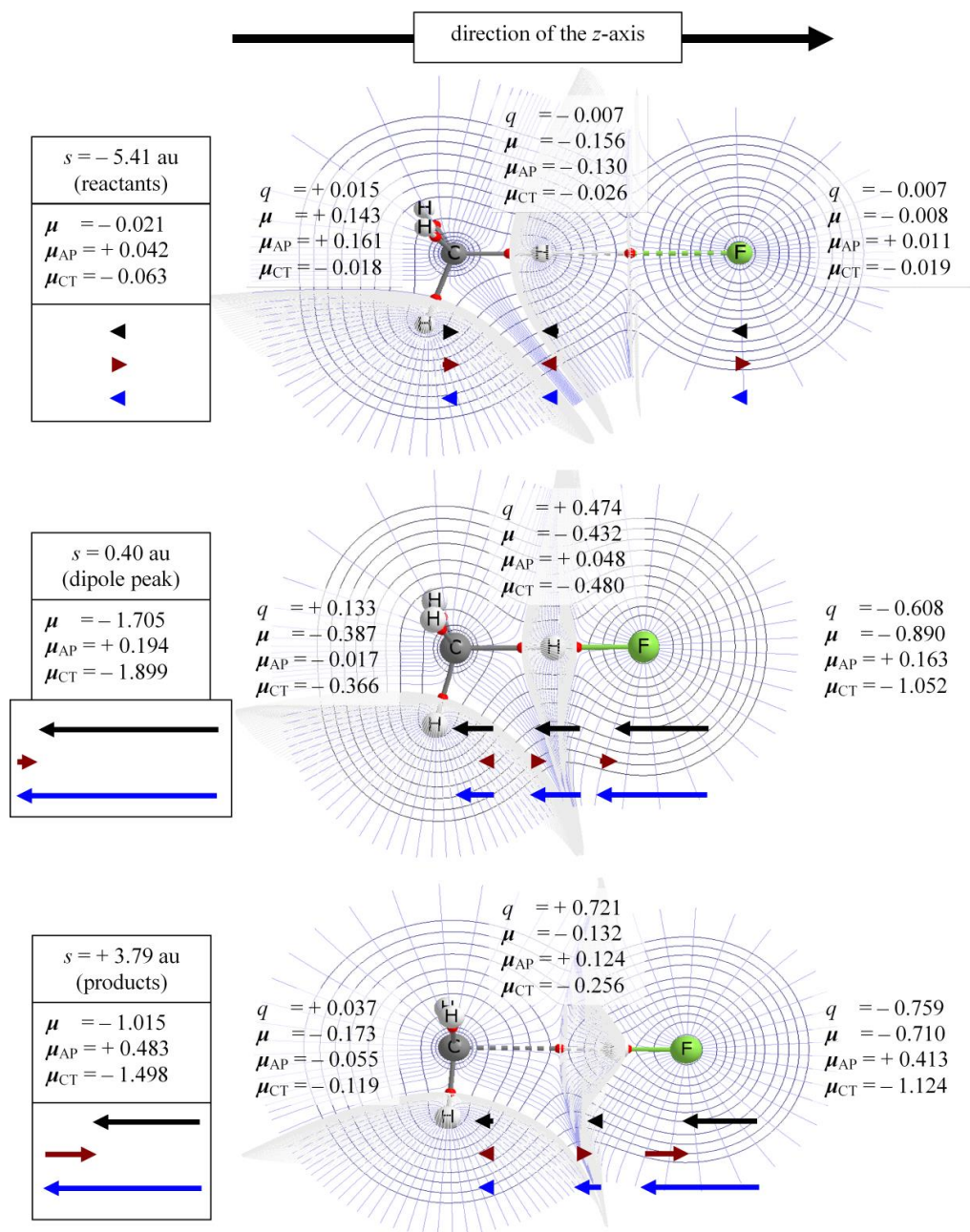


**Figure 8**

Electron density contour maps with their associated gradient vector fields in one of the three H–C–H–F planes along with the three interatomic surfaces intersecting that plane for the  $\text{CH}_4 + \text{F} \rightarrow \text{CH}_3 + \text{HF}$  system as a function of the reaction coordinate ( $s$ ). (The values of the contours from the outside isodensity contour inward are: 0.001, 0.002, 0.004, 0.008, 0.02, 0.04, 0.08, 0.2, 0.4, 0.8, 2.0, 4.0, 8.0 au). The numerical labels from left to right refer to the methyl group ( $\text{CH}_3$ ), H, and F, listing for each its respective charge ( $q$ ), dipole ( $\mu$ ), and the two components of its dipoles [the atomic polarization term ( $\mu_{AP}$ ) and the charge transfer term ( $\mu_{CT}$ )]. The respective total system dipole

moment and its two components are listed in the middle box at the far left. (All numerical entries in this figure are in atomic units). Below each of the three subsystems (CH<sub>3</sub>, H, and F) is a display of the direction and relative magnitude of the dipole moment along the z-axis ( $\mu$  = top/black,  $\mu_{AP}$  = middle/brown-red, and  $\mu_{CT}$  = bottom/blue). (The key interatomic distance  $d(\text{H}_3\text{C}\dots\text{H})/d(\text{H}\dots\text{F})$  in Å are: 1.082/2.433 at  $s = -5.41$  au; 1.323/1.213 at  $s = 0.40$ , and 2.137/0.925 at  $s = 3.79$ . In methane  $d(\text{H}_3\text{C}-\text{H}) = 1.0830$ , and in HF,  $d(\text{H}-\text{F}) = d(\text{H}-\text{F}) = 0.9179$  at the level of theory used in this work).

We then move to the middle panel of **Figure 8**, representing the system with the strongest dipole moment magnitude encountered in this study. Here the hydrogen is shared between the carbon atom and the fluorine atom, being 1.323 Å from the former and 1.213 Å from the latter. The hydrogen atom shares two bond paths, with respective densities at the bond critical points of:  $\rho_{\text{bcp}}(\text{H}|\text{F}) = 0.126$  au and  $\rho_{\text{bcp}}(\text{C}|\text{H}) = 0.159$  au. The weakening of the C–H bond is accompanied with the strengthening of the remaining three C–H methyl bonds for which  $\rho_{\text{bcp}}(\text{C}|\text{H}') = 0.291$  au. At this critical reaction coordinate, *it is the CT term that is at the origin of the deep well in the dipole moment surface, primarily that of F but also those of the H and CH<sub>3</sub>*, as already gleaned from **Figure 7**. The AP terms are insignificant for H and CH<sub>3</sub> (~11 and 4% of the atomic or group dipole moment in magnitude, respectively), and even for F, the AP term of which is more significant, this term is slightly larger than 18% of the atomic dipole of that atom. Further, the sign of  $\mu_{AP}$  of the CH<sub>3</sub> is opposite to that of the H atom and that of the F resulting in some cancellation and a reduction in the overall magnitude of the CT term. As a result, the system's dipole,  $-1.705$  au, is primarily composed of a CT term ( $-1.899$  au) that is slightly opposed by an AP term of  $+0.194$  au, only 10% in magnitude of the former.

In the last step, the hydrogen is detached from the methane molecule leaving behind a CH<sub>3</sub><sup>•</sup> radical and an HF molecule. The density representing that stage is plotted

in the bottom panel of **Figure 8**. At this "products side", and when  $s = 3.79$ ,  $\rho_{\text{bcp}}(\text{H}|\text{F}) = 0.366$  au and  $\rho_{\text{bcp}}(\text{C}|\text{H}) = 0.018$  au and the respective separations are 0.925 and 2.137 Å. Here the principal player is the F atom, primarily the CT term ( $-1.124$  au) which is reduced to  $-0.759$  when added to the oppositely directed AP term of  $+0.413$  au.

### 2.5.5. The Dipole Moment Surface of the $\text{CH}_4 + \text{Cl} \rightarrow \text{CH}_3 + \text{HCl}$ Reaction

We now turn to the  $X = \text{Cl}$  system where **Figure 9** and **Table 3** are the equivalent to **Figure 6** and **Table 2** for  $X = \text{F}$ . A comparison of **Figures 9** and **6**, in addition to revealing differences in the depth and curvatures of the two dipole moment surfaces, also reveals other more subtle differences. First, the  $\mu$  and  $\mu_{\text{CT}}$  curves for  $X = \text{Cl}$  are almost superposed at all values of the reaction coordinate, unlike the corresponding curves for  $X = \text{F}$  where they diverge at the product side of reaction pathway. The total dipole curve follows so closely the CT term for the  $X = \text{Cl}$  system that one can anticipate a negligible role of the AP term, in contrast with the  $X = \text{F}$  system. Further, and unlike the  $X = \text{F}$  case whereby the AP slowly but steadily rises before experiencing a somewhat abrupt jump that starts at the dipole peak coordinate ( $s = 0.40$  au), in the  $X = \text{Cl}$  system, the rise is slower reaching a small peak at the TS ( $s = 0.00$  au) before decreasing back to almost vanish on the products side.

**Figure 10** (comparable to **Figure 7**) breaks down each term into atomic/group contributions. In the  $X = \text{Cl}$  system, the halogen plays a less marked role than F in the  $X = \text{F}$  system, as can be seen from the more even spacing of the atomic and group contributions to  $\mu$  (the top panel of **Figure 10**) compared with the corresponding plot in **Figure 7**. The same conclusion can be reached through a comparison of the

corresponding numerical entries in **Tables 2** and **3**. This remark is particularly visible at the position of the "dipole moment well" (at  $s = 0.00$ ). Finally, the similarity of the all curves in the top and bottom plots in **Figure 10** indicate that not only the full system's  $\mu$  follows its  $\mu_{CT}$  term, but that this is also true on an atom-by-atom basis as well, *i.e.*, every  $\mu(\Omega)$  follows closely every  $\mu_{CT}(\Omega)$ . *The entire dipole moment surface is, thus, primarily governed by charge transfer in the  $X = Cl$  reaction with little influence from the internal polarization of the individual atoms.*

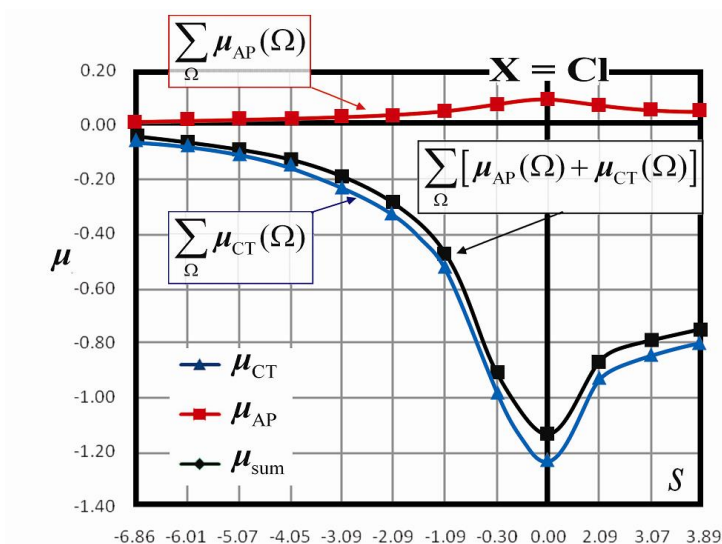


**Figure 9**

Decomposition of the system's total dipole moment of the  $\text{CH}_4 + \cdot\text{Cl} \rightarrow \text{CH}_3 + \text{HCl}$  system as a function of the reaction coordinate,  $\mu = \mu(s)$ , as the vector sum of an atomic polarization terms [itself the vector sum of atomic dipolar polarizations,  $\sum_{\Omega} \mu_{AP}(\Omega)$ ], and a charge transfer terms which is composed of the vector sum of individual atomic charge transfer terms [ $\sum_{\Omega} \mu_{CT}(\Omega)$ ]. (All quantities are in atomic units).

The electron density plots in **Figure 11** are the  $X = Cl$  equivalent plots to those in **Figure 8** for  $X = F$ . At the far reactant side, the coordinate  $s = -6.86$  au corresponds to a system whereby the distance between the C and H is  $1.082 \text{ \AA}$  and that between the H

and Cl is 2.701 Å, the latter smaller than the sum of the van der Waals radii [46] (3 Å). At this stage in the reaction, the hydrogen is basically bound to the carbon only [ $\rho_{\text{bcp}}(\text{H}|\text{Cl}) = 0.007$  au, and  $\rho_{\text{bcp}}(\text{C}|\text{H}) = 0.282$  au, the latter figure indicate that the C–H bonding is practically identical to that between C and each of the three umbrella hydrogen atoms for which  $\rho_{\text{bcp}}(\text{C}|\text{H}) = 0.283$  au]. At this geometry, there is neither charge transfer nor a dipole moment in the system. The methane subsystem at this reaction coordinate is similar (but not identical) to the free methane molecule (compare the individual charges and dipole moment components in **Figures 5** and **11**).

The middle density plot of **Figure 11** is of the transition state system, which occurs at the same reaction coordinate as the peak in the dipole moment,  $s = 0.00$  au. This peak dipole moment, while significant, is less pronounced than that of the X = F reaction and reaches the value of  $-1.141$  au, primarily due to CT terms. At the TS, the hydrogen shares a bond paths with both of its neighbors, the carbon [ $d(\text{C}–\text{H}) = 1.379$  Å] and the chlorine atoms [ $d(\text{H}–\text{Cl}) = 1.446$  Å]. The densities at the bond critical points are:  $\rho_{\text{bcp}}(\text{H}|\text{Cl}) = 0.153$  au,  $\rho_{\text{bcp}}(\text{C}|\text{H}) = 0.120$  au, and is  $\rho_{\text{bcp}}(\text{C}|\text{H}') = 0.291$  au for the three umbrella C–H methyl bonds. Just as in the system with peak dipole moment for the X = F reaction, it is exclusively the CT term (primarily that of the Cl) that gives rise to the deep well in the dipole moment surface (**Figure 11**). In contrast with the corresponding X = F system, the AP term of Cl is far less important [ $\mu_{\text{AP}}(\text{Cl}, s = 0.00 \text{ au}) = + 0.001$  au, *i.e.*, practically zero since it is of the order of magnitude of the integration error) as opposed to  $\mu_{\text{AP}}(\text{F}, s = 0.40 \text{ au}) = + 0.163$  in the case of the F atom. The three CT terms are aligned and reinforce each other, almost unopposed by the two small  $\mu_{\text{AP}}$  of CH<sub>3</sub> and

of H to yield a TS dipole of  $-1.141$  au, which is, again, primarily a CT dipole ( $-1.237$  au) opposed by only  $+0.095$  au of AP contribution.

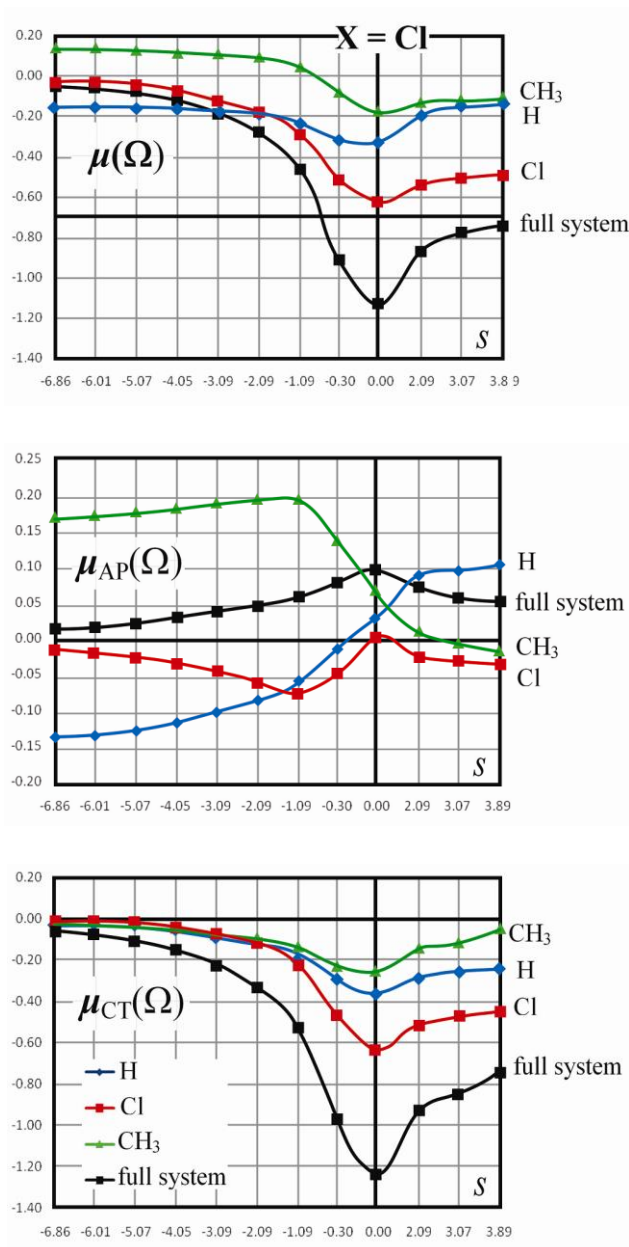


**Figure 10**

Atomic and methyl group total dipolar polarizations,  $\mu(\Omega)$ , and their respective component internal atomic (or group) polarization terms  $\mu_{\text{AP}}(\Omega)$  and charge transfer terms  $\mu_{\text{CT}}(\Omega)$ , as functions of the coordinate ( $s$ ) of the  $\text{CH}_4 + \text{Cl} \rightarrow \text{CH}_3 + \text{HCl}$  reaction. (All quantities are in atomic units).

One important conclusion is that it is at the products side where most of the difference between the  $X = \text{Cl}$  and the  $X = \text{F}$  lies. In the case of  $X = \text{F}$ , the system's dipole is in large part the result of the vector addition of a large CT dipole, primarily belonging to F, but not without an insignificant contribution of a CT contribution from the H as well. At this stage in the reaction, the hydrogen atom has essentially been detached from a trailing  $\bullet\text{CH}_3$  radical forming an HCl molecule (bottom panel of **Figure 11**). This occurs near  $s = 3.89$  when  $\rho_{\text{bcp}}(\text{H}|\text{Cl}) = 0.241$  au and  $\rho_{\text{bcp}}(\text{C}|\text{H}) = 0.019$  au with separations of 1.282 and 2.169 Å, respectively. The CT term ( $\mu_{\text{CT}} = -0.797$  au) is again the principal determinant of the overall dipole moment ( $\mu = -0.798$  au) opposed by only as little as +0.051 of  $\mu_{\text{AP}}$  dipole.



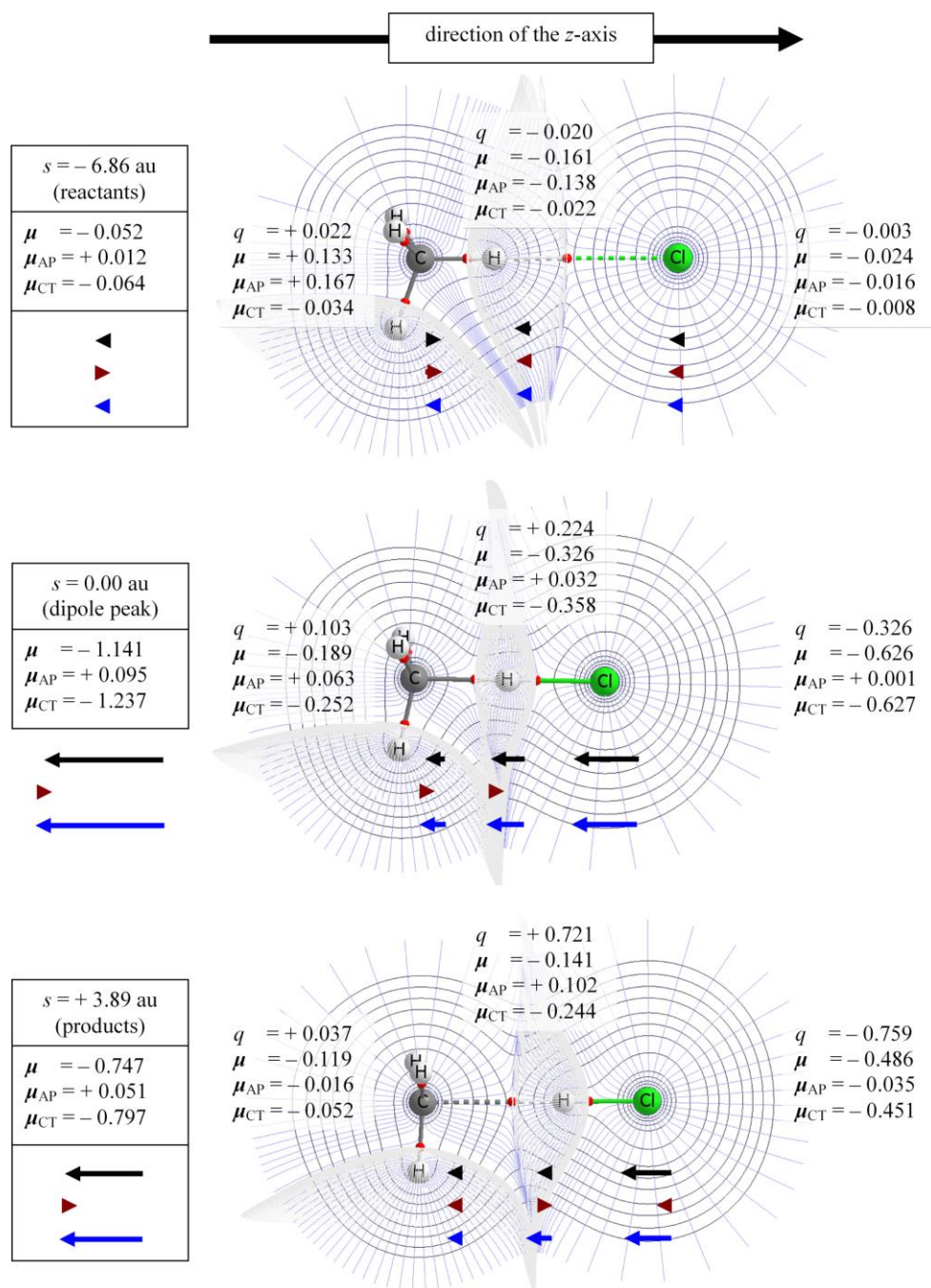


**Figure 11**

Electron density contour maps with their associated gradient vector fields in one of the three H-C-H-Cl planes along with the three interatomic surfaces intersecting that plane for the  $\text{CH}_4 + \cdot\text{Cl} \rightarrow \text{CH}_3 + \text{HCl}$  system as a function of the reaction coordinate ( $s$ ). (The values of the contours from the outside isodensity contour inward are: 0.001, 0.002, 0.004, 0.008, 0.02, 0.04, 0.08, 0.2, 0.4, 0.8, 2.0, 4.0, 8.0 au). The numerical labels from

left to right refer to the methyl group ( $\text{CH}_3$ ), H, and Cl, listing for each its respective charge ( $q$ ), dipole ( $\mu$ ), and the two components of its dipoles [the atomic polarization term ( $\mu_{\text{AP}}$ ) and the charge transfer term ( $\mu_{\text{CT}}$ )]. The respective total system dipole moment and its two components are listed in the middle box at the far left. (All numerical entries in this figure are in atomic units). Below each of the three subsystems ( $\text{CH}_3$ , H, and Cl) is a display of the direction and relative magnitude of the dipole moment along the  $z$ -axis ( $\mu$  = top/black,  $\mu_{\text{AP}}$  = middle/brown-red, and  $\mu_{\text{CT}}$  = bottom/blue). (The key interatomic distance  $d(\text{H}_3\text{C}\dots\text{H})/d(\text{H}\dots\text{Cl})$  in Å are: 1.082/ 2.701 at  $s = -6.86$  au; 1.379/1.446 at  $s = 0.00$ , and 2.169/1.282 at  $s = 3.89$ . In methane  $d(\text{C-H}) = 1.0830$ , and in HCl  $d(\text{H-Cl}) = 1.2703$  at the level of theory used in this work).

## 2.6. Conclusion

A system's dipole moment can be partitioned into origin-independent atomic contributions that arise from the transfer of charge between interacting atoms and also from the resulting distortion of the atomic electron density departing from spherical symmetry. The dipole moment of an interacting system is partitioned in terms of its composing atomic and group contributions. It is found that, with the abstraction of the hydrogen atom in the head-on collinear reaction of a halogen atom (F, Cl) with methane, the charge transfer (CT) term is the most dominant in governing the evolution and the depth of the well in the dipole moment surface. This dominance is more pronounced in the case of the more electronegative and more compact F compared to the less electronegative more diffuse Cl. It is found that for the more polarizable Cl, the extremum in the CT term coincides exactly with the position of the transition state on the reaction path, whereas for the more compact and harder F, this extremum is delayed into the products region shortly after the transition state has been reached. Further studies are needed to formulate rules of thumb in the design of reacting systems that extremize the peaks in the reacting system dipole moment in order to provide an extra layer of control

on the kinetics of the reaction through the exploitation of the permanent dipole-laser interaction as has been previously demonstrated [17,18].

The evolution of the system's dipole and polarizability that accompany the excursions of a reacting system on its potential energy landscape are keys to the control of the kinetics and thermodynamics of the reaction through their constructive or destructive interferences when coupled with external fields [Eq. (1)]. The effect of varying one of the reactants on dipole and polarizability surfaces, and hence on the laser control of reactions as predicted by Eq. (1), and the origins and enhancement or competition of polarizability with the CT dipole interactions in laser-molecule interactions will be the subject of future investigation.

## References

- (1) M. Shapiro, P. Brumer; *Principles of the Quantum Control of Molecular Processes*; Wiley - Inter: New York, **2003**.
- (2) V. S. Letokhov; *Laser Control of Atoms and Molecules*; Oxford University Press: Oxford UK, **2007**.
- (3) H. H. Telle; A. G. Ureña, R. J. Donovan; *Laser Chemistry: Spectroscopy, Dynamics and Applications*; John Wiley and Sons, Ltd.: Chichester, West Sussex, UK, **2007**.
- (4) P. Schmelcher, W. E. Schweizer; *Atoms and Molecules in Strong External Fields*; Plenum Press: New York, **2010**.
- (5) M. Mohan; Ed. *Atoms and Molecules in Laser and External Fields*; Alpha Science Ltd.: Oxford, UK, **2008**.
- (6) G. G. Paulus, F. Lindner, H. Walther, A. Baltuska, E. Goulielmakis, M. Lezius, F. Krausz; Measurement of the phase of few-cycle laser pulses. *Phys. Rev. Lett.* **2003**, *91*, 253004\_1-4.
- (7) V. S. Yakovlev, P. Dombi, G. Tempea, C. Lemell, J. Burgdorfer, T. Udem, A. Apolonski; Phase-stabilized 4-fs pulses at the full oscillator repetition rate for a photoemission experiment. *Appl. Phys. B* **2003**, *76*, 329-332.
- (8) S. Chelkowski, A. D. Bandrauk; Sensitivity of spatial photoelectron distributions to the absolute phase of an ultrashort intense laser pulse. *Phys. Rev. A* **2002**, *65*, 061802\_1-4.
- (9) S. Chelkowski, A. D. Bandrauk, A. Apolonski; Phase-dependent asymmetries in strong-field photoionization by few-cycle laser pulses. *Phys. Rev. A* **2004**, *70*, 013815\_1-9.
- (10) S. Chelkowski, A. D. Bandrauk, A. Apolonski; Measurement of the carrier-envelope phase of few-cycle laser pulses by use of asymmetric photoionization. *Opt. Lett.* **2004**, *29*, 1557-1559.
- (11) A. E. Orel, W. H. Miller; Infrared laser induced chemical reactions. *Chem. Phys. Lett.* **1978**, *57*, 362-363.
- (12) A. E. Orel, W. H. Miller; Infrared laser enhancement of chemical reactions via collision induced absorption. *J. Chem. Phys.* **1979**, *70*, 4393-4399.
- (13) A. E. Orel, W. H. Miller; Classical model for laser-induced non-adiabatic collision processes. *J. Chem. Phys.* **1980**, *73*, 241-246.

- (14) T. T. Nguyen-Dang, A. D. Bandrauk; Molecular dynamics in intense laser fields. I. One-dimensional systems in infrared radiation. *J. Chem. Phys.* **1983**, *79*, 3256-3268.
- (15) P. Dietrich, P. B. Corkum; Ionization and dissociation of diatomic molecules in intense infrared laser fields. *J. Chem. Phys.* **1992**, *97*, 3187-3198.
- (16) A. Conjusteau, A. D. Bandrauk, P. B. Corkum; Barrier suppression in high intensity photodissociation of diatomics: Electronic and permanent dipole moment effects. *J. Chem. Phys.* **1997**, *106*, 9095-1004.
- (17) A. D. Bandrauk, E. S. Sedik, C. F. Matta; Effect of absolute laser phase on reaction paths in laser-induced chemical reactions. *J. Chem. Phys.* **2004**, *121*, 7764-7775.
- (18) A. D. Bandrauk, E. S. Sedik, C. F. Matta; Laser control of reaction paths in ion-molecule reactions. *Mol. Phys.* **2006**, *104*, 95-102.
- (19) M. Y. Ivanov, D. R. Matusek, J. S. Wright; Altered reaction dynamics: Lowered barriers and bound states induced by intense infrared laser fields. *Chem. Phys. Lett.* **1996**, *255*, 232-237.
- (20) F. O. Kannemann, A. D. Becke; Atomic volumes and polarizabilities in density-functional theory. *J. Chem. Phys.* **2012**, *136*, 034109\_1-5.
- (21) J. C. Polanyi; Proposal for an infrared maser dependent on vibrational excitation. *J. Chem. Phys.* **1961**, *34*, 347-348.
- (22) M. Cheng, Y. Feng, Y. Du, Q. Zhu, W. Zheng, G. Czako, J. M. Bowman; Probing the entrance channels of the  $X + CH_4 \rightarrow HX + CH_3$  ( $X = F, Cl, Br, I$ ) reactions via photodetachment of  $X^-CH_4$ . *J. Chem. Phys.* **2011**, *134*, 191102\_1-4.
- (23) R. F. W. Bader; *Atoms in Molecules: A Quantum Theory*; Oxford University Press: Oxford, U.K., **1990**.
- (24) P. L. A. Popelier; *Atoms in Molecules: An Introduction*; Prentice Hall: London, **2000**.
- (25) C. F. Matta, R. J. Boyd; *The Quantum Theory of Atoms in Molecules: From Solid State to DNA and Drug Design*; Wiley-VCH: Weinheim, 2007.
- (26) R. F. W. Bader, T. A. Keith; Properties of atoms in molecules: magnetic susceptibilities. *J. Chem. Phys.* **1993**, *99*, 3683-3693.
- (27) R. F. W. Bader, C. F. Matta; Properties of atoms in crystals: Dielectric polarization. *Int. J. Quantum Chem.* **2001**, *85*, 592-607.

- (28) R. F. W. Bader; Dielectric polarization: A problem in the physics of an open system. *Mol. Phys.* **2002**, *100*, 3333-3344.
- (29) R. F. W. Bader, D. Bayles, G. L. Heard; Properties of atoms in molecules: transition probabilities. *J. Chem. Phys.* **2000**, *112*, 10095-10105.
- (30) T. A. Keith; Chapter 3 in: *The Quantum Theory of Atoms in Molecules: From Solid State to DNA and Drug Design*; C. F. Matta, R. J. Boyd; (Eds), Wiley-VCH: Weinheim, **2007**; pp. 61-95.
- (31) C. Møller, M. S. Plesset; Note on an approximation treatment for many-electron systems. *Phys. Rev.* **1934**, *46*, 618-22.
- (32) C. Gonzalez, H. B. Schlegel; An improved algorithm for reaction path following. *J. Chem. Phys.* **1989**, *90*, 2154-2161.
- (33) M. J. Frisch, G. W. Trucks, H. B. Schlegel, G. E. Scuseria, M. A. Robb, J. R. Cheeseman, V. G. Zakrzewski, J. A. Jr. Montgomery, R. E. Stratmann, J. C. Burant; *et al.* Gaussian98, Revision A.9 (Gaussian Inc., Pittsburgh PA, **1998**).
- (34) D. C. Young; *Computational Chemistry: A Practical Guide for Applying Techniques to Real World Problems*; Wiley-Interscience: New York, **2001**.
- (35) C. F. Matta; How dependent are molecular and atomic properties on the electronic structure method? Comparison of Hartree-Fock, DFT, and MP2 on a biologically relevant set of molecules. *J. Comput. Chem.* **2010**, *31*, 1297-1311.
- (36) K. Fukui; A formulation of the reaction coordinate. *J. Phys. Chem.* **1970**, *74*, 4161-4163.
- (37) K. Fukui; The path of chemical reactions - The IRC approach. *Acc. Chem. Res.* **1981**, *14*, 363-368.
- (38) T. A. Keith; AIMALL (Version 11.05.16, Professional) (aim@tkgristmill.com, **2011**).
- (39) J. W. Hovick, J. C. Poler; Misconceptions in sign conventions: Flipping the electric dipole moment. *J. Chem. Edu.* **2005**, *82*, 889.
- (40) C. A. Coulson; *Electricity*; Oliver and Boyd: London, **1961**.
- (41) A. Szabo, N. S. Ostlund; *Modern Quantum Chemistry: Introduction to Advanced Electronic Structure Theory*; Dover Publications, Inc.: New York, **1989**.

- (42) G. A. Russell; in: Free Radicals; J. K. Kochi; (Ed.), Wiley-Interscience: New York, **1973**.
- (43) J. K. Kerr; in: Free Radicals; J. K. Kochi; (Ed.), Wiley-Interscience: New York, **1973**.
- (44) M. L. Poutsma; in: Free Radicals; J. K. Kochi; (Ed.), Wiley-Interscience: New York, **1973**.
- (45) F. Cortés-Guzmán, R. F. W. Bader; Role of functional groups in linear regression analysis of molecular properties. *J. Phys. Org. Chem.* **2004**, *17*, 95-99.
- (46) L. Pauling; *The Nature of the Chemical Bond, (Third Ed.)*; Cornell University Press: Ithaca, N.Y., **1960**.

## Chapter 3

# Physicochemical properties of exogenous molecules correlated with their biological efficacy as protectors against carcinogenesis and inflammation<sup>3</sup>

### Summary

A large number of molecules referred to here as M, several of which are extracted from plants, belong to different chemical classes and exhibit chemoprotective activity against carcinogenesis and inflammation in rodents and *in vitro* cell culture. The aim of this article is to review and analyse our previous investigations on linear correlations observed between physicochemical parameters of the tested molecules M and their biological efficacies measured *in vivo* and/or *in vitro*. The principal physicochemical parameters studied characterise the energy required to oxidise M into  $M^{*+}$ ,  $E(M^{*+}/M)$ , namely its first vertical ionization potential (IP), and the energy liberated by the addition of an electron to M, *i.e.*, its vertical electron affinity (EA). These physicochemical properties were determined experimentally using diverse techniques and theoretically using mainly semiempirical (AM1) and density functional theory (DFT) quantum mechanical methods.

---

<sup>3</sup> This Chapter is based on the paper: R. V. Bensasson, S. Sowlati-Hashjin, V. Zoete, D. Dauzonne and C. F. Matta "Physicochemical Properties of exogenous molecules correlated with their biological efficacy as protectors against carcinogenesis and inflammation" *Int. Rev. Phys. Chem.* Published online, In press, <http://dx.doi.org/10.1080/0144235X.2013.767669> (2013).



### 3.1. Introduction

The aim of this paper is to examine previously reported correlations of physicochemical parameters of phenol and flavone derivatives, phenylpropenoids, benzoic and salicylic acids, and triterpenoids with their anti-carcinogenic and anti-inflammatory activities in the light of new theoretical results. The biological activities examined include: (i) cancer chemoprevention efficacy *in vivo* [1,2] (ii) induction of quinone reductase, a prototypic cancer-protective enzyme [3-6], (iii) inhibition of topoisomerases involved in DNA replication and transcription and known as targets for anticancer drugs [7], and (iv) quenching of inflammation, a critical root of tumour progression [6,8-11].

The physicochemical parameters used as quantitative structure-activity (QSAR) descriptors of the protective exogenous molecules, M, determined experimentally and quantum mechanically include: (i) The first vertical electron affinity (EA) and the electrophilicity index ( $\omega$ ) which reflect the capability of M to accept an electron, *i.e.*, the energy liberated when an electron is added to M, and (ii) the energy required to detach an electron from the molecule, *i.e.*, namely its first vertical ionisation potential (IP) which measures the ease of oxidation of M into the corresponding radical cation  $M^{\bullet+}$ .

This paper also addresses the question of the interconnection with one another between the experimental and theoretical physicochemical parameters of the protective molecules M.

## 3.2. Methods

### 3.2.1. Biological methods

The experimental methods used for determining the biological efficacies of the families of protective compounds inhibitors of carcinogenesis and of inflammation are reported in the cited literature.

### 3.2.2. Computational methods

#### 3.2.2.1. *Semiempirical quantum mechanical calculations*

Methods used to calculate electron affinity (EA), electrophilicity index ( $\omega$ ), energies of the highest occupied molecular orbital  $E(\text{HOMO})$ , and energies of the lowest unoccupied molecular orbital  $E(\text{LUMO})$  of the protective exogenous molecules M are also detailed in the appropriate articles quoted in the text. However some important aspects of these calculations are emphasised below.

The  $E(\text{HOMO})$  in eV of the different molecules under study were calculated by the semiempirical AM1 quantum mechanical approximation [12] carried out with Hyperchem Ver. 4,6,7.51 programmes [13]. The restricted Hartree-Fock (RHF) formalism [14,15] was used to complete these calculations. Molecular geometries were optimized using Polak-Ribiere minimisation algorithm.

According to the general Koopman's theorem [14,16], within Hartree-Fock theory, the value of  $E(\text{HOMO})$  is a measure of the first ionisation potential of M, *i.e.*, the energy required to remove an electron from the molecule in the gas-phase or the oxidation potential of M in solution  $E(\text{M}^{*+}/\text{M})$ . Moreover, it is important to underline that although the redox potentials can be strongly affected by the surrounding medium, linear correlations are observed between  $E(\text{HOMO})$  of a series of related molecules M

calculated in the gas phase and their ionisation potential measured in the gas phase or their one-electron oxidation potential,  $E(M^{*+}/M)$ , measured in different solvents [17].

The electron affinity of molecules M was determined by calculations of the  $E(\text{LUMO})$  as well as the energy  $E(\text{HOMO})$  of the  $M^{\cdot-}$  anions, since it can be considered as a more precise way to calculate the electron affinity of the neutral molecule M than the calculation of the energy of the lowest unoccupied molecular orbital  $E(\text{LUMO})$  of M.

### 3.2.2.2. *Calculations of the vertical ionisation potential (IP) and of the electron affinity (EA) by density functional theory (DFT)*

Density functional theory (DFT) [18,19] is a widely used approximation to solve the Schrödinger equation and accounting for electron Coulombic correlation at an accuracy comparable with the much more expensive post-Hartree-Fock methods but at a significantly slower scaling with the size of the calculation. DFT is used to generate the new data in the present article.

Becke's hybrid exchange functional and Lee-Yang-Parr correlation functional [20,21] were used in the calculation along with a 6-31+G\*\* Pople basis set, i.e., the level of theory in standard notation is the DFT-B3LYP/6-31+G\*\*//B3LYP/6-31+G\*\*, where the double slash indicates that full unconstrained geometry optimisations were carried out at the same level of theory before the calculation of the final energies. The geometry energy minimisations for all closed-shell species studied by DFT were each followed by a harmonic frequency calculation to confirm that the given optimised structure is a true minimum on its potential energy surface. No imaginary frequencies have been found confirming that all optimised structures studied in this work are all stable minima. All numerical DFT computations and frequency calculations were performed using the

Gaussian 09 program [22].

The DFT-B3LYP/6-31+G\*\*//B3LYP/6-31+G\*\* level of theory has been chosen for this work since it has been demonstrated to outperform other functionals for the theoretical estimation of ionization potentials [23,24].

The unrestricted DFT-B3LYP formulation was employed with the same basis set for computations on open shell radical-ions. No geometry optimisations were conducted on the open-shell species. Instead, a single-point open-shell calculation is conducted at the same optimised geometry of the respective closed-shell species, *i.e.*, invoking the sudden approximation since the time scale of electron attachment or detachment is several orders of magnitude smaller than that necessary for the relaxation of the nuclear configuration. In other words, the ionisation events here are all vertical.

For open shell species, the spin contaminations as measured by the deviation of  $\langle S^2 \rangle$  from the ideal value  $s(s+1) = 0.75$  in the case of doublets ( $s = 1/2$ ) has been found in all cases to be significantly lower than the recommended 10% deviation [25], with an average deviation of 1.46% and a maximal deviation of 3.05% for a total of 128 open-shell calculations.

Vertical ionisation potentials (IP) are calculated in this work by subtracting the energy of neutral molecules from the energy of the corresponding cations. That is, we calculate what is known as the ( $\Delta$ IP) according to:

$$\text{IP} = E(\text{M}^{+\bullet}) - E(\text{M}) \quad (1)$$

where  $E(\text{M}^{+\bullet})$  is the total electronic energy of the radical cation calculated at the same geometry as the neutral molecule, and  $E(\text{M})$  is the corresponding total energy of the neutral closed-shell molecule at its equilibrium geometry.

Similarly, the vertical electron affinities ( $\Delta EA$ ) were calculated according to:

$$EA = E(M) - E(M^{\cdot-}) \quad (2)$$

where the symbols have obvious meaning.

Vertical IP and EA are calculated which means for radicals, frequency calculations are not performed. To be consistent to radicals, ZPE corrections are not included for neutral ones either.

### 3.2.3. Data treatment and analyses

#### 3.2.3.1. Relation of IP, $E(HOMO)$ and the oxidation potential at neutral pH

Comparing the  $E(HOMO)$  calculated by semiempirical AM1 quantum mechanical calculations and IP calculated by DFT method using B3LYP/6-31+G\*\* basis set, will be discussed in more detail in the conclusion section. However, we underline now the fact that, on one hand  $E(HOMO)$  and on the other both IP and the oxidation potential measured electrochemically at pH=7 [ $E_7(M^{+}/M)$ ] are inverse functions. In other words, the signs of the  $E(HOMO)$  are negative, while those of the IP and the  $E_7$  are positive, and both absolute values decrease when the molecule is more reducing (*i.e.*, when the molecule releases electrons more easily).

#### 3.2.3.2. Biological quantitative structure-activity relationships (QSAR)

In biological QSAR between physicochemical properties of a series of compounds determined *ex vivo* and their biological activities measured *in vivo* or in cellular systems, linear correlations can be observed, when these investigations are carried out on congeners of the same general structure [26,27]. The correlation coefficients  $r$  of the linear correlations observed were calculated by the curve fitting analysis of the

Kaleidagraph 3.6.4 graphing software [28].

### **3.3. Results and discussion**

#### **3.3.1. Cancer chemoprevention efficacy *in vivo***

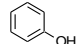
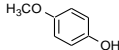
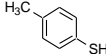
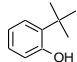
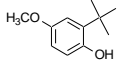
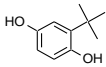
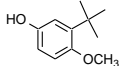
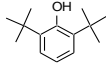
Two studies of cancer chemoprevention *in vivo* were previously carried out by members of our group [1,2]. The first study dealt with the inhibitory effects of phenolic derivatives (P) on abnormal proliferation of cells (called also *neoplasia*) in the forestomach of mice, determined quantitatively by Wattenberg *et al.* [29], the second with the inhibitory effects of a series of 3-nitroflavones (NF) on the onset and progression of aberrant crypt foci (ACF) in the rat colon, ACF being precancerous colon lesions induced by subcutaneous injections of azoxymethane in rats [2].

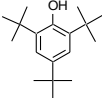
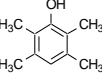
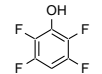
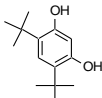
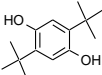
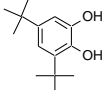
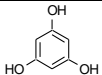
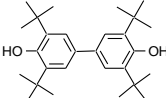
##### *3.3.1.1. Correlations between redox properties of phenolic derivatives (P) and their inhibitory effects on mice neoplasia*

Wattenberg *et al.* [29] have determined quantitatively the inhibitory effects of 22 synthetic phenolic compounds (P) added to the diet on benzo(a)pyrene-induced neoplasia of the forestomach of mice. The chemical names and the structures of these phenolic derivatives, the 3 physicochemical parameters  $\log k(^1\text{O}_2+\text{P})$ ,  $E(\text{HOMO})$ , and IP of P, as well as the ratio  $R$  of the number of tumours per mouse in the treated group over the number of tumours per mouse in the unprotected group are listed in Table 1 along with their Roman numerical numbering used by Wattenberg *et al.* [29]

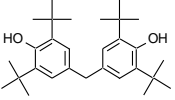
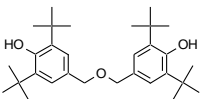
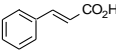
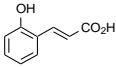
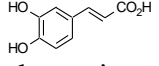
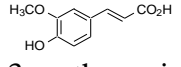
**Table 1**

Physicochemical parameters:  $\log k$  ( $^1\text{O}_2 + \text{P}$ ),  $E(\text{HOMO})$  and IP of phenol derivatives (P) as well as the ratio  $R$  of the number of tumours per mouse in the treated group over the number of tumours per mouse in the unprotected group measured by Wattenberg *et al.* [29].

<b>P<sup>(a)</sup></b>	<b>structures</b>	<b><math>\log k^{(b)}</math></b>	<b><math>E(\text{HOMO})^{(c)}</math></b>	<b>IP<sup>(d)</sup></b>	<b>R</b>
<b>I</b>	 Phenol	4.40	-9.1147	8.46	0.88
<b>II</b>	 <i>p</i> -Methoxyphenol	6.75	-8.6490	7.70	0.22
<b>III</b>	 4-Methylmercaptophenol		-7.9850		0.67
<b>IV</b>	 2- <i>tert</i> -Butylphenol	5.40	-8.9651	8.12	0.60
<b>V</b>	 3- <i>tert</i> -Butyl-4-hydroxyanisole		-8.5279	7.47	0.54
<b>VI</b>	 <i>tert</i> -Butylhydroquinone		-8.6335	7.64	0.58
<b>VII</b>	 2- <i>tert</i> -Butyl-4-hydroxyanisole	7.34	-8.5327	7.45	0.30
<b>VIII</b>	 2,6-Di- <i>tert</i> -butylphenol	5.41	-8.8051	7.76	0.52

<b>P<sup>(a)</sup></b>	<b>structures</b>	<b>log <i>k</i><sup>(b)</sup></b>	<b><i>E</i>(HOMO)<sup>(c)</sup></b>	<b>IP<sup>(d)</sup></b>	<b>R</b>
<b>IX</b>	 2,4,6-Tri- <i>tert</i> -butylphenol	7.40	-8.6335		1.23
<b>X</b>	 2,3,5,6-Tetramethylphenol		-8.7338		0.79
<b>XI</b>	 2,3,5,6-Tetrafluorophenol	4.48	-9.8744	7.43	0.73
<b>XII</b>	 4,6-Di- <i>tert</i> -butylresorcinol	5.54	-8.6308	7.50	0.88
<b>XIII</b>	 2,5-Di- <i>tert</i> -butylhydroquinone		-8.5224	7.33	1.28
<b>XIV</b>	 3,5-Di- <i>tert</i> -butylcatechol	7.40	-8.6942	7.52	0.46
<b>XV</b>	 Phloroglucinol (or 3,5-Dihydroxyphenol)		-9.2328	8.35	0.84
<b>XVI</b>	 4,4-Bis(2,6-di- <i>tert</i> -butylphenol)			6.72	0.84



<b>P<sup>(a)</sup></b>	<b>structures</b>	<b>log <i>k</i><sup>(b)</sup></b>	<b><i>E</i>(HOMO)<sup>(c)</sup></b>	<b>IP<sup>(d)</sup></b>	<b>R</b>
<b>XVII</b>	 Di-(3,5-di- <i>tert</i> -butyl-4-hydroxyphenol)methane			6.95	0.88
<b>XVIII</b>	 Di-(3,5-di- <i>tert</i> -butyl-4-hydroxybenzyl)ether			7.05	0.88
<b>XIX</b>	 Cinnamic acid	3.53	-9.4768	8.60	0.92
<b>XX</b>	 2-Hydroxycinnamic acid	4.32	-9.1806	8.25	0.66
<b>XXI</b>	 3,4-Dihydroxycinnamic acid	5.73	-9.0350	7.91	0.62
<b>XXII</b>	 4-Hydroxy-3-methoxycinnamic acid	5.54	-8.9063	7.73	0.60

<sup>(a)</sup> P are represented in Roman numerals as in Chart 1 of Wattenberg *et al.* [29] and also as listed along with their chemical names in Table 1.

<sup>(b)</sup> The log *k* have been previously determined by flash photolysis for eleven P, the only compounds commercially available at that time among the protective molecules ref. [1].

<sup>(c)</sup> *E*(HOMO) have been calculated by semiempirical AM1 method. Thirteen compounds appear as congeners. Nine compounds have been discarded for the following reasons: compounds IX and XIII are tumourigens (for these molecules the ratio *R* of the number of tumours per mouse in the treated group over those in the control unprotected group is larger than 1); compounds III and XI contain S or F elements making them non-congeners as well as compounds X, XII, XVI, XVII and XVIII which all possess large substituents.

<sup>(d)</sup> The IP have been calculated by DFT methods.

The methods to determine the 3 parameters used to express quantitatively the electron-donor property of P were (i) laser flash photolysis for  $\log k(^1\text{O}_2 + \text{P})$  where  $k$  is the second order rate constant for the quenching of singlet oxygen,  $^1\text{O}_2$ , by P, this parameter is linearly correlated with the ability of P to donate an electron, that is linearly correlated with the standard potential  $E(\text{P}^{*+}/\text{P})$ , called the oxidation potential of P or reduction potential of  $\text{P}^{*+}$ , as demonstrated theoretically and experimentally [5,30-35], (ii) the semiempirical quantum mechanical method AM1 for the energy of the highest occupied molecular orbital  $E(\text{HOMO})$  of P newly calculated as a measure of the first ionization potential of P in the gas-phase or the oxidation potential of P,  $E(\text{P}^{*+}/\text{P})$ , in solution phase as first proposed by Pullman and Pullman [17], (iii) the DFT method as described in the section 2.2.2 for IP, newly calculated vertical ionisation potential.

Out of the 22 phenolic compounds studied by Wattenberg *et al.* [29], 10 to 13 molecules were selected as congeners which could be examined for possible correlations between their physicochemical and cancer chemoprotection properties. The three physicochemical parameters  $\log k(^1\text{O}_2+\text{P})$ ,  $E(\text{HOMO})$ , and IP of P exhibit strong co-linearity according to the following linear regression equations:

$$\log k(^1\text{O}_2+\text{P}) = 47.64 + 4.70 E(\text{HOMO}) \quad [n = 11, r = 0.94] \quad (3)$$

$$\log k(^1\text{O}_2+\text{P}) = 30.07 - 3.08 \text{IP} \quad [n = 10, r = 0.93] \quad (4)$$

$$\text{IP} = -3.29 - 1.26 E(\text{HOMO}) \quad [n = 13, r = 0.95] \quad (5)$$

Such strong correlations interconnecting the three physicochemical parameters demonstrate that these parameters can be considered as equivalent.

These 3 physicochemical parameters exhibit similar linear correlations with the ratio  $R$  of the number of tumours per mouse in the treated group over those in the

control unprotected group:

$$\log k(^1\text{O}_2+\text{P}) = 8.60 - 5.26 R \quad [n = 11, r = 0.89] \quad (6)$$

$$E(\text{HOMO}) = - 8.16 - 1.24 R \quad [n = 13, r = 0.84] \quad (7)$$

$$\text{IP} = 6.96 + 1.61R \quad [n = 13, r = 0.84] \quad (8)$$

If molecules V and VI are excluded from the correlation on the basis of their *tert*iobutyl substitutions at *ortho* position of the phenol, the correlation coefficients are improved for both  $E(\text{HOMO})$  and IP correlations and the corresponding revised equations (7) and (8) become:

$$E(\text{HOMO}) = - 8.26 - 1.16 R \quad [n = 11, r = 0.92] \quad (7')$$

$$\text{IP} = 7.05 + 1.56 R \quad [n = 11, r = 0.89] \quad (8')$$

As an example of the correlations (6), (7), (8), (7') and (8') a diagram of the equation IP versus the ratio  $R$  is shown in Fig.1.

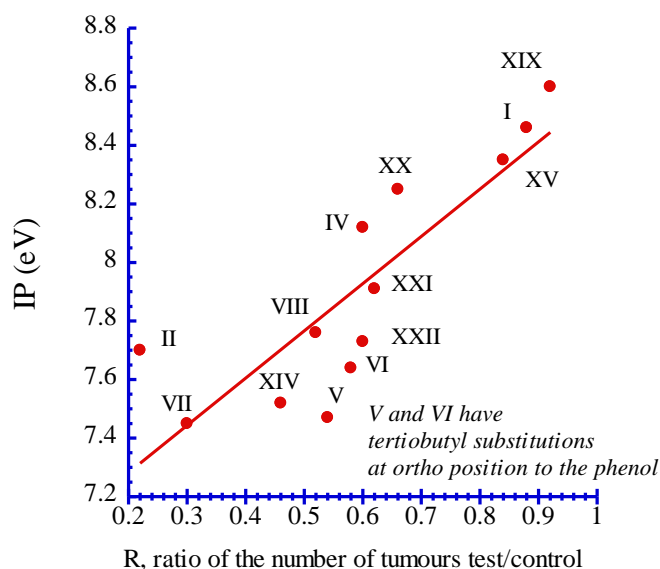


**Figure 1**

Correlation (8) between IP of the phenol derivatives P and the ratio  $R$  of the number of tumours per mouse in the treated group over those in the control unprotected group. Phenol derivatives P are represented in Roman numerals following the same numbering as in Chart 1 of Wattenberg *et al.* [29], correlation coefficient  $r = 0.84$  and increases to

$r=0.89$  if V and VI are discarded from the plot.

The correlations (6), (7), (8), (7') and (8') demonstrate a clear tendency: the smaller is the electron donor energy required to oxidise P, the greater its protection efficacy on benzo(a)pyrene-induced neoplasia of the forestomach of mice. A similar conclusion will be reached in the next example which deals with carcinogenesis inhibition in the rat colon by nitroflavones.

The mechanism of carcinogenesis by benzo(a)pyrene involves metabolic oxidation and covalent bonding to DNA *via* its epoxides [36]. The molecular mechanism of the chemoprotection by phenols is not yet completely understood. This mechanism might be partially related to the ability of phenolic derivatives to induce the activities of cancer-protective enzymes [37,38]. Such inductions of protective enzymes by P and other chemoprotective exogenous molecules will be discussed in a following section.

#### *3.3.1.2. Correlations between electron-donating ability of 3-nitroflavones (NF) and their inhibitory activity of the onset and progression of aberrant crypt foci (ACF) in rat colon*

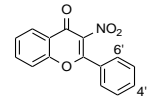
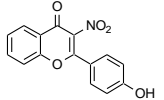
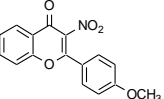
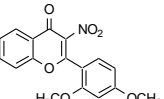
Many studies in patients with colon cancer, as well as in animal models, have shown a positive link between aberrant crypt foci (ACF) formation and colon tumour incidence. We had previously shown that the efficacy of chemoprotection against ACF formation and progression induced by azoxymethane is related to the electronic effects of substituents of the chemoprotective agents [2]. These agents were five 3-nitroflavones (NF1, NF2, NF3, NF5 and NF6) with different substituents at position 4' spanning a

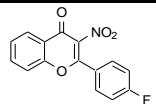
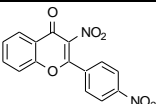
spectrum of Hammett constants ( $\sigma_p^+$ ) going from +0.79 for the electron-withdrawing group  $\text{NO}_2$ , to -0.92 for the electron donating group OH. Figure 2 shows the structure of these molecules and the values of the three physicochemical parameters characterizing their electron-donating property: Hammett constant ( $\sigma_p^+$ ),  $E(\text{HOMO})$  and IP.

For certain studies, in order to extend the range of electron-releasing propensity, we have added a sixth NF, namely, NF4, which has two electron-donating  $-\text{OCH}_3$  substituents at positions 4' and 6' (Table 2). It is difficult to assess the additivity of the Hammett constants of the doubly substituted agent NF4 (see pages 3-5 of [26]). In order to incorporate this new molecule in our NF series, we have calculated two other parameters,  $E(\text{HOMO})$  by the AM1 method and IP by the DFT method, expressing both the electron-donating ability of the six molecules (NF1-6) (Table 2).

**Table 2**

Inhibitory effects of six NF on biomarkers of angiogenesis **(i)** proliferation of human microvascular endothelial cells line HMEC-1 after 72h of incubation, expressed in IC<sub>50</sub> in  $\mu\text{M}$  in column, **(ii)** migration of endothelial cells HMEC-1 expressed in IC<sub>50</sub> in  $\mu\text{M}$  in column, and **(iii)** activity of the critical protease MMP-2, promoter of angiogenesis, expressed in % inhibition of MMP2 at 50 $\mu\text{M}$  in column, data of **(i)**, **(ii)**, and **(iii)** obtained from ref. [43], Hammett constants ( $\sigma_{\text{p}+}$ ),  $E(\text{HOMO})$  in eV, and IP in (eV)

NF	Structures	(i)	(ii)	(iii)	Hammett constants ( $\sigma_{\text{p}+}$ ) <sup>a</sup>	$E(\text{HOMO})$ in eV	IP in eV
NF1	 3-Nitroflavone	154	307	27.5	0	-9.9647	8.65
NF2	 4'-Hydroxy-3-nitroflavone	122	139	45.9	-0.92	-9.6790	8.34
NF3	 4'-methoxy-3-nitroflavone	93	> 100	49.4	-0.78	-9.5565	8.18
NF4	 2',4'-Dimethoxy-3-nitroflavone	19	5.2	73.2	-1.50	-9.3793	7.95

NF	Structures	(i)	(ii)	(iii)	Hammett constants ( $\sigma_{p+}$ ) <sup>a</sup>	$E(\text{HOMO})$ in eV	IP in eV
NF5	 4'-Fluoro-3-nitroflavone	130	n.d.	22.6	-0.07	-10.0109	8.71
NF6	 3,4'-Dinitroflavone	192	315	18.3	+0.79	-10.2912	9.07

<sup>a</sup> For NF1, NF2, NF3, NF5 and NF6 these  $\sigma_{p+}$  are taken from page 7 of [26], for NF6 the  $\sigma_{p+}$  was evaluated by extrapolation of equations (9) and (10).

$E(\text{HOMO})$  and IP values of our six NF correlate linearly to the corresponding Hammett constants of the substituents at position 4' of ring B by the equations:

$$E(\text{HOMO}) = -9.98 - 0.41 \sigma_p^+ \quad [n = 6, r = 0.97] \quad (9)$$

$$\text{IP} = 8.68 + 0.49 \sigma_p^+ \quad [n = 6, r = 0.97] \quad (10)$$

The linear correlations expressed by equations (9) and (10) allow us to calculate, by extrapolation, a  $\sigma_p^+$  value of  $-1.50$  for the double substitution by  $-\text{OCH}_3$  at 4' and 6' in NF4, the most reducing agent in our NF series.

Moreover  $E(\text{HOMO})$  and IP of the 6 NF are correlated with one another by the equation:

$$\text{IP} = -3.36 - 1.21 E(\text{HOMO}) \quad [n = 6, r = 1.00] \quad (11)$$

The linear correlations between the three physicochemical parameters, IP, Hammett constants  $\sigma_p^+$ , and  $E(\text{HOMO})$  have correlation coefficients  $r \geq 0.97$ , an indication of their statistical and predictive equivalence.

In a first assay (called onset or initiation assay, protocol A) the 3-nitroflavone (NF1), as well as the 4' -substituted hydroxy (NF2), methoxy (NF3), fluoro (NF5) and nitro (NF6)- 3-nitroflavones were continuously present in the diet. In a second assay (called post-initiation or progression, protocol B) the protective NF were given for a period of 4 weeks after the last injection of azoxymethane [2]. The animals were fed with two dose regimens of 3-nitroflavones: 63 ppm, 125 ppm, or no test compounds. For both protocols A and B, the percentages of inhibition plotted versus the Hammett substitution constants  $\sigma_p^+$  as well as the  $E(\text{HOMO})$  and IP of the five NF show linear correlations, the most efficient inhibition of aberrant crypt foci (ACF) being produced by the molecules with the most electron-donating substituents. The following



correlations were found for the % inhibitions of ACF versus the three physicochemical parameters,  $\sigma_p^+$ ,  $E(\text{HOMO})$ , and IP of the five NF for protocols A and B and the two dose regimens, 63 and 125 ppm:

*Inhibition of ACF onset (Protocol A) – 63 ppm*

$$\% \text{inhibition} = 15.2 - 18.3 \sigma_p^+ \quad [n = 5, r = 0.95] \quad (12)$$

$$\% \text{inhibition} = 411.6 + 39.67 E(\text{HOMO}) \quad [n = 5, r = 0.86] \quad (13)$$

$$\% \text{inhibition} = 305.7 - 33.9 \text{IP} \quad [n = 5, r = 0.86] \quad (14)$$

*Inhibition of ACF progression (Protocol B) – 63 ppm*

$$\% \text{inhibition} = 13 - 15.3 \sigma_p^+ \quad [n = 5, r = 0.88] \quad (15)$$

$$\% \text{inhibition} = 358.3 + 34.6 E(\text{HOMO}) \quad [n = 5, r = 0.83] \quad (16)$$

$$\% \text{inhibition} = 263.9.3 + 34.6 E(\text{HOMO}) \quad [n = 5, r = 0.83] \quad (17)$$

*Inhibition of ACF onset (Protocol A) – 125 ppm*

$$\% \text{inhibition} = 25.9 - 20.7 \sigma_p^+ \quad [n = 5, r = 0.91] \quad (18)$$

$$\% \text{inhibition} = 464.3 + 43.86 E(\text{HOMO}) \quad [n = 5, r = 0.81] \quad (19)$$

$$\% \text{inhibition} = 346.88 - 36.9 \text{IP} \quad [n = 5, r = 0.81] \quad (20)$$

*Inhibition of ACF progression (Protocol B) – 125 ppm*

$$\% \text{inhibition} = 22 - 23 \sigma_p^+ \quad [n = 5, r = 0.98] \quad (21)$$

$$\% \text{inhibition} = 531.8 + 51.04 E(\text{HOMO}) \quad [n = 5, r = 0.84] \quad (22)$$

$$\% \text{inhibition} = 395.7 - 43 \text{IP} \quad [n = 5, r = 0.84] \quad (23)$$

The correlation coefficients  $r$  are very similar for the correlations using either  $E(\text{HOMO})$  or IP and are satisfactory in all cases. However they are systematically lower than the  $r$  found for the correlations using the Hammett constants. The lower  $r$  found for  $E(\text{HOMO})$  and IP might be due to the fact that the parameters calculated by quantum

mechanical calculations introduce some approximations in the evaluation of the electron-donor property of the NF.

As an example of the 12 observed correlations (Eqs. 12-23), a plot of the equation (23) representing the % of inhibition of ACF progression versus the IP of the NF is shown in Figure 2.

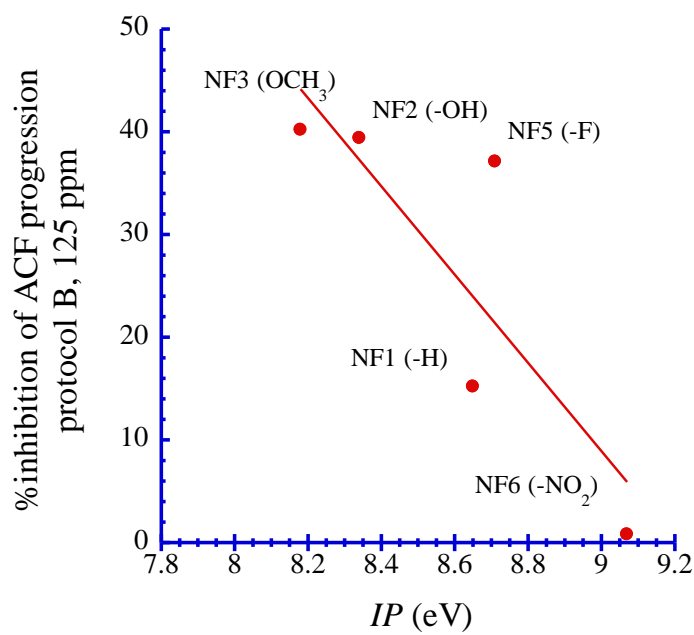


**Figure 2**

Linear correlation (23) observed between the % inhibition of rat colon ACF progression (protocol B) *versus* the IP of the NF, ( $r = 0.84$ ).

The similar degree of ACF inhibition reached in both protocols A (ACF onset) and B (ACF progression) underscores the therapeutic effect as well as the protective effect of these agents [2].

### 3.3.1.3. *Correlations between electron-donating ability of 3-nitroflavones (NF) and their efficacy to inhibit angiogenesis*

Folkman showed that an essential role of new blood-vessel formation, called angiogenesis, is required for invasive tumour growth and metastasis [39,40] and proposed cancer therapies using antiangiogenic agents [41,42]. Antiangiogenic effects of the six NF shown in Figure 2 have been observed by Lichtenberg [43]. The main conclusion of her study is that the smaller the absolute  $E(\text{HOMO})$  value of NF molecules, (*i.e.*, the lower their oxidation potential,  $E(\text{NF}^{++}/\text{NF})$ , the stronger is their electron donor power), the greater are the observed inhibitory effects on certain biomarkers of angiogenesis. These biomarkers include (*i*) proliferation of human microvascular endothelial (HMEC-1), human fibrosarcoma (HT1080), human colorectal carcinoma (HCT116) and non-invasive murine fibroblast (NIH3T3) cell lines, after 24h, 48h, and 72h of incubation (*ii*) migration of microvascular endothelial cells (HMEC-1), analysed by the wound-closure assay, and (*iii*) expression of a critical protease MMP-2 which functions as pathfinder for sprouting blood vessels and facilitates angiogenesis. Table 2 inserted in section 3.1.2 presents an overview of the main representative data of the antiangiogenic effects of the six NF [43,44].

As examples of the linear correlations observed by Lichtenberg between inhibition of angiogenesis biomarkers by the six NF and their  $E(\text{HOMO})$  calculated by AM1 method [43], are equations (24 - 26) shown below, as well as the equations corresponding to the linear correlations that we have observed with the two other new parameters  $\sigma_p^+$  and IP:

(i) The  $IC_{50}$  being the half-maximal concentration of the six NF (between 19  $\mu$ M for NF4 to 192  $\mu$ M for NF6) for inhibition of proliferation of microvascular endothelial cells (HMEC-1), after 72 h of incubation:

$$IC_{50} (\mu\text{M}) = -1487 - 163.6 E(\text{HOMO}) \quad [n = 6, r = 0.93] \quad (24)$$

$$IC_{50} (\mu\text{M}) = 146.16 + 67.33 \sigma_p^+ \quad [n = 6, r = 0.93] \quad (24')$$

$$IC_{50} (\mu\text{M}) = -1039 - 136.50 \text{IP} \quad [n = 6, r = 0.93] \quad (24'')$$

(ii) The  $IC_{50}$  being the half-maximal concentration of six NF (between 5.2 $\mu$ M for NF4 and 307  $\mu$ M for NF6) for inhibition of endothelial migration:

$$IC_{50} (\mu\text{M}) = -3319 + 357 E(\text{HOMO}) \quad [n = 6, r = 0.95] \quad (25)$$

$$IC_{50} (\mu\text{M}) = 242.13 + 142.92 \sigma_p^+ \quad [n = 6, r = 0.94] \quad (25')$$

$$IC_{50} (\mu\text{M}) = -2298.1 + 212.88 \text{IP} \quad [n = 6, r = 0.94] \quad (25'')$$

(iii) The %inhibition being the relative % of inhibition of activity of MMP-2, metalloprotease expressed in angiogenesis, observed at a concentration of 50  $\mu$ M of the six NF (between 73.2% for NF4 and 18.3% for NF6)

$$\% \text{inhibition} = 619 + 59.1 E(\text{HOMO}) \quad [n = 6, r = 0.96] \quad (26)$$

$$\% \text{inhibition} = 29.47 - 24.03 \sigma_p^+ \quad [n = 6, r = 0.94] \quad (26')$$

$$\% \text{inhibition} = 453.98 - 48.87 \text{IP} \quad [n = 6, r = 0.96] \quad (26'')$$

A diagram representing correlation (26''), as an example of these three sets of correlations, is shown in Figure 3, where the % of inhibition of MMP-2, metalloprotease expressed in angiogenesis, plotted versus IP representing the electron-donating ability of the six NF.

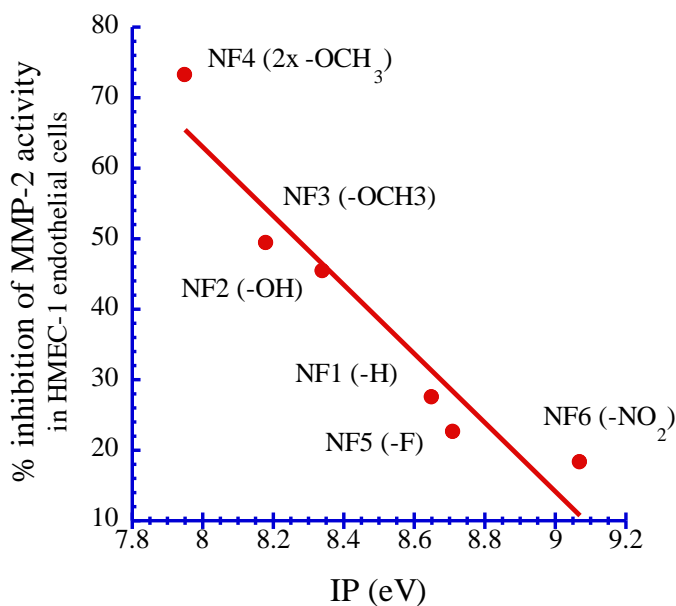


**Figure 3**

Linear correlation (Equation 26") observed by plotting the % of inhibition of the activity of the critical protease MMP-2 expressed during angiogenesis, at 50  $\mu$ M concentration of the 3-nitroflavones, in HMEC-1 endothelial cells *versus* the ionisation potential IP of the NF, ( $r = 0.95$ ).

In agreement with the strong correlations (9), (10) and (11), with  $r \geq 0.97$ , interconnecting the three parameters  $\sigma_p^+$ ,  $E(\text{HOMO})$ , and IP, very similar correlation coefficients are found between the inhibition of angiogenesis biomarkers and these three parameters.

The correlations (24 to 26") suggest that the antiangiogenic properties of our NF observed in cellular systems [43,44] might contribute to the inhibition in onset and in progression of the aberrant crypt foci (ACF) induced by azoxymethane that we studied in the rat colon [2].

### 3.3.2. Induction of a cancer-protective enzyme, NAD(P)H-quinone reductase 1 (NQO1)

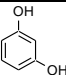
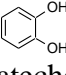
Among the lines of defense against cancer is the induction of phase 2 enzymes [45]. The cancer protective enzyme, NAD(P)H-quinone oxido reductase 1 (NQO1) is a prototypic phase 2 enzyme, that is induced coordinately with other phase 2 enzymes and has opened the way to a better understanding of the chemistry of inducers [45-47]. Induction of NQO1 by many distinct chemical classes, including diphenols (DP), phenylpropenoids (PP), flavonoids (F) and triterpenoids (TP) are analysed below through the correlations between their induction activity of NQO1 and their redox properties.

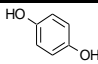
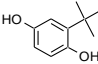
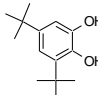
#### 3.3.2.1. Induction of NQO1 by diphenols (DP)

Talalay's team has demonstrated that 1,2 diphenols (catechols) and 1,4 diphenols (hydroquinones) that can undergo facile reversible oxidations to the corresponding quinones Q, are inducers of NQO1 but that 1,3 diphenols (resorcinols) that cannot be oxidized to quinones are not inducers [48]. Induction of the detoxification enzyme NAD(P)H-quinone oxidoreductase 1 (NQO1) was determined in murine Hepa 1c1c7 hepatoma cells. The structures of the five DP studied are indicated in Table 3.

**Table 3**

Structures, redox properties and NQO1 induction efficacy of diphenols DP.

Diphenols (DP)	$\log k^{(a)}$	$E_7^{(a)}$ (mV)	$E(\text{HOMO})^{(a)}$ (eV)	$\text{IP}^{(b)}$ (eV)	NQO1 activity <sup>(a)</sup>
 Resorcinol	5.81	810	-8.9820	8.18	0.9
 Catechol	6.23	530	-8.8841	8.13	1.4

Diphenols (DP)	$\log k^{(a)}$	$E_7^{(a)}$ (mV)	$E(\text{HOMO})^{(a)}$ (eV)	$\text{IP}^{(b)}$ (eV)	NQO1 activity <sup>(a)</sup>
 Hydroquinone	7.15	460	-8.7344	7.91	1.7
 <i>tert</i> -butylhydroquinone	7.74	260	-8.6120	7.64	2.1
 3,5-di- <i>tert</i> -butylcatechol	7.40	290	-8.6365	7.55	2.2

<sup>(a)</sup> Data obtained from Ref. [3].

<sup>(b)</sup> Newly calculated data by DFT method (see Section 3.2.2.2).

The demonstration, that only DP able to undergo oxidation to Q are inducers of NQO1, was followed by the realisation that many inducers, such as quinones Q were electrophilic Michael acceptors [38]. Induction of NQO1 is regulated by the Keap1-Nrf2-ARE system. Certain inducers oxidise two highly reactive cysteine residues of the sensor protein Keap1, resulting in disulfide formation and conformation change, which allows the transcription factor Nrf2 to undergo nuclear translocation and binding to the antioxidant response element (ARE) followed by the induction of NQO1. The ARE is also known as the electrophile response element (EpRE). After recruitment of the basic transcriptional machinery, the ultimate result is activation of the transcription of NQO1 and other ARE-regulated protective enzymes [49-53]. These results suggest that the induction of NQO1 by DP occurs by a two-step mechanism [3] involving (i) oxidation of phenolic inducers to their quinone derivatives Q by autooxidation, by antioxidant action with reactive oxygen species (ROS) or enzymatic oxidations, and in a second step (ii) oxidation of highly reactive thiols of the protein sensor Keap1 by quinones Q activating transcription factor Nrf2. These two putative routes are supported by quantitative

structure-activity relationships correlating NQO1 induction with electron-donating property of DP for the first step and for the second step with the electron-attracting property of the corresponding quinones Q.

We consider this two-step mechanism as a possible model underlying the mechanism of action of other phenolic inducers as phenylpropenoids PP (section 3.3.2.2) and flavonoids F (section 3.3.2.3). In Table 3 are reported the induction of NQO1 in Hepa 1c1c7 cells by 10  $\mu\text{M}$  of DP expressed as relative specific activity (treated/control), data being extracted from Figure 3 of Ref. [48] and four parameters expressing relative values of the energy required to detach an electron from DP: (i)  $\log k(^1\text{O}_2+\text{DP})$ , (ii) the one-electron oxidation,  $E_7(\text{DP}^{*+}/\text{DP})$  in mV measured at pH 7 versus NHE, (iii) the  $E(\text{HOMO})$  in eV, and (iv) the IP in eV. The first three parameters [ $\log k$ ,  $E_7$  and  $E(\text{HOMO})$ ] have been previously determined as reported in [3], the fourth, IP, being newly determined and presented herewith (Table 3).

These four parameters expressing the energy required to detach an electron from the five DP are linearly inter-correlated with one another by the following equations:

$$\log k(^1\text{O}_2+\text{DP}) = 51.22 + 5.057 E(\text{HOMO}) \quad [n = 5, r = 0.99] \quad (27)$$

$$\log k(^1\text{O}_2+\text{DP}) = 27.89 - 2.67 \text{ IP} \quad [n = 5, r = 0.93] \quad (28)$$

$$E(\text{HOMO}) = -4.51 - 0.54 \text{ IP} \quad [n = 5, r = 0.96] \quad (29)$$

Moreover, the potency of induction of NQO1 for each DP is linearly correlated with the four parameters expressing the energy required to detach an electron from DP by the equations:

$$\text{NQO1 activity} = -2.62 + 0.623 \log k(^1\text{O}_2+\text{DP}) \quad [n = 5, r = 0.95] \quad (30)$$

$$\text{NQO1 activity} = 2.77 - 0.00237 E_7(\text{DP}^{*+}/\text{DP}) \quad [n = 5, r = 0.98] \quad (31)$$



$$\text{NQO1 activity} = 30.36 + 3.27 E(\text{HOMO}) \quad [n = 5, r = 0.98] \quad (32)$$

$$\text{NQO1 activity} = 15.84 - 1.80 \text{ IP} \quad [n = 5, r = 0.96] \quad (33)$$

As an example, the linear correlation (33) is displayed in Figure 4.

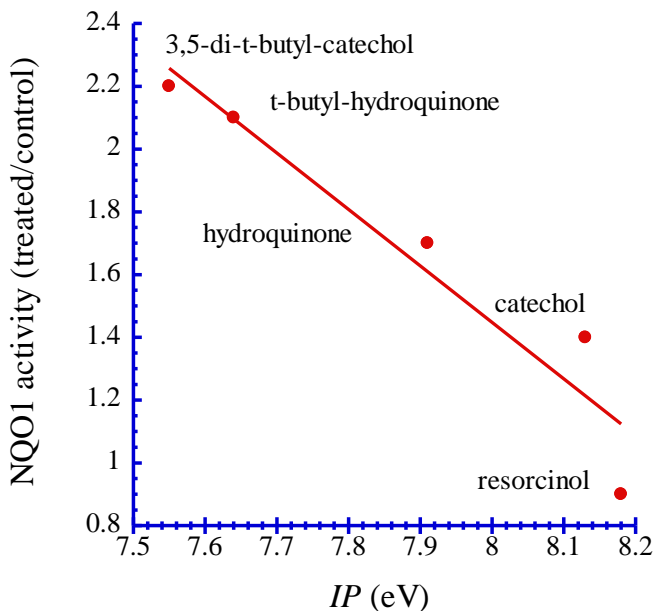


**Figure 4**

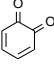
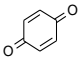
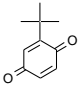
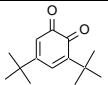
Linear correlation (33) between NQO1 activity and the ionisation potential IP of DP ( $r = 0.96$ ), data are reported in Table 4.

As already alluded to in section 2.3.1 above,  $E(\text{HOMO})$  and the  $E_7$ , and the  $E(\text{HOMO})$  and the  $IP$  are inverse functions, respectively. In other words, the signs of the  $E(\text{HOMO})$  are negative, while those of the  $E_7$  and those of the  $IP$  are positive, and the absolute values of these parameters decrease when the molecule is more reducing, *i.e.*, when the molecule releases an electron more easily. The correlations (27) to (33) are observed for four DP in a narrow range of parameter values. However in the case of equations (27), (28) and (30) the correlations occur with a change of  $\log k$  involving almost two orders of magnitude. These correlations allow us to conclude that the stronger is the electron-

donating property of the DP, the easier will be its transformation into its corresponding quinone Q and the greater is its inducer efficacy.

The NQO1 induction occurs *via* the quinones Q resulting from the oxidised DP. The reduction potentials of the quinone/semiquinone couples, corresponding to the electron affinity of the neutral molecule Q are essential for understanding their reactions with thiols of Keap1. In absence of reliable one-electron reduction potentials, the  $E(\text{HOMO})$  of the  $\text{Q}^{\cdot-}$  anions, considered as more precise than the calculation of the energy of the lowest unoccupied molecular orbital  $E(\text{LUMO})$  of Q had been calculated previously by the semiempirical AM1 method [3]. In Table 4 are presented the induction efficacy of NQO1, the  $E(\text{HOMO})$  of the quinone anions, calculated by the AM1 method and the electron affinity (EA) of Q calculated by DFT method.

**Table 4**  
Redox properties and NQO1 induction efficacy of quinones Q.

Quinones (Q)	$E(\text{HOMO})^{(a)}$ of $\text{Q}^{\cdot-}$ (eV)	EA <sup>(b)</sup> (eV)	NQO1 activity <sup>(a)</sup>
 1,2-benzoquinone	0.64363	-1.97	1.4
 1,4-benzoquinone	0.56943	-1.90	1.7
 <i>tert</i> -butyl-1,4-benzoquinone	0.47822	-1.83	2.1
 3,5-di- <i>tert</i> -butyl-1,2-benzoquinone	0.43736	-1.78	2.2

<sup>(a)</sup> Data obtained from Ref. [3].

<sup>(b)</sup> Newly calculated data by DFT method (see section 2.2.2).

Plotting the EA(DFT) against the  $E(\text{HOMO})$  of the anion, we get the expression:

$$\text{EA(DFT)} = -1.39 - 0.89 E(\text{HOMO}) \text{ of } \text{Q}^{\bullet-} \text{ (AM1)} \quad [n = 4, r = 0.99] \quad (34)$$

which indicates a strong interconnection between the two values of the physicochemical parameters characterising the electron-attracting property of the Q obtained *via* DFT and semiempirical AM1 methods.

Plotting the induction of NQO1, expressed as relative specific activity of the enzyme, as a function of  $E(\text{HOMO})$  of the anion  $\text{Q}^{\bullet-}$ , and as a function of EA of Q, we observe respectively two linear correlations with identical correlation coefficients  $r$ :

$$\text{NQO1 activity} = 3.97 - 3.98 E(\text{HOMO}) \text{ (AM1) of } \text{Q}^{\bullet-} \quad [n = 4, r = 0.99] \quad (35)$$

$$\text{NQO1 activity} = 10.11 + 4.42 \text{ EA (DFT) of Q} \quad [n = 4, r = 0.99] \quad (36)$$

These correlations indicate that the stronger the electron-attracting power of the quinone Q, the greater is its induction efficacy of NQO1 synthesis.

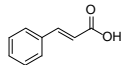
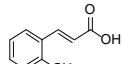
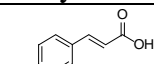
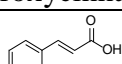
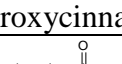
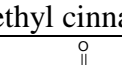
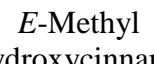
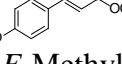
### 3.3.2.2. Induction of NQO1 by phenylpropenoids (PP)

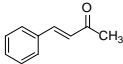
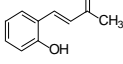
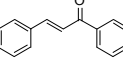
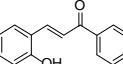
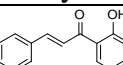
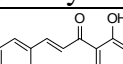
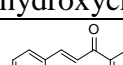
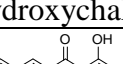
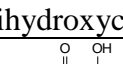
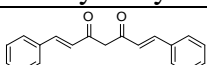
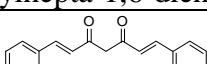
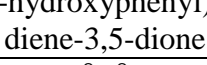
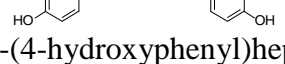
The potency of the NQO1 induction has also been studied in the case of 34 molecules, many naturally occurring plant phenylpropenoids, *e.g.*, cinnamic acids and their esters, chalcones, curcuminoids, and coumarins, as well as synthetic analogues, such as phenyl butenones, bis(benzylidene)acetones, and bis(benzylidene)cycloalkanones. Thirty one PP molecules, out of 34, have been shown to induce the activity of NQO1 in Hepa 1c1c7 murine hepatoma cells [54]. The inducer potency of each active compound was expressed as the concentration required to double NQO1 (CD value). The tendency to release electrons of each PP is expressed by their  $E(\text{HOMO})$  in eV calculated by an AM1

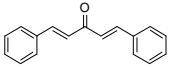
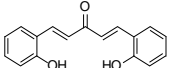
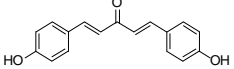
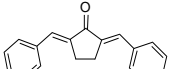
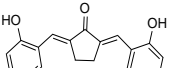
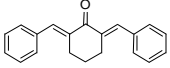
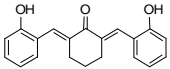
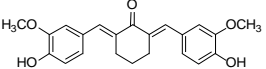
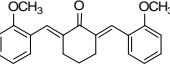
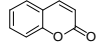
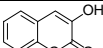
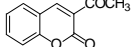
semiempirical quantum mechanical method and by their IP in eV newly calculated by a DFT method.

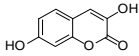
The tendency to attract electron of each PP is expressed by their electron affinity EA in eV that has been calculated by a DFT method. The structures of the PP, their *p*CD, *E*(HOMO), IP and EA values are indicated in Table 5.

**Table 5**  
*p*CD, *E*(HOMO), IP and EA values of the 34 PP

PP <sup>a</sup>	Formula	<i>p</i> CD	<i>E</i> (HOMO) in eV <sup>(a)</sup>	IP in eV	EA in eV
1	 <i>E</i> -Cinnamic acid	inactive e	-9.503	8.60	-0.588
2	 <i>E</i> -2-Hydroxycinnamic acid	4.72	-9.210	8.22	-0.518
3	 <i>E</i> -4-Hydroxycinnamic acid	inactive e	-9.125	8.13	-0.432
4	 <i>E</i> -3-Hydroxycinnamic acid	inactive e	-9.332	8.39	-0.585
5	 <i>E</i> -Methyl cinnamate	4.09	-9.434	8.45	-0.479
6	 <i>E</i> -Methyl 2-hydroxycinnamate	4.82	-9.156	8.14	-0.414
7	 <i>E</i> -Methyl 4-hydroxycinnamate	4.08	-9.068	7.97	-0.302
8	 <i>E</i> -Methyl 3-hydroxycinnamate	4.08	-9.282	8.29	-0.458

PP <sup>a</sup>	Formula	pCD	<i>E</i> (HOMO) in eV <sup>(a)</sup>	<i>IP</i> in eV	<i>EA</i> in eV
9	 <i>E</i> -4-Phenylbut-3-en-2-one	4.82	-9.364	8.42	-0.631
10	 <i>E</i> -4-(2-Hydroxyphenyl)but-3-en-2-one	5.27	-9.113	8.36	-0.453
11	 Chalcone	4.51	-9.286	8.19	-1.029
12	 2-Hydroxychalcone	4.92	-9.047	8.11	-1.059
13	 2'-Hydroxychalcone	5.01	-9.216	7.92	-0.847
14	 2,2'-Dihydroxychalcone	5.33	-9.093	7.69	-0.772
15	 4-Hydroxychalcone	4.48	-8.950	7.82	-0.891
15	 2',4'-Dihydroxychalcone	4.80	-9.266	7.94	-0.927
17	 2,2',4'-Trihydroxychalcone	5.32	-9.069	7.60	-0.696
18	 1,7-Diphenylhepta-1,6-diene-3,5-dione	4.90	-9.166	7.94	-1.314
19	 1,7-Bis-(2-hydroxyphenyl)hepta-1,6-diene-3,5-dione	6.52	-8.902	7.78	-1.473
20	 1,7-Bis-(4-hydroxyphenyl)hepta-1,6-diene-3,5-dione	4.94	-8.873	7.46	-1.124
21	 1,7-Bis-(4-hydroxy-3-methoxyphenyl)hepta-1,6-diene-3,5-dione (or Curcumin)	5.12	-8.669	7.17	-1.087

PP <sup>a</sup>	Formula	pCD	<i>E</i> (HOMO) in eV <sup>(a)</sup>	<i>IP</i> in eV	<i>EA</i> in eV
22	 1,5-Diphenylpenta-1,4-dien-3-one	>4.70	-9.175	7.81	-1.293
23	 1,5-Bis-(2-hydroxyphenyl)-penta-1,4-dien-3-one	6.82	-8.863	7.41	-1.136
24	 1,5-Bis-(4-hydroxyphenyl) penta-1,4-dien-3-one	4.85	-8.844	7.31	-1.092
25	 2,5-Dibenzylidenecyclopentanone	4.80	-9.082	7.57	-1.240
26	 2,5-Bis-(2-hydroxybenzylidene) cyclopentanone	7.12	-8.783	7.45	-1.415
27	 2,6-Dibenzylidenecyclohexanone	5.54	-9.172	7.47	-0.784
28	 2,6-Bis-(2-hydroxybenzylidene) cyclohexanone	6.55	-8.846	7.27	-0.868
29	 2,6-Bis-(4-hydroxy-3-methoxybenzylidene) cyclohexanone	6.05	-8.865	6.76	-0.883
30	 2,6-Bis-(2-methoxybenzylidene) cyclohexanone	5.56	-8.757	7.34	-0.736
31	 Chromen-2-one (or Coumarin)	3.30	-9.460	8.67	-0.489
32	 3-Hydroxychromen-2-one	5.82	-9.197	8.29	-0.268
33	 3-Acetylchromen-2-one	3.70	-9.697	8.71	-1.134

PP <sup>a</sup>	Formula	pCD	E(HOMO) in eV <sup>r(a)</sup>	IP in eV	EA in eV
34	 3,7-Dihydroxychromen-2-one	3.30	-9.232	8.29	-0.339

<sup>a</sup> pCD is the logarithm of the reciprocal of CD (concentration of each PP required to double NQO1 specific activity expressed in M units).

A redox ranking of these PP as inducers of NQO1 *via* their E(HOMO) has been reported by Zoete *et al.* [4].

The correlations observed between pCD of the PP and their E(HOMO) previously calculated at the AM1 level of semiempirical theory or their newly calculated IP at DFT level can be considered as statistically valid when the molecular structures belong to series of congener compounds with related features. Plotting pCD versus E(HOMO) and versus EA for the 31 active PP non-congeners that belong to nine chemical classes, the following expressions are found:

$$pCD = 29.74 + 2.71 E(\text{HOMO}) \quad [n = 31, r = 0.67] \quad (37)$$

$$pCD = 4.06 - 1.14 EA \quad [n = 31, r = 0.42] \quad (38)$$

the fact that the correlation coefficient of (37) is much larger than that of (38) suggests that although these 31 molecules have in common Michael reaction acceptor functionalities (*i.e.*, olefinic function conjugated to electron-withdrawing set(s)) that are electrophilic, these PP inducers would rather act *via* a mechanism involving their electron-donor property than *via* their electron-acceptor property.

In the search of more satisfactory correlations, we have formed three groups (a), (b) and (c) of PP molecules with structures more strongly related to one another in the case of (a) and (c) and in the case of group (b) with structures belonging to many different classes but all with Michael acceptor functionalities:

(a) The first linear correlations observed with six molecules **7**, **15**, **20**, **21**, **24** and **34** with

one or two hydroxyl substituent(s) at a position *para* to ethylene group(s) (Tables 6 and 7) are expressed by the equations:

$$pCD = 34.5 + 3.36 E(\text{HOMO}) \quad [n = 6, r = 0.96] \quad (39)$$

$$pCD = 16.14 - 1.52 \text{IP} \quad [n = 6, r = 0.96] \quad (40)$$

These two physicochemical parameters  $E(\text{HOMO})$  and IP being strongly intercorrelated by:

$$\text{IP} = -11.5 - 2.14 E(\text{HOMO}) \quad [n = 6, r = 0.97] \quad (41)$$

If we now plot  $pCD$  versus their electron affinity EA of these six molecules, we obtain:

$$pCD = 3.17 - 1.60 \text{EA} \quad [n = 6, r = 0.90] \quad (42)$$

The correlations (39) and (40) suggest that the presence of OH substituents on the aromatic rings of the PP increases the ease of the molecule to be oxidised as a whole and increases also locally the electron affinity of the ethylenic  $\alpha, \beta$  unsaturated carbonyl system. This might indicate that PP would rather act as electron donors in the first step and in the second step that the oxidised PP would act as electrophiles in the mechanism of NQO1 induction. This will be more clearly established by the study (b) of 23 other PP.

(b) The second linear correlation can be observed with all the other molecules that have no hydroxyl substituents at the *para* position relative to an ethylene (**2, 5, 6, 8, 9, 10, 11, 12, 13, 14, 16, 17, 18, 19, 23, 25, 26, 27, 28, 30, 31, 32, 33**). Although these 23 molecules belong to different chemical classes, their correlations are:

$$pCD = 38.40 + 3.63 E(\text{HOMO}) \quad [n = 23, r = 0.86] \quad (43)$$

$$pCD = 18.75 - 1.71 \text{IP} \quad [n = 23, r = 0.77] \quad (44)$$

The lower IP correlation coefficient of (44) obtained as compared to that of  $E(\text{HOMO})$  correlation (43) can be explained by the presence of the ten molecules **2, 6,**



**10, 12, 14, 17, 19, 23, 26,** and **28** among the 23 PP molecules examined in this paragraph (b). In paragraph (c), dealing exclusively with the ten molecules **2, 6, 10, 12, 14, 17, 19, 23, 26,** and **28**, characterized by one hydroxyl or two hydroxyl substituents at a position(s) *ortho* to ethylene group(s), it will be observed that IP correlation (51) has a correlation coefficient  $r=0.80$  significantly lower than the  $r=0.96$  observed for the  $E(\text{HOMO})$  correlation (50). Thus, this discrepancy between (50) and (51) explains the lower  $r$  of IP expression (44) as compared to the  $r$  of  $E(\text{HOMO})$  expression (43) as due to the presence of the ten molecules **2, 6, 10, 12, 14, 17, 19, 23, 26,** and **28** among the 23 PP molecules examined.

Molecule **29** which has two OH substituent at the *para* position relative to an ethylenic group should be with group (a), however its data point falls into group (b) [4]. Further, if molecule **22** is added to the 23 molecules of this group (b) with  $p\text{CD} = 4.70$ , although  $p\text{CD}$  is indicated as larger than 4.70 (from CD reported in Ref. [54]). The expressions of the correlations show a similar tendency:

$$p\text{CD} = 38.43 + 3.64 E(\text{HOMO}) \quad [n = 24, r = 0.85] \quad (45)$$

$$p\text{CD} = 18.52 - 1.68 \text{IP} \quad [n = 24, r = 0.76] \quad (46)$$

For the 24 molecules that are not perfect congeners, plotting the IP calculated by DFT methods against the  $E(\text{HOMO})$  calculated by a semiempirical AM1 gives

$$\text{IP}(\text{DFT}) = -6.87 - 1.62 E(\text{HOMO}) (\text{AM1}) \quad [n = 24, r = 0.85] \quad (47)$$

It is important to underline that these 23 or 24 molecules PP, do not act as electrophiles in a first step, since there is no correlation of  $p\text{CD}$  with their electron affinity (EA):

$$p\text{CD} = 4.22 - 1.10 \text{EA} \quad [n = 23, r = 0.40] \quad (48)$$

and with molecule **22**:

$$pCD = 4.31 - 0.96 EA \quad [n = 24, r = 0.35] \quad (49)$$

This absence of correlation with their EA suggests that although these PP molecules contain electrophilic Michael reaction acceptors (electrophilic unsaturated bond conjugated with a carbonyl group) they should be considered as electrophiles only after a first step involving their oxidation as in the case of diphenols (DP) reported above in section 3.2.1 and as in the case of flavonoids (F) reported in section 3.2.3.

(c) Inductions of NQO1 by molecules **2**, **6**, **10**, **12**, **14**, **17**, **19**, **23**, **26**, and **28**, with a hydroxyl or two hydroxyl substituents at a position(s) *ortho* to ethylene group(s) (Tables 6 and 7) are expressed by the equations:

$$pCD = 59.5 + 5.96 E(\text{HOMO}) (\text{AM1}) \quad [n = 10, r = 0.96] \quad (50)$$

$$pCD = 22.03 - 2.09 \text{IP} (\text{DFT}) \quad [n = 10, r = 0.80] \quad (51)$$

As already noted above, in the case of these 10 molecules with a hydroxyl or two hydroxyl substituents at a position(s) *ortho* to ethylene group(s), the correlation coefficient obtained using the IP calculated by a DFT method is significantly lower than that obtained using the  $E(\text{HOMO})$  calculated by a semiempirical AM1 method.

Plotting  $pCD$  versus  $EA(\text{DFT})$  gives the following expression:

$$pCD = 4.10 - 1.91 EA \quad [n = 10, r = 0.75] \quad (52)$$

The correlations (50) and (51) dealing with the electron-donating parameters  $E(\text{HOMO})$  and IP as compared to correlation (52) dealing with electron-attracting parameter EA might indicate that the induction of NQO1 by these 10 molecules might occur *via* their acting as electron-donor molecules. The best inducers with hydroxyl substituents among all PP studied are **23**, **26**, and **28**. Thus, the presence of OH substituents on the aromatic rings of the PP at a position *ortho* to ethylene group is

important and increases the ease of the molecule to be oxidised as a whole. For all the examined PP, the correlations found suggest a general tendency: the stronger is their electron-donating propensity, the greater is their induction potency.

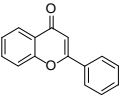
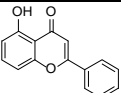
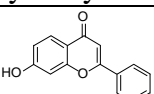
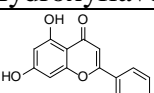
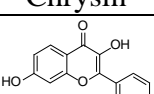
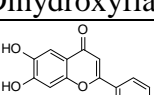
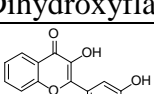
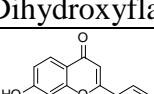
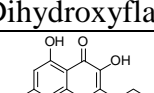
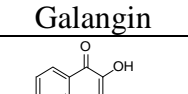
The mechanism of action of the PP is not yet fully understood. On the basis of the observation that the PP activity can be ranked *via* their electron releasing power with rather satisfactory correlation coefficients, it is possible to consider that, after a metabolic oxidation, the oxidized PP become electrophile agents and that they react covalently with highly reactive sulfhydryl groups of a protein Keap1, according to the prevailing view accepted for all electrophile inducers. This modification of Keap1 disrupts the Keap1-Nrf2 complex and enables the transcription factor Nrf2 to migrate to the nucleus, where it binds to the antioxidant response element (ARE) regions of phase 2 genes and activates the transcription of NQO1 and other ARE regulated protective enzymes.

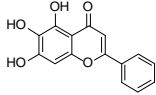
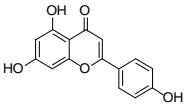
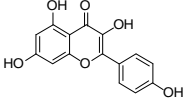
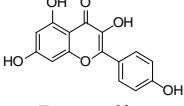
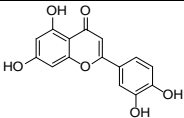
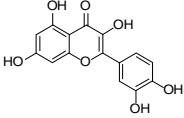
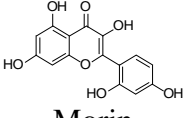
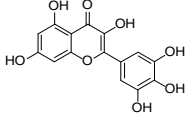
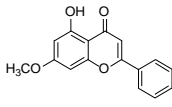
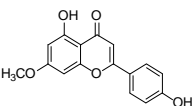
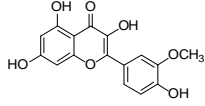
#### 3.3.2.3. *Induction of NQO1 by flavonoids (F)*

Flavonoids are a subclass of polyphenols present in vegetables and fruits, and may provide beneficial health effects. An overview dealing with the flavonoids in cancer prevention and therapy has been published by Chabot *et al.* [55]. Lee-Hilz *et al.* [56] have reported the relationship between the  $E(\text{HOMO})$  values of 21 flavonoids (F) calculated by the AM1 approximation and the experimental induction factor (IF) of the EpRE-mediated gene transcription leading to induction of detoxifying enzymes such as NQO1 and glutathione S-transferases (GSTs) in Hepa-1c1c7 hepatoma cells (Table 6).

**Table 6**

Structures of the flavones (F) studied by Lee-Hilz *et al.* [56] their E(HOMO) calculated by AM1, their ionisation potential IP calculated by DFT and their induction factor IF.

Compounds (F)	Formula	E(HOMO) <sup>(a)</sup> (eV)	IP <sup>(b)</sup> (eV)	IF <sup>(a)</sup>
1	 Flavone	-9.27	8.22	2.8
2	 5-Hydroxyflavone	-9.12	7.98	2.5
3	 7-Hydroxyflavone	-9.36	8.22	2.5
4	 Chrysin	-9.25	7.88	2.1
5	 3,7-Dihydroxyflavone	-8.89	7.68	3
6	 6,7-Dihydroxyflavone	-9.10	8.34	3
7	 3-3'-Dihydroxyflavone	-8.88	7.68	5.8
8	 7,8-Dihydroxyflavone	-9.23	7.89	2.2
9	 Galangin	-8.90	7.48	4.0
10	 Resokaempferol	-8.72	7.41	6.5

11	 <p><b>Baicalein</b></p>	-8.99	7.69	2.5
12	 <p><b>Apigenin</b></p>	-9.15	7.65	2.0
13	 <p><b>Kaempferol</b></p>	-8.74	7.20	7.1
14	 <p><b>Luteolin</b></p>	-9.09	7.97	3.0
15	 <p><b>Fisetin</b></p>	-8.69	7.28	8.0
16	 <p><b>Quercetin</b></p>	-8.72	7.13	10
17	 <p><b>Morin</b></p>	-8.81	7.17	8.4
18	 <p><b>Myricetin</b></p>	-8.80	7.17	9
19	 <p><b>Tectochrysin</b></p>	-9.16	7.84	4.4
20	 <p><b>Genkwanin</b></p>	-9.09	7.62	5
21	 <p><b>Isorhamnetin</b></p>	-8.65	7.08	7.8

<sup>(a)</sup> $E(\text{HOMO})$  and IF values taken from [56]

<sup>b)</sup>IP ionisation potentials newly calculated by DFT

The flavonoids are commonly known to have electron-donating properties and they would act as pro-oxidant compounds in their induction of EpRE-mediated gene expression after donating electrons by antioxidant action, enzymatic oxidation or autooxidation that lead to the corresponding quinones or semiquinones [56]. The structures of the 21 flavonoids, their induction factors (IF), the  $E(\text{HOMO})$  calculated by Lee-Hilz *et al.* and the IP which we have newly calculated by DFT methods are reported in Table 7. Plotting IP against  $E(\text{HOMO})$ , we get:

$$\text{IP} = -6.25 - 1.55 E(\text{HOMO}) \quad [n = 21, r = 0.88] \quad (53)$$

showing that both expressions of the electron-donating property of the 21 F are satisfactorily interconnected.

Plotting IF versus the  $E(\text{HOMO})$ , we obtain :

$$\text{IF} = 95.35 + 10.10 E(\text{HOMO}) \quad [n = 21, r = 0.84] \quad (54)$$

which gives  $r^2 = 0.71$  a value identical to that reported by Lee-Hilz *et al.* [56]

For comparison, plotting IF versus IP, we have:

$$\text{IF} = 48.88 - 5.76 \text{IP} \quad [n = 21, r = 0.84] \quad (55)$$

and  $r^2 = 0.71$ .

These results demonstrate that calculation of  $E(\text{HOMO})$  by the semiempirical AM1 quantum mechanical method or calculation of IP by DFT method can lead to linear correlations with identical correlation coefficients  $r$ . They show that the stronger is the electron-donor property of F, the greater is their induction potency. As observed above in section 3.2.1, only the diphenols DP able to undergo oxidation to quinones Q are inducers of NQO1; similar to DP, flavonoids might undergo an oxidation to flavonoid

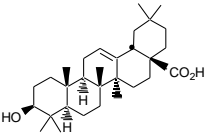
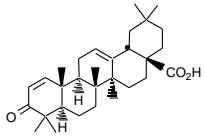
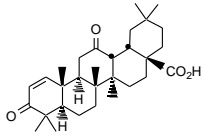
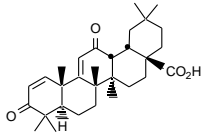
quinones that will react with cysteine residues of Keap1, leading successively to conformational change of Keap1, release of the transcription factor Nrf2 and induction of detoxifying enzymes such as NQO1.

#### 3.3.2.4. *Induction of NQO1 by triterpenoids (TP)*

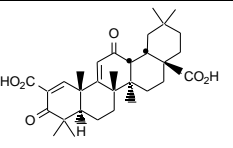
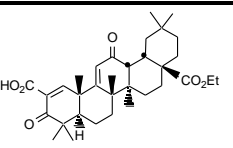
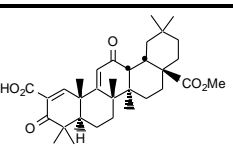
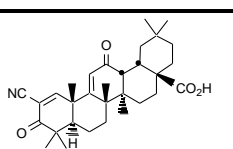
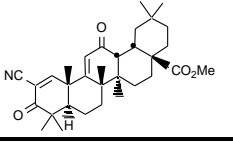
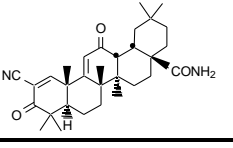
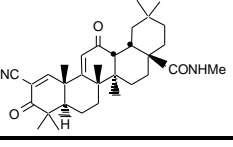
Triterpenoids (TP) are electrophiles which interact in one step *via* their Michael acceptors functionalities with sulfhydryl groups of Keap1. The physicochemical property involved in this redox interaction of TP with thiol groups should be their reduction potential  $E(\text{TP}/\text{TP}^{\bullet-})$ . In a previous work using self-consistent field (SCF) calculations by the AM1 quantum mechanical procedure with Hyperchem 7.5.1 program [13] and restricted Hartree-Fock (RHF) formalism, standard AM1 basis sets of atomic orbitals were used for computing the orbital energy levels of TP and  $\text{TP}^{\bullet-}$  systems [6]. The structures of these TP are shown in Table 7, as well as the energy of their lowest unoccupied molecular orbital  $E(\text{LUMO})$ , the energy of their singly occupied molecular orbital  $E(\text{SOMO})$  and the  $E(\text{HOMO})$  of the anions  $\text{TP}^{\bullet-}$ , all three representing the ease of TP molecules to attract an electron (see pp. 132-135 of Ref. [17] and [6]), and all three being linearly correlated with EA of TP and reduction potential  $E(\text{TP}/\text{TP}^{\bullet-})$ . The inducer potency of each TP is expressed as the concentration CD (in  $\mu\text{M}$ ) required to double NQO1 specific activity in Hepa1c1c7 murine hepatoma cells. Table 7 reports also the induction potencies expressed as the logarithm of reciprocal CD,  $p\text{CD}$  values for convenience.

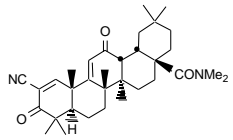
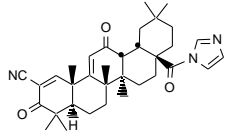
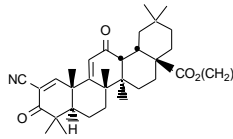
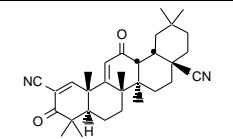
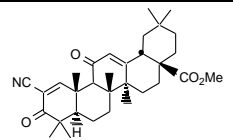
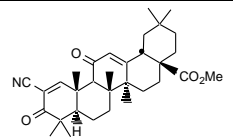
**Table 7**

Structures of the TP,  $E(\text{LUMO})$  of TP,  $E(\text{HOMO})$  of TP,  $E(\text{HOMO})$  of TP<sup>-</sup>,  $E(\text{SOMO})$  of TP<sup>-</sup>, electrophilicity index  $\omega$ , and  $p\text{CD}$ .

TP	Formula	$E(\text{LUMO})$ of TP	$E(\text{HOMO})$ of TP	$E(\text{HOMO})$ of TP anion	$E(\text{SOMO})$ of TP anion	$\omega$	$p\text{CD}$
<b>Oleanolic acid</b>		1.1517	-9.2948				inactive
<b>TP 46</b>		0.0847	-9.4198	-1.8999	2.3050	1.1460	5.41
<b>TP 69</b>		-0.0326	-10.1753	-2.0420	2.2300	1.2841	5.74
<b>TP 82</b>		-0.1660	-10.1038	-2.1102	1.6210	1.3266	6.55



<b>TP191</b>		-0.6704	-10.2660	-2.9702	1.2870	1.5580	6.66
<b>TP 222</b>		-0.6506	-10.2308	-2.9673	1.3050	1.5449	7.66
<b>TP 190</b>		-0.6541	-10.2397	-2.9647	1.3020	1.5475	7.74
<b>TP 151</b>		-0.7185	-10.3069	-2.8980	1.1370	1.5847	8.64
<b>TP 155</b>		-0.7051	-10.2788	-2.8866	1.1690	1.5752	9.00
<b>TP 223</b>		-0.6721	-10.2028	-2.9424	1.2110	1.5511	8.89
<b>TP 224</b>		-0.6705	-10.0514	-2.9451	1.2090	1.5318	9.00

<b>TP 226</b>		-0.6656	-9.6932	-2.9289	1.2130	1.4857	8.17
<b>TP 235</b>		-0.7697	-9.6187	-3.0019	0.9075	1.524	8.48
<b>TP 233</b>		-0.7059	-10.2794	-2.8957	1.1420	1.5756	6.66
<b>TP 225</b>		-0.7670	-10.4076	-2.9271	1.0530	1.6200	9.55
<b>TP 162</b>		-0.4550	-10.2278	-2.6002	1.2770	1.4596	7.00
<b>TP 156</b>		-90.5381	-9.5244	-2.6670	1.7280	1.4084	5.82

(\*)All data

in this table are taken from [6].

Plotting the logarithm of  $pCD$  of 15 active congener triterpenoids versus  $E(\text{LUMO})$ ,  $E(\text{HOMO})$ , and  $E(\text{SOMO})$  of the TP anions gives:

$$pCD = 5.50 - 4.15 E(\text{LUMO}) \quad [n = 15, r = 0.85] \quad (56)$$

$$pCD = 0.19 - 2.92 E(\text{HOMO}) \text{ of the TP anion} \quad [n = 15, r = 0.83] \quad (57)$$

$$pCD = 11.75 - 2.89 E(\text{SOMO}) \text{ of the TP anion} \quad [n = 15, r = 0.88] \quad (58)$$

TP-233 and TP-191 are outliers of the above plots since their structures are dissimilar to the other compounds in the series [6]. These correlations (56-58) demonstrate that the higher is the electron affinity of TP, the greater its potency as NQO1 inducer.

In the frame of the molecular orbital method, it is possible to describe the efficacy of TP compounds by another reactivity parameter expressed in terms of  $E(\text{HOMO})$  and  $E(\text{LUMO})$  energies of the neutral TP, namely the electrophilicity index defined by Parr *et al.* [57] as:

$$\omega = \frac{\chi^2}{2\eta} \quad (59)$$

where  $\chi$  is the electronegativity and  $\eta$  is the chemical hardness of the molecule. Use of  $\omega$  was suggested empirically by Maynard *et al.* [58] and theoretically justified by Parr *et al.* in the frame of the DFT theory [57]. Using DFT calculations would be interesting if theoretical values could be obtained by a simple procedure. Now the  $E(\text{HOMO})(\text{DFT})$  values are generated by the so-called non-interacting electron model and therefore are lower than the exact one by a deviation  $\Delta E$ , the evaluation of which would necessitate an intricate linear response procedure [59]. Moreover, the determination of realistic  $E(\text{LUMO})$  values *via* DFT with respect to experimental EA is still debated [60]. The

equations for the calculations of  $\chi$  and  $\eta$  are [18]:

$$\chi = \frac{\text{IP} + \text{EA}}{2}$$

(60)

$$\eta = \text{IP} - \text{EA} \quad (61)$$

In terms of orbital energies, equation 59 can be expressed in terms of (60) and (61) as:

$$\omega = \frac{[E(\text{HOMO}) + E(\text{LUMO})]^2}{8[E(\text{LUMO}) - E(\text{HOMO})]} \quad (62)$$

The concept of electrophilicity index, its usefulness as well as the electrophilicity scales based on different physicochemical properties have been reviewed by Chattaraj *et al.* [61].

The electrophilicity index,  $\omega$  of every TP reported in Table 7, is calculated in terms of  $E(\text{HOMO})$  and  $E(\text{LUMO})$  orbital energies of the neutral TP [6]. Plotting the electrophilicity index  $\omega$  of every TP versus  $E(\text{SOMO})$  gives a linear correlation expressed by:

$$\omega = 1.90 - 0.30 E(\text{SOMO}) \quad [n = 15, r = 0.92] \quad (63)$$

showing that both scales, based on distinct physicochemical parameters are very similar. Again, TP-233 and TP-191 are outliers for reasons related to their structure and are taken out of the plots.

Compared with the correlation coefficient  $r = 0.88$  of the plot of  $p\text{CD}$  versus  $E(\text{SOMO})$  of equation (63), plots of  $p\text{CD}$  versus the electrophilicity index  $\omega$  indicates a very similar  $r$ :

$$p\text{CD} = -5.67 + 9.1 \omega \quad [n = 15, r = 0.89] \quad (64)$$

The induction of the cancer-protective enzyme NQO1 by electrophilic exogenous

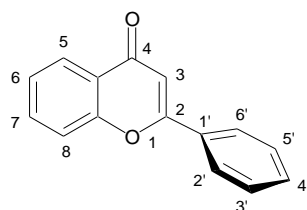
triterpenoids TP as well as by electrophilic metabolites of other exogenous molecules such as diphenols DP, phenylpropanoids PP and flavonoids F is considered as similar to the induction by endogenous oxidants such as reactive oxygen and nitrogen species (ROS, RNS) produced in aerobic and anaerobic metabolisms. This induction by exogenous and endogenous oxidants involves targeted aminoacids in proteins that are highly reactive cysteine residues of the sensor protein Keap1 [49,62].

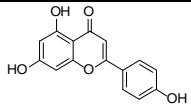
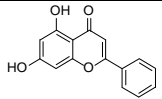
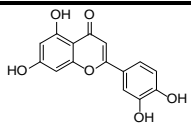
### **3.3.3. Inhibition of topoisomerases involved in DNA replication and transcription**

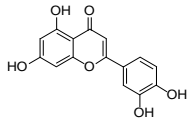
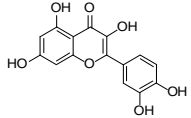
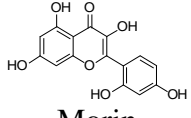
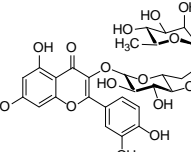
Human DNA topoisomerase enzymes are involved in key processes including DNA replication, transcription, recombination and repair. These enzymes are the targets of several drug inhibitors that generate DNA single and double stranded breaks and consequently lead to apoptosis and cell death. Among these inhibitors, some flavonoids are being tested in the clinical development of cancer chemotherapy. The most potent topoisomerase I poisons are the flavones and flavonols, that generally are found to be DNA intercalators. In a previous study [7], we have determined two redox parameters expressing the electron-donor property of seven flavones (Fl), apigenin, chrysin, fisetin, kaempferol, quercetin, morin and rutin, the structures of which are shown in Table 7.

**Table 8**

Redox parameters:  $E(\text{HOMO})$  in eV, IP in eV,  $\log k(^1\text{O}_2+\text{Fl})$ , structural parameter (dihedral angle  $\text{O}_1\text{-}2\text{-}1'\text{-}2'$ ), and activity  $A^*$  for inhibiting eukaryotic topoisomerase I of the seven flavones Fl.



Compounds (Fl)	$E(\text{HOMO})$ (eV)	IP (eV)	$\log k$	$A^*$	Dihedral angle $\text{O}_1\text{-}2\text{-}1'\text{-}2'$ ( $^\circ$ )
 Apigenin	-9.1487	7.64	6.83	1.68	25
 Chrysin	-9.2462	7.88	6.25	1.10	28
 Fisetin	-8.6941	7.28	7.20	1.96	27

Compounds (Fl)	$E(\text{HOMO})$ (eV)	IP (eV)	$\log k$	$A^*$	Dihedral angle $\text{O}_1\text{-}2\text{-}1'\text{-}2'$ ( $^\circ$ )
 <b>Kaempferol</b>	-8.7474	7.20	7.23	1.79	27
 <b>Quercetin</b>	-8.7548	7.13	7.60	2.19	27
 <b>Morin</b>	-8.6681	7.17	7.99	1.40	40
 <b>Rutin</b>	-8.6849	7.29	7.19	0.92	37

\* This activity  $A$  is taken from the data reported by Boege *et al.* [63] in Table 1.  $A$  values correspond to the concentration of open circular DNA obtained under inhibition conditions by flavones relative to control.

These two parameters are  $\log k(^1\text{O}_2+\text{Fl})$  determined by laser flash photolysis and  $E(\text{HOMO})$  of Fl calculated by the AM1 method, reported in Table 7. Using DFT level of theory, we have calculated a third redox parameter, the IP, expressing also the electron-donor property of every Fl (Table 7).

The main purpose of our study is to discuss the correlations observed between, on the one hand, the three redox parameters  $\log k$ ,  $E(\text{HOMO})$  and IP of Fl, and, on the other hand the topoisomerase I inhibition activity  $A$  of these Fl at a concentration of 1mM, determined in by Boege *et al.* [63]. A fourth property of these molecules, the dihedral angle, O1-2-1'-2' (Table 7), had also been calculated; the changes in this angle modifies the interaction of the Fl with the topoisomerase-DNA complex and consequently their inhibition activity  $A$  [7].

Plotting the topoisomerase inhibition activity  $A$  exerted by the five flavones, apigenin, chrysin, fisetin, kaempferol, quercetin that have a minimum conformational energy at a dihedral angle O<sub>1-2-14-2'</sub>, 25-28° versus their  $\log k(^1\text{O}_2+\text{Fl})$ ,  $E(\text{HOMO})$ , and IP give the expressions:

$$A = -3.8 + 0.79 \log k(^1\text{O}_2+\text{Fl}) \quad [n = 5, r = 0.98] \quad (65)$$

$$A = 13.61 + 1.33 E(\text{HOMO}) \quad [n = 5, r = 0.84] \quad (66)$$

$$A = 10.34 - 1.16 \text{IP} \quad [n = 5, r = 0.91] \quad (67)$$

showing a correlation coefficient for  $E(\text{HOMO})$  lower that for IP. Rutin and morin are outliers of the linear correlations (64, 65, 66) as their large dihedral angles O<sub>1-2-14-2'</sub>, in the range 40-37°, decreases significantly their topoisomerase inhibition activity, and probably prevents their intercalation in DNA. Figure 5 shows the linear correlation between topoisomerase inhibition activity  $A$  exerted by the five flavones, apigenin,



chrysin, fisetin, kaempferol, quercetin *versus* their IP and the two outliers rutin and morin.

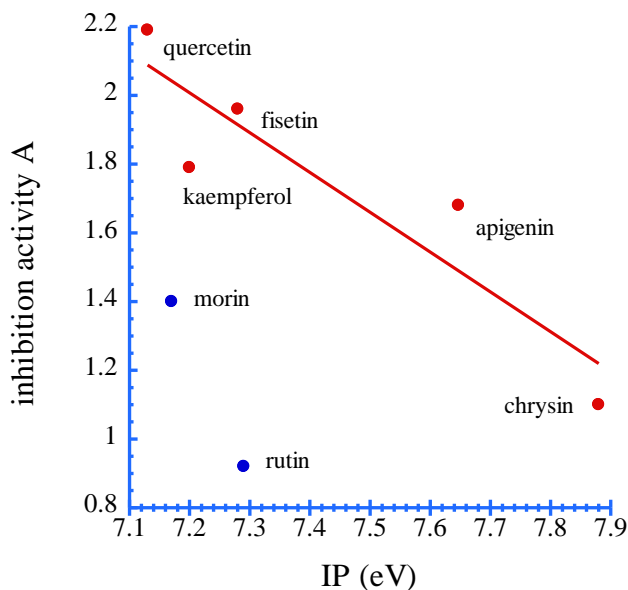


**Figure 5**

Linear correlation (58) observed by plotting the inhibition activity  $A$  *versus* the ionisation potential IP. A correlation coefficient  $r = 0.91$  is obtained for this linear correlation involving the five flavones (Fl) quercetin, fisetin, kaempferol, apigenin, chrysin that have a dihedral angle  $O_1-2-14-2'$  in the range  $25-28^\circ$ . Morin and rutin are outliers with dihedral angle  $O_1-2-14-2'$  in the range  $37-40^\circ$ .

Both,  $E(\text{HOMO})$  obtained by AM1 method and IP obtained by DFT calculations lead to correlations showing similar sensitivity to the molecular structures of the flavonoids. Such sensitivity was already noticed in correlations (7' and 8') where tertibutyl substitutions at ortho positions of phenols P transformed molecules V and VI into outliers (Fig.1). Our results indicate that the ability of our Fl to inhibit topoisomerase is connected with (i) their electron-donor property related to their affinity to DNA as well

as their possibility to be transformed into the corresponding quinones and (ii) their 3-dimensional structure related to the feasibility of formation of the ternary complex, inhibitor-topoisomerase-DNA.

#### **3.3.4. Inflammation suppressive capacity**

The 19<sup>th</sup> century hypothesis advanced by Rudolf Virchow's of a link between inflammatory processes and a predisposition to certain cancers [64] has been expanded by recent investigations. It is now widely accepted that many carcinogenesis processes can be promoted by inflammatory cells [65].

Inhibition of prostaglandin synthesis is considered as a primary mechanism for the anti-inflammatory effects of non-steroidal anti-inflammatory drugs (NSAID). Habicht and Brune have determined the anti-inflammatory efficacy of salicylic acid and phenol derivatives and expressed it as  $pIC_{50}$ , that is the logarithm of the reciprocal of  $IC_{50}$ , the 50% inhibitory concentration of the prostaglandin production in mouse macrophages [66].

Employing DFT, and using the B3LYP and PBEPBE functionals with and without Koopmans theorem, Shakman and Mazziotti calculated the ionisation potentials of 27 molecules (12 salicylic acids and 15 phenols) [67]. The correlation coefficients  $r$ , obtained by Shakman and Mazziotti for the plots between the DFT ionisation potentials of their 27 selected molecules and their anti-inflammatory potency expressed as their  $pIC_{50}$ , are  $r=0.69$  (from B3LYP) and  $r=0.72$  (from PBEPBE). For the same 27 molecules, using a semiempirical AM1 method carried out with the Hyperchem 4 program [8] we obtain a linear correlation expression:

$$pIC_{50} = 31 + 2.89 E(\text{HOMO}) \quad [n = 27, r = 0.83] \quad (68)$$

Shakman and Mazziotti selected their 27 molecules from a previous study of 32 molecules (benzoic and salicylic acids and phenol derivatives) performed by Mehlers and Gerhards [68]. Calculating the  $E(\text{HOMO})$  of these 32 molecules by using a semiempirical AM1 method, carried out with the Hyperchem 4 program, we obtain the expression:

$$pIC_{50} = 28.90 + 2.66 E(\text{HOMO}) \quad [n = 32, r = 0.86] \quad (69)$$

while for the same 32 molecules the  $E(\text{HOMO})$  calculated by an *ab initio* method by Mehler and Gerhards [68] yields:

$$pIC_{50} = 21.54 + 0.076 E(\text{HOMO}) \quad [n = 32, r = 0.82] \quad (70)$$

The better correlation coefficient  $r$  of the semiempirical method with respect to the DFT and *ab initio* ones will be discussed in the general conclusion.

The above linear correlations are consistent with correlations observed in the case of several types of anti-inflammatory compounds (triterpenoids, 4,5-diarylpyrroles, benzoic and salicylic acids and phenol derivatives, and imidazole derivatives), for which the stronger is the electron-donating property of the tested agents, the greater is their anti-inflammation efficacy [6,9-11].

### 3.4. Conclusion

Two main general conclusions can be drawn from the observed correlations of physicochemical parameters of phenol and flavone derivatives, phenylpropanoids, benzoic and salicylic acids, and triterpenoids with their biological efficacies against carcinogenesis and inflammation *in vivo* and in cellular systems:

The first principal conclusion is the equivalence between the different experimental and theoretical determinations of the physicochemical parameters involved in our studies.

Electron donor properties of exogenous protective molecules M have been mainly represented by five physico chemical parameters including (i) Hammett constants,  $\sigma_p^+$ , of different substituents in M, (ii)  $\log k(^1\text{O}_2+\text{M})$  measured by laser flash photolysis in solution, (iii) one-electron oxidation potential,  $E_7(\text{DP}^{+\cdot}/\text{DP})$  measured by electrochemical methods, (iv) energy of the highest occupied molecular orbital  $E(\text{HOMO})$  of M calculated by a semiempirical AM1 quantum mechanical method, and (v) ionisation potential IP of M calculated by DFT, specifically at the B3LYP/6-31+G\*\* level, all linearly correlated with the oxidation potential of M  $E(\text{M}^{+\cdot}/\text{M})$  in solution. The  $E(\text{HOMO})$  and IP theoretical values are related to the energy required to remove a  $\pi$  electron from the molecule M in the dilute gas phase. The correlations involving the three experimental parameters (i), (ii), (iii) have slightly higher correlation coefficients  $r$ . The two experimental parameters (i) and (ii), are either simply found in Hammett constant tables or measured by time resolved flash photolysis in any adequate solvent, and the two theoretical parameters (iv) and (v) are easily calculated, in contrast to the determination by electrochemical techniques such as cyclic voltametry [69], that is often complicated by irreversible processes or by pulse radiolysis that can only be applied to water-soluble molecules [70]. Moreover, the three experimental parameters and the two theoretical parameters are interconnected to one another by linear correlations with high correlation coefficients  $r$ .

Electron-acceptor properties of a molecule M have been represented by the energy of the

lowest unoccupied molecular orbital  $E(\text{LUMO})$  of  $M$  or by the  $E(\text{HOMO})$  of the anion  $M^{\ominus}$  or by the energy of the singly occupied molecular orbital  $E(\text{SOMO})$  of the anion  $M^{\ominus}$ . These theoretical parameters are linearly correlated with the electron affinities EA of  $M$  in the diluted gas phase and with the reduction potential  $E(M/M^{\ominus})$  in solution. The electron affinity of  $M$  has also been calculated *via* DFT methods using B3LYP/6-31+G\*\* functionals. These different methods give similar correlation coefficients  $r$ .

Out of eighteen correlations studied using DFT methods and semiempirical AM1 method, fifteen have very similar correlation coefficients  $r$ , while in three cases the correlation coefficients observed are different. In two cases, the  $r$  found for  $E(\text{HOMO})$  calculated by a semiempirical method AM1 are higher than those obtained with IP calculated by DFT methods. The AM1 method is parametrised to reproduce experimental heats of formations and therefore it is not that surprising that it performs so well, even can outperform DFT for most protective agents studied herein, if used for the type of molecules for which it has been parametrised. However in a third case the DFT method gives a higher  $r$  than the semiempirical method AM1.

The first case is that noted in section 3.2.2 (c) where the inductions of NQO1 by PP molecules **2**, **6**, **10**, **12**, **14**, **17**, **19**, **23**, **26**, and **28**, with a hydroxyl or two hydroxyl substituents at a position(s) *ortho* to ethylene group(s) were expressed by:

$$p\text{CD} = 59.5 + 5.96 E(\text{HOMO}) \quad [n = 10, r = 0.96] \quad (50)$$

$$p\text{CD} = 22.03 - 2.09 \text{IP} \quad [n = 10, r = 0.80] \quad (51)$$

The second case, noted in section 3.4, deals with the study of 27 anti-inflammatory molecules (12 salicylic acids and 15 phenols) selected by Shakman and Mazziotti [67].

These authors employed the Hartree-Fock method and the B3LYP and PBEPBE functionals of DFT with and without Koopmans theorem. In this case, the correlation coefficients  $r$ , obtained for the plots between the ionisation potentials of their 27 selected molecules and their anti-inflammatory potency expressed as their  $pIC_{50}$ , are  $r=0.69$  (from B3LYP) and  $r=0.72$  (from PBEPBE). For the same 27 molecules, using a semiempirical AM1 method [8] we obtain a linear correlation expression with a better correlation coefficient  $r$ :

$$pIC_{50} = 31 + 2.89 E(\text{HOMO}) \quad [n = 27, r = 0.83] \quad (68)$$

The third case, noted in section 3.3, deals with the inhibition activity  $A$  of human topoisomerase by flavonoids where the correlation coefficient obtained *via* semiempirical AM1 calculation is lower than that obtained *via* a DFT method:

$$A = 13.61 + 1.33 E(\text{HOMO}) \quad [n = 5, r = 0.84] \quad (66)$$

$$A = 10.34 - 1.16 IP \quad [n = 5, r = 0.91] \quad (67)$$

Nevertheless these three cases do not modify the equivalence and the strong interconnections between the two theoretical determinations and the three experimental measurements of the physicochemical parameters involved in our studies.

Our second conclusion deals with the importance of physicochemical parameters in tackling mechanisms of complex biological processes and in managing improvements of biological efficacies of protective exogenous molecules. An observed linear co-variation is a necessary but not sufficient condition for causality, however the correlations obtained in QSAR investigations can be considered as fruitful in the search of the best possible agents against carcinogenesis and inflammation: they open new strategies with predictive value, which are quantitatively based on correlations between redox physicochemical

parameters of exogenous molecules M and their potency against carcinogenesis and inflammation. As underlined by several authors [26,71-73], the QSAR methods are rapid and low-cost tools for predicting biological, environmental, toxicological, and physicochemical properties of chemicals. In this context, our QSAR studies show that systematic evaluation by quantum mechanical methods of redox parameters can guide the understanding of biochemical mechanisms involved in carcinogenesis and inflammation. Another example demonstrating the importance of physicochemical tools in biology is the project carried out by Oxford University's Centre for Computational Drug Discovery which screened up to 3.5 billion molecules for cancer-fighting potential [74,75].

Moreover, our *in silico* evaluations of biological activity should orient the rational design of new congeners with greater potency against carcinogenesis and inflammation and might reduce the expensive use of *in vivo* and *in vitro* bioassays.

## References

- (1) R. Scurlock, M. Rougée, R. V. Bensasson; Redox properties of phenols, their relationships to singlet oxygen quenching and to their inhibitory effects on benzo(a)pyrene-induced neoplasia, *Free Radic. Res. Commun.* **1990**, *8*, 251, erratum *Free Rad. Res. Commun.* **1992**, *16*, 205.
- (2) V. E. Steele, C. W. Boone, D. Dauzonne, C. V. Rao, R. V. Bensasson; Correlation between electron-donating ability of a series of 3-nitroflavones and their efficacy to inhibiting the onset and progression of aberrant crypt foci in the rat colon, *Cancer Res.* **2002**, *62*, 6506.
- (3) R. V. Bensasson, V. Zoete, A. T. Dinkova-Kostova, P. Talalay; Two-step mechanism of induction of the gene expression of a prototypic cancer-protective enzyme by diphenols, *Chem. Res. Toxicol.* **2008**, *21*, 805.
- (4) V. Zoete, M. Rougée, A. T. Dinkova-Kostova, P. Talalay, R. V. Bensasson; Redox ranking of inducers of a cancer protective enzyme *via* the energy of their highest occupied molecular orbital, *Free Rad. Biol. Med.* **2004**, *36*, 1418.
- (5) R. Scurlock, M. Rougée, R. V. Bensasson; Redox properties of diphenols and their correlation to induction of enzyme synthesis, *Z. Phys. Chem.* **1996**, *196*, 85.
- (6) R. V. Bensasson, G. Berthier, V. Zoete, P. Talalay, A. T. Dinkova-Kostova; Potency ranking of triterpenoids as inducers of a cytoprotective enzyme and asinhibitors of a cellular inflammatory response *via* their electron affinity and their electrophilicity index, *Chem.-Biol. Interact.* **2010**, *186*, 118.
- (7) R. V. Bensasson, V. Zoete, A. Jossang, B. Bodo, P. B. Arimondo, E. J. Land; Potency to inhibit human DNA topoisomerase I by flavones assessed through physicochemical parameters, *Free Rad. Biol. Med.* **2011**, *51*, 1406.
- (8) R. V. Bensasson, G. Berthier, V. Zoete; Comment on “Assessing the efficacy of nonsteroidal anti-inflammatory drugs through the quantum computation of molecular ionization energies”, *J. Phys. Chem. A* **2009**, *113*, 12337.
- (9) V. Zoete, F. Maglia, M. Rougée, R. V. Bensasson; Mechanism of action of a 4,5-diarylpyrrole series of selective cyclo-oxygenase-2 inhibitors, *Free Rad. Biol. Med.* **2000**, *28*, 1638.
- (10) V. Zoete, F. Bailly, F. Maglia, M. Rougée, R. V. Bensasson; Molecular orbital theory applied to the study of non-steroidal anti-inflammatory drug efficiency, *Free Radical Biol. Med.* **1999**, *26*, 1261.
- (11) R. V. Bensasson, J. Frederiksen, M. Rougée, D. Lexa, N. Harrit; Correlations between the rate constant of singlet oxygen quenching by imidazole derivatives and anti-inflammatory activity in rats, *Mol. Pharmacol.* **1992**, *42*, 718.



- (12) M. J. S. Dewar, E. G. Zoebisch, E. F. Healy, J. J. P. Stewart; Development and use of quantum mechanical molecular models. 76. AM1: a new general purpose quantum mechanical molecular model, *J. Am. Chem. Soc.* **1985**, *107*, 3902.
- (13) HyperCube, Inc.: Canada, (<http://www.hyper.com/>) **2012**.
- (14) A. Szabo, N. S. Ostlund; *Modern Quantum Chemistry: Introduction to Advanced Electronic Structure Theory* (Dover Publications, Inc., New York, **1989**).
- (15) I. N. Levine; *Quantum Chemistry*, Sixth Edition (Pearson Prentice Hall: Upper Saddle River, New Jersey, **2009**).
- (16) R. S. Mulliken; Molecular orbital method and molecular ionization potential. *Phys. Rev.* **74**, 736 (**1948**).
- (17) B. Pullman, A. Pullman; *Quantum Biochemistry* (Interscience Publishers, New York, **1963**).
- (18) R. G. Parr, W. Yang; *Density-Functional Theory of Atoms and Molecules* (Oxford University Press, Oxford, **1989**).
- (19) W. Koch, M. C. Holthausen; *A Chemist's Guide to Density Functional Theory*, 2<sup>nd</sup> ed. (Wiley-VCH, New York, **2001**).
- (20) C. Lee, W. Yang, R. Parr; Development of the Colle-Salvetti correlation-energy formula into a functional of the electron-density. *Phys. Rev. B* **1988**, *37*, 785.
- (21) A. D. Becke; Density-functional thermochemistry .3. The role of exact exchange. *J. Chem. Phys.* **1993**, *98*, 5648.
- (22) M. J. Frisch, G. W. Trucks, H. B. Schlegel, G. E. Scuseria, M. A. Robb, J. R. Cheeseman, G. Scalmani, V. Barone, B. Mennucci, G.A. Petersson, H. Nakatsuji, M. Caricato *et al.*; Gaussian 09 - Rev. B01, (Gaussian Inc., Wallingford CT, **2010**).
- (23) U. Salzner, J. B. Lagowski, P. G. Pickup, R. A. Poirier; Design of low band gap polymers employing density functional theory-hybrid functionals ameliorate band gap problem, *J. Comput. Chem.* **1997**, *18*, 1943.
- (24) L. Barrio, J. Catalan, J. L. G. de Paz; DFT study of ionization potentials for aza-substituted aromatic rings. *Int. J. Quant. Chem.* **91**, 432 (**2003**).
- (25) D. C. Young; *Computational Chemistry: A Practical Guide for Applying Techniques to Real World Problems* (Wiley-Interscience, New York, **2001**).
- (26) C. Hansch, A. Leo; *Exploring QSAR: Fundamentals and Applications in Chemistry and Biology* (American Chemical Society, Washington, DC, **1995**).
- (27) M. S. Tute; Principles and practice of Hansch analysis: a guide to structure-activity

- correlation for the medicinal chemist. *Advances in Drug Research* (Vol. 6); Academic Press: London, **1971**, pp 1-77.
- (28) Kaleidagraph 3.6.4 (<http://www.synergy.com/prodinfo.htm>).
- (29) L. W. Wattenberg, J. B. Coccia, L. K. T. Lam; Inhibitory effects of phenolic compounds on benzo(a)pyrene induced neoplasia, *Cancer Res.***1980**, *40*, 2820.
- (30) D. Bellus; Quenchers of singlet oxygen - A critical review, in *Singlet Oxygen*, edited by B. Rånby and J. F. Rabek (John Wiley and Sons, Chichester, **1978**) pp 61-110.
- (31) C. S. Foote; Quenching of singlet oxygen, in *Singlet Oxygen*, edited by H. H. Wasserman and R. Murray (Academic Press, New York, **1979**), Vol. 40, pp 139-171.
- (32) R. H. Young, D. R. Brewer; The mechanism of quenching of singlet oxygen, in *Singlet Oxygen*, edited by B. Rånby and J. F. Rabek (John Wiley and Sons, Chichester, **1978**) pp 36-47.
- (33) I. Saito, T. Matsuura; The oxidation of electron-rich aromatic compounds, in *Singlet Oxygen*, edited by H.H. Wasserman and R. Murray (Academic Press, New York, **1979**), vol. 40 pp 511-574.
- (34) M. J. Thomas and C. S. Foote; Chemistry of singlet oxygen. XXVI. Photooxygenation of phenols, *Photochem. Photobiol.* **1978**, *27*, 683.
- (35) K. Yamaguchi; Theoretical calculations of singlet oxygen reactions in *Singlet Oxygen* (CRC, Boca Raton, New York, **1985**), Vol. 3, pp 119-251.
- (36) N. E. Geacintov; Mechanisms of reaction of polycyclic aromatic epoxide derivatives with nucleic acids, *Polycyclic Aromatic Hydrocarbon Carcinogenesis; Structure Activity Relationships (Vol. II)* (CRC Press, Boca Raton, **1988**) pp 181-206.
- (37) V. L. Sporn, L. W. Wattenberg; Enhancement of glutathione transferase activity of the mouse forestomach by inhibitors of benzo(a)pyrene-induced neoplasia of the forestomach, *J. Natl. Cancer Inst.***1981**, *66*, 769.
- (38) P. Talalay, M. J. De Long, H. J. Prochaska; Identification of a common signal regulating the induction of enzymes that protect against chemical carcinogenesis, *Proc. Natl. Acad. Sci. USA* **1988**, *85*, 8261.
- (39) J. Folkman; Tumor angiogenesis: Therapeutic implications. *N. Engl. J. Med.* **1971**, *285*, 1182.
- (40) J. Folkman, M. Klagsbrun; Angiogenic factors, *Science* **1987**, *235*, 442.

- (41) J. Folkman; Fighting cancer by attacking its blood supply. *Sci. Amer.* **1996**, 275, 150.
- (42) J. Folkman; Role of angiogenesis in tumor growth and metastasis, *Semin. Oncol.* **2002**, 29, 15.
- (43) M. Lichtenberg; *Diplomarbeit. Investigation of anti-angiogenic effects displayed by 3-nitroflavone and 3-nitroflavone 8-acetic acid derivatives.*; Fakultät für Biowissenschaften der Ruprecht-Karls-Universität: Heidelberg, **2005**.
- (44) M. Lichtenberg, D. Dauzonne, V. Zoete, C. Gerhäuser, R. V. Bensasson; Quantitative structure activity relationships of 3-nitroflavones acting as potential inhibitors of angiogenesis, target of cancer inhibition, *Chem.-Biol. Interact.* **2006**, 161, 217.
- (45) P. Talalay; Chemoprotection against cancer by induction of phase 2 enzymes, *Biofactors* **2000**, 12, 5.
- (46) J. W. Fahey, A. T. Dinkova-Kostova, K. K. Stephenson, P. Talalay; The “Prochaska” microtiter plate bioassay for inducers of NQO1, *Methods in Enzymol.: Quinones and Quinone Enzymes, Part B* **2004**, 382, 243.
- (47) T. W. Kensler; Chemoprevention by inducers of carcinogen detoxication enzymes, *Environ. Health Perspect.* **1997**, 105 (Suppl. 4), 965.
- (48) H. J. Prochaska, M. J. De Long, P. Talalay; On the mechanisms of induction of cancer-protective enzymes: A unifying proposal, *Proc. Natl. Acad. Sci. USA* **1985**, 82, 8232.
- (49) A. T. Dinkova-Kostova, W. D. Holtzclaw, R. N. Cole, K. Itoh, N. Wakabayashi, Y. Katoh, M. Yamamoto, P. Talalay; Direct evidence that sulfhydryl groups of Keap1 are the sensors regulating induction of phase 2 enzymes that protect against carcinogens and oxidants, *Proc. Natl. Acad. Sci. USA* **2002**, 99, 11908.
- (50) A. T. Dinkova-Kostova, W. D. Holtzclaw, T. W. Kensler; The role of Keap1 in cellular protective responses, *Chem. Res. Toxicol.* **2005**, 18, 1779.
- (51) H. Motohashi, M. M. Yamamoto; Nrf2-Keap1 defines a physiologically important stress response mechanism, *Trends Mol. Med.* **2004**, 10, 549.
- (52) M. Kobayashi, M. Yamamoto; Molecular mechanisms activating the Nrf2-Keap1 pathway of antioxidant gene regulation. *Antioxid. Redox Signal.* **2005**, 7, 385.
- (53) M. Kobayashi, M. Yamamoto; Nrf2-Keap1 regulation of cellular defense mechanisms against electrophiles and reactive oxygen species. *Adv. Enzyme Regul.* **2006**, 46, 113.
- (54) A. T. Dinkova-Kostova, M. A. Massiah, R. E. Bozak, R. J. Hicks, P. Talalay;

- Potency of Michael reaction acceptors as inducers of enzymes that protect against carcinogenesis depends on their reactivity with sulfhydryl groups, *Proc. Natl. Acad. Sci. USA*, **2001**, *98*, 3404.
- (55) G. G. Chabot, Y. S. Touil, M. H. Pham, D. Dauzonne; Flavonoids in Cancer Prevention and Therapy: Challenges and perspectives for drug discovery. *Alternative and Complementary Therapies for Cancer* (Springer, New York, **2010**) pp. 583-612.
- (56) Y. Y. Lee-Hilz, A.-M. J. F. Boerboom, A. H. Westphal, W. J. H. van Berkel, J. M. M. J. G. Aarts, I.M.C.M. Rietjens; Pro-oxidant activity of flavonoids induces EpRE-mediated gene expression, *Chem. Res. Toxicol.* **2006**, *19*, 1499.
- (57) R. G. Parr, L. V. L. Szeentpály, S. Liu; Electrophilicity index, *J. Am. Chem. Soc.* **1999**, *121*, 1922.
- (58) A. T. Maynard, M. Huang, W. C. Rice, D. G. Covell; Reactivity of the HIV-1 nucleocapsid protein p7 zinc finger domains from the perspective of density-functional theory, *Proc. Natl. Acad. Sci. USA* **1998**, *95*, 11578.
- (59) D. P. Chong, O. V. Gritsenko, E. J. Baerends; Interpretation of the Kohn-Sham orbital energies as approximate vertical ionization potential, *J. Chem. Phys.* **2002**, *116*, 1760.
- (60) A. Filipetti; Electron affinity in density functional theory in the local spin-density approximation, *Phys. Rev. A* **1998**, *57*, 914.
- (61) P. K. Chattaraj, U. Sarkar, D. R. Roy; Electrophilicity index, *Chem. Rev.* **2006**, *106*, 2065.
- (62) Y. M. W. Janssen-Heininger, B. T. Mossman, N. H. Heintz, H. J. Forman, B. Kalyanaram, T. Finkel, J. S. Tamler, S. Goo Rhee, A. van der Vliet; Redox-based regulation of signal transduction: Principles, pitfalls and promises, *Free Radic. Biol. Med.* **2008**, *45*, 1.
- (63) F. Boege, T. Straub, A. Kehr, C. Boesenberg, K. Christiansen, A. Andersen, F. Jakob, J. Kohrle; Selected novel flavones inhibit the DNA binding or the DNA religation step of eukaryotic topoisomerase I, *J. Biol. Chem.* **1996**, *271*, 2262.
- (64) R. L. K. Virchow; *Cellular pathology as based upon physiological and pathological histology* (J. B. Lippincott, Philadelphia, 1863).
- (65) L. M. Coussens, Z. Werb; Inflammation and cancer, *Nature* **2002**, *420*, 860.
- (66) J. Habicht, K. Brune; Inhibition of prostaglandin E2 release by salicylates, benzoates and phenols: A quantitative structure-activity study, *J. Pharm. Pharmacol.* **1983**, *35*, 718.

- (67) K. B. Shakman, D. A. Mazziotti; Assessing the efficacy of nonsteroidal anti-inflammatory drugs through the quantum computation of molecular ionization energies, *J. Phys. Chem. A* **2007**, *111*, 7223.
- (68) E. L. Mehler, J. Gerhards; Interaction model for the anti-inflammatory action of benzoic and salicylic acids and phenols, *Int. J. Quantum Chem.* **1989**, *35*, 205.
- (69) A. Bard, L. Faulkner; *Electrochemical Methods* (John Wiley, New York, **1980**).
- (70) P. Wardman; Reduction potentials of one-electron couples involving free radicals in aqueous solution, *J. Phys. Ref. Data* **1989**, *18*, 1637.
- (71) C. Hansch; Structure-activity relationships of chemical mutagens and carcinogens, *Sci. Total Environ.* **1991**, *109/110*, 17.
- (72) R. Benigni; Alternatives to the carcinogenicity bioassay for toxicity prediction: are we there yet? *Exp. Opin. Drug Metab. Toxicol.* **2012**, *8*, 1.
- (73) C.F. Matta, A.A. Arabi; Electron-density descriptors as predictors in quantitative structure-activity/property relationships and drug design, *Future Med. Chem.* **2011**, *3*, 969.
- (74) W. G. Richards; Virtual screening using grid computing: the screensaver project, *Nat. Rev. Drug Discov.* **2002**, *1*, 551.
- (75) E. K. Davies, M. Glick, K. N. Harrison, W.G. Richards; Pattern recognition and massively distributed computing, *J. Comput.Chem.* **2002**, *23*, 1544.

## Chapter 4

### Closing Remarks

Three separate computational quantum chemical studies have been conducted and reported in this thesis, each of which investigates atomic and molecular properties and their changes in response to their electronic environment, and in the last chapter their predictive empirical correlation with anticancer and anti-inflammatory activity. A conclusion is provided at the end of every research chapter. All three research chapters are based on published papers (Chapters 2, and 3) or accepted for publication (Chapter 1).

The first research chapter reports a computational study of the effect of increasingly strong external electric fields on a number of molecular and bond properties in diatomic molecules. The properties studied for their response to the imposition of external fields include: Total energy, dipole moment, bond length, bond force constant, and vibrational frequency. This chapter fills an important gap in the literature that lacks a systematic computational investigation of the perturbing effect of strong electric fields on the chemical bond. The fields included in the study are of strength commonly encountered in the active sites of cellular receptors, in the crystalline state, in typical nanotechnological applications such as the scanning tunnelling microscope (STM), or (oscillating) in a femtosecond laser pulse. A precise phenomenological description of the changes under the field is presented, but the study did not stop there. Instead, and building on the work of B. Delley, a simple yet physically sound theoretical framework that explains the observed computational trends has been formulated. The model can *predict what happens in the chemical bond under an electric field from quantities that are experimentally measurable in absence of any external fields*, which is the principal strength of the model. An example of properties predicted well by the model is the bond's infrared absorption spectrum in the field, i.e., how does the field alter the wavelength of IR light absorbed by the molecule - the so called Stark shift. The paper upon which this chapter is based has been accepted for publication as a "full paper" in the *Journal of Chemical Physics* (Published by the *American Institute of Physics*). A second manuscript

that further elaborate on the calculations presented in Chapter 1 is being finalized for submission to publication at this time but has not been included in the thesis. This study, to be submitted during 2013 reports an in-depth investigation of the change of the topological properties of the electron density under the external electric fields in the same nine diatomic molecules and under the same fields investigated in Chapter 1.

Chapter 2 elucidates the atomic origins of the peaks in the dipole moment surfaces of reactions of the type  $\text{CH}_4 + \text{X} \rightarrow \text{CH}_3 + \text{HX}$  ( $\text{X}=\text{F}, \text{Cl}$ ), reactions previously studied Bandrauk *et al.* as an example of tuneable laser-controllable reactions. Results of the current study reveal that the halogen plays the main role in the observed changes in the dipole moment surface, and hence is the atom that plays the most dominant role in the laser-molecule interaction. This knowledge has been gained by decomposing the dipole moment of the systems into its two origin-independent contributions namely, atomic polarization (AP) and charge transfer (CT). It is shown that in both cases the CT term dominates. To complete this study in the future, the last missing piece in the jigsaw so to speak, is to trace the origin of the peaks in the *polarizability* surfaces that accompany the peaks in the dipole moment surface, since the energy expression of laser-molecule interaction includes one term for each. In other words, the dipole moment and polarizability terms, together, explain the changes in potential energy surface of the reaction under the laser fields regarding the absolute phase of the field - Chapter 2 explains the origin of the dipole term, in the future the polarizability term will be investigated. The significance of this chapter is in the field of laser control of chemical reactivity. The work, in collaboration with the group of Professor Bandrauk of the *Université de Sherbrooke*, has been published in the *Journal of Physical Chemistry A* (Published by the *American Chemical Society*).

Chapter 3 falls under the quantitative structure-to-activity relationship (QSAR) studies, a common and powerful method used in the early phases of *in silico* drug design (and also used in as diverse fields as toxicology and material design) in both academia and industry. This final study uses calculated quantum chemical physicochemical parameters in the construction of QSAR models for the prediction and understanding of the anti-carcinogenic and anti-inflammatory activities of a wide variety of chemical compounds (150 different chemical compound, in round numbers). This study has

revealed that different experimental and theoretical determinations of the physicochemical parameters involved can be employed interchangeably as they are highly correlated statistically. Importantly, the results suggest that semiempirical electronic structure calculation methods such as AM1 or PM3, much computationally cheaper than *ab initio* methods, yield QSAR models of the same statistical quality and strength as the much more expensive methods such as DFT. This result can be of industrial importance in considerably speeding the early stages of computer-aided drug discovery process. Further, the correlated physicochemical parameters shed insight into the mechanisms of complex biological processes involved in the fight against carcinogenesis and inflammation. This study has been conducted in collaboration with the group of Dr. René Bensasson, Director of Research in the *Centre National de Recherche Scientifique (CNRS)* and the *Musée National d'Histoire Naturelle* (France), and has been published in *International Reviews in Physical Chemistry* (Published by *Taylor and Francis, Inc.*)

During the time of his M.Sc. studies, the author of this thesis has also contributed the paper [Groves, B. R.; Crawford, S. M.; Lundrigan, T.; S. Sowlati-Hashjin; Matta, C. F.; Thompson, A. "Improved synthesis and chemical manipulation of the simplest F-BODIPY framework", *Chemical Communications* **49**, 816-818 (2013)], but this paper has not been included in the thesis since its principal result is in synthetic organic chemistry, and the author's contribution was in providing supporting quantum chemical calculations.



# **APPENDIX**

# APPENDIX

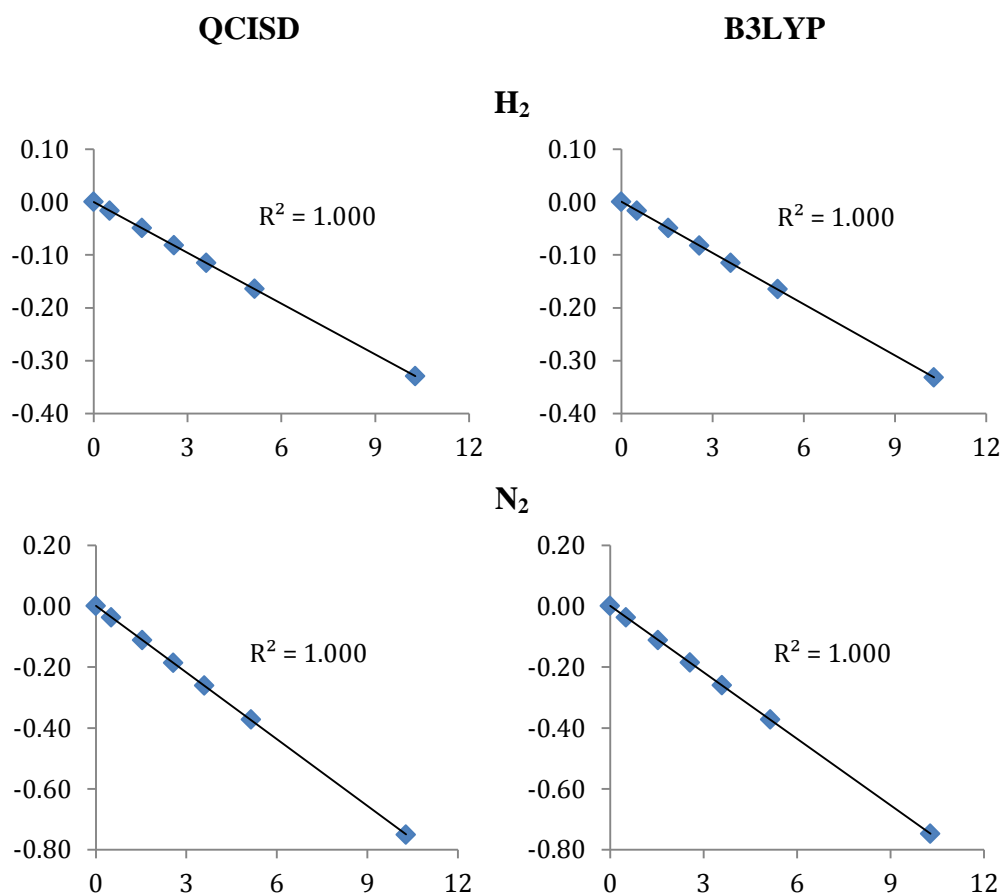
## (Supporting Information for Chapter 1)

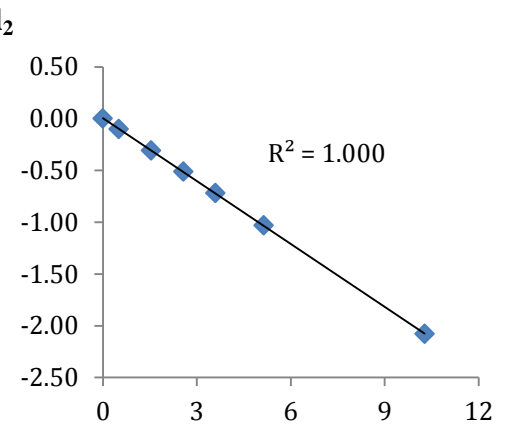
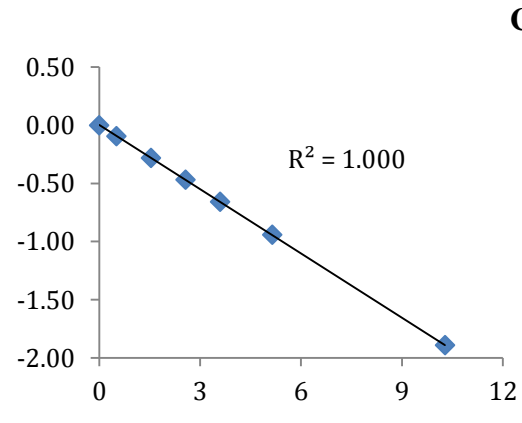
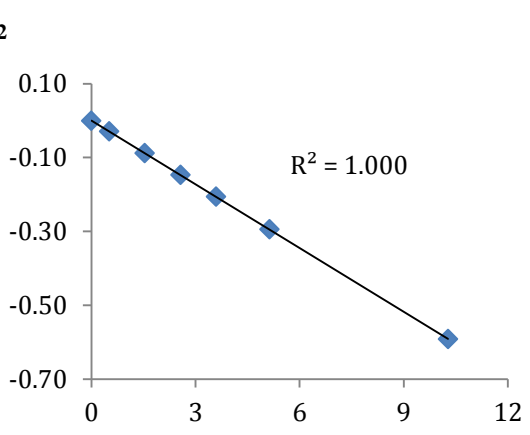
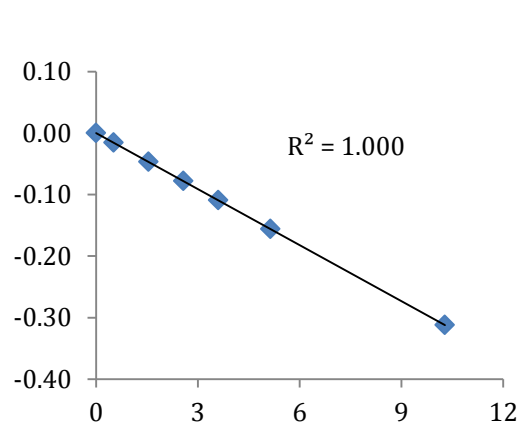
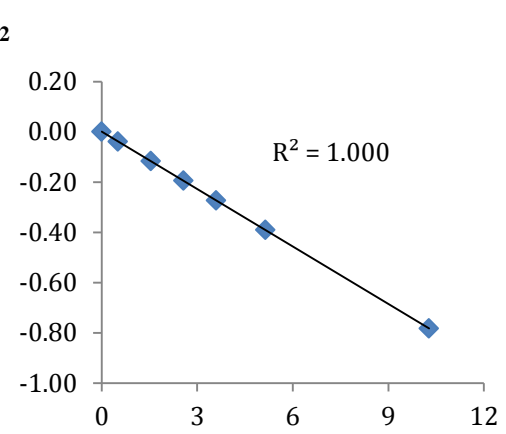
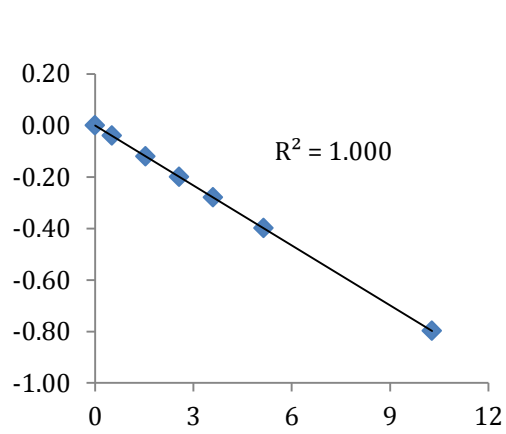
### Figures

#### Dipole moment

z-component of the dipole moment of the molecules (debye) as a function of the applied external electric field ( $\times 10^9 \text{ Vm}^{-1}$ ), at QCISD/6-311++G(3df,2pd) (left) and B3LYP/6-311++G(3df,2pd) (right)

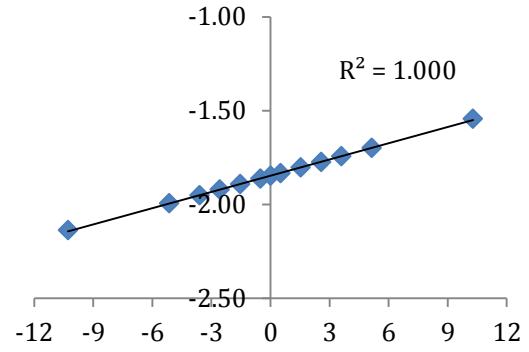
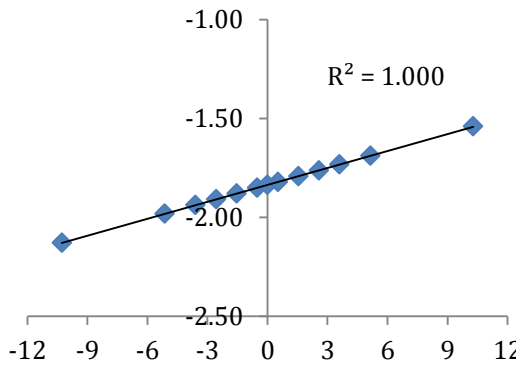
#### Homonuclear molecules



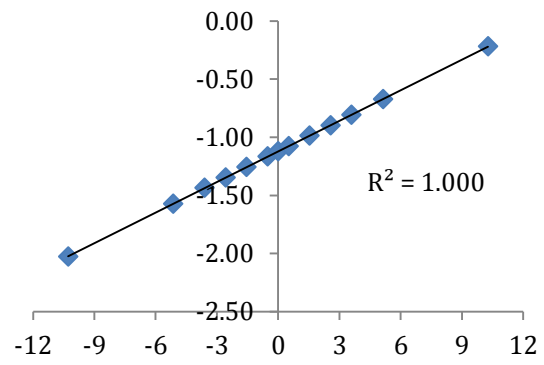
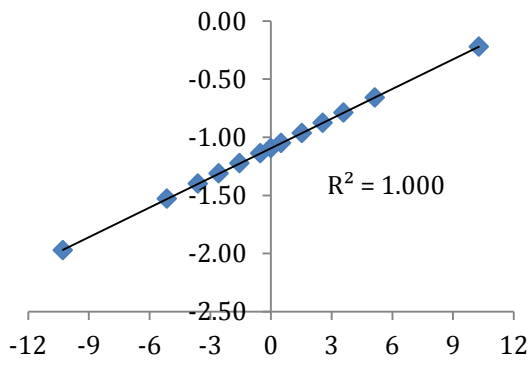


## Heteronuclear molecules

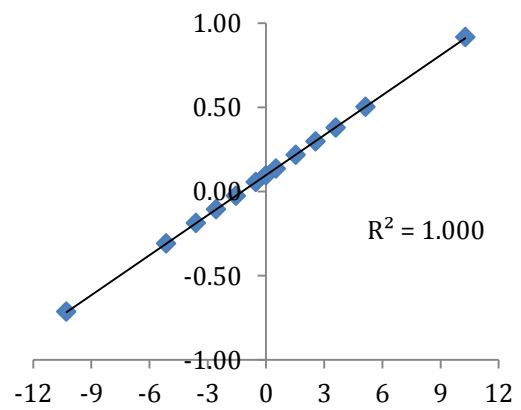
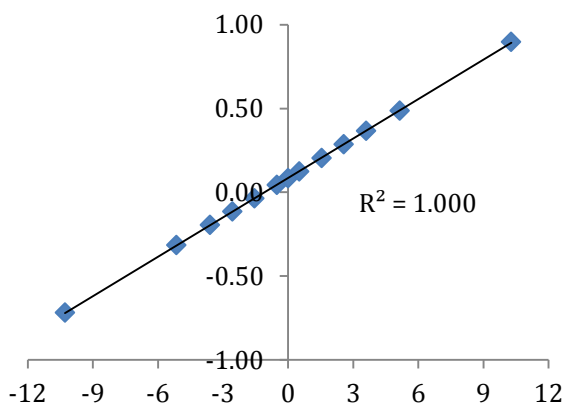
### HF



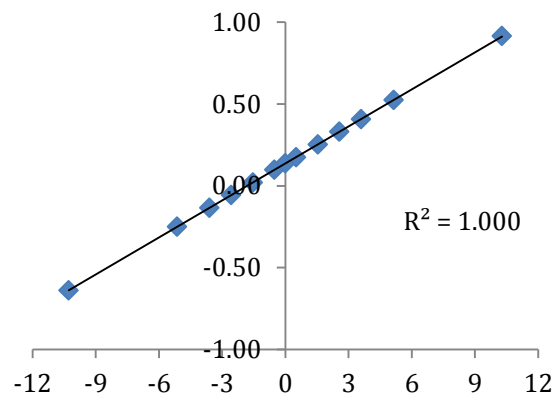
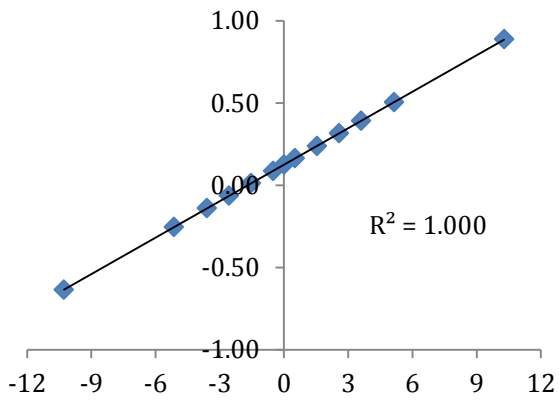
### HCl



### CO



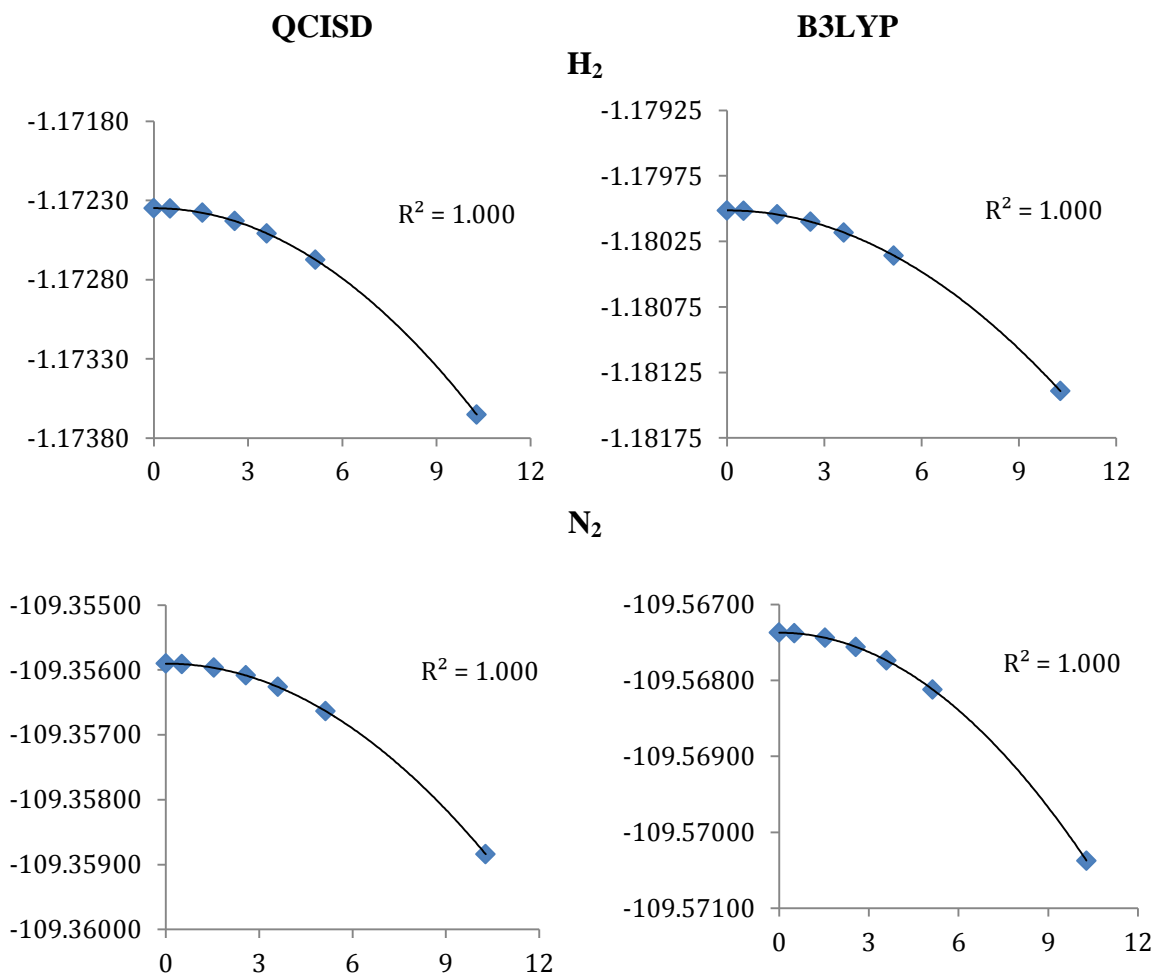
NO



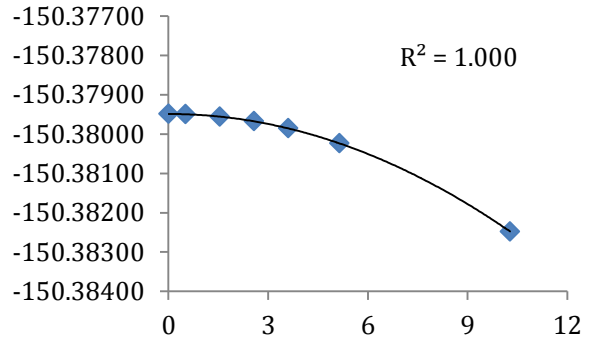
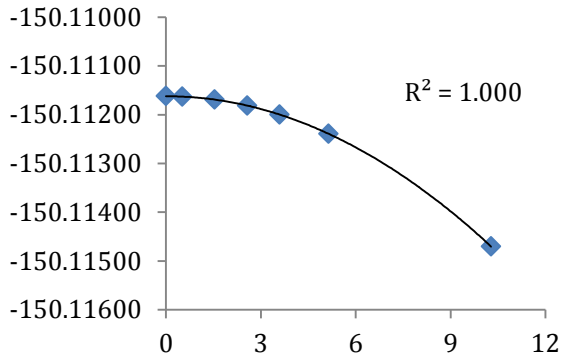
## Energy

Total energy of the molecules (hartree) as a function of the applied external electric field ( $\times 10^9 \text{ Vm}^{-1}$ ), at QCISD/6-311++G(3df,2pd) (left) and B3LYP/6-311++G(3df,2pd) (right)

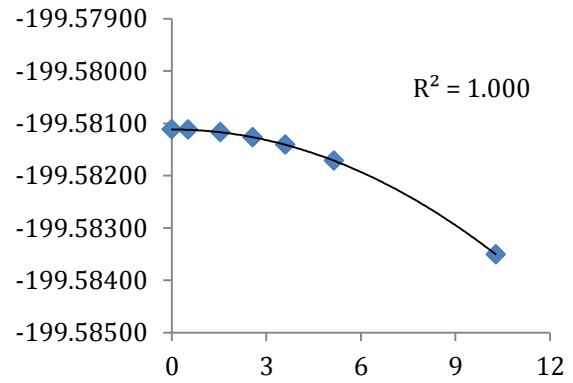
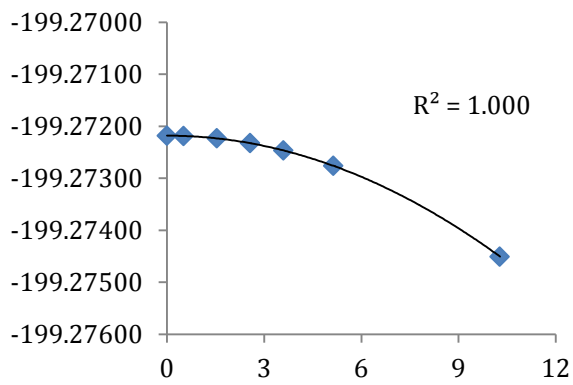
### Homonuclear molecules



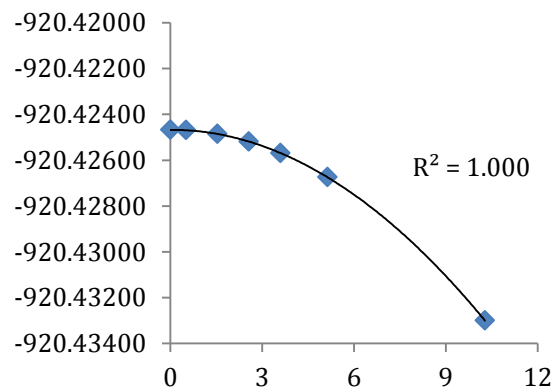
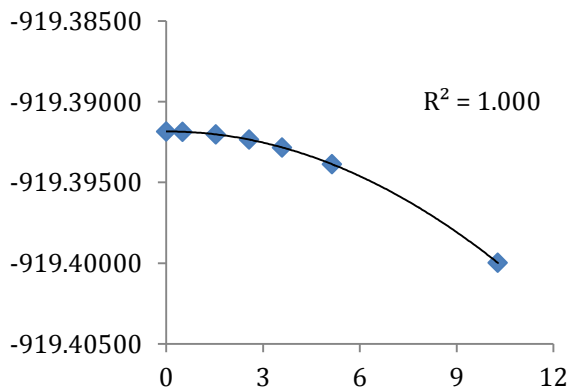
**O<sub>2</sub>**



**F<sub>2</sub>**

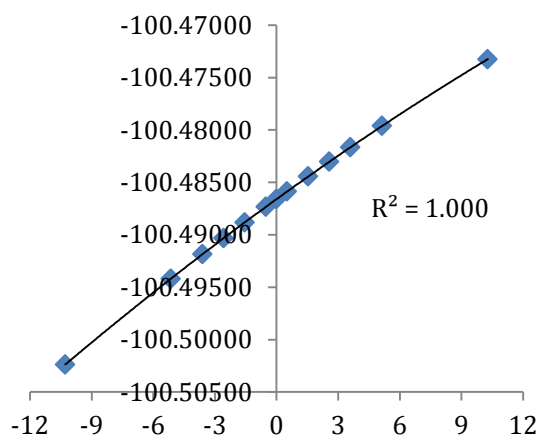
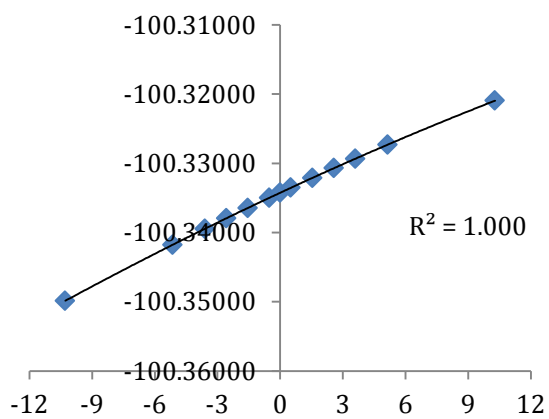


**Cl<sub>2</sub>**

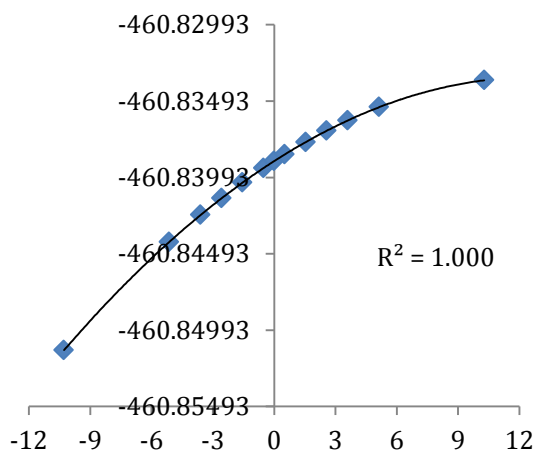
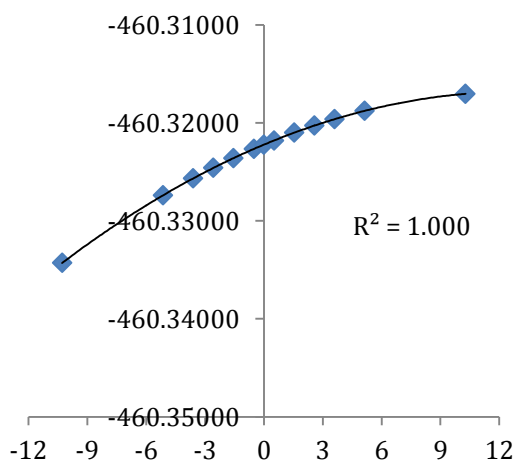


## Homonuclear molecules

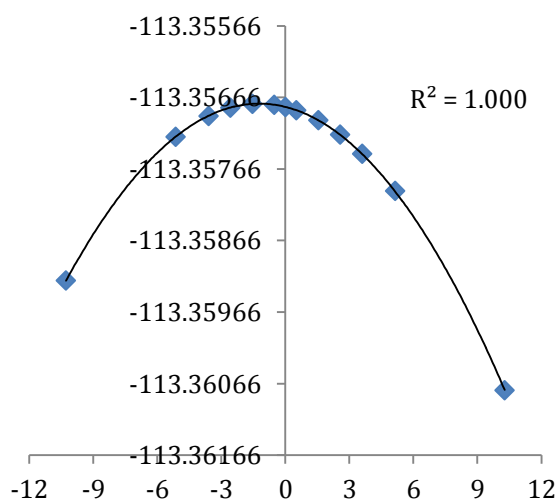
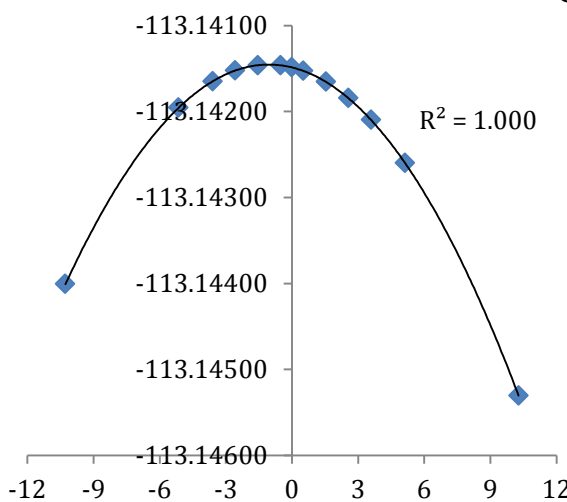
### HF



### HCl

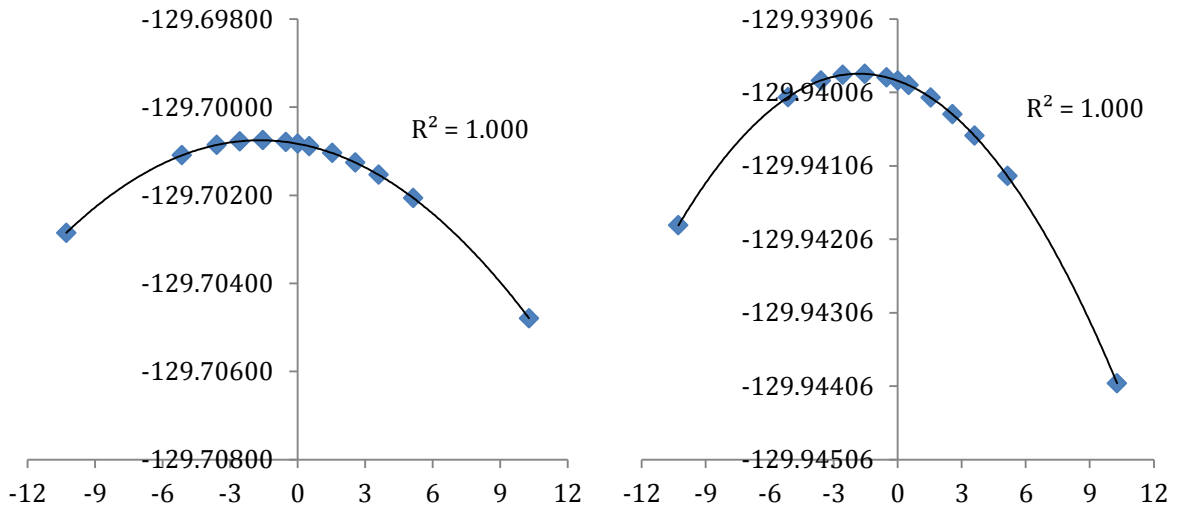


### CO





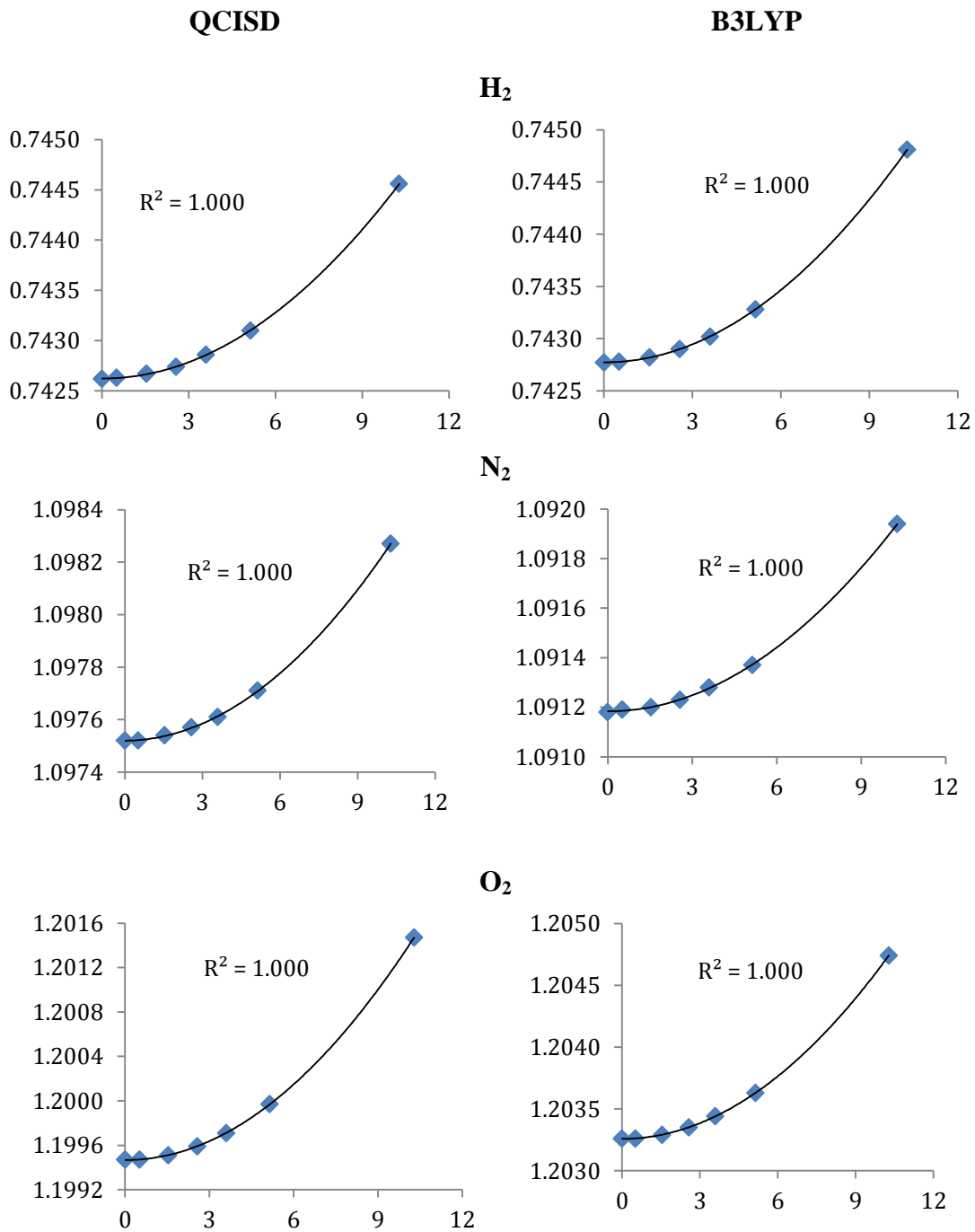
**NO**

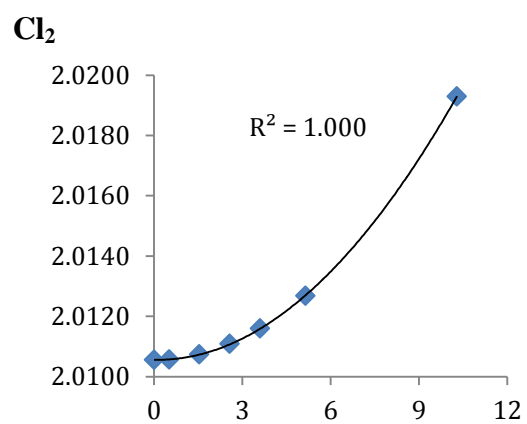
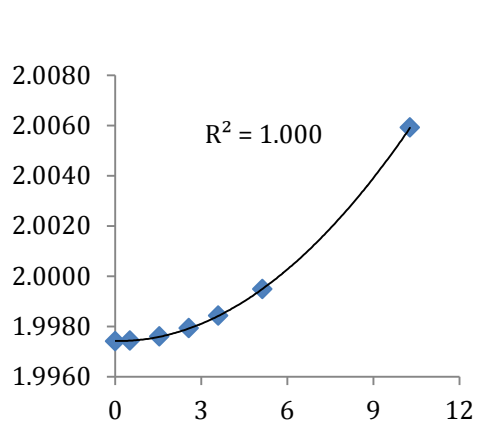
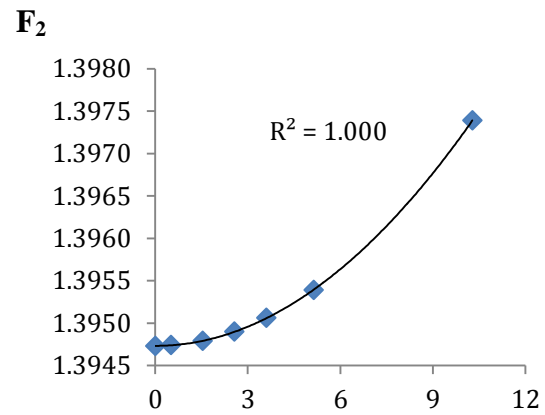
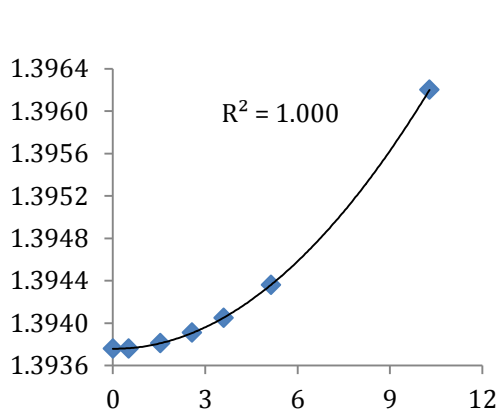


### Bond Length

Bond length (Ångstrom) as a function of the applied external electric field ( $\times 10^9 \text{ Vm}^{-1}$ ), at QCISD/6-311++G(3df,2pd) (left) and B3LYP/6-311++G(3df,2pd) (right)

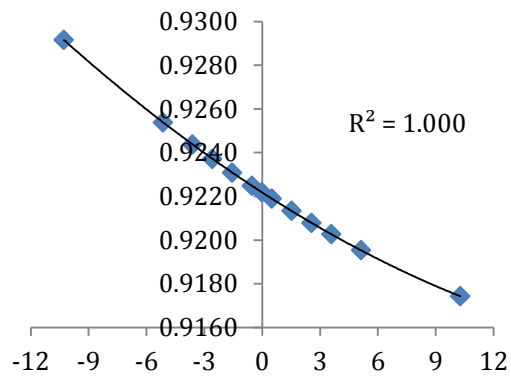
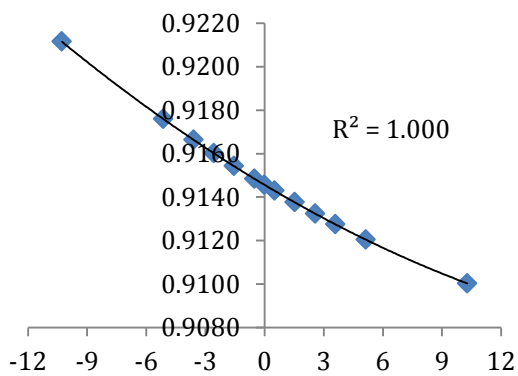
### Homonuclear molecules



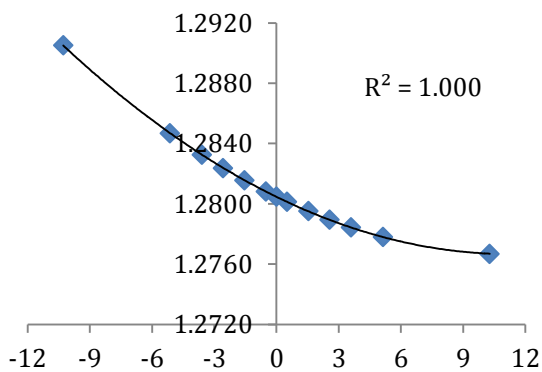
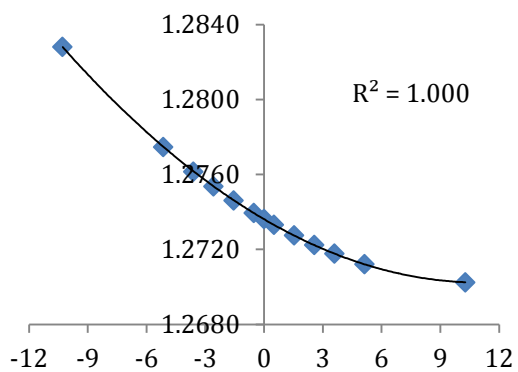


### Heteronuclear molecules

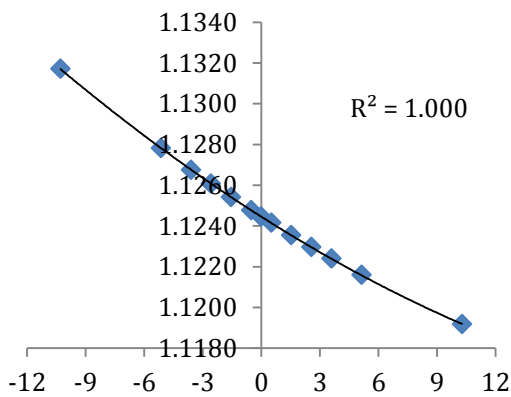
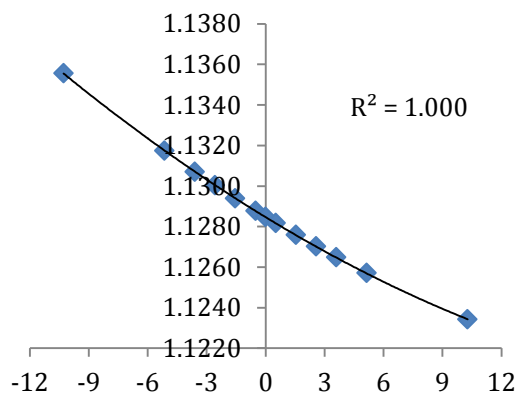
### HF



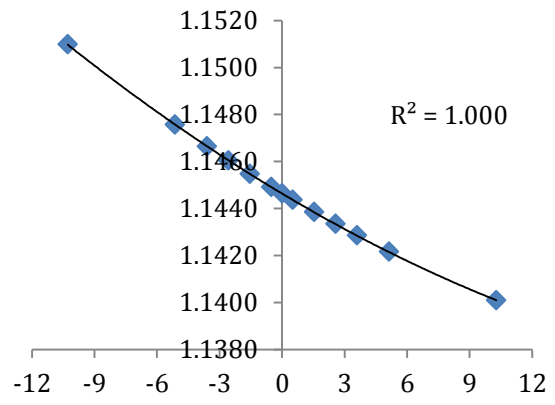
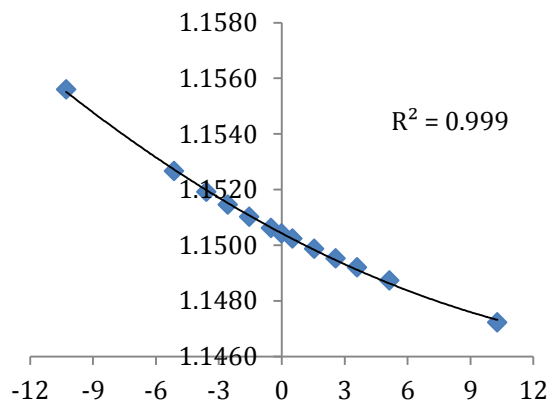
### HCl



### CO



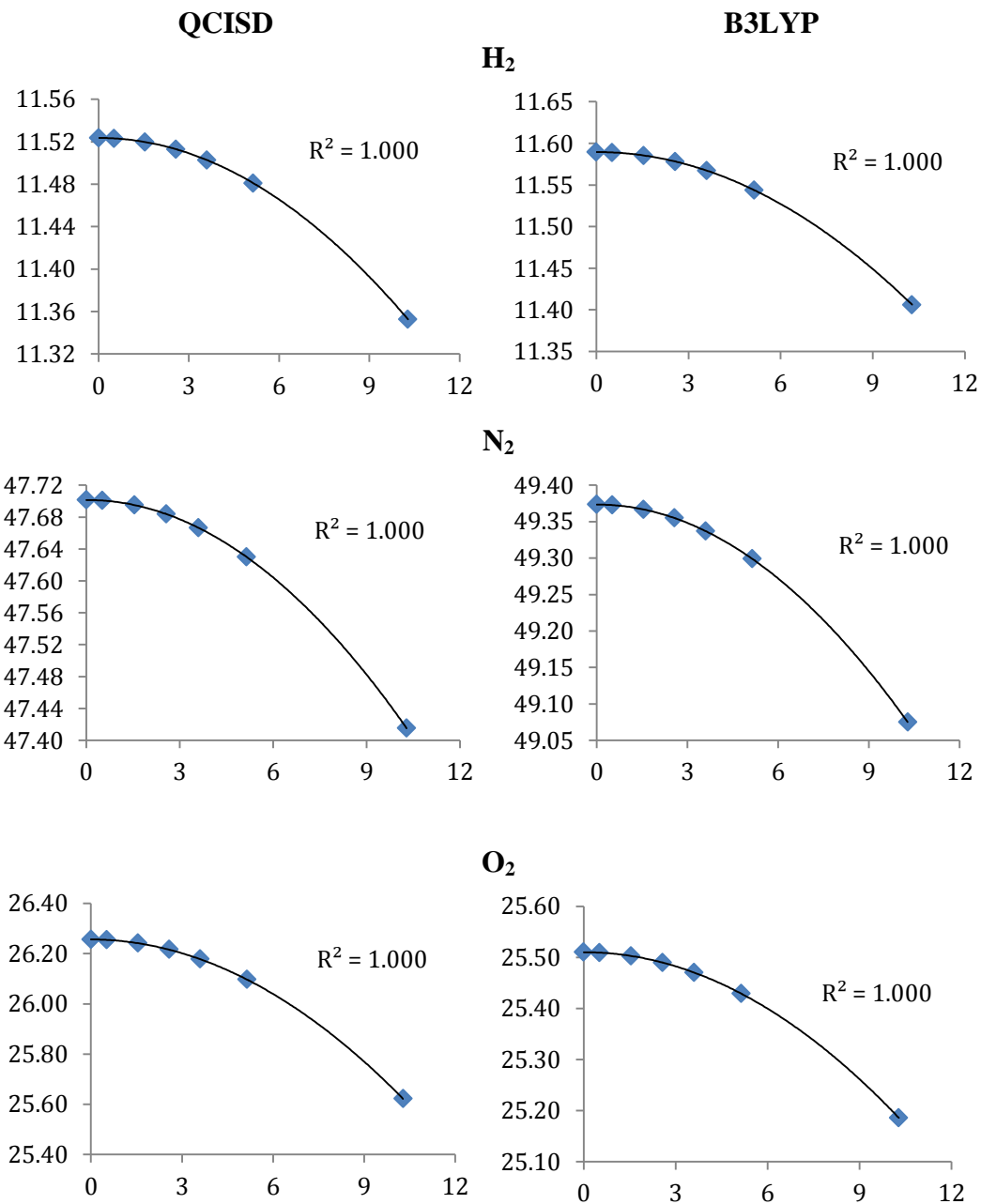
NO

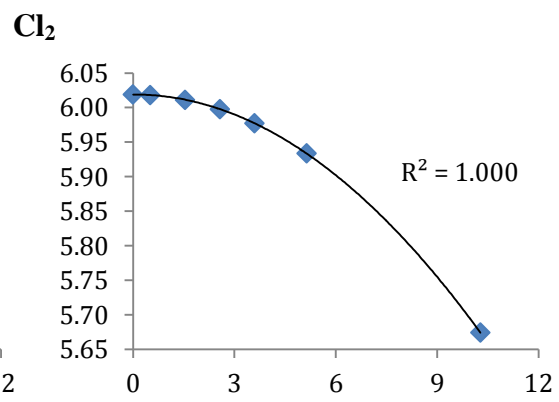
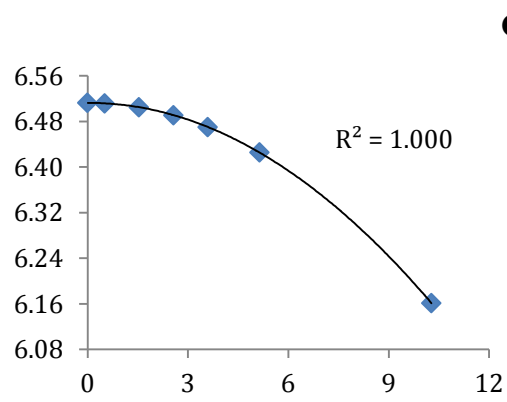
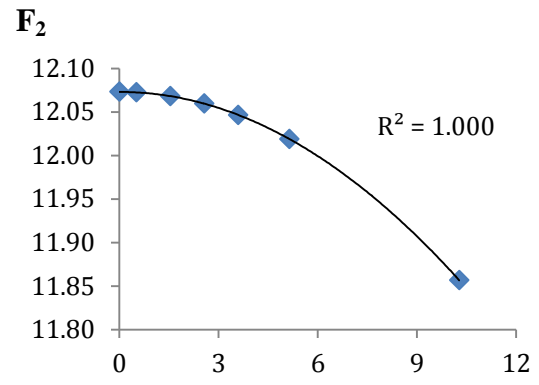
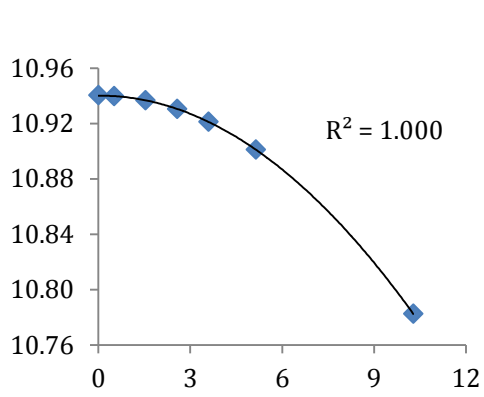


### Force constant ( $k$ )

Force constants,  $k$  (mDyne/Å) as a function of the applied external electric field ( $\times 10^9$  Vm<sup>-1</sup>) at QCISD/6-311++G(3df,2pd) (left) and B3LYP/6-311++G(3df,2pd) (right)

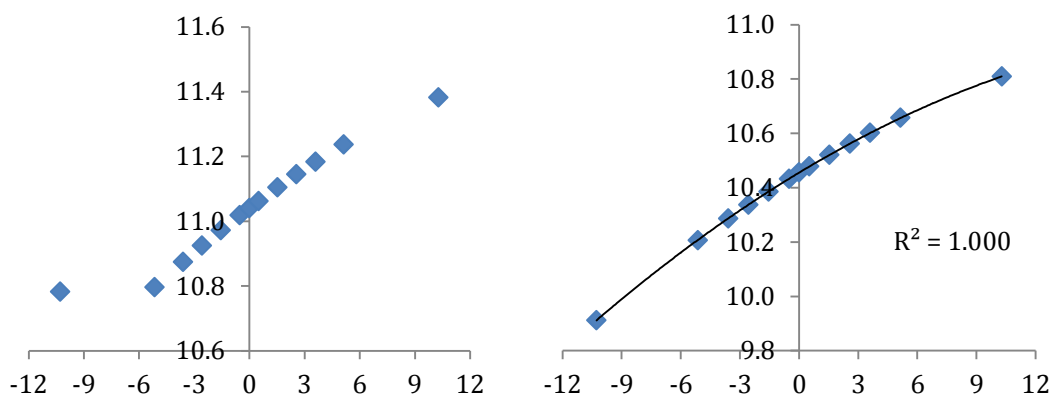
### Homonuclear molecules



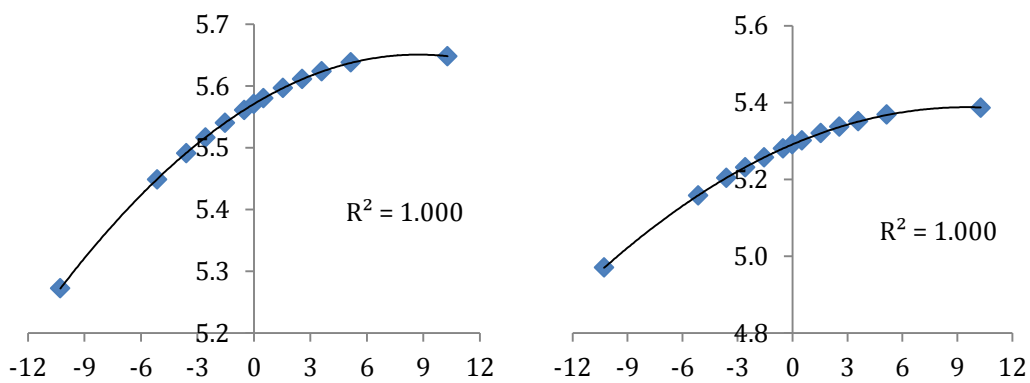


## Heteronuclear molecules

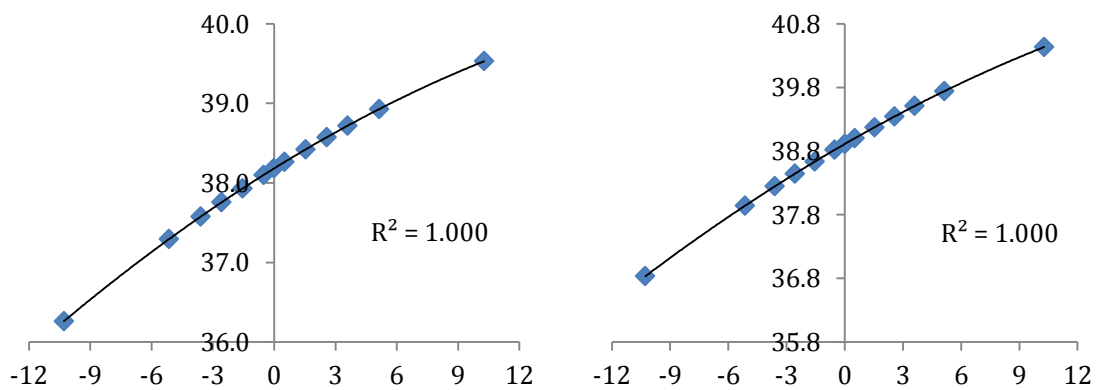
### HF



### HCl

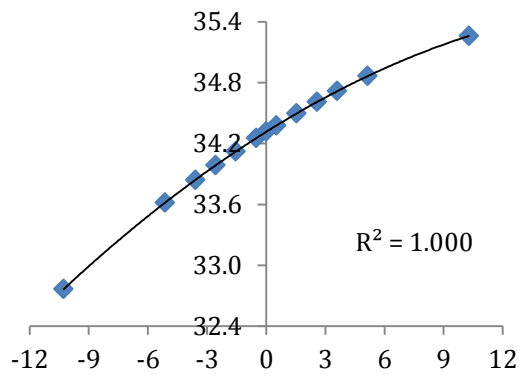
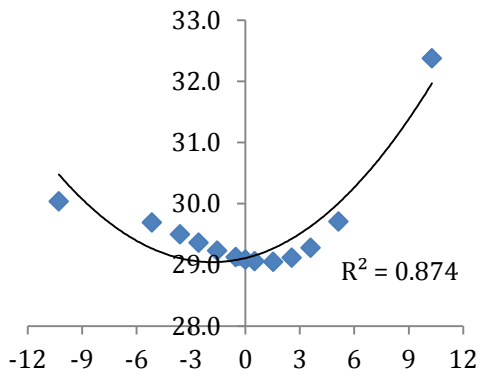


### CO





NO



### Harmonic frequencies

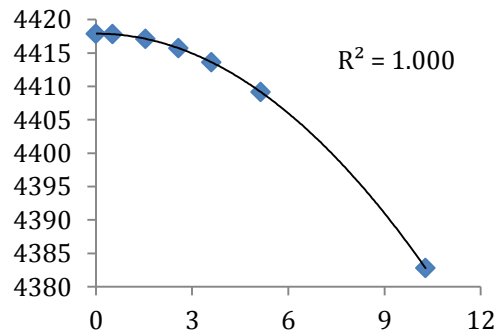
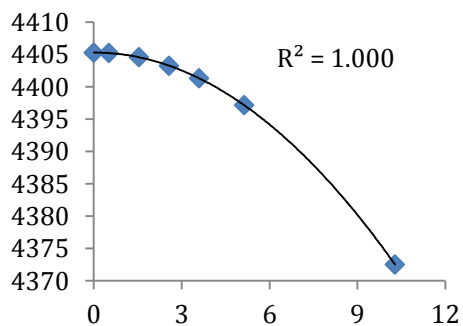
Harmonic frequencies,  $\nu$  ( $\text{cm}^{-1}$ ) as a function of the applied external electric field ( $\times 10^9 \text{ Vm}^{-1}$ ) at QCISD/6-311++G(3df,2pd) (left) and B3LYP/6-311++G(3df,2pd) (right)

#### Homonuclear molecules

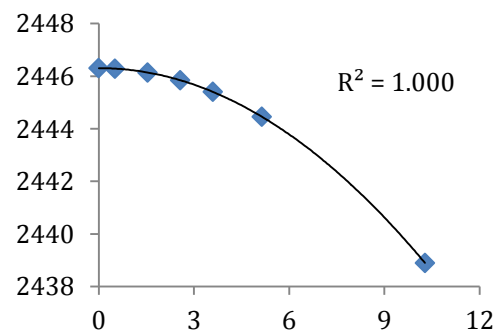
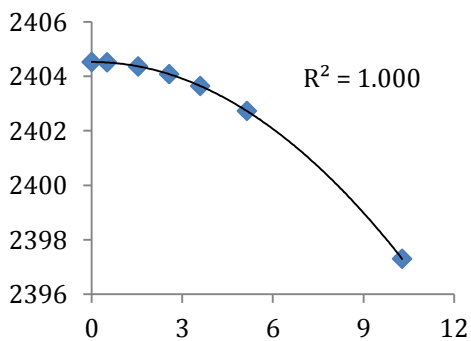
QCISD

B3LYP

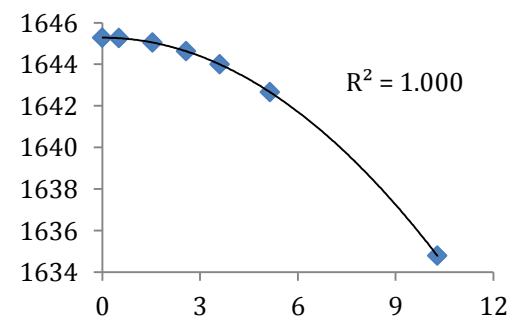
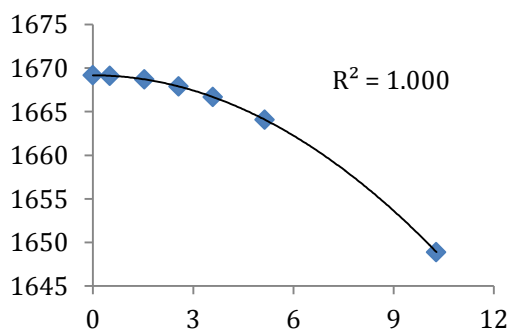
H<sub>2</sub>

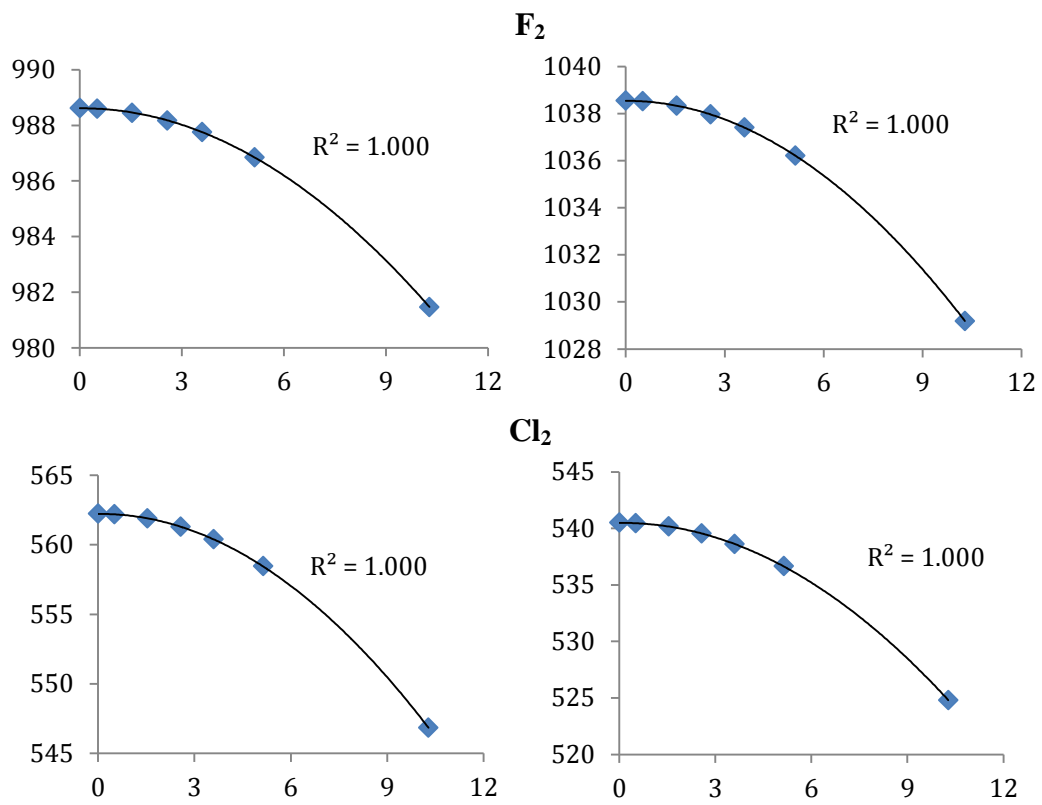


N<sub>2</sub>

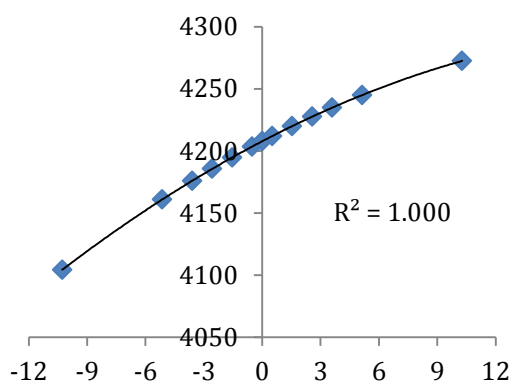


O<sub>2</sub>

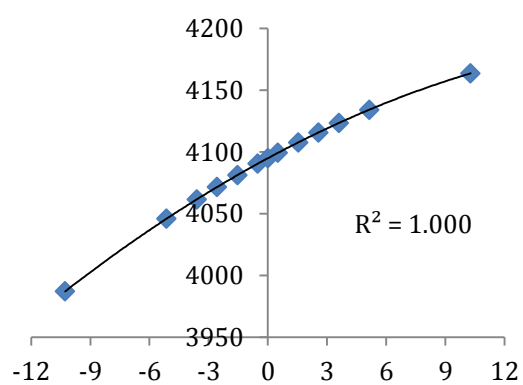




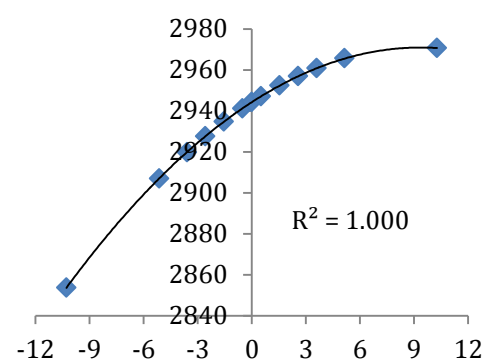
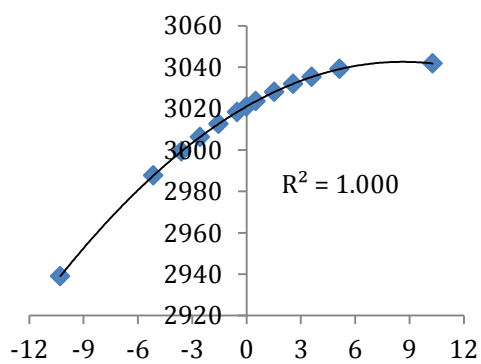
### Homonuclear molecules



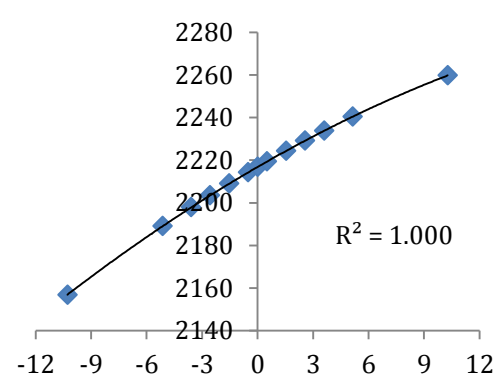
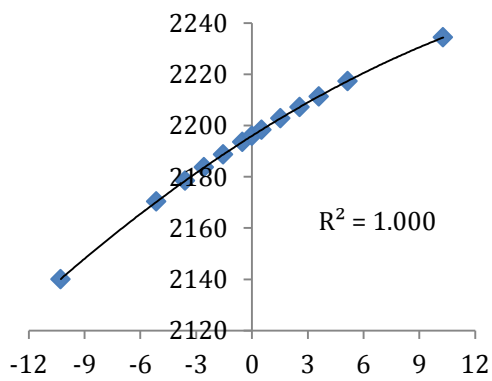
### HF



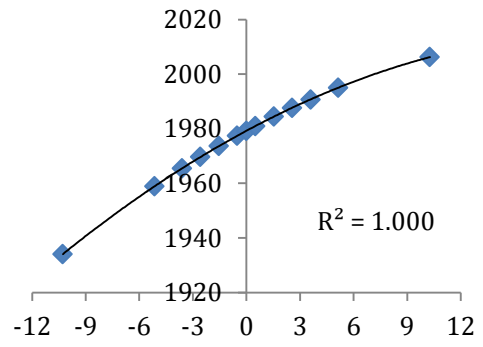
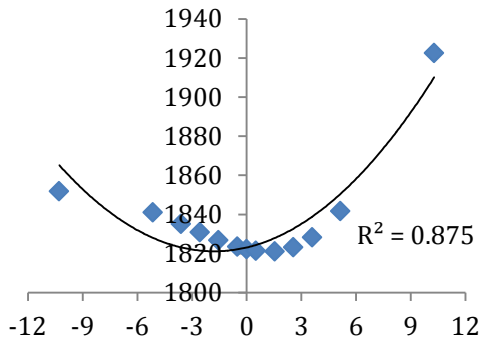
### HCl



### CO



NO



## Tables

### Dipole moment

z-component of the dipole moment of the molecules (debye) as a function of the applied external electric field ( $\times 10^9 \text{ Vm}^{-1}$ ), at QCISD/6-311++G(3df,2pd) and B3LYP/6-311++G(3df,2pd)

### Homonuclear molecules

#### QCISD

	<b>H<sub>2</sub></b>	<b>N<sub>2</sub></b>	<b>O<sub>2</sub></b>	<b>F<sub>2</sub></b>	<b>Cl<sub>2</sub></b>
<b>0.000</b>	0.0000	0.0000	0.0000	0.0000	0.0000
<b>0.514</b>	-0.0164	-0.0374	-0.0399	-0.0156	-0.0940
<b>1.542</b>	-0.0493	-0.1121	-0.1198	-0.0467	-0.2821
<b>2.570</b>	-0.0821	-0.1868	-0.1996	-0.0779	-0.4703
<b>3.598</b>	-0.1150	-0.2616	-0.2794	-0.1090	-0.6586
<b>5.140</b>	-0.1643	-0.3723	-0.3991	-0.1558	-0.9416
<b>10.280</b>	-0.3294	-0.7505	-0.7976	-0.3121	-1.8909

#### B3LYP

	<b>H<sub>2</sub></b>	<b>N<sub>2</sub></b>	<b>O<sub>2</sub></b>	<b>F<sub>2</sub></b>	<b>Cl<sub>2</sub></b>
<b>0.000</b>	0.0000	0.0000	0.0000	0.0000	0.0000
<b>0.514</b>	-0.0165	-0.0372	-0.0390	-0.0294	-0.1028
<b>1.542</b>	-0.0494	-0.1115	-0.1171	-0.0883	-0.3086
<b>2.570</b>	-0.0824	-0.1860	-0.1952	-0.1472	-0.5145
<b>3.598</b>	-0.1154	-0.2604	-0.2733	-0.2062	-0.7208
<b>5.140</b>	-0.1650	-0.3723	-0.3906	-0.2947	-1.0310
<b>10.280</b>	-0.3317	-0.7477	-0.7830	-0.5916	-2.0783

**Heteronuclear molecules****QCISD**

	<b>HF</b>	<b>HCl</b>	<b>CO</b>	<b>NO</b>
<b>-10.280</b>	-2.1284	-1.9721	-0.7190	-0.6352
<b>-5.140</b>	-1.9820	-1.5310	-0.3160	-0.2544
<b>-3.598</b>	-1.9381	-1.3999	-0.1958	-0.1406
<b>-2.570</b>	-1.9089	-1.3126	-0.1157	-0.0648
<b>-1.542</b>	-1.8797	-1.2255	-0.0356	0.0110
<b>-0.514</b>	-1.8504	-1.1384	0.0445	0.0868
<b>0.000</b>	-1.8358	-1.0949	0.0846	0.1247
<b>0.514</b>	-1.8211	-1.0514	0.1247	0.1627
<b>1.542</b>	-1.7918	-0.9645	0.2050	0.2385
<b>2.570</b>	-1.7624	-0.8775	0.2854	0.3145
<b>3.598</b>	-1.7330	-0.7905	0.3660	0.3905
<b>5.140</b>	-1.6888	-0.6599	0.4872	0.5046
<b>10.280</b>	-1.5403	-0.2219	0.8965	0.8865

**B3LYP**

	<b>HF</b>	<b>HCl</b>	<b>CO</b>	<b>NO</b>
<b>-10.280</b>	-2.1379	-2.0280	-0.7141	-0.6386
<b>-5.140</b>	-1.9942	-1.5726	-0.3081	-0.2501
<b>-3.598</b>	-1.9506	-1.4373	-0.1871	-0.1341
<b>-2.570</b>	-1.9214	-1.3473	-0.1064	-0.0569
<b>-1.542</b>	-1.8921	-1.2574	-0.0257	0.0203
<b>-0.514</b>	-1.8626	-1.1676	0.0550	0.0975
<b>0.000</b>	-1.8478	-1.1227	0.0954	0.1361
<b>0.514</b>	-1.8330	-1.0779	0.1359	0.1747
<b>1.542</b>	-1.8033	-0.9882	0.2168	0.2520
<b>2.570</b>	-1.7734	-0.8984	0.2980	0.3293
<b>3.598</b>	-1.7434	-0.8086	0.3794	0.4067
<b>5.140</b>	-1.6981	-0.6737	0.5019	0.5230
<b>10.280</b>	-1.5442	-0.2207	0.9168	0.9135

## Energy

Total energy of the molecules (hartree) as a function of the applied external electric field ( $\times 10^9 \text{ Vm}^{-1}$ ), at QCISD/6-311++G(3df,2pd) and B3LYP/6-311++G(3df,2pd)

### Homonuclear molecules

#### QCISD

	<b>H<sub>2</sub></b>	<b>N<sub>2</sub></b>	<b>O<sub>2</sub></b>	<b>F<sub>2</sub></b>	<b>Cl<sub>2</sub></b>
<b>0.000</b>	-1.17235	-109.35590	-150.11162	-199.27218	-919.39185
<b>0.514</b>	-1.17235	-109.35591	-150.11163	-199.27219	-919.39187
<b>1.542</b>	-1.17238	-109.35597	-150.11169	-199.27223	-919.39203
<b>2.570</b>	-1.17243	-109.35609	-150.11181	-199.27233	-919.39235
<b>3.598</b>	-1.17251	-109.35626	-150.11200	-199.27246	-919.39284
<b>5.140</b>	-1.17267	-109.35664	-150.11239	-199.27276	-919.39387
<b>10.280</b>	-1.17365	-109.35884	-150.11470	-199.27451	-919.39999

#### B3LYP

	<b>H<sub>2</sub></b>	<b>N<sub>2</sub></b>	<b>O<sub>2</sub></b>	<b>F<sub>2</sub></b>	<b>Cl<sub>2</sub></b>
<b>0.000</b>	-1.18001	-109.56737	-150.37949	-199.58112	-920.42467
<b>0.514</b>	-1.18002	-109.56738	-150.37950	-199.58112	-920.42469
<b>1.542</b>	-1.18004	-109.56744	-150.37956	-199.58117	-920.42486
<b>2.570</b>	-1.18010	-109.56756	-150.37967	-199.58127	-920.42519
<b>3.598</b>	-1.18018	-109.56774	-150.37985	-199.58141	-920.42569
<b>5.140</b>	-1.18036	-109.56812	-150.38023	-199.58171	-920.42675
<b>10.280</b>	-1.18139	-109.57037	-150.38248	-199.58351	-920.43300



Heteronuclear molecules

QCISD

	HF	HCI	CO	NO
<b>-10.280</b>	-100.34986	-460.33429	-113.14401	-129.70285
<b>-5.140</b>	-100.34176	-460.32740	-113.14196	-129.70109
<b>-3.598</b>	-100.33945	-460.32567	-113.14165	-129.70086
<b>-2.570</b>	-100.33793	-460.32460	-113.14152	-129.70078
<b>-1.542</b>	-100.33644	-460.32360	-113.14146	-129.70075
<b>-0.514</b>	-100.33497	-460.32267	-113.14146	-129.70079
<b>0.000</b>	-100.33424	-460.32223	-113.14149	-129.70083
<b>0.514</b>	-100.33352	-460.32181	-113.14153	-129.70089
<b>1.542</b>	-100.33210	-460.32101	-113.14165	-129.70104
<b>2.570</b>	-100.33070	-460.32029	-113.14184	-129.70126
<b>3.598</b>	-100.32933	-460.31963	-113.14210	-129.70154
<b>5.140</b>	-100.32730	-460.31877	-113.14260	-129.70206
<b>10.280</b>	-100.32095	-460.31704	-113.14531	-129.70479

B3LYP

	HF	HCI	CO	NO
<b>-10.280</b>	-100.50237	-460.85125	-113.35922	-129.94187
<b>-5.140</b>	-100.49418	-460.84417	-113.35721	-129.94013
<b>-3.598</b>	-100.49184	-460.84239	-113.35692	-129.93990
<b>-2.570</b>	-100.49032	-460.84129	-113.35680	-129.93982
<b>-1.542</b>	-100.48881	-460.84027	-113.35675	-129.93981
<b>-0.514</b>	-100.48733	-460.83931	-113.35676	-129.93986
<b>0.000</b>	-100.48660	-460.83886	-113.35679	-129.93990
<b>0.514</b>	-100.48587	-460.83843	-113.35684	-129.93996
<b>1.542</b>	-100.48444	-460.83762	-113.35698	-129.94013
<b>2.570</b>	-100.48303	-460.83688	-113.35718	-129.94036
<b>3.598</b>	-100.48165	-460.83620	-113.35745	-129.94065
<b>5.140</b>	-100.47962	-460.83533	-113.35797	-129.94120
<b>10.280</b>	-100.47324	-460.83357	-113.36075	-129.94402

### Bond Length

Bond length (Ångstrom) as a function of the applied external electric field ( $\times 10^9 \text{ Vm}^{-1}$ ), at QCISD/6-311++G(3df,2pd) and B3LYP/6-311++G(3df,2pd)

#### Homonuclear molecules

##### QCISD

	<b>H<sub>2</sub></b>	<b>N<sub>2</sub></b>	<b>O<sub>2</sub></b>	<b>F<sub>2</sub></b>	<b>Cl<sub>2</sub></b>
<b>0.000</b>	0.74262	1.09752	1.19947	1.39376	1.99741
<b>0.514</b>	0.74263	1.09752	1.19947	1.39376	1.99743
<b>1.542</b>	0.74267	1.09754	1.19951	1.39381	1.99760
<b>2.570</b>	0.74274	1.09757	1.19959	1.39391	1.99793
<b>3.598</b>	0.74286	1.09761	1.19971	1.39405	1.99842
<b>5.140</b>	0.74310	1.09771	1.19997	1.39436	1.99948
<b>10.280</b>	0.74456	1.09827	1.20147	1.3962	2.00591

##### B3LYP

	<b>H<sub>2</sub></b>	<b>N<sub>2</sub></b>	<b>O<sub>2</sub></b>	<b>F<sub>2</sub></b>	<b>Cl<sub>2</sub></b>
<b>0.000</b>	0.74277	1.09118	1.20326	1.39473	2.01055
<b>0.514</b>	0.74278	1.09119	1.20326	1.39474	2.01057
<b>1.542</b>	0.74282	1.09120	1.20329	1.39479	2.01074
<b>2.570</b>	0.74290	1.09123	1.20335	1.39490	2.01108
<b>3.598</b>	0.74302	1.09128	1.20344	1.39506	2.01159
<b>5.140</b>	0.74328	1.09137	1.20363	1.39539	2.01268
<b>10.280</b>	0.74481	1.09194	1.20474	1.39739	2.01929

## Heteronuclear molecules

### QCISD

	<b>NO</b>	<b>CO</b>	<b>HF</b>	<b>HCl</b>
<b>-10.280</b>	1.15560	1.13556	0.92115	1.28281
<b>-5.140</b>	1.15266	1.13174	0.91759	1.27746
<b>-3.598</b>	1.15192	1.13070	0.91663	1.27615
<b>-2.570</b>	1.15145	1.13003	0.91601	1.27536
<b>-1.542</b>	1.15102	1.12939	0.91542	1.27462
<b>-0.514</b>	1.15061	1.12877	0.91484	1.27394
<b>0.000</b>	1.15042	1.12847	0.91456	1.27362
<b>0.514</b>	1.15023	1.12817	0.91429	1.27331
<b>1.542</b>	1.14987	1.12758	0.91376	1.27275
<b>2.570</b>	1.14952	1.12702	0.91324	1.27224
<b>3.598</b>	1.14920	1.12648	0.91275	1.27178
<b>5.140</b>	1.14873	1.12570	0.91205	1.27121
<b>10.280</b>	1.14722	1.12342	0.91003	1.27024

### B3LYP

	<b>NO</b>	<b>CO</b>	<b>HF</b>	<b>HCl</b>
<b>-10.280</b>	1.15098	1.13171	0.92916	1.29052
<b>-5.140</b>	1.14757	1.12782	0.92538	1.28468
<b>-3.598</b>	1.14664	1.12675	0.92436	1.28325
<b>-2.570</b>	1.14604	1.12607	0.92371	1.28237
<b>-1.542</b>	1.14547	1.12541	0.92308	1.28156
<b>-0.514</b>	1.14491	1.12477	0.92247	1.28082
<b>0.000</b>	1.14464	1.12446	0.92218	1.28047
<b>0.514</b>	1.14437	1.12415	0.92189	1.28013
<b>1.542</b>	1.14385	1.12355	0.92133	1.27951
<b>2.570</b>	1.14334	1.12296	0.92078	1.27895
<b>3.598</b>	1.14285	1.12240	0.92027	1.27844
<b>5.140</b>	1.14216	1.12159	0.91953	1.27780
<b>10.280</b>	1.14009	1.11918	0.91742	1.27668

**Force constant ( $k$ )**

Force constants,  $k$  (mDyne/Å) as a function of the applied external electric field ( $\times 10^9$  Vm<sup>-1</sup>) at QCISD/6-311++G(3df,2pd) and B3LYP/6-311++G(3df,2pd)

**Homonuclear molecules****QCISD**

	<b>H<sub>2</sub></b>	<b>N<sub>2</sub></b>	<b>O<sub>2</sub></b>	<b>F<sub>2</sub></b>	<b>Cl<sub>2</sub></b>
<b>0.000</b>	11.5236	47.7015	26.2565	10.9403	6.5125
<b>0.514</b>	11.5231	47.7008	26.2548	10.9397	6.5116
<b>1.542</b>	11.5197	47.6951	26.2419	10.9366	6.5047
<b>2.570</b>	11.5129	47.6838	26.2164	10.9304	6.4908
<b>3.598</b>	11.5027	47.6665	26.178	10.9212	6.4699
<b>5.140</b>	11.481	47.6301	26.0966	10.9012	6.4255
<b>10.280</b>	11.3527	47.4152	25.622	10.7824	6.1611

**B3LYP**

	<b>H<sub>2</sub></b>	<b>N<sub>2</sub></b>	<b>O<sub>2</sub></b>	<b>F<sub>2</sub></b>	<b>Cl<sub>2</sub></b>
<b>0.000</b>	11.5896	49.3735	25.5101	12.0730	6.0191
<b>0.514</b>	11.5891	49.3728	25.5093	12.0724	6.018
<b>1.542</b>	11.5855	49.3668	25.5028	12.0681	6.0113
<b>2.570</b>	11.5782	49.3549	25.4899	12.0595	5.9978
<b>3.598</b>	11.5672	49.3371	25.4704	12.0465	5.9771
<b>5.140</b>	11.5439	49.2991	25.4291	12.0189	5.9336
<b>10.280</b>	11.4061	49.0749	25.1859	11.8565	5.6743

**Heteronuclear molecules****QCISD**

	<b>NO</b>	<b>CO</b>	<b>HF</b>	<b>HCl</b>
<b>-10.280</b>	30.0363	36.2623	10.7824	5.2725
<b>-5.140</b>	29.6911	37.2951	10.7956	5.4487
<b>-3.598</b>	29.4979	37.5764	10.8739	5.4910
<b>-2.570</b>	29.3621	37.7566	10.9239	5.5165
<b>-1.542</b>	29.2331	37.9311	10.9718	5.5399
<b>-0.514</b>	29.1258	38.0998	11.0179	5.5610
<b>0.000</b>	29.0856	38.1821	11.0402	5.5707
<b>0.514</b>	29.0581	38.2630	11.0621	5.5799
<b>1.542</b>	29.0481	38.4203	11.1043	5.5967
<b>2.570</b>	29.1156	38.5721	11.1445	5.6112
<b>3.598</b>	29.2763	38.7182	11.1827	5.6235
<b>5.140</b>	29.7085	38.9268	11.2364	5.6378
<b>10.280</b>	32.3748	39.5309	11.3821	5.6476

**B3LYP**

	<b>NO</b>	<b>CO</b>	<b>HF</b>	<b>HCl</b>
<b>-10.280</b>	32.7650	36.8332	9.9123	4.9708
<b>-5.140</b>	33.6157	37.9422	10.2068	5.1580
<b>-3.598</b>	33.8414	38.2473	10.2862	5.2036
<b>-2.570</b>	33.9843	38.4438	10.3369	5.2314
<b>-1.542</b>	34.1211	38.6347	10.3857	5.2570
<b>-0.514</b>	34.2520	38.8200	10.4327	5.2803
<b>0.000</b>	34.3151	38.9107	10.4555	5.2912
<b>0.514</b>	34.3768	38.9999	10.4778	5.3015
<b>1.542</b>	34.4955	39.1742	10.5210	5.3203
<b>2.570</b>	34.6082	39.3431	10.5622	5.3370
<b>3.598</b>	34.7149	39.5065	10.6016	5.3513
<b>5.140</b>	34.8635	39.7413	10.6569	5.3685
<b>10.280</b>	35.2593	40.4352	10.8090	5.3865

### Harmonic frequencies

Harmonic frequencies,  $\nu$  ( $\text{cm}^{-1}$ ) as a function of the applied external electric field ( $\times 10^9 \text{ Vm}^{-1}$ ) at QCISD/6-311++G(3df,2pd) and B3LYP/6-311++G(3df,2pd)

#### Homonuclear molecules

##### QCISD

	<b>H<sub>2</sub></b>	<b>N<sub>2</sub></b>	<b>O<sub>2</sub></b>	<b>F<sub>2</sub></b>	<b>Cl<sub>2</sub></b>
<b>0.000</b>	4405.304	2404.526	1669.176	988.622	562.221
<b>0.514</b>	4405.223	2404.507	1669.122	988.596	562.184
<b>1.542</b>	4404.572	2404.363	1668.712	988.455	561.886
<b>2.570</b>	4403.270	2404.078	1667.900	988.174	561.285
<b>3.598</b>	4401.314	2403.643	1666.679	987.759	560.382
<b>5.140</b>	4397.153	2402.725	1664.085	986.854	558.454
<b>10.280</b>	4372.513	2397.298	1648.884	981.465	546.845

##### B3LYP

	<b>H<sub>2</sub></b>	<b>N<sub>2</sub></b>	<b>O<sub>2</sub></b>	<b>F<sub>2</sub></b>	<b>Cl<sub>2</sub></b>
<b>0.000</b>	4417.901	2446.303	1645.281	1038.541	540.504
<b>0.514</b>	4417.815	2446.284	1645.255	1038.518	540.454
<b>1.542</b>	4417.119	2446.137	1645.046	1038.332	540.156
<b>2.570</b>	4415.727	2445.842	1644.628	1037.960	539.547
<b>3.598</b>	4413.636	2445.400	1644.001	1037.402	538.618
<b>5.140</b>	4409.185	2444.458	1642.668	1036.214	536.651
<b>10.280</b>	4382.795	2438.894	1634.793	1029.188	524.795

**Heteronuclear molecules****QCISD**

	<b>HF</b>	<b>HCl</b>	<b>CO</b>	<b>NO</b>
<b>-10.280</b>	4104.383	2939.010	2140.046	1851.748
<b>-5.140</b>	4160.953	2987.715	2170.307	1841.075
<b>-3.598</b>	4176.013	2999.295	2178.476	1835.075
<b>-2.570</b>	4185.593	3006.253	2183.693	1830.848
<b>-1.542</b>	4194.772	3012.604	2188.735	1826.822
<b>-0.514</b>	4203.573	3018.351	2193.598	1823.464
<b>0.000</b>	4207.826	3020.991	2195.965	1822.207
<b>0.514</b>	4211.983	3023.485	2198.289	1821.345
<b>1.542</b>	4220.011	3028.025	2202.805	1821.031
<b>2.570</b>	4227.650	3031.943	2207.151	1823.145
<b>3.598</b>	4234.890	3035.273	2211.326	1828.170
<b>5.140</b>	4245.052	3039.113	2217.276	1841.615
<b>10.280</b>	4272.470	3041.762	2234.414	1922.481

**B3LYP**

	<b>HF</b>	<b>HCl</b>	<b>CO</b>	<b>NO</b>
<b>-10.280</b>	3987.095	2853.698	2156.826	1934.032
<b>-5.140</b>	4045.878	2906.909	2189.054	1958.978
<b>-3.598</b>	4061.596	2919.758	2197.839	1965.543
<b>-2.570</b>	4071.588	2927.533	2203.476	1969.688
<b>-1.542</b>	4081.191	2934.677	2208.941	1973.651
<b>-0.514</b>	4090.406	2941.189	2214.233	1977.431
<b>0.000</b>	4094.868	2944.208	2216.816	1979.253
<b>0.514</b>	4099.233	2947.069	2219.357	1981.030
<b>1.542</b>	4107.677	2952.314	2224.312	1984.449
<b>2.570</b>	4115.726	2956.921	2229.101	1987.688
<b>3.598</b>	4123.381	2960.887	2233.725	1990.748
<b>5.140</b>	4134.133	2965.636	2240.353	1995.005
<b>10.280</b>	4163.533	2970.606	2259.827	2006.299



**Saint Mary's  
University**

Halifax, Nova Scotia  
Canada B3H 3C3

Patrick Power Library

tel 902.420.5534

fax 902.420.5561

web [www.stmarys.ca](http://www.stmarys.ca)

## **Copyright Permission Notice**

Documentation regarding permissions for the use of copyrighted material in this thesis is on file at the Saint Mary's University Archives. Contact us if you wish to view this documentation:

Saint Mary's University, Archives  
Patrick Power Library  
Halifax, NS  
B3H 3C3

Email: [archives@smu.ca](mailto:archives@smu.ca)

Phone: 902-420-5508

Fax: 902-420-5561